Scaling up production of reprogrammed cells for biomedical applications

Skalierung der Produktion von reprogrammierten Zellen für biomedizinische Anwendungen

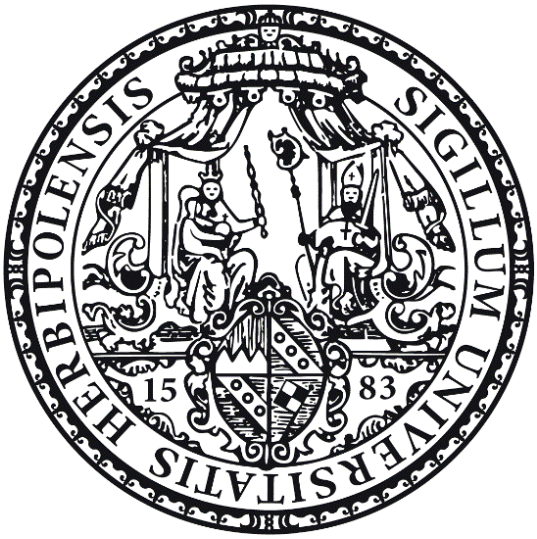

Doctoral Thesis

for the conferral of the degree
"Doctor rerum naturalium" (Dr. rer. nat.)

at the Graduate School of Life Sciences, Biomedicine Section
Julius-Maximilians-Universität Würzburg

Submitted by
Chee Keong Kwok
born in Singapore on 2nd May 1986

Würzburg, 2019

Submitted on: _____

Office stamp

Members of the “Promotionskomitee”:

Chairperson:	Prof. Dr. Thomas Dandekar
Primary Supervisor:	Prof. Dr. Frank Edenhofer
Second Supervisor:	Prof. Dr. Jürgen Groll
Third Supervisor:	Prof. Dr. Thomas Scheibel
Fourth Supervisor:	Prof. Dr. Heike Walles

Date of public defence: _____

Date of receipt of certificates: _____

To my family,

and my chosen family,

both in equal measure.

Table of Contents

Summary

Induced pluripotent stem cells (iPSCs) have been recognised as a virtually unlimited source of stem cells that can be generated in a patient-specific manner. Due to these cells' potential to give rise to all differentiated cell types of the human body, they have been widely used to derive differentiated cells for drug screening and disease modelling purposes. iPSCs also garner much interest as they can potentially serve as a source for cell replacement therapy. Towards the realisation of these biomedical applications, this thesis aims to address challenges that are associated with scale-up, safety and biofabrication.

Firstly, the manufacture of a high number of human iPSCs (hiPSCs) will require standardised procedures for scale-up and the development of a flexible bioprocessing method, since standard adherent hiPSC culture exhibits limited scalability and is labour-intensive. While the quantity of cells that are required for cell therapy depends largely on the tissue and defect that these replacing cells are meant to correct, an estimate of 1×10^9 has been suggested to be sufficient for several indications, including myocardial infarction and islet replacement for diabetes. Here, the development of an integrated, microcarrier-free workflow to transition standard adherent hiPSC culture (6-well plates) to scalable stirred suspension culture in bioreactors (1 L working volume, 2.4 L maximum working volume) is presented. The two-phase bioprocess lasts 14 days and generates hiPSC aggregates measuring 198 ± 58 µm in diameter on the harvesting day, yielding close to 2×10^9 cells. hiPSCs can be maintained in stirred suspension for at least 7 weeks with weekly passaging, while exhibiting pluripotency-associated markers TRA-1-60, TRA-1-81, SSEA-4, OCT4, and SOX2. These cells retain their ability to differentiate into cells of all the three germ layers *in vitro*, exemplified by cells positive for AFP, SMA, or TUBB3. Additionally, they maintain a stable karyotype and continue to respond to specification cues, demonstrated by directed differentiation into beating cardiomyocyte-like cells. Therefore, the aim of manufacturing high hiPSC quantities was met using a state-of-the-art scalable suspension bioreactor platform.

Secondly, multipotent stem cells such as induced neural stem cells (iNSCs) may represent a safer source of renewable cells compared to pluripotent stem cells. However, pre-conditioning of stem cells prior to transplantation is a delicate issue to ensure not only proper function in the host but also safety. Here, iNSCs which are normally maintained in the presence of factors such as hLIF, CHIR99021, and SB431542 were cultured in basal medium for distinct periods of time. This wash-out procedure results in lower proliferation while maintaining key neural stem cell marker PAX6, suggesting a transient pre-differentiated state. Such pre-treatment may aid transplantation studies to

suppress tumourigenesis through transplanted cells, an approach that is being evaluated using a mouse model of experimental focal demyelination and autoimmune encephalomyelitis.

Thirdly, biomedical applications of stem cells can benefit from recent advancements in biofabrication, where cells can be arranged in customisable topographical layouts. Employing a 3DDiscovery bioprinter, a bioink consisting of hiPSCs in gelatin-alginate was extruded into disc-shaped moulds or printed in a cross-hatch infill pattern and cross-linked with calcium ions. In both discs and printed patterns, hiPSCs recovered from these bioprints showed viability of around 70% even after 4 days of culture when loaded into gelatin-alginate solution in aggregate form. They maintained pluripotency-associated markers TRA-1-60 and SSEA-4 and continued to proliferate after re-plating. As further proof-of-principle, printed hiPSC 3D constructs were subjected to targeted neuronal differentiation, developing typical neurite outgrowth and resulting in a widespread network of cells throughout and within the topology of the printed matrix. Staining against TUBB3 confirmed neuronal identity of the differentiated cellular progeny. In conclusion, these data demonstrate that hiPSCs not only survive the 3D-printing process but were able to differentiate along the printed topology in cellular networks.

Zusammenfassung

Induzierte pluripotente Stammzellen (iPSZ) stellen eine praktisch unbegrenzte Stammzellquelle dar, welche patientenspezifisch erzeugt werden kann. Da diese Zellen das Potenzial haben, alle differenzierten Zelltypen des menschlichen Körpers hervorzubringen, werden sie für die Herstellung differenzierter Zellen für Arzneimitteltests und für die Krankheitsmodellierung verwendet. Sie erfahren auch großes Interesse, weil sie als Zellquelle in der Zellersatztherapie Anwendung finden könnten. Die vorliegende Dissertation beschäftigt sich mit drei zentralen Herausforderungen, die im Rahmen der biomedizinischen Anwendung von iPSZ auftreten.

Die Herstellung einer großen Zahl von humanen iPSZ (hiPSZ) erfordert die Entwicklung standardisierter Verfahren für die Skalierung, welche durch die Entwicklung einer flexiblen Bioprozessmethode realisiert werden kann. Bisher wird die Skalierbarkeit durch eine standardmäßig adhärente Zellkultur und den damit verbundenen hohen Arbeitsaufwand begrenzt. Die Menge an Zellen, die für die Zelltherapie benötigt wird, hängt stark vom Gewebetyp ab, welcher von den ersetzenden Zellen korrigiert werden soll. Berechnungen legen nahe, dass eine Anzahl 1×10^9 Zellen für eine Vielzahl von Indikationen ausreicht – einschließlich Myokardinfarkt und Inselzelltransplantation für Diabetes. Im Rahmen dieser Arbeit wurde ein integrierter Arbeitsablauf zur skalierbaren Zellsuspensionskultur von hiPSZ ohne Verwendung von *microcarrier* entwickelt, um die standardmäßig adhärente Kultur (6-Well-Platten) in Bioreaktoren (1 L Arbeitsvolumen, 2,4 L maximales Arbeitsvolumen) zu überführen. Der zweiphasige Produktionsprozess dauert 14 Tage und erzeugt hiPSZ-Aggregate mit einem finalen Durchmesser von 198 ± 58 µm, der annähernd 2×10^9 Zellen beinhaltet. hiPSZ können mindestens 7 Wochen lang in einer gerührten Zellsuspension bei wöchentlichem Passagieren gehalten werden, wobei sie Pluripotenz-assoziierte Marker wie TRA-1-60, TRA-1-81, SSEA-4, OCT4 und SOX2 beibehalten. Die Zellen behalten weiterhin ihre Fähigkeit, sich *in vitro* in Zellen mit AFP-, SMA- oder TUBB3-Immunoreaktivität und damit in Zellen aller drei Keimblätter zu differenzieren. Darüber hinaus halten sie einen stabilen Karyotyp aufrecht und reagieren auf gezielt eingesetzte externe Differenzierungsstimuli, wie durch eine gezielte Differenzierung in schlagende Kardiomyozyten-ähnliche Zellen demonstriert werden konnte. Somit wurde das Ziel, eine großen Anzahl hiPSCs herzustellen, mit einer hochmodernen, skalierbaren Suspensionsbioreaktorplattform erreicht.

Multipotente Stammzellen wie induzierte neurale Stammzellen (iNSZ) gelten verglichen mit iPSZ als sicherere Zellquelle für Ersatztherapien. Die Vorkonditionierung

von Stammzellen vor der Transplantation ist jedoch ein heikles Thema, da sowohl die einwandfreie Funktion im Wirtsgewebe als auch Sicherheit gewährleistet werden müssen. Im Rahmen dieser Arbeit wurden iNSZ, die normalerweise im Kulturmedium mit Faktoren wie hLIF, CHIR99021 und SB431542 gehalten werden, für eine definierte Zeitspanne in basalem Medium kultiviert. Die Vorbehandlung führt zu einer geringeren Proliferation, jedoch unter Erhalt der Expression des wichtigen neuralen Stammzellmarkers PAX6, was auf einen transienten vordifferenzierten Zustand hindeutet. Eine solche Vorbehandlung könnte bei zukünftigen Transplantationsstudien angewandt werden, um die Tumorentstehung durch transplantierte Zellen zu unterdrücken. Dieser Ansatz wird in Zukunft mit einem Mausmodell der experimentellen fokalen Demyelinisierung und der autoimmunen Enzephalomyelitis untersucht.

Schließlich kann die Zellersatztherapie von den jüngsten Fortschritten in der Biofabrikation profitieren, bei der die Zellen durch das Drucken in anpassbare topographische Profile angeordnet werden können. Mit einem 3DDiscovery Biodrucker wurde eine Biotinte bestehend aus Gelatine-Alginat und hiPSZ in scheibenförmig extrudiert oder in einem Kreuzschraffurmuster gedruckt und mittels Kalziumionen-Zugabe vernetzt. Gedruckte hiPSZ zeigten auch nach 4 Tagen Kultivierung eine Lebensfähigkeit von etwa 70 % und weiterhin das Auftreten der Pluripotenz-assoziierten Marker TRA-1-60 und SSEA-4. Zudem konnten sie sich anschließend mit standardmäßig adhärenter Zellkultur weiter vermehren. Zudem konnte gezeigt werden, dass die gedruckten Konstrukte einer gezielten neuronalen Differenzierung unterzogen werden können, die zu einem typischen Neuritenauswuchs und zu einer weitreichenden interzellulären Vernetzung durch und innerhalb der Topologie der gedruckten Matrix führte. Die Färbung gegen TUBB3 bestätigte die neuronale Identität der differenzierten Zellen. Zusammenfassend zeigen diese Daten, dass bei Verwendung des in dieser Studie erarbeiteten Protokolls hiPSZ nicht nur den 3D-Druckprozess überleben, sondern auch entlang der gedruckten 3D Topologie in Netzwerke Neurone differenzieren können.

Übersetzt von Philipp Wörsdörfer

List of Abbreviations

7-AAD	7-amino-actinomycin D
ACTA2	Actin, alpha 2, same as SMA
ACTN2	Actinin, alpha 2 (sarcomeric actinin)
ADF4	Dragline silk fibroin 4
AFP	Alpha-fetoprotein
APC	Allophycocyanin
BDNF	Brain-derived neurotrophic factor
bMG	Basement membrane Matrigel, growth factor reduced
BMP4	Bone morphogenetic protein 4
BSA	Bovine serum albumin
CAD	Computer-aided design
cAMP	Cyclic adenosine monophosphate
CBM	Cardiac basal medium
cDNA	Complementary DNA
CEM	Cardiac enrichment medium
CIM	CVPC induction medium
CPC	Cardiac progenitor cells
CPM	CVPC propagation medium
CSM	Cardiac specification medium
CVPC	Cardiovascular progenitor cells
DABCO	1,4-Diazabicyclo[2.2.2]octane
DAPI	4’,6-Diamidino-2-phenylindole
DAPT	N-[N-(3,5-Difluorophenacetyl)-L-alanyl]-S-phenylglycine t-butyl ester
DMEM	Dulbecco’s modified Eagle medium
DMSO	Dimethyl sulphoxide
DNA	Deoxyribonucleic acid
DPBS	Dulbecco’s phosphate buffered saline
ECM	Extracellular matrix
EDTA	Ethylenediaminetetraacetate dihydrate
ESC	Embryonic stem cells

FCS	Foetal calf serum
FIPD	Fold increase per day
GAPDH	Glyceraldehyde 3-phosphate dehydrogenase
GDNF	Glia cell-derived neurotrophic factor
hESC(s)	Human embryonic stem cell(s)
hES MG	Human ESC-qualified basement membrane Matrigel
hiNSC(s)	Human induced neural stem cell(s)
hiPSC(s)	Human induced pluripotent stem cell(s)
hPSC(s)	Human pluripotent stem cell(s)
HSA	Human serum albumin
iNSC(s)	Induced neural stem cell(s)
iPSC(s)	Induced pluripotent stem cell(s)
ISL1	ISL LIM homeobox 1
IWR-1	Inhibitor of Wnt response 1
KDR	Kinase insert domain receptor
KSR	KnockOut serum replacement
LIF	Leukaemia inhibitory factor
MACS	Magnet-activated cell sorting
MEF(s)	Mouse embryonic fibroblast(s)
MESP1	Mesoderm posterior 1 homolog
mRNA	Messenger RNA
MSC(s)	Mesenchymal stem/stromal cell(s)
NDM	Neuronal differentiation medium
NEAA	Non-essential amino acids
NEM	Neural expansion medium
NES	Nestin
NIM	Neural induction medium
NSC(s)	Neural stem cell(s)
OCT4	Octamer-binding transcription factor 4
PAX6	Paired box 6
PCR	Polymerase chain reaction
PDGFRa	Platelet-derived growth factor receptor alpha

PE	Phycoerythrin
PFA	Paraformaldehyde
PMA	Purmorphamine
PSA-NCAM	Polysialic acid-neural cell adhesion molecule
PSC(s)	Pluripotent stem cell(s)
RNA	Ribonucleic acid
RPM	Revolutions per minute
RT	Reverse transcription
SCID	Severe combined immunodeficiency
SCNT	Somatic cell nuclear transfer
SIRPA	Signal regulatory protein alpha
SMA	Smooth muscle actin, same as ACTA2
smNPC(s)	Small molecule-derived neural progenitor cell(s)
SOX1	Sex determining region Y-box 1
SOX2	Sex determining region Y-box 2
SSEA-1	Stage-specific embryonic antigen 1
SSEA-4	Stage-specific embryonic antigen 4
TNNT2	Troponin T2, cardiac type
TRA-1-60	Trafalgar-1-60
TRA-1-81	Trafalgar-1-81
TUBB3	Tubulin, beta 3 class III
VitC	Vitamin C (ascorbic acid)
Wnt	Wingless-type MMTV integration site

1. Introduction

1.1 Stem cells

The term “stem cell” was coined by Ernst Haeckel who used it to refer to an ancestral cell from which all multicellular organisms evolved (Haeckel, 1868; Ramalho-Santos and Willenbring, 2007). The term was also used by others to refer to the cells which today are called primordial germ cells and cells of the germline lineage (Häcker, 1892). The current understanding of the term “stem cells” — defined as cells that are capable of unlimited proliferation and self-renewal, and possess the potential to differentiate into more specialised cells (Jaenisch and Young, 2008; Morrison, Shah, and Anderson, 1997) — was borne out of early studies into the haematopoietic system in mice. The pioneering work on the haematopoietic system showed that irradiated mice could be rescued by bone marrow transplants, and that the donor cells themselves were responsible for the reconstitution of the blood cells and not the host cells (Ford *et al.*, 1956). Expanding on those findings, James Till and Ernest McCulloch and colleagues were able to convincingly show clonality of colonies from the transplants (Becker, McCulloch, and Till, 1963; Siminovitch, McCulloch, and Till, 1963), thus laying the groundwork for the concept of haematopoietic stem cells, and stem cells in general. Stem cells can be further classified by the extent of their development potential.

From the widest to the narrowest potential, these are totipotent, pluripotent, multipotent, and unipotent (Jaenisch and Young, 2008). In mammals, totipotent cells include the zygote and the blastomeres after the first cleavage and give rise to extraembryonic (e.g. trophectoderm) as well as embryonic cells. These potencies are illustrated in Figure 1.1.

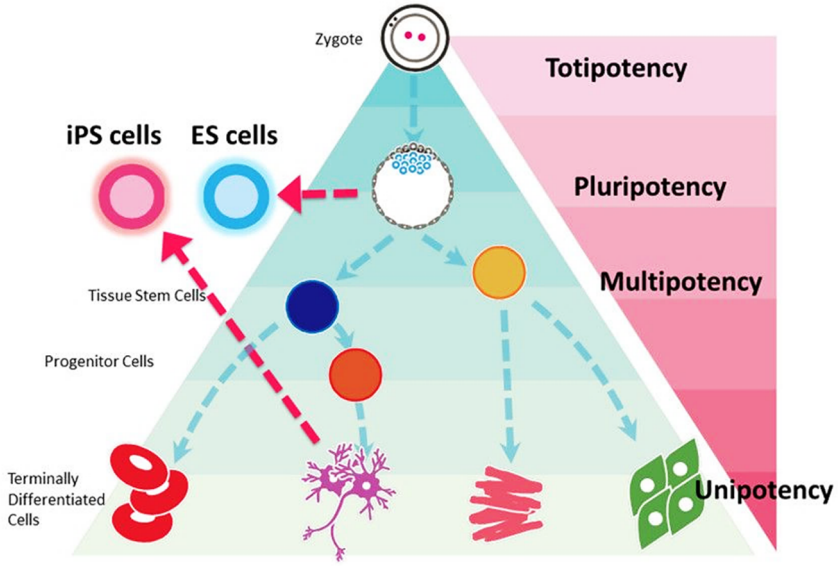

Figure 1.1 Overview of hierarchy of cell potency. Starting from the cell with the widest potency at the top, totipotent cells such as the zygote can form all embryonic and extraembryonic cells. As the zygote develops, the cells of the inner cell mass of the blastocyst can be isolated as embryonic stem cells (ESCs), an example of pluripotent stem cells (PSCs). During development, the ESCs further differentiate into multipotent, lineage-committed tissue stem cells and progenitors, such as neural stem cells. As the cells further develop, they become terminally differentiated somatic cell types. Somatic cells can be reprogrammed and induced into a pluripotent state, called induced pluripotent stem cells (iPSCs). (Sugawara *et al.*, 2012)

1.1.1 Pluripotent stem cells (PSCs)

Pluripotent stem cells (PSCs) have a wide differentiation potential and can contribute to all the cell lineages of the body (Jaenisch and Young, 2008). These can be classified into embryonic stem cells (ESCs) or induced pluripotent stem cells (iPSCs).

1.1.1.1 Embryonic stem cells (ESCs)

Embryonic stem cells (ESCs) were firstly isolated and characterised from mice in 1981 (Evans and Kaufman, 1981; Martin, 1981) by culturing them on a feeder layer of mitotically-inactivated mouse embryonic fibroblasts (MEFs). In Evans and Kaufman's study, they predicted that ESCs could be "use[d] as a vehicle for the transfer into the mouse genome of mutant alleles, either selected in cell culture or inserted into the cells via transformation with specific DNA fragments". Indeed, the marriage of Evans and Kaufman's ESC culture technologies with targeted recombinant DNA technologies developed by Capecchi and colleagues (Thomas, Folger, and Capecchi, 1986) and Smithies and colleagues (Smithies *et al.*, 1985) led to the development of transgenic mice with targeted genome modifications, building the basis of the 2007 Nobel Prize in Physiology or Medicine. Expanding on Evans and Kaufman's work, elements of the culture conditions that were required for the

maintenance of an undifferentiated state were elucidated, such as leukaemia inhibitory factor (LIF) which was provided by the MEFs (Smith *et al.*, 1988; Williams *et al.*, 1988) and bone morphogenetic proteins (BMP) which could be derived from the foetal calf serum present in the culture medium (Ying *et al.*, 2003).

After the isolation of mouse ESCs, it took another 17 years for the first human ESCs (hESCs) to be isolated by James Thomson and colleagues from the inner cell mass of a developing blastocyst (Thomson *et al.*, 1998), using human embryos produced by *in vitro* fertilisation. These cells were cultured on MEFs as well and were shown to stain strongly for cell surface antigens such as stage-specific embryonic antigens 3 and 4 (SSEA-3, SSEA-4), and Trafalgar-1-60 and -1-81 (TRA-1-60, TRA-1-81), could form teratomas containing cells of various lineages in SCID mice, and expressed telomerase. In order to further culture hESCs in a way that minimises the risk of xenogeneic contaminants such as MEFs, groups worked to identify extracellular matrices or substrata that could support feeder-free culture of hESCs (reviewed by Hagbard *et al.*, 2018). One of the earliest examples of such substrata that was identified and now commonly used for feeder-free culture of hESCs is Matrigel (abbreviated as MG in this thesis; Xu *et al.*, 2001), which is the basement membrane extracted from Engelbreth-Holm-Swarm mouse sarcoma cells, containing a mix of extracellular matrix (ECM) molecules such as laminin, entactin, and collagen (Kleinman *et al.*, 1982).

Since the establishment of hESCs involved the destruction of a human embryo, the derivation and use of hESCs for research is ethically controversial, and various countries have varying stances towards the use of hESCs in research. In Germany, the Embryo Protection Act was enacted in 1990 that makes it illegal to use human embryos "for any purpose that does not serve its preservation", while the Stem Cell Act of 2002 permits limited and controlled import of hESC lines established before 1st January 2002 (later being postponed to 1st May 2007) from extra embryos generated from *in vitro* fertilisation (Wiedemann *et al.*, 2004). In contrast, other countries such as the UK permit the derivation of hESC lines from surplus embryos generated by *in vitro* fertilisation. In the light of these sentiments, methods to derive PSCs without destruction of a human embryo have been developed. For example, the generation of hESC lines from single blastomeres was demonstrated (Klimanskaya *et al.*, 2006), using single-cell biopsy techniques that are similar to those used for pre-implantation genetic diagnosis. Additionally, in the context of transplantation or cell replacement therapy, the problem of tissue rejection arising

from immune mismatch between the donor and recipient of the cells is not overcome by this development in hESC derivation. Earlier work in amphibians (Gurdon, 1962) and other mammals (Wilmut *et al.*, 1997) showed the possibility of somatic cell nuclear transfer (SCNT) into enucleated oocytes as an approach to generate clones. Some have envisioned the transfer of human somatic nuclei into oocytes in order to generate embryos from which hESCs could be isolated (reviewed in Gurdon and Melton, 2008), thereby creating personalised hESC lines. However, the generation of nuclear transfer-embryonic stem cells (NT-ESCs) could not be achieved for a long time due to early arrest of SCNT embryos (Egli *et al.*, 2011). More recently, the generation of hESCs using SCNT has been achieved, after the elucidation of key factors leading to early arrest (Tachibana *et al.*, 2013). However, SCNT to derive hESCs has not been widely adopted, possibly due to the breakthrough discovery in 2006 of a method to induce pluripotency from somatic cells. This is discussed in the following section.

1.1.1.2 Induced pluripotent stem cells (iPSCs)

Inspired by earlier work establishing the possibility of cellular reprogramming (Briggs and King, 1952; Cowan *et al.*, 2005; Gurdon, 1962; Wilmut *et al.*, 1997), Takahashi and Yamanaka elaborated on a list of candidate genes that were crucial for the maintenance of ESC identity in order to identify a combination of factors that may have the potential to artificially induce pluripotency. In their seminal report in 2006 (Takahashi and Yamanaka, 2006), the reprogramming of mouse embryonic fibroblasts and adult mouse tail tip fibroblasts into a pluripotent state through retrovirus-mediated transduction of *Oct4*, *Sox2*, *Klf4*, and *cMyc* was demonstrated. This showed that somatic cells could be reprogrammed into an ESC-like state, and they named these "induced pluripotent stem cells" (iPSCs). In the following year, two groups reported the induction of pluripotency from human fibroblasts using a similar approach. While Yamanaka's group achieved this through *OCT4*, *SOX2*, *KLF4*, and *cMYC* (Takahashi *et al.*, 2007), Yu and colleagues accomplished this through lentivirus-mediated transduction of *OCT4*, *SOX2*, *NANOG*, and *LIN28* (Yu *et al.*, 2007) to also generate iPSCs from human fibroblasts. Importantly, the human iPSCs (hiPSCs) generated by both groups met the criteria for characterising hESCs, other than the fact that they were generated from somatic cells and not embryos.

These first two hiPSC reports used fibroblasts of foetal, postnatal foreskin, or adult facial dermal origin for reprogramming. Because the derivation of these

fibroblasts can involve some degree of invasiveness, such as through a skin punch biopsy, various groups searched for other cell types that could be obtained through less invasive means. Other cell types that have been successfully reprogrammed into hiPSCs include keratinocytes which can be isolated from a single plucked hair (Aasen *et al.*, 2008; Maherali *et al.*, 2008), peripheral blood cells (Staerk *et al.*, 2010) and terminally differentiated T cells (Loh *et al.*, 2010; Seki *et al.*, 2010) that can be obtained through a blood draw, and exfoliated renal epithelial cells that can be collected from urine (Zhou *et al.*, 2012).

In the first reports which used integrating retro- and lentiviral mediated transduction to introduce the reprogramming factors into cells, the potential for insertional mutagenesis was already recognised as a problem that future research would have to address and overcome. Additionally, while transgenes are silenced in the fully reprogrammed iPSCs, there is the risk of uncontrolled reactivation of the transgenes. In particular, reactivation of *cMyc* was shown to correlate with tumour formation in mice (Okita, Ichisaka, and Yamanaka, 2007). In the light of these risks, numerous other methods have been investigated to induce pluripotency avoiding integration. These include the development of non-integrating viruses that deliver the reprogramming factors, such as adenovirus carrying the factors in DNA vectors (Stadtfeld *et al.*, 2008a) and Sendai virus carrying the factors in RNA vectors (Ban *et al.*, 2011; Fusaki *et al.*, 2009; Seki *et al.*, 2010), or virus-free methods such as electroporation of episomal DNA vectors (Yu *et al.*, 2009), transfection of synthetic mRNA (Warren *et al.*, 2010), and application of recombinant proteins (Bosnali and Edenhofer, 2008; Thier, Münst, and Edenhofer, 2011; Zhou *et al.*, 2009). Another approach involves the use of excisable integrating lentivirus reprogramming cassettes (Kadari *et al.*, 2014; Somers *et al.*, 2010; Sommer *et al.*, 2008), where the reprogramming cassette can be excised using Cre recombinase once the iPSCs have been derived, or by using an inducible *piggyBac* transposon system for excision of inserts (Kaji *et al.*, 2009; Woltjen *et al.*, 2009). A summary of these methods is presented in Figure 1.2.

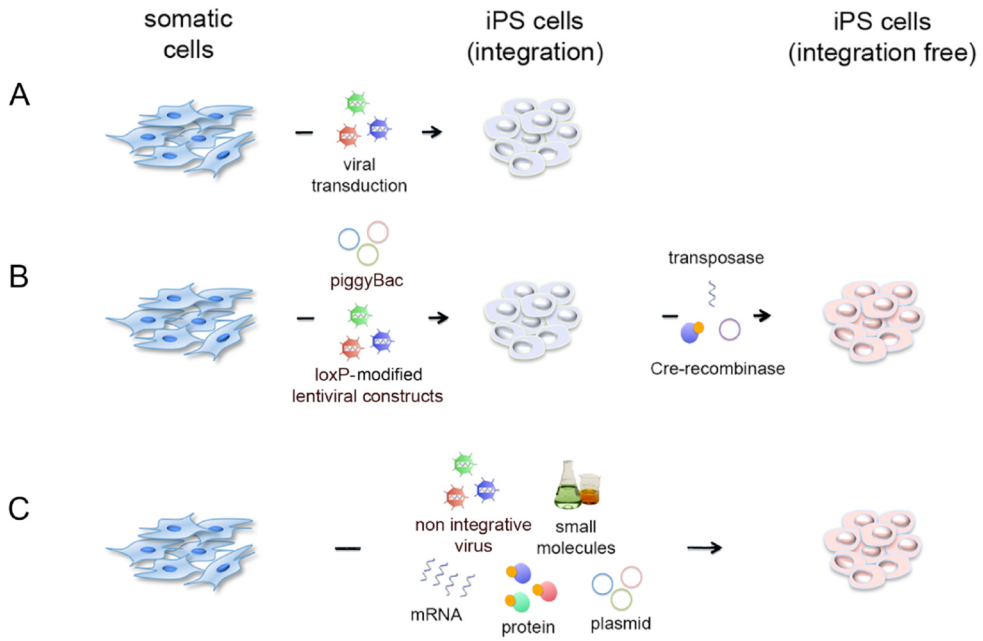

Figure 1.2 Overview of methods to introduce reprogramming factors into cells. (A) Integrating methods such as retro- and lentivirus-mediated transduction of DNA. (B) Two-step methods to first reprogram using integrating inserts, followed by excision of inserts with recombinase or transposase. (C) Non-integrating virus and virus-free methods for integration-free reprogramming. (Wörsdörfer *et al.*, 2013)

Since the discovery of methods to induce pluripotency, several groups have sought to gain mechanistic insights into reprogramming trajectories. Reprogramming to pluripotency is a low efficiency process, and investigations into the underlying reasons for this suggest that the acquisition of pluripotency occurs in two waves. In the first wave which the majority of cells pass through, downregulation of somatic cell genes and upregulation of pluripotency-associated genes occurs (Stadtfeld *et al.*, 2008b); in the second wave, a small proportion of the cells then proceed to continuously maintain the core pluripotency network (Polo *et al.*, 2012). Two different models have been proposed, a stochastic model and a deterministic model, to explain why pluripotency is only established in this small proportion of cells (Yamanaka, 2009). The stochastic model proposes that all cells can be reprogrammed, but reprogramming involves random events, therefore acquisition of pluripotency depends on time, and this model is supported by various studies (Buganim *et al.*, 2012; Hanna *et al.*, 2009). Conversely, the deterministic or "elite" model posits that some cells in a population are intrinsically predisposed to reprogramming, and there is evidence to support such a model where certain "privileged" cells are quick to acquire pluripotency (Guo *et al.*, 2014). With evidence such as this, the previously held assumption that reprogramming follows the stochastic model is called into question (Theunissen and Jaenisch, 2014).

Nevertheless, the development of iPSC technology has and will continue to revolutionise the study of cell biology and the way biomedical research is being carried out (see Section 1.1.3, Table 1.1). For this discovery, the 2012 Nobel Prize in Physiology or Medicine was awarded to John Gurdon and Shinya Yamanaka for discovering that somatic cells can be reprogrammed to a pluripotent state (Nobel Media, 2012).

1.1.2 Multipotent stem cells

While PSCs possess the ability to differentiate into cells of all three germ layers, multipotent stem cells in contrast possess the ability to differentiate into cells of one lineage only. Examples include neural stem cells (NSCs) which can give rise to cells of the neural lineage, namely neurons, astrocytes, and oligodendrocytes (Conti and Cattaneo, 2010; Gage and Temple, 2013), and cardiac progenitor cells (CPCs) which can differentiate into cardiomyocytes, endothelial cells, and vascular smooth muscle cells (Kattman, Huber, and Keller, 2006).

Multipotent stem cells can be derived from various sources. Firstly, they can be isolated from their niche in the human body. For example, mesenchymal stem/stromal cells (MSCs) can be isolated from the bone marrow (Friedenstein *et al.*, 1974) and colonic stem cells can be isolated from the colonic epithelium (Jung *et al.*, 2011). Secondly, multipotent stem cells can be derived from PSCs by subjecting the PSCs to controlled differentiation conditions. This approach has been adopted for a variety of stem cells such as NSCs (Chambers *et al.*, 2009; Günther *et al.*, 2016; Reinhardt *et al.*, 2013; Yan *et al.*, 2013), MSCs (Lian *et al.*, 2010; Villa-Diaz *et al.*, 2012), and cardiovascular progenitor cells (CVPCs; Birket *et al.*, 2015; Cao *et al.*, 2013). Notably, while conditions to isolate and reliably expand NSCs are well-defined, in contrast the successful prolonged culture of CVPCs *in vitro* has proven to be challenging (Birket and Mummery, 2015; Chen and Wu, 2016). Thirdly, multipotent stem cells can also be directly induced from somatic cells without passing through a pluripotent state. This process is also termed transdifferentiation or direct conversion, and our laboratory has demonstrated transdifferentiation of fibroblasts or blood cells into induced NSCs (iNSCs) (Meyer *et al.*, 2015; Thier *et al.*, 2012, 2019). Others have directly converted peripheral blood mononuclear cells into iNSCs (Tang *et al.*, 2016), as well as fibroblasts into blood progenitors (Szabo *et al.*, 2010).

Despite having a more restricted differentiation potential, multipotent stem cells may be more suited for cell therapy (Biehl and Russell, 2009). Their limited

differentiation potential can be considered a virtue as it narrows down the possible cell fates and reduces the chances of off-target differentiation, in contrast to the tumorigenic capacity of PSCs which represents a potential obstacle to clinical application (Lee *et al.*, 2013). Multipotent stem cells are therefore safer for cell therapy. In a study comparing NSCs, iNSCs, MSCs, ESCs, and iPSCs for their immunogenicity and tumourigenicity in mice, grafted NSCs, iNSCs, and MSCs did not result in any tumour formation, while ESC and iPSC grafts did. Additionally, ESC and iPSC grafts were associated with infiltration by immune cells and upregulation of immunogenicity-associated genes, whereas with the NSC, iNSC, and MSC grafts, immune cells were only rarely detected and immunogenicity-associated genes were only weakly expressed (Gao *et al.*, 2016).

1.1.3 Biomedical applications of stem cells

Since stem cells possess self-renewal capability and can differentiate into a plethora of different specialised cell types, they have become appealing candidates as a source of different cell types for a range of biomedical applications (Bellin *et al.*, 2012; Das and Pal, 2010). These applications include drug discovery and toxicity testing (Inoue and Yamanaka, 2011; Ko and Gelb, 2014), modelling of development and disease (Clevers, 2016; Soldner and Jaenisch, 2012), and potential cell therapy (Lu and Zhao, 2013; Martin, 2017).

While animals such as mice have been frequently used for drug discovery and modelling of disease and development (Perlman, 2016), their use in research has been heavily debated. From an ethics perspective, the use of animals for research can be controversial and there has been significant drive to reduce the use of animals in drug testing (Doke and Dhawale, 2015; Ford, 2016; Garattini and Grignaschi, 2017). From a scientific perspective, animal models may not faithfully recapitulate the human situation (Seok *et al.*, 2013; Takao and Miyakawa, 2015), which can complicate the interpretation of animal studies and even call into question their relevance to the study of human development and disease. For example, candidate drugs identified based on animal-based studies may have little to no effect in humans (DiBernardo and Cudkowicz, 2006; Scott *et al.*, 2008), or in worse cases result in detrimental effects to humans that were not present in animals due to differences in their biology (Suntharalingam *et al.*, 2006). Therefore, while the contribution of animal-based studies cannot be understated, the study of human cells *in vitro* may more accurately describe the human situation. However, in some cases, the collection or isolation of

such human cells may be too invasive or not possible, such as brain biopsies for cerebral disorders. To circumvent this problem, iPSCs can be derived by reprogramming other human cells that require comparatively less invasive methods to harvest, such as fibroblasts through a skin punch biopsy or peripheral blood mononuclear cells through blood collection. The generated iPSCs can then be differentiated into other cell types like neurons or cardiomyocytes, and the differentiated cells can then be studied.

To drive drug discovery and aid in drug toxicity screening, iPSCs have been differentiated into various cell types. For example, these include cardiac cells such as cardiomyocytes (Bruyneel *et al.*, 2018; Ebert, Liang, and Wu, 2012), neural cells such as neurons (Han *et al.*, 2018; Hung *et al.*, 2017), as well as other cell types such as hepatocyte-like cells (Cayo *et al.*, 2017). Since iPSCs are self-renewing and have unlimited proliferation capacity under maintenance conditions, these offer the possibility to generate large quantities of differentiated cells *in vitro* to test drugs in a high throughput manner and to screen drugs for potential toxic effects.

For disease modelling, iPSCs have been derived from patients with a range of diseases, such as Alzheimer's disease (Peitz *et al.*, 2018), arrhythmogenic cardiomyopathy (Khudiakov *et al.*, 2017), attention-deficit/hyperactivity disorder (Jansch *et al.*, 2018), cystic fibrosis (Merkert *et al.*, 2017), Fabry disease (Klein *et al.*, 2018), long QT syndrome (Fatima *et al.*, 2013), etc. Normal as well as disease-associated iPSC lines can then be differentiated into various cell types through the application of a multitude of differentiation protocols. A few examples of the cell types that can be generated include cardiomyocytes through modulation of GSK3B and Wnt pathways (Burridge *et al.*, 2014; Kadari *et al.*, 2014; Lian *et al.*, 2012), neural cells through dual SMAD inhibition (Chambers *et al.*, 2009; Reinhardt *et al.*, 2013), and pancreatic beta cells through sequential signalling modulation (Bose and Sudheer, 2016; Pagliuca *et al.*, 2014). More recently, stem cells have been cultured in 3D formats to form structures that mimic organs, termed organoids. Some of these organoids start from PSCs, which are then instructed to differentiate into a particular cell lineage. Studying the differentiation trajectories of these stem cells can offer insights into the development of those organs. For example, the generation of cerebral organoids (Lancaster *et al.*, 2013) showed that these cerebral organoids could faithfully recapitulate aspects of the human brain, such as brain regionalisation and cortical organisation, and could also be used to model microcephaly. A list of

biomedical studies utilising iPSCs to investigate disease is presented below in Table 1.1.

Table 1.1 List of biomedical studies employing iPSCs (Modified from Liu *et al.*, 2018; Singh *et al.*, 2015)

Disease	Major affected tissue/cell(s)	Culture format	Reference(s)
Amyotrophic lateral sclerosis	Nervous system	Planar	Chestkov *et al.*, 2014
Diabetes mellitus, type 1	Pancreas, blood vessels	Planar	Park *et al.*, 2008; reviewed in Soejitno and Prayudi, 2011
Down's syndrome/ Trisomy 21	Heart, brain, etc.	Planar	Park *et al.*, 2008; reviewed in Briggs *et al.*, 2013
Drug-induced lethal liver failure	Liver	Organoid	Takebe *et al.*, 2013
Haemophilia A	Blood	Planar	Park *et al.*, 2015
Hutchinson-Gilford progeria syndrome	Blood vessels	Planar	Liu *et al.*, 2011
Hutchinson-Gilford progeria syndrome	Blood vessels	Engineered tissue	Atchison *et al.*, 2017
Idiopathic pulmonary fibrosis	Lungs	Organoid	Firth *et al.*, 2015; Wilkinson *et al.*, 2017
Microcephaly	Brain	Organoid	Lancaster *et al.*, 2013
Parkinson's disease	Brain	Planar	Soldner *et al.*, 2009
Polycystic liver disease	Liver	Organoid	Sampaziotis *et al.*, 2015
Retinal degeneration	Retina	Organoid	Völkner *et al.*, 2016
Salmonella infection	Intestine	Organoid	Forbester *et al.*, 2015
Spinal muscular atrophy	Nervous system	Planar	Ebert *et al.*, 2009
Zika virus infection	Brain	Organoid	Qian *et al.*, 2016

Another potential application of stem cells is their use for cell replacement therapy in diseases such as age-related macular degeneration (Mandai *et al.*, 2017), myocardial infarction (Hartman, Dai, and Laflamme, 2016), and type 1 diabetes mellitus (Calne, Gan, and Lee, 2010). Taking the example of myocardial infarction, an attack leads to the loss of cardiomyocytes, and these cardiomyocytes would need

to be replaced. Unfortunately, endogenous cardiomyocyte generation in the adult human heart appears to be a very slow process (Laflamme and Murry, 2011), and cannot generate cardiomyocytes quickly enough to replace the lost cells. Therefore, the prospect of rapidly culturing hiPSCs and differentiating them into cardiomyocytes as a source for cell replacement is highly attractive. However, it has been estimated that a typical myocardial infarction involves the loss of $1–2 \times 10^9$ heart cells (Laflamme and Murry, 2011; Mummery, 2005; Zweigerdt, 2009), and cell therapy in this context would therefore require the production of $1–2 \times 10^9$ cardiomyocytes. An example of a cell replacement treatment referred to as the Edmonton protocol (Shapiro *et al.*, 2000) uses cadaveric donor pancreatic islets to treat patients with type 1 diabetes mellitus, and the quantity of β-cells infused in that protocol has been estimated to be 1×10^9 (Docherty, Bernardo, and Vallier, 2007). While the quantities of cells required for cell therapy largely depends on the disease or type of injury (Serra *et al.*, 2012), $1–2 \times 10^9$ cells appears to be a good ballpark estimate for many cell therapy approaches.

The generation of $1–2 \times 10^9$ cells would require intensive cell culture and is hardly feasible given the lack of scalability of adherent culture formats for hiPSC cultivation. Another hurdle that needs to be addressed is the question of how to transplant these cells for cell therapy, as the transplanted cells should be introduced in a format that is compatible with its eventual function. Given these two criteria of cell quantity and transplantation format, the next sections elaborate on methods to scale up cell production (Section 1.2), and ways to arrange cells in orientations for transplantation (Section 1.3).

1.2 Scaling strategies for cell production

Cell culturing processes must increase in scale in order to achieve the 1–2 × 10^9 cells. In the following, "scale out" is used to refer to one manufacturing lot multiplied across a number of units in parallel (e.g. one T75 culture flask × 10 for a total of 750 cm^2 culture surface area), whereas "scale up" is used to refer to cases where each manufacturing lot is increased in scale (e.g. increasing the size of the culture flask so that one culture flask has a culture surface area of 750 cm^2) (Kropp, Massai, and Zweigerdt, 2017). An overview of various scaling strategies is presented in Figure 1.3 and further described in this chapter.

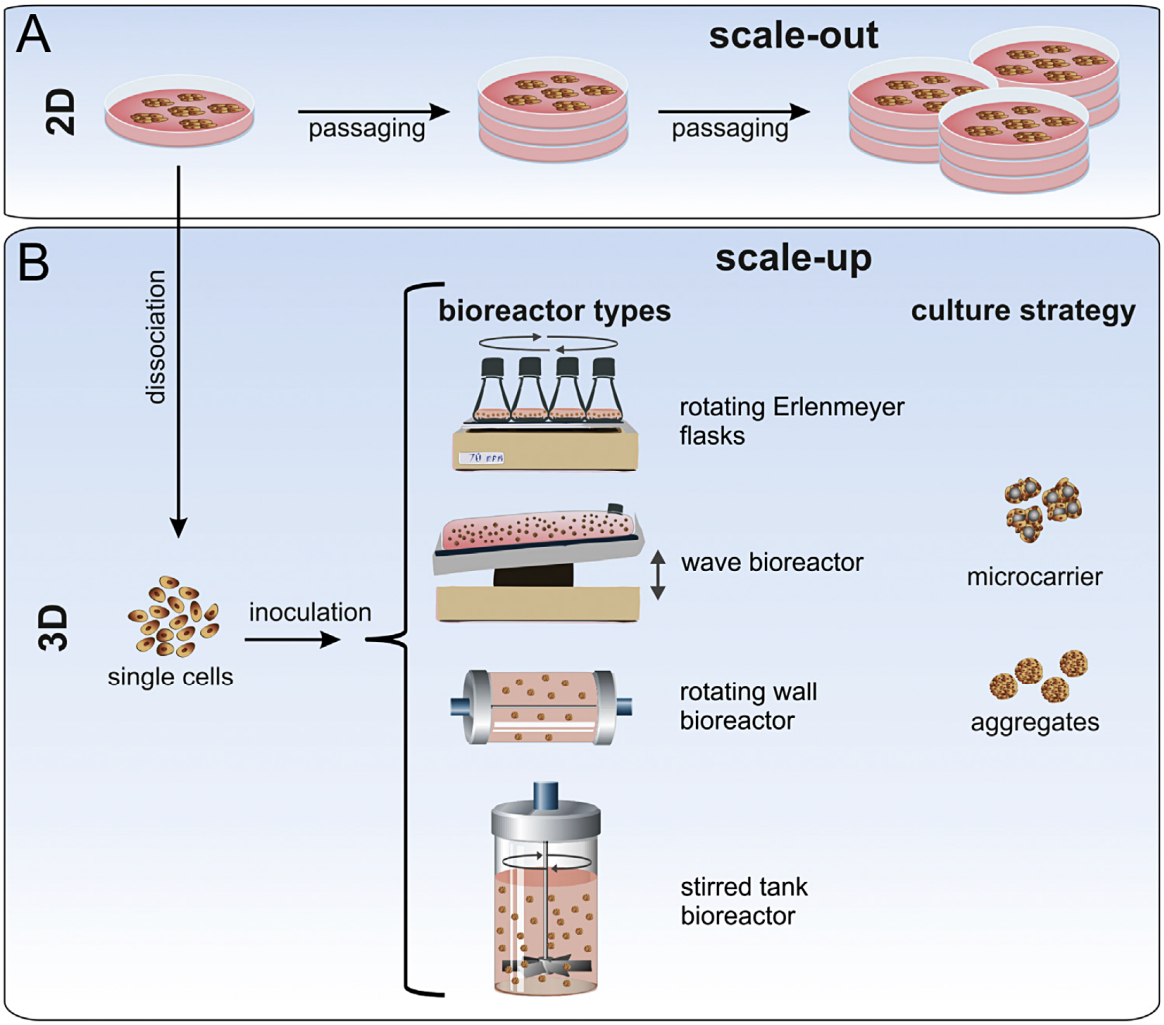

Figure 1.3 Overview of scaling strategies for human PSC (hPSC) production. (A) Static adherent "2D" scale out strategy multiplies one lot (e.g. one dish) by several units in parallel to increase the number of cells produced. (B) "3D" scale up strategies utilise various vessels such as rotating Erlenmeyer flasks, wave bioreactors, rotating wall bioreactors, and stirred tank bioreactors to achieve the target cell quantity. Optionally, in these systems, microcarriers may be used to increase the surface area for hPSC attachment. The hPSCs are otherwise able to be cultured as cell-only aggregates. (Kropp, Massai, and Zweigerdt, 2017).

1.2.1 Scaling of adherent culture

Most routine hiPSC culture is performed under adherent conditions, either with feeder layers of varying origins (Mallon *et al.*, 2006; Thomson *et al.*, 1998) or in feeder-free formats (Chen *et al.*, 2014b; Dakhore, Nayer, and Hasegawa, 2018). For clinical applications, feeder layers may be incompatible due to undefined and/or xenogeneic factors, and therefore feeder-free methods are more suitable. Feeder-free methods involve the culture of PSCs on basement membrane extracts such as Matrigel (Xu *et al.*, 2001), recombinant human ECM proteins such as laminins (Rodin *et al.*, 2014), or other synthetic materials (Mei *et al.*, 2010; Villa-Diaz *et al.*, 2010). These are summarised in Figure 1.4

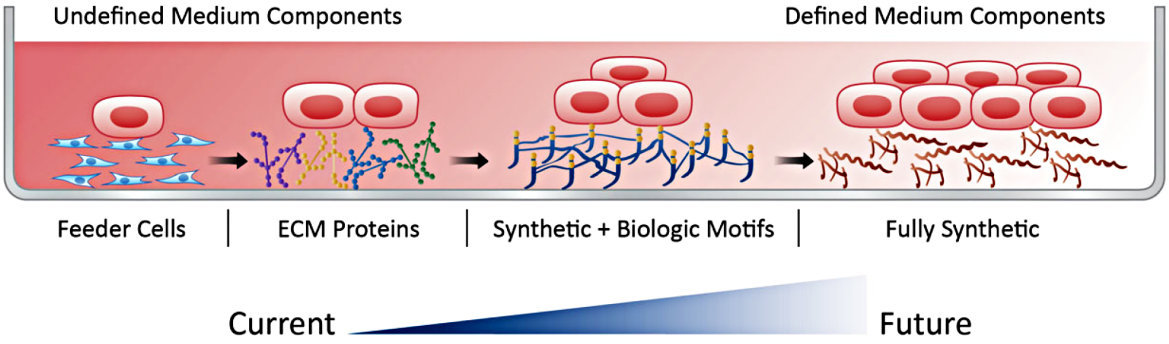

Figure 1.4 Adherent culture of hiPSCs requires substrata for attachment on plasticware. Earliest hPSC reports involved their adherent culture on feeder layers. Following that, hPSCs have been cultured on plasticware coated with mixes of ECM proteins such as Matrigel, or recombinant human proteins such as laminins. Further development has produced synthetic materials coupled with bioinspired peptides and motifs such as RGD, with the future aim of developing completely synthetic adhesion materials. (Villa-Diaz *et al.*, 2013)

One of the limitations in scalability of adherent culture of hPSCs is the labour required to culture these sensitive cells, and therefore two approaches have been used to mitigate the amount of labour required to produce these cells. The first approach uses automation to greatly reduce the amount of hands-on time required for hPSC culture, and the second involves the use of alternative culture vessels.

Machines have been developed that approximate workflows to expand hESCs (Thomas *et al.*, 2008), cardiac stem cells (Kami *et al.*, 2013), and more recently hiPSCs (Konagaya *et al.*, 2015; Soares *et al.*, 2014). To summarise, these machines represent integrated cell manufacturing platforms that can plate and incubate cells, perform medium exchange, optically inspect cells to ensure morphological consistency, and passage cells through cell dissociation and centrifugation. The hiPSCs cultured using this machine express pluripotency markers, maintain a stable karyotype, form

teratomas in immunodeficient mice, and can differentiate into all 3 germ layers *in vitro*. Multi-layer culture flasks by companies such as Nunc (marketed as Cell Factory systems) and Corning (Abraham *et al.*, 2011; marketed as Multi-Flask, CellSTACK, and HYPERStack systems) have also been proposed as a method to scale out the production of cells (Rowley *et al.*, 2012). However, these approaches continue to rely on coating substrata such as Matrigel and laminin to coat the plasticware before plating hiPSCs, remain costly, and represent a scale out of existing culture protocols. Adherent cultures are also generally static with no medium agitation, and this can lead to build-up of nutrient and metabolite gradients that can limit the growth of hiPSCs (Chen *et al.*, 2010b; Rodrigues *et al.*, 2011). Despite these limitations, scaled out production of hiPSCs using adherent culture methods remain relevant for the production of patient-specific hiPSCs, for example in drug screening (Rowley *et al.*, 2012).

1.2.2 Scaling up through suspension culture

Suspension culture can be further classified into two major sub-categories, namely microcarrier-based suspension culture, and microcarrier-free suspension culture. Both involve the use of an agitation mechanism to allow the microcarriers or cell-only aggregates to be suspended in the culture medium, and the culture may be coupled to inline sensors and controllers for monitoring culture parameters such as pH and dissolved oxygen. Currently, suspension culture of hPSCs can be performed using several types of culture vessels (Figure 1.3B, reviewed in Jenkins and Farid, 2015; Kropp, Massai, and Zweigerdt, 2017; Kumar and Starly, 2015), including Erlenmeyer flasks on rotators (Amit *et al.*, 2011), cell bags or wave bioreactors, rotating wall bioreactors, and stirred tank bioreactors (Kehoe *et al.*, 2010; Kwok *et al.*, 2018; Olmer *et al.*, 2012).

Examples of commercially available wave bioreactors include BioWave, Wave Bioreactor, BIOSTAT CultiBagRM, AppliFlex, Tsunami Bioreactor, and CELL-tainer (Eibl, Werner, and Eibl, 2010). Rotating wall bioreactors include slow turning lateral vessels and high aspect ratio vessels (both from Synthecon, Cellon S.A. Bereldange, Luxembourg), and controlled and monitored by the Bioprofile 400 from Nova Biomedical (Côme *et al.*, 2008; Gerecht-Nir, Cohen, and Itskovitz-Eldor, 2004). Stirred tank bioreactors can for example be sourced from Merck/MilliporeSigma (Mobius Single-use Bioreactor, also referred to as CellReady Bioreactors), Sartorius Stedim (UniVessel), and Eppendorf (DASGIP/DASbox Parallel Bioreactor Systems).

Standalone bioreactors like the Mobius bioreactors can be controlled and monitored by connection to an external controller such as the Applikon ezControl Platform, which can control agitation speed, temperature, pH, and dissolved oxygen through gas lines. In contrast, Eppendorf's DASGIP system provides a completely integrated platform.

1.2.2.1 Microcarrier-based suspension culture

Microcarriers are small spheres, discs, or rods that serve as a solid surface which provides structural support for cells to attach and grow on. They can be made from different materials such as cellulose, glass, and polystyrene (reviewed in Chen, Reuveny, and Oh, 2013). They can be added to liquid media and agitation of the media keeps these microcarriers dispersed in suspension, effectively increasing the culture surface area many times more than planar cultures (Chen *et al.*, 2010a; Kehoe *et al.*, 2010).

In most cases, such microcarriers require coatings similar to adherent cultures, such as Matrigel (Oh *et al.*, 2009), laminins, or vitronectin (Heng *et al.*, 2011). As before, such coating materials can be of animal origin (e.g. Matrigel) or can be expensive to produce and purify (e.g. laminins), and therefore their continued necessity for microcarrier-based expansion does not significantly improve upon established adherent culture methods, at least when it comes to the requirement of coatings. Interestingly, non-coated positive-charged cellulose microcarriers (DE-53) have been shown to support attachment and survival of hPSCs and their long-term propagation, if the culture medium was continuously supplemented with ROCK inhibitor Y27632 or Blebbistatin (Chen *et al.*, 2013). Y27632 permits survival of dissociated hESCs (Watanabe *et al.*, 2007) and is a common supplement to improve cell recovery after passaging at low density or as single cells, and is usually applied for 1–2 days. However, in the report of Chen and colleagues (2013), exposure to Y27632 for only 1–2 days was insufficient to support cell proliferation and pluripotency maintenance and resulted in an unsuccessful culture.

When culturing hPSCs on microcarriers, cell harvesting requires the removal of microcarriers prior to further downstream processes such as cell differentiation or further expansion. The hPSCs can be released from the microcarriers by treatment with dissociation enzymes such as TrypLE Express (Oh *et al.*, 2009) or Accutase (Ashok *et al.*, 2016), and the microcarriers can be removed by straining the cell-microcarrier suspension through a 40 µm cell sieve. While the removal of

microcarriers may be relatively trivial at laboratory scales, it is an additional step to be added to the workflow, and complexity of this step can increase with the scale of the culture. More recently, the development of dissolvable microcarriers, made of calcium-crosslinked polygalacturonic acid polymer chains, has made it possible to eliminate the microcarrier straining step by culturing hiPSC on dissolvable microcarriers coated with Synthemax II (Rodrigues *et al.*, 2018). The cultured hiPSCs on dissolvable microcarriers are treated with a harvest solution containing Accutase to dissociate hiPSCs from each other, EDTA to chelate and remove the crosslinking calcium ions, and pectinase to degrade the polymer chains. In effect, the microcarriers were dissolved in the harvest solution and could be washed away in downstream washing steps, leaving only the remaining cells.

Despite their drawbacks, microcarrier-based cultures have advantages over adherent culture methods in terms of process efficiency. Numerous studies consistently show greater fold increase in cell numbers when cultured on microcarriers when compared to adherent culture methods over the same time period (Oh *et al.*, 2009; Phillips *et al.*, 2008; Serra *et al.*, 2010; Thomas *et al.*, 2008). This could be due to better nutrient circulation in suspension culture, and better dispersion of growth limiting concentrations of waste products such as lactate (Chen *et al.*, 2010b).

1.2.2.2 Microcarrier-free suspension culture

During the years where microcarrier-based suspension was investigated as a scale up strategy for mass production of hPSCs, the culture of hPSCs as cell-only aggregates was stymied by the observation that dissociated hPSCs were very sensitive and were apoptotic in suspension (Watanabe *et al.*, 2007). This could be overcome by supplementing the culture medium with Y27632, which permitted the formation of self-aggregating cell-only aggregates in suspension without microcarrier support. Following this discovery, various groups developed suspension culture protocols that demonstrated the feasibility of expanding hPSCs as cell-only aggregates in suspension (Amit *et al.*, 2011; Krawetz *et al.*, 2009; Olmer *et al.*, 2010; Zweigerdt *et al.*, 2011).

The ability to culture hPSCs as cell-only aggregates offers several advantages. Firstly, hPSCs cultured in this format may more accurately reflect the conditions of the inner cell mass of a blastocyst, which is the source of hESCs. It has been suggested that this closer mimicking of the *in vivo* niche may arise through activation of

endogenous signalling, and might result in better differentiation efficiency (Fridley *et al.*, 2010; Sart *et al.*, 2014). Secondly, it eliminates the requirement of using coating materials like Matrigel, vitronectin, and laminin, which can significantly add to the cost. Instead, it relies on the hPSCs to synthesise their own ECM and maintain cell-cell contact in 3D (Kim, Takeuchi, and Kino-oka, 2018; Serra *et al.*, 2012). Thirdly, it is possible to optimise bioreactor hydrodynamic conditions to exert control over the sizes of the hPSC aggregates (Abbasalizadeh *et al.*, 2012), resulting in more homogeneously cultivated cells. Lastly, the cultivated hPSC aggregates can be directly used for downstream differentiation processes without the requirement to remove microcarriers and this can be performed in the same culture vessel by changing the medium. Differentiation studies utilising hPSC aggregates as a starting point include cardiac cells (Fonoudi *et al.*, 2016; Kempf *et al.*, 2015), pancreatic cells (Pagliuca *et al.*, 2014), and hepatocyte-like cells (Vosough *et al.*, 2013).

While microcarrier-free suspension culture offers a multitude of advantages, it is also associated with various intricacies that must be dealt with. Agitation rates of differing bioreactors require specific tuning to bioreactor impeller designs (Olmer *et al.*, 2012), in order to minimise detrimental effects such as shear stress to hPSCs seeded as single cells. Additionally, medium feeding strategy has a profound effect on process efficiency and growth dynamics (Kropp *et al.*, 2016), with batch feeding leading to lower efficiencies than perfusion based feeding strategies. Moreover, in rare cases some hPSC lines are intrinsically refractory to aggregation in suspension and spontaneously differentiate after a few passages (Singh *et al.*, 2010); it has thus been suggested that screening of hPSC lines for their amenability to suspension culture should be performed before large scale expansion (Zweigerdt *et al.*, 2011).

1.3 3D printing for tissue engineering and regenerative medicine

Additive manufacturing, otherwise popularly known as 3D printing, is a technology that has captured the imagination of the scientific community and public. The availability of computer-aided design (CAD) software to rapidly design goods coupled with 3D printers has enabled the manufacture of customised goods at relatively low cost (Berman, 2012). Additive manufacturing technology now sees widespread application, such as in the electronics, engineering, aerospace, automotive, and fashion industries (Lipson and Kurman, 2013).

Consequently, there has also been significant effort in applying additive manufacturing to the tissue engineering and regenerative medicine fields, most notably in the manufacture of scaffolds and other implantable medical devices (Groll *et al.*, 2016; Mota *et al.*, 2015; Youssef, Hollister, and Dalton, 2017). However, some of these manufacture techniques use conditions that are incompatible with live cells (e.g. heat, use of UV for polymerisation). Therefore, these approaches use additive manufacturing only to create the scaffolds and devices, and any introduction of cells is performed only after the manufacturing process. For example, Holzapfel and colleagues (Holzapfel *et al.*, 2015) used melt electrospinning to first produce medical-grade polycaprolactone tubular scaffolds, and then seeded human- or mouse-derived mesenchymal progenitor cells on these scaffolds to create tissue engineered bone constructs; Chen and colleagues (Chen *et al.*, 2014a) used selective laser sintering to fabricate polycaprolactone scaffolds, further coated these scaffolds with gelatin or collagen, before seeding the modified scaffolds with chondrocytes as an approach to engineer cartilage. Therefore, to make it possible to print using cells, materials and techniques must be developed that are compatible with conditions that are cytocompatible.

1.3.1 Biocompatible printable materials

The terms “bioprinting”, “cell printing”, “tissue printing” and even “organ printing” have been used to refer to printing using cell-laden materials (Boland *et al.*, 2003; Mironov *et al.*, 2003) or even scaffold-free cell aggregates (Norotte *et al.*, 2009). This enables precise control over spatial position of cell types in relation to other cells, in conjunction with the provision of a matrix to provide structural or adherent support, as well as other biochemical signals such as growth factor gradients (Campbell *et al.*, 2005; McMurtrey, 2016). Materials that have been used for bioprinting include natural biopolymers like alginate, chitosan, collagen, gelatin, and hyaluronic acid

(Jüngst *et al.*, 2016; Malda *et al.*, 2013; Murphy and Atala, 2014), and recombinantly produced proteins such as spider silk protein (Aigner, DeSimone, and Scheibel, 2018). In the following, two of such materials are further described.

1.3.1.1 Gelatin-alginate hydrogel

Sodium alginate is a widely used hydrogel precursor for biofabrication (Duan *et al.*, 2013; Faulkner-Jones *et al.*, 2015; He *et al.*, 2016; Song *et al.*, 2011), and can be used in combination with gelatin to confer thermoresponsivity to the gelatin-alginate mixture (Paxton *et al.*, 2017; Wüst, Müller, and Hofmann, 2015). This allows the tuning of the viscosity of the mixture by modulating the temperature; by keeping the mixture warm, low viscosity can be maintained for extrusion at the nozzle. Conversely, the extruded fibre can be collected onto a cooled collecting platform, which results in a rapid increase in viscosity of the mixture to form a gel-like construct. Thereafter, the extruded construct can be exposed to calcium ions in the form of a calcium chloride solution, which cross-links the alginate and contributes to the rigidity of the resulting alginate hydrogel. Duan and colleagues (2013) additionally reported that gelatin was gradually leached out from the cross-linked constructs over time. As gelatin and alginate are both innocuous to cells, cells can be mixed into the gelatin-alginate mixture before extrusion to allow printing of a cell-laden material. Moreover, alginate molecules can be functionalised by covalent linking to peptide sequences such as RGD and VAPG (Yu *et al.*, 2010), a process that can be exploited to enhance attachment to certain cell types and may impact cell differentiation and phenotype (Hunt *et al.*, 2017). A summary of the cell-laden gelatin-alginate hydrogel extrusion is shown in Figure 1.5.

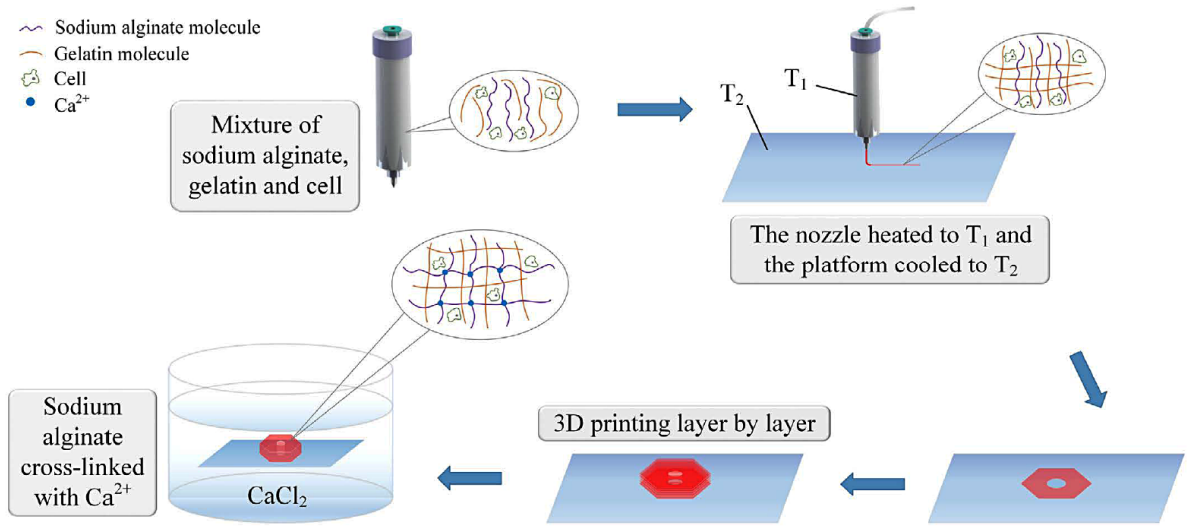

Figure 1.5 Schematic of 3D printing using gelatin-alginate hydrogel. Combined alginate and gelatin solutions can be mixed and kept warm at T_1 to maintain low viscosity for extrusion. Cells can be mixed into such gelatin-alginate mixtures to create cell-laden bioinks. After extrusion through the nozzle, the extruded material can be deposited onto a collection platform cooled to T_2, which causes a rapid increase in viscosity (gelation). By movement of the platform and/or nozzle, a series of layers can be deposited to form the bioprinted construct. Thereafter, the bioprinted construct can be cross-linked by immersion in calcium chloride solution to maintain its structure for further culture and investigation. (He *et al.*, 2016)

1.3.1.2 Recombinant spider silk proteins

Another material that shows promise for biofabrication is recombinant spider silk protein, as it exhibits minimal toxicity, low immunogenicity, slow biodegradability, and has remarkable tensile strength (Leal-Egaña and Scheibel, 2010; MacIntosh *et al.*, 2008). The repetitive core sequences of dragline silk fibroin 4 (ADF4) of the European garden spider *Araneus diadematus* were identified and engineered into a vector for expression in *Escherichia coli* bacteria (Huemmerich *et al.*, 2004). Figure 1.6 gives an overview of the generation of such recombinant spider silk protein, using eADF4(C16) as an example (Aigner, DeSimone, and Scheibel, 2018). An advantage of this recombinant expression system is that it offers the possibility to make amino acid residue changes to change biochemical properties of the spider silk protein, as well as add peptide sequences to enhance adhesion properties for various kinds of cells. For example, eADF4(C16) has been modified to form eADF4(C16)-RGD, using chemical means or genetic means to include the integrin recognition motif RGD (Wohlrab *et al.*, 2012); the RGD motif mediates cell attachment and can be found in fibronectin for example (Ruoslahti, 1988). Furthermore, eADF4(C16) is normally negatively charged due to the glutamic acid residue (bolded E in Figure 1.6) in the consensus sequence of the C-module. By genetic engineering of the DNA sequences

in the expression vector, a substitution of a single amino acid residue of the glutamic acid residue to the positively charged lysine residue was made, thus generating a positively charged variant of this spider silk protein called eADF4(K16) (Doblhofer and Scheibel, 2015).

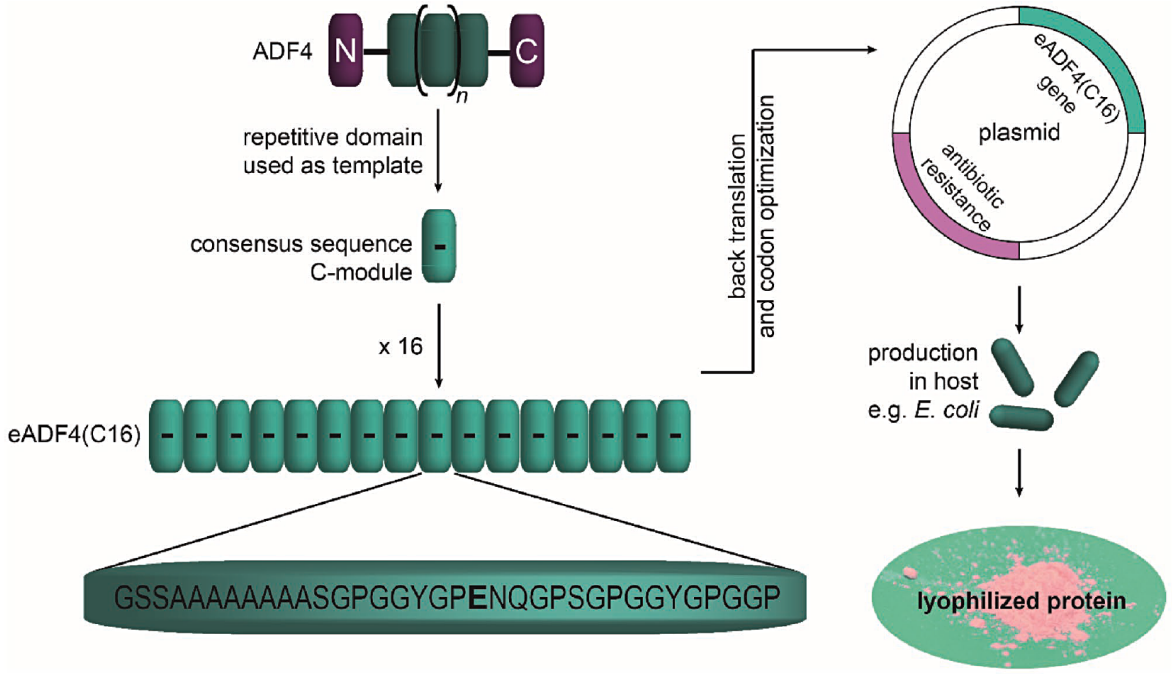

Figure 1.6 Generation of recombinant spider silk protein. The core repetitive domain from ADF4 was used as a template to generate a consensus sequence C-module and repeated 16 times to form eADF4(C16). Using codon optimisation techniques, the DNA sequences encoding eADF4(C16) were introduced into an expression vector that could be inserted into *E. coli* for expression of eADF4(C16) protein. This protein can then be purified and lyophilised. (Aigner, DeSimone, and Scheibel, 2018).

The resultant recombinant spider silk proteins and variants can be then further processed to form fibrils, emulsion capsules, small particles, foams, and cast as films on glass (Aigner, DeSimone, and Scheibel, 2018). They can also be processed into a hydrogel that gels upon exposure to heating at 37 °C. At high concentrations, the spider silk solutions exhibit shear thinning properties, where it can flow when under shear stress (such as when printed through a nozzle), but regains viscosity once extruded. Because of this, eADF4(C16) and eADF4(C16)-RGD have both been used for bioprinting with human and mouse fibroblasts (Schacht *et al.*, 2015), which were maintained viably in culture for at least 48 h. A diagram describing the bioprinting of human fibroblasts loaded in recombinant spider silk hydrogel is shown in Figure 1.7.

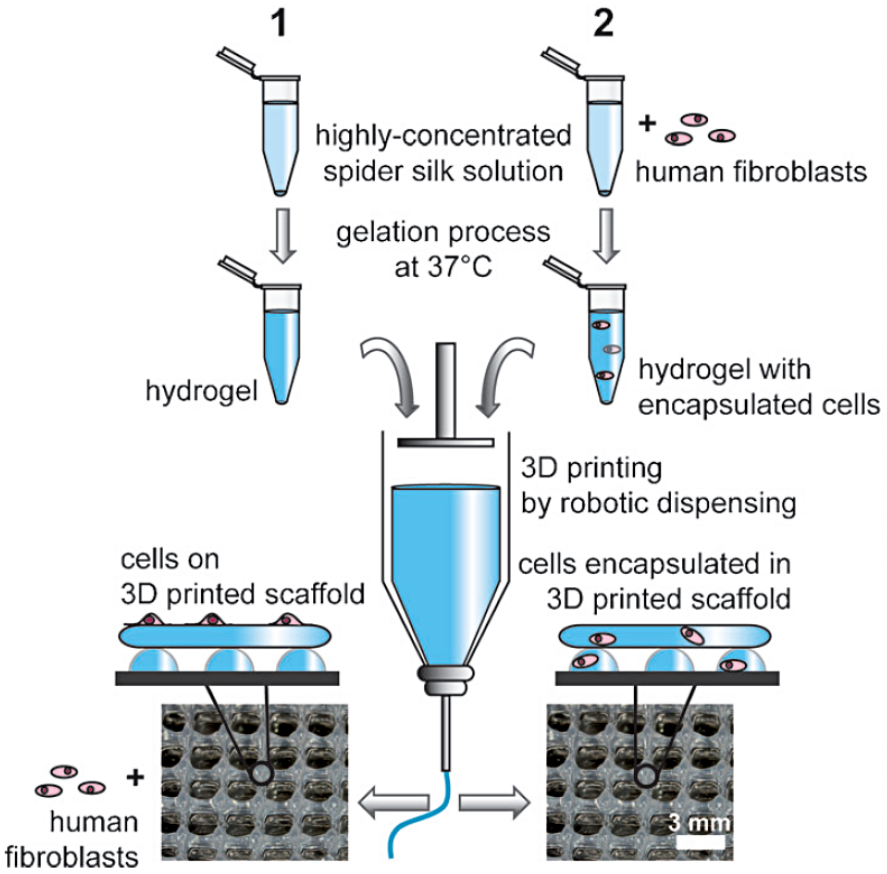

Figure 1.7 Schematic of 3D bioprinting of human fibroblasts in a recombinant spider silk protein hydrogel. Concentrated spider silk solutions form hydrogels at 37 °C, and can be extruded by microvalve-based extrusion printing, either as hydrogel only, or as a cell-loaded hydrogel. (Schacht *et al.*, 2015)

1.4 Aims of the thesis

Stirred suspension culture is a promising culture technique to produce hPSCs, as outlined in Section 1.2.2. However, most of these studies are based on culture vessels at the 100–300 mL scale, and the claimed scalability has been mostly theoretical. Moreover, many of the studies employ the use of reusable glassware like Erlenmeyer flasks (Amit *et al.*, 2011) or reusable mini-bioreactors (Olmer *et al.*, 2012). For industrial scale production of cells, the use of single-use consumables is ideal to prevent problems such as cross-contamination. While technologies using disposable consumables like cell bags on wave bioreactors meet this criteria, they face limitations such as the requirement of floor space that impedes scalability (Kumar and Starly, 2015).

The aim of this thesis is therefore to demonstrate the *scalability* of stirred suspension culture by establishing suspension cultures and optimising them first in medium volume spinner flasks, and secondly to scale the protocol to 3 L Mobius Single-use Bioreactors with a maximum working volume of 2.4 L. From these bioreactors, we aim to produce a quantity of cells that is in line with current estimates for cell therapy ($1–2 \times 10^9$ cells). To increase confidence in the established method, we use two hiPSC lines generated by our laboratory. To ensure the quality of the generated hiPSCs, we perform characterisation and quality control checks to ensure the maintenance of pluripotency and stable karyotype (Martí *et al.*, 2013), and perform directed differentiation to cardiomyocytes to illustrate the utility of the hiPSCs expanded in stirred suspension culture.

After the establishment of the protocol, we seek to further utilise the generated cells for 3D biofabrication, by developing a bioink consisting of a printable hydrogel material with encapsulated hiPSCs and using this bioink to 3D print a construct that can be maintained in culture. As a proof-of-principle, we aim also to differentiate the 3D printed construct into neurons. Alongside these aims, we also seek to answer the question of whether our stirred suspension culture protocol can be applied to other stem cell types, such as the iNSCs that were developed in our laboratory.

2. Materials and Methods

2.1 Materials

2.1.1 Equipment

Table 2.1 List of equipment

Item	Manufacturer
Autoclaves	
DX-23	Systec, Wettenberg, Germany
Hiclave HG-133	HMC Europe, Tüßling, Germany
Varioklav Classic 400E	HP Medizintechnik, Oberschleißheim, Germany
Biological safety cabinets	
Airstream	Esco Micro, Singapore
BSB4	Gelaire Pty Ltd, Sydney, Australia
CellGard ES NU-480-400	NuAire, Plymouth, MN, USA
LabGard NU-S437-500E	NuAire, Plymouth, MN, USA
Bioprinter	
3DDiscovery	RegenHU, Fribourg, Switzerland
Bioreactor controller	
ez-Control	Applikon Biotechnology, Delft, Netherlands
Centrifuges	
Heraeus Multifuge X1R	Thermo Fisher Scientific, Waltham, MA, USA
Heraeus Pico 17	Thermo Fisher Scientific, Waltham, MA, USA
J2-21	Beckman Coulter, Brea, CA, USA
Rotanta	Hettich, Tuttlingen, Germany
Sorvall Evolution RC	Thermo Fisher Scientific, Waltham, MA, USA
Sorvall SLA-1500 Rotor	Thermo Fisher Scientific, Waltham, MA, USA
Sorvall SS-34 Rotor	Thermo Fisher Scientific, Waltham, MA, USA
Microcentrifuge IR	Carl Roth, Karlsruhe, Germany
Centrifuge 5430R	Eppendorf, Hamburg, Germany
Microspin FV2400	Biosan, Riga, Latvia
Cryostorage	
ARP 110	Air Liquide, Paris, France
Cryo 1°C Cooler	Nalgene, Roskilde, Denmark
Electrophoresis	
PerfectBlue Mini M/L	Peqlab, Erlangen, Germany
PowerPac Basic	Bio-Rad, Munich, Germany
Flow cytometer	
BD FACSCanto II	BD Biosciences, San Jose, CA, USA
Fume hood	
Type AS	Vinitex, Coswig, Germany

Table 2.1 List of equipment (continued)

Item	Manufacturer
Heaters	
TDB-100	Biosan, Riga, Latvia
WiseStir MSH-20A	Witeg, Wertheim, Germany
Ice machine	
AF-100	Scotsman, Vernon Hills, IL, USA
Incubators	
C150	Binder, Tuttlingen, Germany
Heraeus Heracell 240	Thermo Fisher Scientific, Waltham, MA, USA
MCO-19AIC(UV)	Panasonic, Gunma, Japan
Magnetic separators	
MiniMACS/MidiMACS Separator	Miltenyi Biotec, Bergisch Gladbach, Germany
Metabolite analyser	
Stat Profile PRIME CCS Analyser	Nova Biomedical, Waltham, MA, USA
Microscopes	
Axioskop 2 mot plus	Carl Zeiss Microscopy GmbH, Jena, Germany
Axiovert 40 CFL	Carl Zeiss Microscopy GmbH, Jena, Germany
Biorevo BZ-9000	Keyence, Neu-Isenburg, Germany
DFC450 C Camera	Leica Microsystems GmbH, Wetzlar, Germany
DMIL LED	Leica Microsystems GmbH, Wetzlar, Germany
pH meter	
inoLab pH 720	WTW GmbH, Weilheim, Germany
Pipettes	
accu-jet pro	Brand, Wertheim, Germany
Microman E, positive displacement	Gilson, Middleton, WI, USA
Peqpette	Peqlab, Erlangen, Germany
Research Plus	Eppendorf, Hamburg, Germany
Research Pro	Eppendorf, Hamburg, Germany
Transferpette S	Brand, Wertheim, Germany
Rocker	
Multi MR-12	Biosan, Riga, Latvia
Scales	
EG 2200-2NM	Kern & Sohn GmbH, Balingen, Germany
PLJ 2100-2M	Kern & Sohn GmbH, Balingen, Germany
AB104	Mettler Toledo, Gießen, Germany
Stirrers	
WiseStir MS-20A	Witeg, Wertheim, Germany
bioMIXdrive 2	2mag, Munich, Germany

Table 2.1 List of equipment (continued)

Item	Manufacturer
Spectrophotometer	
NanoDrop 2000c	Thermo Fisher Scientific, Waltham, MA, USA
Thermocyclers	
Veriti	Thermo Fisher Scientific, Waltham, MA, USA
StepOnePlus	Thermo Fisher Scientific, Waltham, MA, USA
Tube welder	
SCDIIB Sterile Tubing Welder	Terumo Corporation, Tokyo, Japan
UV transilluminator	
Quantum-ST4	Vilber Lourmat, Eberhardzell, Germany
Vortex	
Vortex-2 Genie	Scientific Industries, Bohemia, NY, USA
Water baths	
W12	Labortechnik Medingen, Arnsdorf, Germany
WNB14	Memmert, Schwabach, Germany

2.1.2 Disposable consumables

Table 2.2 List of disposable consumables

Item	Manufacturer
Bioreactors, single-use (Mobius, 3 L)	Merck KGaA, Darmstadt, Germany
Capillary pistons (1000 µl)	Gilson, Middleton, WI, USA
Cell culture dishes (3.5, 6, 10 cm)	Greiner Bio-one, Kremsmünster, Austria
Cell culture flasks (T25, T75, T175)	Greiner Bio-One, Kremsmünster, Austria
Cell culture plates (6-, 12-, 24-, 96-wells)	Greiner Bio-One, Kremsmünster, Austria
Cell strainers (40, 70, 100 µm)	Corning, Corning, NY, USA
Centrifuge tubes (15 ml)	Greiner Bio-One, Kremsmünster, Austria
Centrifuge tubes (15, 50 ml)	Sarstedt, Nümbrecht, Germany
Coverslips, glass (15 mm diameter)	Glaswarenfabrik Karl Hecht GmbH, Sondheim/Rhön, Germany
Cryovials (1.8 ml)	Sarstedt, Nümbrecht, Germany
Flow cytometry tubes	Sarstedt, Nümbrecht, Germany
Gauze swabs	MaiMed GmbH, Neuenkirchen, Germany
Gloves, latex	care integral GmbH, Bad Schwartau, Germany
Gloves, nitrile	Meditrade GmbH, Kiefersfelden, Germany
Haemocytometer (Neubauer improved)	Brand, Wertheim, Germany
Hypodermic needles	B.Braun, Melsungen, Germany
MACS separation columns (MS, LS)	Miltenyi Biotec, Bergisch Gladbach, Germany
Microcentrifuge tubes (0.5, 1.5, 2 ml)	Sarstedt, Nümbrecht, Germany
Microscope slides, glass	Marienfeld, Lauda-Königshofen, Germany
Parafilm M	Bemis, Neenah, WI, USA
Pasteur pipettes, glass	Kimble Chase, Rockwood, TN, USA

Table 2.2 List of disposable consumables (continued)

Item	Manufacturer
PCR microtube strips	Brand, Wertheim, Germany
PCR plates (96-well)	Thermo Fisher Scientific, Waltham, MA, USA
PCR plates optical adhesive film	Thermo Fisher Scientific, Waltham, MA, USA
Petri dishes (3.5, 6, 10 cm)	Greiner Bio-One, Kremsmünster, Austria
Pipette tips (10, 100, 1000 µl)	Sarstedt, Nümbrecht, Germany
Pipette tips, filter (20, 100, 200, 1000 µl)	Sorenson BioScience, Salt Lake City, UT, USA
Precision wipes, lint-free	Kimberley-Clark, Dallas, TX, USA
Printing syringe (3 mL)	Nordson EFD, Westlake, OH, USA
Printing nozzle tips (inner diameter 330 µm)	Nordson EFD, Westlake, OH, USA
SCDIIb wafers	Terumo Corporation, Tokyo, Japan
Serological pipettes (5, 10, 25, 50 ml)	Greiner Bio-One, Kremsmünster, Austria
Spinner flasks (125 ml)	Corning, Corning, NY, USA
Syringe filters (0.2 µm)	Pall Corporation, Port Washington, NY, USA
Syringes (10, 20, 50 ml)	BD, East Rutherford, NJ, USA
Tygon tubing (outer diameter 5.6 mm, wall thickness 0.8 mm)	Sigma-Aldrich, St Louis, MO, USA

2.1.3 Chemicals

Table 2.3 List of chemicals

Item	Manufacturer
1,4-diazabicyclo[2.2.2]octane (DABCO)	Carl Roth, Karlsruhe, Germany
4',6-diamidino-2-phenylindole (DAPI)	Sigma-Aldrich, St Louis, MO, USA
7-amino-actinomycin D (7-AAD)	BD, East Rutherford, NJ, USA
Acetic acid	Merck KGaA, Darmstadt, Germany
Agarose	Biozym Scientific GmbH, Oldendorf, Germany
Calcein acetomethylester (AM)	Thermo Fisher Scientific, Waltham, MA, USA
Calcium chloride ($CaCl_2$)	Merck KGaA, Darmstadt, Germany
Disodium phosphate (Na_2HPO_4)	Carl Roth, Karlsruhe, Germany
Disodium ethylenediaminetetraacetate dihydrate (EDTA)	Sigma-Aldrich, St Louis, MO, USA
Ethanol	Applichem, Darmstadt, Germany
Ethidium homodimer 1	Thermo Fisher Scientific, Waltham, MA, USA
Fixable viability dye (Viobility 405/452)	Miltenyi Biotec, Bergisch Gladbach, Germany
Giemsa stain solution	Sigma-Aldrich, St Louis, MO, USA
Isopropanol	Carl Roth, Karlsruhe, Germany
Magnesium chloride ($MgCl_2$)	Merck KGaA, Darmstadt, Germany
Methanol	Carl Roth, Karlsruhe, Germany
Midori Green Advance DNA stain	Nippon Genetics Europe, Düren, Germany
Monopotassium phosphate (KH_2PO_4)	Carl Roth, Karlsruhe, Germany
Mowiol 4-88	Sigma-Aldrich, St Louis, MO, USA
Paraformaldehyde (PFA)	Applichem, Darmstadt, Germany
Potassium chloride (KCl)	Applichem, Darmstadt, Germany
Sodium chloride (NaCl)	Carl Roth, Karlsruhe, Germany
Tris-HCl	Sigma-Aldrich, St Louis, MO, USA
Triton X-100	Sigma-Aldrich, St Louis, MO, USA
TRIzol reagent	Thermo Fisher Scientific, Waltham, MA, USA
Water, RNAse- and DNAse-free	Promega, Madison, WI, USA
Water, sterile, for injection	Fresenius Kabi, Bad Homburg, Germany

2.1.4 Cell culture media, supplements, and growth factors

Table 2.4 List of cell culture media, supplements, and growth factors

Item	Manufacturer
1-thioglycerol	Sigma-Aldrich, St Louis, MO, USA
A83-01	Tocris, Bristol, UK
Accutase	Thermo Fisher Scientific, Waltham, MA, USA
Activin A	Miltenyi Biotec, Bergisch Gladbach, Germany
Advanced DMEM/F12	Thermo Fisher Scientific, Waltham, MA, USA
Alk5 inhibitor (Alk5)	Enzo Life Sciences, Lörrach, Germany
Antifoam C	Sigma-Aldrich, St Louis, MO, USA
Ascorbic acid (VitC)	Sigma-Aldrich, St Louis, MO, USA
B27 supplement (50×)	Thermo Fisher Scientific, Waltham, MA, USA
B27 supplement, without insulin (50×)	Thermo Fisher Scientific, Waltham, MA, USA
B27 supplement, without Vitamin A (50×)	Thermo Fisher Scientific, Waltham, MA, USA
Bone morphogenetic protein 4 (BMP4)	PeproTech, Rocky Hill, NJ, USA
Brain-derived neurotrophic factor (BDNF)	PeproTech, Rocky Hill, NJ, USA
cAMP	Sigma-Aldrich, St Louis, MO, USA
CHIR99021	Axon Medchem, Groningen, Netherlands
Collagenase B	Sigma-Aldrich, St Louis, MO, USA
DAPT, γ-secretase inhibitor	Promocell, Heidelberg, Germany
Dimethyl sulphoxide (DMSO)	Carl Roth, Karlsruhe, Germany
DMEM	Thermo Fisher Scientific, Waltham, MA, USA
DMEM/F12	Thermo Fisher Scientific, Waltham, MA, USA
Dorsomorphin	Sigma-Aldrich, St Louis, MO, USA
Dulbecco's phosphate buffered saline, without calcium or magnesium (DPBS)	Thermo Fisher Scientific, Waltham, MA, USA
Foetal calf serum (FCS)	Biochrom, Berlin, Germany
Gelatin	Sigma-Aldrich, St Louis, MO, USA
Glia cell-derived neurotrophic factor (GDNF)	PeproTech, Rocky Hill, NJ, USA
IWR-1	Sigma-Aldrich, St Louis, MO, USA
KaryoMAX Colcemid solution	Thermo Fisher Scientific, Waltham, MA, USA
KnockOut serum replacement (KSR)	Thermo Fisher Scientific, Waltham, MA, USA
Leukaemia inhibitory factor, human (LIF)	Miltenyi Biotec, Bergisch Gladbach, Germany
L-glutamine (200 mM)	Thermo Fisher Scientific, Waltham, MA, USA
Matrigel, growth factor reduced (bMG)	Corning, Corning, NY, USA
Matrigel, human ESC-qualified (hES MG)	Corning, Corning, NY, USA
mTeSR-1	STEMCELL Technologies, Vancouver, Canada
N2 supplement (100×)	Thermo Fisher Scientific, Waltham, MA, USA
Neurobasal medium	Thermo Fisher Scientific, Waltham, MA, USA
Non-essential amino acids (NEAA; 100×)	Thermo Fisher Scientific, Waltham, MA, USA
Penicillin/streptomycin (100×)	Thermo Fisher Scientific, Waltham, MA, USA
Poloxamer 188	Sigma-Aldrich, St Louis, MO, USA
Purmorphamine (PMA)	Miltenyi Biotec, Bergisch Gladbach, Germany
ReLeSR	STEMCELL Technologies, Vancouver, Canada
SB431542 (SB)	Miltenyi Biotec, Bergisch Gladbach, Germany
Serum albumin, bovine (BSA)	Sigma-Aldrich, St Louis, MO, USA
Serum albumin, human (HSA)	Sigma-Aldrich, St Louis, MO, USA
Sodium alginate (Protanal® LF 10/60)	FMC BioPolymer, Philadelphia, PA, USA
Sodium lactate	Sigma-Aldrich, St Louis, MO, USA
StemMACS iPS-Brew XF, human	Miltenyi Biotec, Bergisch Gladbach, Germany
SU5402	Sigma-Aldrich, St Louis, MO, USA
Y27632 Rho kinase inhibitor	Miltenyi Biotec, Bergisch Gladbach, Germany
β-mercaptoethanol (50 mM)	Thermo Fisher Scientific, Waltham, MA, USA

2.1.5 Specialty cell culture media

Table 2.5 List of specialty cell culture media and formulations

Item	Formulation	Reference(s)
Cardiac Basal Medium (CBM)	RPMI1640 1× B27 2 mM L-glutamine 100 µM β-mercaptoethanol 50 µg/ml VitC	Kadari *et al.*, 2014
Cardiac Enrichment Medium (CEM)	RPMI1640 without glucose 4 mM sodium lactate	Kadari *et al.*, 2014; Tohyama *et al.*, 2013
Cardiac Specification Medium (CSM)	RPMI1640 1× B27 (without insulin) 2 mM L-glutamine 100 µM β-mercaptoethanol 50 µg/mL VitC	Kadari *et al.*, 2014
CVPC Expansion Medium (BACS)	Adv. DMEM/F12:Neurobasal (1:1) 1× N2 1× B27 without Vitamin A 1× NEAA 2 mM L-glutamine 100 µM β-mercaptoethanol 0.05% (w/v) HSA 250 µM VitC 5 ng/mL BMP4 10 ng/mL Activin A 3 µM CHIR99021 2 µM SU5402	Modified from Zhang *et al.*, 2016
CVPC Induction Medium (CIM)	48.5 mL DMEM/F12 1× B27 without Vitamin A 2 mM L-glutamine 400 µM 1-thioglycerol 50 µg/mL VitC 25 ng/mL BMP4 3 µM CHIR99021	Cao *et al.*, 2013
CVPC Propagation Medium (CPM)	47.5 mL DMEM/F12 1× N2 1× B27 without Vitamin A 1× NEAA 2 mM L-glutamine 100 µM β-mercaptoethanol 400 µM 1-thioglycerol 50 µg/mL VitC 3 µM CHIR99021 2 µM dorsomorphin 0.5 µM A83-01	Cao *et al.*, 2013
Cell freezing medium	KSR 10% DMSO	Modified from Merkle and Eggan, 2017

Table 2.5 List of specialty cell culture media and formulations (continued)

Item	Formulation	Reference(s)
N2B27 medium	DMEM/F12:Neurobasal (1:1) 0.5× N2 0.5× B27 without Vitamin A 2 mM L-glutamine	Reinhardt *et al.*, 2013
Neural expansion medium (NEM)	DMEM/F12:Neurobasal (1:1) 1× N2 1× B27 2 mM L-glutamine 200 µM VitC 18.2 mg/L BSA fraction V 4 µM CHIR99021 5 µM Alk5 0.5 µM PMA	Jovanovic *et al.*, 2018
Neural Induction Medium (NIM)	DMEM/F12:Neurobasal (1:1) 1× N2 1× B27 2 mM L-glutamine 10 ng/mL LIF 3 µM CHIR99021 2 µM SB431542	Meyer *et al.*, 2015
Neuronal differentiation medium (NDM)	Neurobasal 1× N2 1× B27 1× NEAA 2 mM L-glutamine 20 ng/mL BDNF 20 ng/mL GDNF 300 ng/mL cAMP 200 µM VitC 2 µM DAPT	Modified from Borghese *et al.*, 2010; Yan *et al.*, 2013
smNPC induction medium	DMEM 20% KSR 1 mM β-mercaptoethanol 1% NEAA 2 mM L-glutamine 10 µM SB431542 1 µM dorsomorphin 3 µM CHIR99021 0.5 µM PMA	Modified from Reinhardt *et al.*, 2013
smNPC propagation medium	DMEM/F12:Neurobasal (1:1) 0.5× N2 0.5× B27 without Vitamin A 2 mM L-glutamine 3 µM CHIR99021 0.5 µM PMA 150 µM VitC	Reinhardt *et al.*, 2013

Table 2.5 List of specialty cell culture media and formulations (continued)

Item	Formulation	Reference(s)
Undirected differentiation medium	DMEM 10% FCS 1× NEAA 4 µM L-glutamine 100 µM β-mercaptoethanol	Modified from Aasen *et al.*, 2008

2.1.6 Cells

Table 2.6 List of cell lines and typical culture medium

Cell line identifier	Typical culture medium	Reference(s)
fl-AR1034ZIMA 001 (AFiPS)	mTeSR-1, StemMACS iPS-Brew XF	Kadari *et al.*, 2014
STEMCCA-FSiPS clone 2 (FSiPS)	mTeSR-1, StemMACS iPS-Brew XF	Kwok *et al.*, 2018
mRNA-BJ-iPS clone 6 (BJiPS)	StemMACS iPS-Brew XF	In-house iPSC line generated by Dr. Katharina Günther from BJ fibroblasts
BJ-iNSC clone 5d (BJ-iNSC)	NIM, NEM	Meyer *et al.*, 2015, Peruzzotti-Jametti *et al.*, 2018

2.1.7 Buffers and solutions

Table 2.7 List of general buffers and solutions

Item	Formulation
Dulbecco's phosphate buffered saline (DPBS)	In double distilled water, 1.5 mM KH_2PO_4 2.7 mM KCl 8.1 mM Na_2HPO_4 137 mM NaCl
Fixation buffer	DPBS 4% (w/v) PFA Store at -20 °C, thaw and keep at 4 °C for use.
Mowiol 4-88 mounting solution	6.0 mL double distilled water 2.4 g Mowiol 4-88 6.0 g glycerol 12.0 mL of 0.2 M Tris-HCl 25 mg/mL DABCO Mix water, Mowiol, and glycerol for 2 h at room temperature. Add Tris-HCl, and further mix at 50 °C for 2 h. Add DABCO, and gently rotate overnight at room temperature to mix. Divide into aliquots and store at -20 °C.

Table 2.7 List of general buffers and solutions (continued)

Item	Formulation
Staining buffer	DPBS 2% (w/v) BSA Optionally 0.2% Triton X-100 for permeabilisation

2.1.8 Antibodies

Table 2.8 List of primary antibodies and typical working concentrations

Target	Host species/ Clonality	Manufacturer	RRID/ Cat#	Working dilution
AFP	Rabbit polyclonal	Dako, Glostrup, Denmark	AB_2650473 A0008	1:400
ACTA2 (SMA)	Mouse monoclonal IgG2a	Abcam, Cambridge, UK	AB_262054 ab7817	1:200
ACTN2	Mouse monoclonal IgG2a	Sigma-Aldrich, St Louis, MO, USA	AB_476766 A7811	1:400
ISL1	Mouse monoclonal IgG2b	DSHB, Iowa City, IA, USA	AB_2314683 39.4D5	1:50
Ki67	Rabbit monoclonal IgG	Thermo Fisher Scientific, Waltham, MA, USA	AB_10979488 MA5-14520	1:200
MESP1	Rabbit polyclonal	Aviva Systems Biology, San Diego, CA, USA	AB_2047045 ARP39374_P050	1:100
NANOG	Rabbit monoclonal IgG	Cell Signaling Technology, Danvers, MA, USA	AB_10559205 4903S	1:100
NES	Mouse monoclonal IgG1	R&D Systems, Minneapolis, MN, USA	AB_2251304 MAB1259	1:100
OCT4	Mouse monoclonal IgG2b	Santa Cruz Biotechnology, Dallas, TX, USA	AB_628051 sc-5279	1:100
PAX6	Rabbit polyclonal IgG	BioLegend, San Diego, CA, USA	AB_2565003 901301	1:100
SOX1	Goat polyclonal IgG	R&D Systems, Minneapolis, MN, USA	AB_2239879 AF3369	1:100
SOX2	Mouse monoclonal IgG2a	R&D Systems, Minneapolis, MN, USA	AB_358009 MAB2018	1:200
SSEA-4	Mouse monoclonal IgG3	DSHB, Iowa City, IA, USA	AB_528477 MC-813-70	1:100
TNNT2	Mouse monoclonal IgG1	Abcam, Cambridge, UK	AB_306445 ab8295	1:100
TRA-1-81	Mouse monoclonal IgM	STEMCELL Technologies, Vancouver, Canada	AB_1118559 01556	1:50
TUBB3 (Tuj1)	Mouse monoclonal IgG2a	BioLegend, San Diego, CA, USA	AB_10063408 801202	1:1000

Table 2.9 List of secondary antibodies and typical working concentrations

Target	Host species	Manufacturer	RRID/ Cat#	Working dilution
Goat IgG (H+L)-Cy3	Donkey IgG	Jackson ImmunoResearch, West Grove, PA, USA	AB_2307351 705-165-147	1:800
Mouse IgG (H+L)- Cy2	Goat IgG	Jackson ImmunoResearch, West Grove, PA, USA	AB_2307343 115-225-146	1:500
Mouse IgG (H+L)-Cy3	Goat IgG	Jackson ImmunoResearch, West Grove, PA, USA	AB_2338690 115-165-146	1:800
Mouse IgG (H+L)-Cy5	Goat IgG	Jackson ImmunoResearch, West Grove, PA, USA	AB_2338713 115-175-146	1:500
Rabbit IgG (H+L)-Cy3	Goat IgG	Jackson ImmunoResearch, West Grove, PA, USA	AB_2338006 111-165-144	1:800

Table 2.10 List of antibodies for flow cytometry

Target-Conjugate	Species/ Isotype	Manufacturer	RRID/ Cat#	Working dilution
CD133-pure	Mouse $IgG1_K$	Miltenyi Biotec, Bergisch Gladbach, Germany	AB_244339 130-090-422	1:11
KDR-PE	Mouse $IgG1_K$	Miltenyi Biotec, Bergisch Gladbach, Germany	AB_2660806 130-098-905	1:11
PDGFRa-APC	Human IgG1	Miltenyi Biotec, Bergisch Gladbach, Germany	AB_2726952 130-115-239	1:11
PSA-NCAM-PE	Mouse IgM	Miltenyi Biotec, Bergisch Gladbach, Germany	AB_1036069 130-093-274	1:11
SIRPA-PE	Human IgG1	Miltenyi Biotec, Bergisch Gladbach, Germany	AB_2655602 130-099-781	1:11
SOX1-PE	Human IgG1	Miltenyi Biotec, Bergisch Gladbach, Germany	AB_2653488 130-111-158	1:11
SOX2-FITC	Human IgG1	Miltenyi Biotec, Bergisch Gladbach, Germany	AB_2653500 130-104-940	1:11
SSEA-1-APC-Vio770	Human IgG1	Miltenyi Biotec, Bergisch Gladbach, Germany	AB_2653516 130-104-939	1:11
SSEA-4-APC	Human IgG1	Miltenyi Biotec, Bergisch Gladbach, Germany	AB_2653520 130-098-347	1:11
TRA-1-60-PE	Human IgG1	Miltenyi Biotec, Bergisch Gladbach, Germany	AB_2654227 130-100-347	1:11

2.1.9 Oligonucleotide primers

Oligonucleotide primers were purchased from and synthesised by Thermo Fisher.

Table 2.11 Primer sequences used for RT-PCR and qRT-PCR. Fwd indicates the forward primer, Rev indicates the reverse primer.

Target	Sequence	Reference
GAPDH-Fwd	TGACAACTTTGGTATCGTGGA	Koch *et al.*, 2011
GAPDH-Rev	CCAGTAGAGGCAGGGATGAT	Koch *et al.*, 2011
hOCT4-endo-Fwd	GACAGGGGGAGGGGAGGAGCTAGG	Kishino *et al.*, 2014
hOCT4-endo-Rev	CTTCCCTCCAACCAGTTGCCCCAAAC	Kishino *et al.*, 2014
Nanog-Fwd	TTTGTGGGCCTGAAGAAAACT	Wang *et al.*, 2016
Nanog-Rev	AGGGCTGTCCTGAATAAGCAG	Wang *et al.*, 2016
hAFP-Fwd	CTTTGGGCTGCTCGCTATGA	Wang *et al.*, 2015
hAFP-Rev	GCATGTTGATTTAACAAGCTGCT	Wang *et al.*, 2015
hBRACHYURY-Fwd	TATGAGCCTCGAATCCACATAGT	Wang *et al.*, 2015
hBRACHYURY-Rev	CCTCGTTCTGATAAGCAGTCAC	Wang *et al.*, 2015
hSOX1-Fwd	CAGCAGTGTCGCTCCAATTCA	Frank *et al.*, 2012
hSOX1-Rev	GCCAAGCACCGAATTCACAG	Frank et al., 2012

2.1.10 Kits

Table 2.12 List of commercially available kits

Item	Manufacturer
Cytometer Setup & Tracking Beads Kit	BD, East Rutherford, NJ, USA
GoScript™ Reverse Transcriptase	Promega, Madison, WI, USA
Luna® Universal qPCR Master Mix	New England Biolabs, Ipswich, MA, USA
MACS Comp Bead Kit, anti-REA	Miltenyi Biotec, Bergisch Gladbach, Germany
MACS Comp Bead Kit, anti-rat	Miltenyi Biotec, Bergisch Gladbach, Germany
SSEA-4-MicroBeads MACS Kit	Miltenyi Biotec, Bergisch Gladbach, Germany
TRA-1-60-MicroBeads MACS Kit	Miltenyi Biotec, Bergisch Gladbach, Germany

2.1.11 Software

Table 2.13 List of software used

Software	Application	Manufacturer/Reference
Adobe Photoshop CS5.1	Image stitching, Z- and focus-stacking	Adobe Inc, San Jose, CA, USA
AxioVision v4.8	Image acquisition	Carl Zeiss Microscopy GmbH, Jena, Germany
BD FACSDiva v6.1.3	Flow cytometry data acquisition	BD Biosciences, San Jose, CA, USA
RegenHU Software Suite v	Parameter specification for bioprinter	RegenHU, Fribourg, Switzerland
CorelDraw Graphics Suite X7	Figure preparation	Corel Corporation, Ottawa, Canada
FIJI v1.49m	Image analysis, labelling, multichannel overlays	Schindelin *et al.*, 2012
FlowJo v10.0.7	Flow cytometry analysis	Tree Star Inc, Ashland, OR, USA
GraphPad Prism 6	Graphing	GraphPad Software, San Diego, CA, USA
Leica LAS v4.12	Image acquisition	Leica Microsystems, Wetzlar, Germany
Leica LAS X Core	Image acquisition	Leica Microsystems, Wetzlar, Germany
Office 365	Word processing and documentation	Microsoft, Redmond, WA, USA
StepOne Software v2.3	qRT-PCR acquisition and analysis	Thermo Fisher Scientific, Waltham, MA, USA

2.2 Methods

2.2.1 Standard adherent culture

Unless otherwise stated, cells were cultured at 37 °C, 5% CO_2 under normoxia conditions. All handling of cells was performed under sterile conditions in a biological safety cabinet. Cells were routinely tested for *Mycoplasma* contamination using a PCR assay.

2.2.1.1 Coating of cell culture plasticware

In many cases, the surfaces of cell culture plasticware required coating with growth factor reduced Matrigel (bMG), human ESC-qualified Matrigel (hES MG), or gelatin. For subsequent imaging applications such as immunocytochemistry, sterile autoclaved glass coverslips were placed in cell culture plasticware before coating. Frozen aliquots of bMG or hES MG were thawed on ice. Using pre-chilled pipettes, tubes, and media, a 1 mL aliquot of bMG was diluted in 30 mL of DMEM/F12, while a hES MG aliquot of varying volume (depending on batch) was diluted in 24 mL of DMEM/F12. The 0.1% gelatin (w/v), diluted bMG, or hES MG solutions were then swiftly dispensed onto cell culture plasticware, using 1 mL of coating solution per 10 cm^2 (e.g. 1 mL/well of a 6-well plate). Cell culture plasticware containing coating solutions were then sealed with Parafilm and stored at 4 °C for up to 2 weeks. Before use, these plates were incubated at 37 °C for at least 30 min to allow gelation before plating cells.

2.2.1.2 Thawing of cells

A frozen cryovial of cells was retrieved from liquid nitrogen or -80 °C storage and placed on ice for short-term transport. Working quickly, the cells were thawed in a 37 °C water bath with gentle swirling until only a small ice crystal remained. The thawed cell suspension was transferred to a 15 mL centrifuge tube containing 5 mL DMEM/F12 in a dropwise manner, and gently pipetted to resuspend. The cell suspension was then centrifuged at 300 *g* for 5 min at 4 °C to pellet the cells. After removing the supernatant, the cell pellet was resuspended in appropriate culture medium and optionally counted before seeded into pre-warmed, pre-coated cell culture vessels.

2.2.1.3 Cultivation of cells

Human induced pluripotent stem cells (hiPSCs)

hiPSCs were cultivated under feeder-free conditions on hES MG-coated plasticware with either mTeSR-1 or StemMACS iPS-Brew XF culture medium, with daily medium exchange. At approximately 80% confluency, cells were passaged; medium was completely aspirated, and cells were incubated with 500–1000 µL Accutase per 10 cm^2 for 3–5 min at 37 °C to dissociate the cells from the plate. The cells were then harvested by resuspending in DMEM/F12, transferred into a centrifuge tube and centrifuged at 300 *g* for 5 min at 4 °C. The supernatant was aspirated, and the cell pellet was resuspended in culture medium supplemented with 10 µM Y27632 before plating onto a new hES MG-coated plate. Split ratios of 1:6 to 1:12 were used. After the first 24 h after passaging, a medium exchange was done using culture medium without Y27632.

Human induced neural stem cells (hiNSCs)

hiNSCs were cultivated on bMG-coated plasticware with either NIM or NEM culture medium, with medium exchange every other day. Cells were passaged at approximately 60–70% confluency, using 500–1000 µL Accutase per 10 cm^2 and incubated for 3–5 min at 37 °C. The cells were then collected by resuspending in DMEM/F12, transferred into a centrifuge tube and centrifuged at 300 *g* for 5 min at 4 °C. The supernatant was aspirated, and the cell pellet was resuspended in culture medium supplemented with 10 µM Y27632 before plating onto a new bMG-coated plate. Split ratios of 1:12 to 1:24 were used. After the first 24–48 h after passaging, a medium exchange was done using culture medium without Y27632.

2.2.1.4 Cryopreservation of cells

For hiPSCs and hiNSCs, the cells were harvested and pelleted as described above. The cell pellet was then resuspended in freezing medium, with a minimum cell density of 1×10^6 cells/mL. The cell suspension was then dispensed into cryovials. The cryovials of cells were placed in a Cryo 1°C Cooler freezing container filled with isopropanol, and the container was placed in a -80 °C freezer overnight to allow controlled freezing at a rate of 1 °C loss per min. The next day, the cryovials were transferred to a liquid nitrogen tank in the vapour phase for long-term storage.

2.2.1.5 Cell counting

To determine cell quantities for further downstream processes such as passaging and flow cytometry, cells were counted using a Neubauer counting chamber. Cell suspensions were prepared as previously described. Depending on cell density, cells were further diluted in cell culture medium or cell culture grade DPBS. After thorough resuspension of the cells, 10 µL of the homogeneous cell suspension was loaded into a Neubauer chamber and visualised under a microscope. The counting field consists of a large square field divided into a 3×3 counting grid, and cells in each of the four corner squares were counted and added together. Dividing by four to obtain the average number of cells in one corner square, the number of cells in the original cell suspension could then be calculated using the following equations.

$$\frac{\text{cells}}{\text{mL}} = \text{average cells per corner square} \times 10^4$$

$$\text{total number of cells} = \frac{\text{cells}}{\text{mL}} \times \text{total volume of cell suspension}$$

2.2.2 Stirred suspension culture

2.2.2.1 Stirred suspension culture in spinner flasks

hiPSCs growing under standard adherent conditions were harvested from the cultureware by Accutase and incubation for 5 min at 37 °C. The dissociated cells were collected with DMEM/F12 and transferred into centrifuge tubes and centrifuged at 300 *g* for 5 min at 4 °C. The resulting cell pellet was then gently pipetted and resuspended in culture medium, strained through a 40 µm cell strainer that was pre-moistened with culture medium, and collected into a fresh centrifuge tube. Cells were counted as previously described and brought into 125 mL spinner flasks (henceforth referred to as spinners) in varying cell densities in 100 mL culture medium during the optimisation phase. For inoculation, the culture medium was supplemented with 10 µM Y27632 for the first two days without any medium refreshment. The spinners containing cells and medium were incubated in a 37 °C, 5% CO_2 incubator with the side-arm caps slightly loosened to permit gas exchange. The spinners were stirred by the bioMIXdrive 2 device inside the incubator, and a range of stirring rates were tested, from 65–95 revolutions per minute (RPM), to determine the optimal stirring rate. Optimal results were obtained at 85 RPM.

With the regular medium exchange protocol, medium *exchange* was first done after 48 h of stirred suspension culture. To perform the medium exchange, spinners

were brought under the biosafety cabinet and aggregates were allowed to sediment by gravity for 5–8 min. The spinners were then tilted side-ways and the culture medium was aspirated through a side-arm reserved for medium removal, removing about 75–80% of the culture medium. Fresh pre-warmed medium was then fed to the cells through the other side-arm reserved for feeding culture medium, up to a total volume of 100 mL. Thereafter, the spinners were transferred back onto the bioMIXdrive 2 in the incubator, and the medium was exchanged daily until 7 days post-inoculation.

With the optimised medium exchange protocol, cells were inoculated in 80 mL culture medium at a cell density of 2×10^5 cells/mL, and medium *addition* was first done after 48 h of stirred suspension culture. At 48 h and 72 h of stirred suspension culture, 20 mL of fresh pre-warmed medium was added to the cells without medium aspiration. Thereafter, on day 4 post-inoculation, spent medium was aspirated as previously described, and fresh pre-warmed medium was added to the cells up to a culture volume of 100 mL. Medium *exchange* then continued until day 7 post-inoculation.

To harvest the cells, hiPSC aggregates in culture medium were transferred to 50 mL centrifuge tubes and centrifuged at 200 *g* for 3 min at 4 °C to collect the aggregates. After carefully aspirating the supernatant, the cell pellets were resuspended in 10 mL of pre-warmed Accutase and incubated horizontally at 37 °C for up to 10 min with periodic gentle tilting to resuspend the aggregates and cells. To this Accutase suspension of cells, 20 mL of DMEM/F12 was then added and gently triturated to generate the cell suspension. The cells were then pelleted by centrifugation as previously described, and then resuspended in 10 mL of culture medium, strained through a pre-moistened 40 µm cell strainer, and the single cell suspension was collected in a fresh 50 mL centrifuge tube. This single cell suspension was then used for further downstream analysis such as flow cytometry, cryopreservation, passaging under standard adherent conditions, or further passaging in spinners or bioreactors.

2.2.2.2 Stirred suspension culture in bioreactors

In this study, the Mobius 3 L Single-use Bioreactors were used (henceforth referred to as bioreactor). After culturing cells in spinners to generate the cell numbers required for inoculation into bioreactors, the single cell suspensions generated were transferred into the bioreactors at a cell density of 2×10^5 cells/mL, in a volume of

1,000 mL of culture medium supplemented with 10 µM Y27632. This cell density is identical to the cell density used for seeding spinners.

These bioreactors were controlled by an external ez-Control machine, and were maintained at 37 °C, supplied with sterile-filtered air and CO_2 through a gas exchange port through an overlay of gas, and stirred at 164 RPM. The stirring rate of 164 RPM was determined by using the optimised 85 RPM found in spinners and applying it to the energy dissipation rate (Mollet *et al.*, 2007).

Like the optimised medium exchange protocol described earlier in spinners, 250 mL of fresh pre-warmed medium was added to the bioreactor cultures on day 2 and 3 post-inoculation. Medium *addition* was carried out using a functionally closed system by using the SCDIIB Tube Welder to fuse tubing on the bioreactor with tubing connected to bottle cap adapters on medium bottles. From day 4 post-inoculation onwards, medium *exchange* was performed daily by stopping the stirring for 8–10 min, removing spent medium through a side-port on the bioreactor and feeding fresh pre-warmed medium using tube welding up to a culture volume of 1,000 mL, before resuming stirring at 164 RPM. After 7 days of culture in bioreactors, the hiPSC aggregates could be harvested through tube welding through a bottom-port on the bioreactor into a sterile empty bottle fitted with a bottle cap adapter connected to tubing. The aggregates could then be processed into a single cell suspension as previously described for spinners.

2.2.3 Quantification of hiPSC aggregate sizes

Samples of aggregates from spinners and bioreactors were transferred to 12-well plates and spread evenly to clearly separate individual aggregates. Images of the aggregates were taken with a DM IL LED inverted microscope using Leica LAS X Core software. Images were opened in FIJI v1.49m (Schindelin *et al.*, 2012) to measure aggregate diameters and exported using the Region-Of-Interest Manager and Measure functions. A minimum of 100 aggregates were measured at each data point and repeated 3 times. Statistical analysis and generation of plots were done in GraphPad Prism 6.

2.2.4 Undirected differentiation of hiPSCs

A standard assay for characterising pluripotency is to demonstrate the differentiation of cells to all three germ layers. To accomplish this, hiPSC aggregates were cultured in static suspension in non-tissue culture-treated Petri dishes using serum-containing

undirected differentiation medium. After 7 days of static suspension culture, 5–7 aggregates were evenly plated into each well of a 6-well plate precoated with gelatin. The attached differentiating aggregates were further cultured for another 3 weeks in undirected differentiation medium. Under both conditions, medium was exchanged every 3 days. Then, among this heterogeneous population of cells, representatives of each of the three germ layers could be identified by immunocytochemical analysis using antibodies against a marker for each germ layer. To mark cells from the ectoderm, mesoderm, and endoderm, βIII-tubulin (TUBB3), smooth muscle actin (ACTA2, or SMA), and alpha-fetoprotein (AFP) were used respectively.

2.2.5 Directed differentiation of hiPSCs into cardiomyocytes

To demonstrate that bioreactor-grown hiPSCs could continue to respond to signalling cues and differentiate into more specific cells, a cardiomyocyte differentiation protocol was applied (Kadari *et al.*, 2014). Bioreactor-grown hiPSC aggregates were processed into a single cell suspension as previously described and plated onto hES MG-coated plates in mTeSR-1 supplemented with 10 µM Y27632. At 80–90% confluency, cardiac differentiation was started by switching the medium to cardiac basal medium (CBM) supplemented with 25 ng/mL BMP4 and 5 µM CHIR99021. On the next day, the medium was switched to CBM with 5 µM CHIR99021. One day later, the medium was replaced with cardiac specification medium (CSM). On the following day, Wnt-signalling was inhibited by changing the medium to CSM supplemented with 10 µM IWR-1. This Wnt-inhibiting medium was refreshed daily for the next days until beating cells could be observed, which typically occurred after 5–6 days of Wnt inhibition. Once beating cells were observed, the culture medium was switched back to cardiac basal medium for 4 days. To further enrich this culture for cardiomyocyte-like cells, the medium was switched to cardiac enrichment medium (CEM) for the next 5 days (Tohyama *et al.*, 2013). After enrichment, the cells were maintained in CBM and optionally passaged onto bMG-coated plates and glass coverslips for further analyses.

2.2.6 Immunocytochemical analysis

For imaging, cells were cultured on appropriately coated glass coverslips to the desired confluency, then fixed with 4% PFA for 15 min at room temperature, and then washed with DPBS three times for 5 min each. Fixed cells were blocked for 1 h at room temperature with staining buffer; in the case of intracellular markers, permeabilisation and blocking were done in one step by adding 0.2% Triton X-100 to

the staining buffer. Next, the cells were incubated at 4 °C overnight with the desired primary antibodies (Table 2.8) diluted in staining buffer. The samples were then washed three times with DPBS for 5 min each, and then incubated in the dark for up to 2 h at room temperature with fluorophore-conjugated secondary antibodies (Table 2.9) against the host species of the primary antibody. Thereafter, the samples were washed twice with DPBS, cell nuclei were counter-stained with 0.2 µg/mL DAPI in DPBS for 15 min protected from light, and finally washed another three times with DPBS. Glass coverslips of stained cells were then mounted on glass microscope slides with Mowiol 4-88 + DABCO, dried overnight at room temperature protected from light, and visualised with fluorescence microscopes using filter sets appropriate to the fluorochrome. To control for background fluorescence and non-specific binding of the secondary antibodies, unstained samples and primary antibody-omitted samples were prepared.

2.2.7 Flow cytometry

For each test, 0.5–1 × 10^6 cells in a single cell suspension were used. First, cell suspensions were washed with DPBS (without Ca^{2+}/Mg^{2+}) and then optionally incubated with fixable viability stain Viobility 405/452 for 15 min at room temperature according to the manufacturer's instructions. Next, the cells were washed twice with staining buffer, then pelleted and resuspended in staining buffer. To detect cell surface markers, antibodies against the antigens of interest were added to the cell suspension up to a total of 110 µL volume, and incubated at 4 °C for 15–45 min before washing with DPBS. When using non-directly conjugated primary antibodies (e.g. CD133 pure), the primary antibody was then detected with another incubation at 4 °C for 15 min with a secondary antibody (e.g. goat anti-mouse-Cy5) in staining buffer at a staining volume of 110 µL. To detect intracellular markers, the cells were then fixed with 4% PFA for 15 min, followed by washing with DPBS and permeabilisation with 0.2% Triton X-100 in staining buffer for 15 min. Permeabilised cells were then washed with staining buffer, resuspended in staining buffer, and incubated with antibodies against the intracellular targets for 15 min at 4 °C in a total staining volume of 110 µL. Antibodies used for flow cytometry are listed in Table 2.10. Cells were then washed and resuspended in DPBS. If cells were not previously labelled using Viobility 405/452, 5 µL 7-AAD solution was added per 500 µL cell suspension and incubated for 10 min in the dark before analysis. Isotype and unstained controls were included to control for nonspecific binding and background fluorescence. Data were acquired with BD FACSDiva 6.1.3 software on a BD

FACSCanto II flow cytometer using appropriate laser and filter sets, with 10,000–50,000 events recorded per sample. Raw .FCS files were exported from FACSDiva, then analysed and graphed in FlowJo 10.0.7.

2.2.8 Magnet-activated cell sorting

Magnet-activated cell sorting (MACS) was used in the initial optimisation of the stirred suspension culture protocol to demonstrate that it was feasible to recover hiPSCs from a heterogeneous population of undifferentiated and differentiated cells. However, after the stirred suspension culture protocols were optimised, the resultant hiPSC populations had little to no spontaneously differentiating cells, thus obviating the need for MACS to recover pluripotent cells from suspension cultures. To perform MACS on a heterogeneous mix of differentiating and undifferentiated cells, the cell mixture was resuspended in mTeSR-1 supplemented with 10 µM Y27632 and passed through a 30 µm pore size pre-separation filter to remove cell clumps. Single cells were then centrifuged at 300 *g* for 5 min at 4 °C, and the supernatant was removed. 2×10^6 cells were resuspended in 80 µL of mTeSR-1 + 10 µM Y27632, and then 20 µL of anti-TRA-1-60 or anti-SSEA-4 MicroBeads were added to the cell suspension for labelling. The cell suspension was mixed by pipetting, and then incubated for 5 min at 4 °C. Thereafter, the cell suspension was diluted by adding 900 µL mTeSR-1 + 10 µM Y27632 to bring the total volume to 1 mL. An MS Column was then placed in the magnetic field of a MACS Separator, and the column was rinsed with 500 µL of mTeSR-1 + 10 µM Y27632. Then, the labelled cell suspension was applied onto the column, and the flow-through containing unlabelled cells was collected. The column containing labelled cells was rinsed three times with 500 µL mTeSR-1 + 10 µM Y27632, and the flow-throughs were pooled with the first flow-through. The column was then removed from the MACS Separator and placed on a 15 mL centrifuge tube ready to collect the labelled cells. 1 mL of mTeSR-1 + 10 µM Y27632 was added to the column, and the plunger on the column was firmly and quickly pushed such that the labelled cells would be flushed out of the column and into the 15 mL centrifuge tube. The collected cells were then ready to be used for further downstream applications such as flow cytometry.

2.2.9 Karyotype analysis

T25 flasks were coated with hES MG as previously described, and hiPSCs were plated and cultured in mTeSR-1, in the presence of 10 µM Y27632 only for the first day after passaging. At approximately 70% confluency, hiPSCs were incubated at 37 °C with

100 ng/mL KaryoMAX Colcemid for 3 h. Thereafter, the cells were dissociated into a single cell suspension with Accutase, collected in DMEM/F12, and pelleted by centrifugation at 300 *g* for 8 min at 4 °C. After removing the supernatant, the cell pellet was first resuspended in 1 mL of pre-warmed 75 mM KCl solution, and then further diluted in an additional 14 mL of 75 mM KCl solution. The tube was gently inverted to mix, and then incubated for 16 min at 37 °C. The cells were recovered by another round of centrifugation, then resuspended in ice-cold, freshly-prepared 1:3 acetic acid and methanol for fixation at -20 °C overnight. Fixed cells in suspension were spread onto cleaned glass microscope slides in a dropwise manner and air-dried at room temperature. After visual inspection to confirm the presence of visible metaphase chromosomes, the samples were aged and stained with filtered Giemsa stain solution, then analysed with microscopy. The karyotyping procedures described here were performed in collaboration with Julia Flunkert and Anna Maierhofer from the laboratory of Prof. Dr. Thomas Haaf, Department of Human Genetics, University of Würzburg.

2.2.10 Reverse transcription (RT)-polymerase chain reaction (PCR)

RNA extraction

Cells grown under standard adherent or stirred suspension culture conditions were harvested with Accutase, pelleted by centrifugation as previously described, and washed twice with DPBS. For each sample, total RNA from 5×10^6 cells was extracted using 1 mL TRIzol reagent. Cells were homogenised in TRIzol by pipetting and incubated for 5 min at room temperature. Then, 200 µL chloroform was added and the mixture was shaken for 15 s to mix, and then incubated for another 3 min. Thereafter, the samples were centrifuged for 15 min at 12,000 *g* at 4 °C. After centrifugation, the sample separated into three layers, with RNA isolated in the uppermost aqueous layer. The aqueous layer containing RNA was transferred to fresh RNAse-free microcentrifuge tubes, and 500 µL isopropanol was added to each tube, mixed thoroughly, and then incubated on ice for 10 min. The samples were then centrifuged for 10 min at 12,000 *g* at 4 °C to pellet the precipitated RNA. The supernatant was removed, and the pellet was washed with 75% ethanol and vortexed briefly. Following another centrifugation step at 7,500 *g* for 10 min at 4 °C, the supernatant was removed, and the pellet was air dried for 5–10 min without allowing the pellet to completely dry out. The RNA pellet was dissolved in 20–50 µL of RNAse-free water and then warmed to 60 °C for 15 min to allow complete dissolution.

The RNA yield was determined with a NanoDrop 2000 spectrophotometer and quality was checked by observing the A260/A280 (approximately 2.0) and A260/A230 (approximately 2.0–2.2) ratios. The RNA solutions were stored at -80 °C and used for further downstream processes.

Reverse transcription of RNA into complementary DNA (cDNA)

All frozen components of the GoScript Reverse Transcription kit were thawed except the Reverse Transcriptase. For each sample, an RNA+Primer mix was prepared, containing 1 µg of total RNA, 1.25 µL oligo(dT)$_{15}$, and adjusted to 5 µL volume with nuclease-free water. The RNA+Primer mix was heated at 70 °C for 5 min, then immediately chilled on ice water for at least 5 min. The RNA+Primer mix was then quick spun on a centrifuge to gather all the liquid components, and then stored on ice.

An RT-reaction mix was then prepared as a master mix, consisting of the following for each RNA sample. A 15 µL RT-reaction mix for one reaction consisted of 4 µL of GoScript 5X Reaction Buffer, 6.4 µL of 25 mM $MgCl_2$, 1 µL of 10 mM nucleotide mix, 1 µL of GoScript Reverse Transcriptase, and 2.6 µL of nuclease-free water. An additional 10% of master mix was prepared to ensure enough RT-reaction mix for all RNA samples.

To each 5 µL RNA+Primer mix, 15 µL of RT-reaction mix was added and mixed well by pipetting. The mixture was then placed in a thermocycler and set at 25 °C for 5 min to allow annealing. Thereafter, extension was performed by increasing the temperature to 42 °C and incubating for 1 h. The Reverse Transcriptase was then deactivated at 70 °C for 15 min. The reaction mixtures containing the reverse transcribed cDNA were then ready to use for further downstream processes and were stored at -20 °C.

Quantitative PCR (qPCR)

qPCR was performed to quantify and compare gene expression of selected genes between FSiPS cells grown as monolayers or as cell-only aggregates in stirred suspension culture. For each cDNA sample which was the product of 1 µg of total RNA, a 1:10 dilution was made with nuclease-free water. The qPCR reactions were made using the Luna Universal qPCR Master Mix, following the manufacturer's instructions. Briefly, the Master Mix, gene-specific primer solutions, and cDNA samples were thawed at room temperature. Gene-specific primers are listed in

Table 2.11; *GAPDH* was used as an internal reference for normalisation. Each individual component was then separated pipetted to ensure homogeneity of the reagents and samples. Each 20 µL reaction consisted of 10 µL Luna Universal qPCR Master Mix. 0.5 µL of 10 µM forward primer, 0.5 µL of 10 µM reverse primer, 2 µL of diluted cDNA template, and 7 µL nuclease-free water. However, the assay mixes were prepared without cDNA template in a total volume required for the number of cDNA templates, plus an additional 10% to ensure enough assay mix, and pipetted to ensure homogeneity before quick centrifugation to collect the assay mix. The assay mixes were carefully pipetted into 96-well qPCR plates to minimise the formation of air bubbles. cDNA templates were then added to the qPCR plate. Each gene-cDNA combination was pipetted in triplicate. The plates were then sealed with optically transparent film such that all the edges of the wells were properly sealed to minimise artifacts due to evaporation. Sealed plates were then centrifuged for 1 min at 3,000 rpm to collect the reaction mixes and remove bubbles. The StepOne Plus instrument was then programmed with StepOne Software v2.3 to use the SYBR scan mode with Fast ramp speed and to execute the following thermocycling conditions, with a plate read included after each extension step. Data were collected and analysed with the $\Delta\Delta C_t$ method in StepOne Software v2.3, then exported and graphed in GraphPad Prism 6.

Table 2.14 Thermocycling conditions used for qPCR

Step	Temperature	Time	Cycles
Initial Denaturation	95 °C	120 s	1
Denaturation	95 °C	15 s	45
Extension	60 °C	60 s (+ plate read)	
Melt Curve	60–95 °C	5 s for each 0.5 °C increment	1

2.2.11 Metabolite analysis

Samples of spent culture medium were taken from stirred suspension cultures prior to medium addition or medium exchange. These samples were centrifuged at 900 *g* for 5 min at room temperature to pellet cells, aggregates, and debris. Thereafter, the supernatant containing the spent medium was transferred to another microcentrifuge tube for direct measurement or stored frozen at -20 °C for future analysis. Glucose and lactate concentrations were measured using a Stat Profile PRIME CCS Analyser, and data was collected and graphed in GraphPad Prism 6.

2.2.12 Small molecule withdrawal for pre-differentiation of iNSCs

BJ-iNSCs were passaged and plated on bMG-coated plates at a cell density of 1×10^5 cells/cm^2 in NIM supplemented with 10 µM Y27632 on Day -2 and incubated for 2 days. Thereafter, on Day 0 the medium was replaced with NIM without CHIR99021, SB431542, or LIF (denoted as NIM−), with daily medium exchange for another 3 days. As a control, BJ-iNSCs were also cultured in NIM for comparison.

2.2.13 Differentiation of hiPSCs into cardiovascular progenitor cells

To initiate the differentiation of hiPSCs into cardiovascular progenitor cells (CVPCs), hiPSCs were plated at 5×10^4 cells/cm^2 on hES MG-coated plates in CVPC Induction Medium (CIM) containing 5 µM Y27632. After 24 h, the medium was exchanged daily with fresh CIM for another 2 days. Thereafter, the cells were passaged by treatment with Accutase for 5 min at 37 °C, and replated on hES MG-coated plates at 1:3–1:10 split ratio using CVPC Propagation Medium (CPM) containing 5 µM Y27632. Medium was exchanged every other day with CPM, and passaged at 80% confluency using a 1:3 split ratio (Cao *et al.*, 2013).

To better support CVPC propagation and isolation, an alternative prospective approach was tested. After the first 3 days of induction of CVPCs with CIM as described above, resulting cells were replated on hES MG-coated plates at a 1:3 split ratio using the alternative CVPC Expansion Medium (BACS) with 5 µM Y27632 (Zhang *et al.*, 2016). BACS medium was exchanged every other day for up to an additional 18 days of BACS exposure before analysis.

2.2.14 Biofabrication of constructs with bioink

The preparation of hydrogels and bioinks described below were done in collaboration with Dr. Tomasz Jüngst and Annarita Di Lascio from the laboratory of Prof. Dr. Jürgen Groll, Department for Functional Materials in Medicine and Dentistry, University of Würzburg.

2.2.14.1 Generation of gelatin-alginate hydrogel and bioink

Preparation of hydrogel

Sodium alginate powder and gelatin powder were separately sterilised by overnight suspension in evaporating 70% ethanol under a sterile biosafety cabinet. The next day, sterile DPBS without Ca^{2+} was added to the powders to produce 20% (w/v) gelatin and 4% (w/v) alginate solutions. During the optimisation phases,

gelatin and alginate solutions were also dissolved in hES MG/DPBS solutions to investigate the effects of hES MG supplementation during hydrogel preparation. These solutions were incubated overnight in a 37 °C incubator to ensure that all the powders were dissolved. The next day, equal volumes of the 20% gelatin solution was mixed with the 4% alginate solution using wide-bore pipette tips or positive displacement tips, resulting in a 10% gelatin/2% alginate mixture. The 10% gelatin/2% alginate mixture was then incubated at 37 °C for at least another 1 h to remove air bubbles and allow better homogenisation of the mixture.

Preparation of hiPSCs

hiPSCs were prepared for dispensing or printing as a single cell suspension or as hiPSC aggregates. To generate single cells, hiPSCs were grown as monolayers on hES MG-coated plates until approximately 80% confluency and were subsequently treated with Accutase for 5 min at 37 °C to generate a single cell suspension. This was centrifuged at 300 *g* for 5 min to pellet the cells. The supernatant was aspirated, and the single cells were resuspended in 100 µL of DPBS without Ca^{2+}.

To generate hiPSC aggregates, a hiPSC single cell suspension was placed into a 100 mm non-tissue culture-treated Petri dish in StemMACS iPS-Brew XF supplemented with 10 µM Y27632 at a cell density of 200,000 cells/mL. This was then placed on an orbital rotator, set at 20 RPM, in the incubator. 24 h later, the small aggregates of hiPSCs that were generated (~80 µm diameter) while suspended in culture medium were centrifuged at 100 *g* for 3 min to pellet the aggregates. The culture medium was removed, and the remaining aggregates were resuspended in 100 µL of DPBS without Ca^{2+}.

Preparation of bioink

The 100 µL of hiPSCs was added into the 10% gelatin/2% alginate hydrogel as either single cells or as aggregates, and the mixture was mixed by stirring with a sterile pipette tip to evenly distribute the cells or aggregates within the hydrogel. The mixture was then transferred into a 3 mL printer syringe, sealed, and stored at 37 °C in the incubator for 15–30 min to remove air bubbles. The bioink was then ready for dispensing and printing.

2.2.14.2 Generation and culture of dispensed and printed constructs

For dispensing the non-printed reference samples, the bioink was pushed out of the syringe without a printing nozzle tip into silicone moulds to create bioink discs of

approximately 1 mm height and 6 mm diameter. For printing of the constructs, the RegenHU 3DDiscovery bioprinter was used. The bioprinter syringe containing the prepared bioinks was paired with a printing nozzle tip of internal diameter 330 µm and loaded into a cartridge heater set at 30 °C to prevent gelation. Using a pressure-assisted microvalve printhead (PH1, CF-300N/H) set at 1 bar or 3 bar pressure, the bioink was extruded from the syringe into silicone moulds to create printed bioink discs. Both the non-printed and printed bioink discs in silicone moulds were then cross-linked with an overlay of 2% (w/v) $CaCl_2$ and incubated at room temperature for 10 min. The 2% (w/v) $CaCl_2$ was then removed, and the cross-linked bioink discs were briefly washed with DPBS, and then dislodged from the silicone moulds with a spatula and transferred to 12-well plates containing pre-warmed StemMACS iPS-Brew XF. For discs made from bioink containing hiPSCs as single cells, the medium was supplemented with 10 µM Y27632, whereas discs made from bioink containing hiPSCs as aggregates were cultured without Y27632 supplementation.

To define a construct or shape to be printed, instead of printing into silicone moulds, the bioink was instead printed onto glass microscope coverslips placed on a custom chilled collector plate set at 4 °C to trigger gelation of the bioink. Square grids measuring 12 × 12 mm were printed with crosshatch infill and with 1.5 mm between printed fibres of approximately 400–450 µm thickness; these parameters were specified in Gcode using RegenHU Software Suite by Dr. Tomasz Jüngst. At the start of the printing, 1 bar pressure was used with a needle height set at 220 µm from the collector plate and the collector plate speed was set at 10 mm/s. Optimisation of these printing parameters was performed based on the quality and integrity of the printed fibres. If excessive amounts of bioink was deposited, especially around corners, then the speed was increased. In contrast, if breaks in the fibres were present during the deposition, then the speed was lowered. After printing, the glass coverslips with the printed constructs on them were lifted off the chilled collector plate and covered with 2% (w/v) $CaCl_2$ for cross-linking as previously described. The cross-linked printed constructs were then washed off the glass coverslips into 6-well plates using DPBS, and the DPBS was aspirated out from the well plate. Thereafter, fresh pre-warmed StemMACS iPS-Brew XF was pipetted into the well plates to cover the printed constructs.

Non-printed and printed bioink discs, as well as printed square grid constructs were all incubated at 37 °C in StemMACS iPS-Brew XF. One day after printing,

medium exchange was performed daily for up to 4 days, with samples imaged and analysed on day 1 and day 4 after printing.

2.2.14.3 Differentiation of printed constructs towards neuronal lineage

To assess the possibility of differentiating the hiPSCs in biofabricated constructs into neuronal cells, two consecutive protocols were applied to the biofabricated constructs; the first protocol triggered the differentiation of hiPSCs into small molecule-derived neural progenitor cells (smNPCs; Reinhardt *et al.*, 2013), and the second protocol further differentiated the smNPCs into neurons (adapted from Borghese *et al.*, 2010; Yan *et al.*, 2013), as described in the following. The biofabricated construct was removed from the regular culture medium of StemMACS iPS-Brew XF, transferred into a 35 mm Petri dish, and fed with smNPC induction medium for 2 days to start neural induction. Then, the medium was switched to N2B27 medium supplemented with 10 µM SB431542, 1 µM dorsomorphin, 3 µM CHIR99021, and 0.5 µM PMA, and incubated for another 2 days. The medium was then switched to smNPC propagation medium for 2 days, and the biofabricated construct was visually inspected for neuroepithelial outgrowth. Following that, the medium was changed to neuronal differentiation medium (NDM) and cultured for another 3 weeks, with medium exchange every other day.

After neuronal differentiation, the construct was briefly washed with DPBS with 0.9 mM Ca^{2+} and imaged. From this point on, all staining buffer and washing solutions described were supplemented with 0.9 mM Ca^{2+} to minimise dissolving the hydrogel construct. The washed construct was fixed with 4% PFA in DPBS for 20 min at room temperature, and washed twice with DPBS, then blocked and permeabilised at room temperature for 2 h in staining buffer with 0.2% Triton X-100. To label neuronal cells, the construct was incubated with βIII-tubulin (TUBB3/Tuj1) primary antibody in staining buffer with 0.2% Triton X-100 overnight at 4 °C. The following day, the primary antibody was removed from the construct, followed by two washes with DPBS. Then, the primary antibody was detected by incubation with a Cy2-conjugated secondary antibody for 2 h at room temperature. Thereafter, the construct was washed twice with DPBS, and counter-stained with 0.2 µg/mL DAPI in DPBS for 15 min protected from light, and finally washed another two times in DPBS. To control for background fluorescence, a separate sample was prepared with the secondary antibody but without the primary antibody. For imaging of unfixed and stained samples, images were taken on a fluorescence microscope at various focal

planes, and these images were processed in Adobe Photoshop to generate a focus-Z-stacked image. The focus-stacked images were then aligned and stitched together. Further overlaying of fluorescence channels and annotation were performed using FIJI.

2.2.14.4 Cell viability analysis

To visualise live and dead hiPSCs encapsulated in the gelatin-alginate hydrogel, calcein acetoxymethyl ester (calcein AM) and ethidium homodimer-1 was used to label live and dead cells respectively. Cell-loaded hydrogels were briefly washed twice with DPBS containing 0.9 mM Ca^{2+}, then covered in live-dead labelling buffer comprising 2 µM calcein AM and 2 µM ethidium homodimer-1 dissolved in DPBS with 0.9 mM Ca^{2+}, and incubated for 30 min at 37 °C in an incubator. The live-dead labelling buffer was then aspirated, and the constructs were washed twice with DPBS with 0.9 mM Ca^{2+}, covered in DPBS with 0.9 mM Ca^{2+} and then immediately imaged using a fluorescence microscope.

For the quantification of cell viability, cells and cell aggregates were firstly released from the encapsulating hydrogel by incubation with 2 mM EDTA for 25 min at 37 °C. Then, DPBS was added and the mixture was pipetted to homogenise the suspension. The cells and cell aggregates were pelleted by centrifugation at 300 *g* at 4 °C for 5 min, and the EDTA/DPBS supernatant was removed. Then, the cells and cell aggregates were incubated with Accutase for 8–10 min at 37 °C to generate a cell suspension. Then, the cell suspension was mixed with double volume DPBS, pipetted several times to homogenise. This cell suspension was then strained through a 40 µm cell strainer to remove residual undissolved hydrogel and cell clumps. Finally, the single cell suspension was labelled for viability and pluripotency marker analysis by flow cytometry as described earlier in Section 2.2.7. The cell suspension was also plated onto hES MG-coated plates for qualitative verification of cell viability and morphology analysis.

3. Results

3.1 Production of high quantities of hiPSCs

3.1.1 Expansion of hiPSCs using scalable stirred suspension culture

Numerous methods exist for the culture of hiPSCs, such as on feeder layers of mouse embryonic fibroblasts, or feeder-free conditions using various matrices such as Matrigel (MG) or vitronectin (reviewed in Chen *et al.*, 2014b). The method of choice for routine small-scale maintenance of hiPSCs in many laboratories is to culture them on hES MG-coated cell culture plasticware, which will in this thesis be referred to as standard adherent culture. Under these conditions, hiPSCs typically grow as colonies with well-defined edges and high nucleus-to-cytoplasm ratio, express pluripotency-associated markers such as the nuclear markers Nanog homeobox (NANOG), octamer-binding transcription factor 4 (OCT4), and SRY-box 2 (SOX2), as well as exhibit cell surface markers such as stage-specific embryonic antigen-4 (SSEA-4) and epitopes of podocalyxin Trafalgar-1-60 (TRA-1-60) and Trafalgar-1-81 (TRA-1-81). They are able to generate cells of all three germ layers which can be assessed using *in vitro* differentiation assays, and maintain a stable karyotype (Martí *et al.*, 2013). However, such adherent culture formats are laborious and hardly scalable to achieve the target of $>1 \times 10^9$ hiPSCs. Therefore, we sought to adopt stirred suspension culture as a bioprocessing strategy to transition from growing cells in standard adherent culture to stirred suspension culture, by optimising their culture first in 125 mL spinner flasks, and later scaling up the culture protocol to a larger 3 L bioreactor.

3.1.1.1 Adapting adherent culture to stirred suspension culture in spinners

Pilot experiment to culture hiPSCs in spinner flasks

Spinner flasks, comprising a sterile flask and magnetic stirrer, represent a versatile and reliable means to gradually scale mammalian cell cultures from standard adherent format to 3D suspension format (Chen *et al.*, 2014b). In order to inoculate a spinner flask with hiPSCs, AFiPS cells were grown under standard adherent conditions on hES MG-coated 6-well plates. On the day of inoculation, AFiPS cells were dissociated from the plate with Accutase and recovered by centrifugation. AFiPS cells were then transferred to a spinner flask in 100 mL mTeSR-1 medium supplemented with 10 µM Y27632, with a cell seeding density of 5×10^5 cells/mL. The spinner flask was incubated with the side arm caps loosened to

permit gas exchange in an incubator at 37 °C, 5% CO_2 for 2 days. For this pilot experiment, we started with a stirring rate of 65 RPM, based on a survey of the literature which suggested values of 50–90 RPM depending on cell lines, vessel shapes and volumes, and impeller designs (Amit *et al.*, 2011; Chen *et al.*, 2012; Olmer *et al.*, 2012; Pagliuca *et al.*, 2014). Thereafter, the medium was exchanged daily by allowing aggregates to sediment by gravity for 6–8 min and aspirating the supernatant while avoiding aspiration of the sedimented aggregates. This corresponded to about 70–80% of the medium being removed. Fresh medium was fed to the cells up to 100 mL, and the spinner flask was brought back into the incubator. A schematic of this pilot experiment is presented in Figure 3.1.

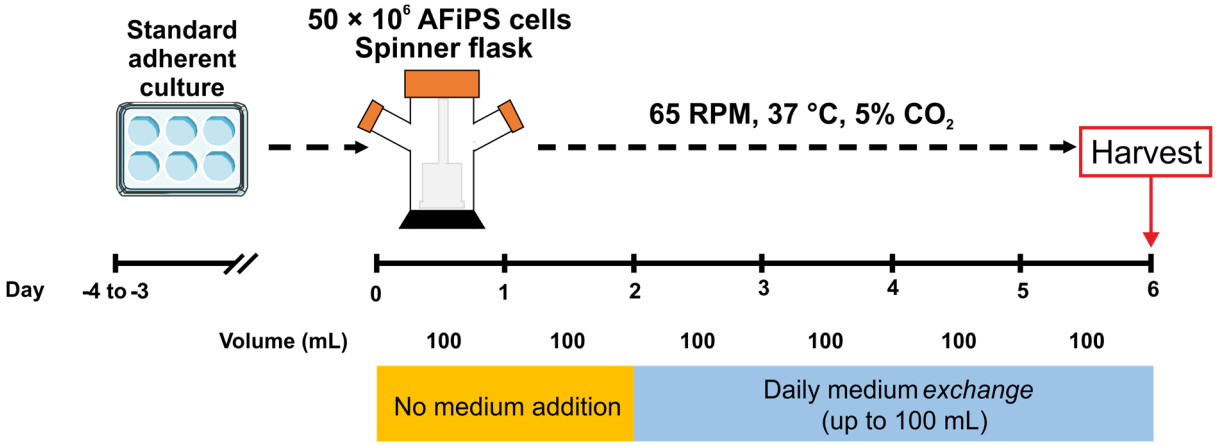

Figure 3.1 Schematic of pilot experiment to culture hiPSC in a stirred spinner flask. AFiPS cells were inoculated into a spinner flask in 100 mL mTeSR-1 supplemented with 10 µM Y27632 and 100 U/mL penicillin-streptomycin, at a cell seeding density of 5×10^5 cells/mL and stirred at 65 RPM. After 2 days, the medium was exchanged daily, with fresh medium added up to 100 mL. After a total of 6 days, the aggregates were harvested for analysis.

While aggregates could be generated using these parameters, they were of irregular shapes and appeared to have coalesced to each other to form large agglomerates of varying sizes (Figure 3.2A). The cells recovered from these aggregates after 6 days of stirred suspension culture also demonstrated the loss of the pluripotency-associated marker TRA-1-60 as shown by flow cytometry (Figure 3.2B), with only 55.4% of the cells positive for TRA-1-60. By culturing the cells from these irregular aggregates on hES MG-coated plates and further immunocytochemical analysis for the pluripotency-associated marker OCT4 (Figure 3.2C), the loss of OCT4 in a portion of these cells was also shown. Taken together, these data suggest that unintended differentiation of some of these cells had occurred during the initial suspension culture, and that optimisation steps were necessary to culture these hiPSCs in stirred suspension while preserving their pluripotency.

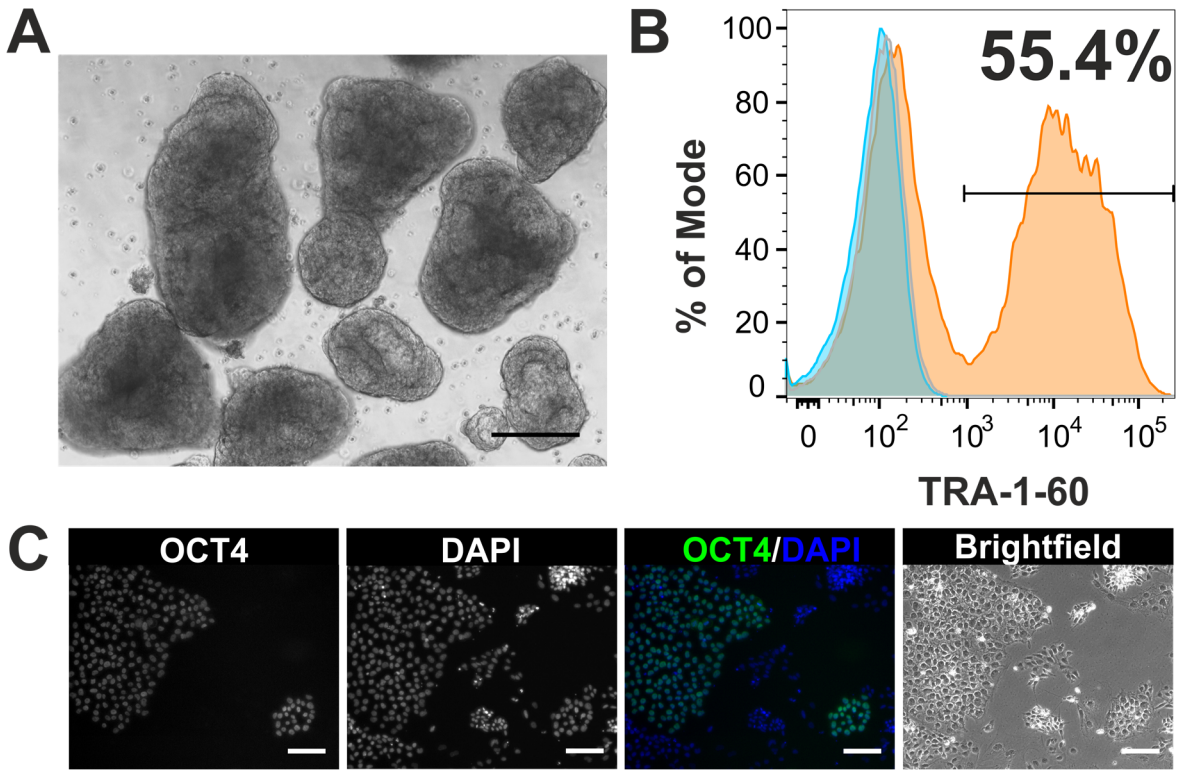

Figure 3.2 Pilot experiment to culture hiPSC in a stirred spinner flask generated sub-optimal aggregates. (A) After 3 days of suspension culture, aggregates were generated but they were of irregular shape and appeared to have fused to each other to form large agglomerates. Representative aggregates and agglomerates are shown. Scale bar = 100 µm. (B) After 6 days of suspension culture, flow cytometric analysis revealed that the pluripotency-associated marker TRA-1-60 was present on only 55.4% of cells recovered from these aggregates, suggesting that 44.6% of the cells were no longer pluripotent cells. Grey histogram: unstained control; blue histogram: isotype control; orange histogram: TRA-1-60-PE stained sample. (C) Cells from sub-optimal aggregates on day 4 were plated on hES MG-coated plates and cultured for another 3 days and then stained for OCT4. While some cells remained OCT4-positive, a significant portion of the remaining cells were negative for OCT4, suggesting a loss of pluripotency of these cells. Scale bar = 100 µm.

Recovering PSCs from heterogeneous, differentiated populations

To recover the pluripotent cells from this mix of pluripotent and differentiating/differentiated cells, we labelled pluripotent cells with TRA-1-60 or SSEA-4 antibodies conjugated to magnetic microbeads and sorted the labelled cells out with magnet-activated cell sorting (MACS). After MACS, regardless of whether the cells were sorted for TRA-1-60 or SSEA-4, the recovered cells were then analysed by flow cytometry and in both cases >95% of the recovered cells were positive for TRA-1-60 (Figure 3.3). This served as a proof-of-principle that MACS could be used to rescue pluripotent cells from a heterogeneous mixture of pluripotent and differentiating/differentiated cells if the culture conditions could not fully support the maintenance of pluripotency.

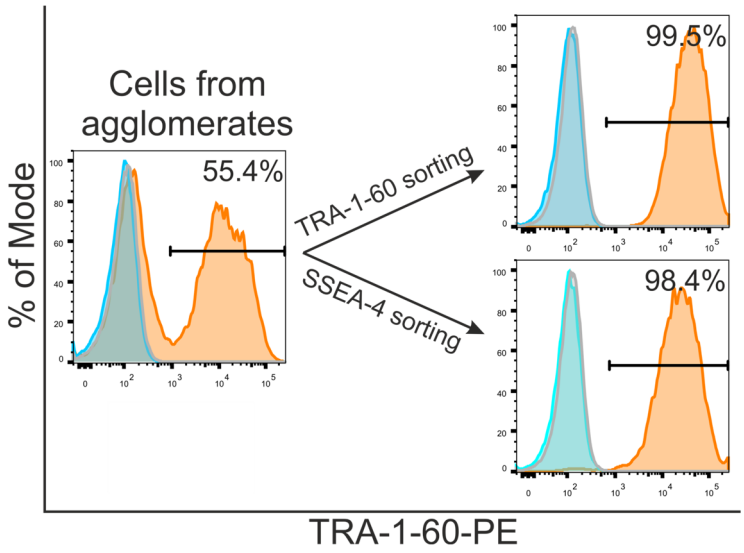

Figure 3.3 Magnet-activated cell sorting (MACS) can be used to recover pluripotent cells from a mixture of pluripotent and differentiating/differentiated cells. The mixture of pluripotent and differentiating/differentiated cells was labelled with either TRA-1-60 or SSEA-4 antibodies conjugated to magnetic microbeads. Labelled cells were captured on a magnetic column, washed, and flushed out. Flushed-out cells were then stained with TRA-1-60-PE and analysed by flow cytometry. Before MACS, 55.4% of the cells were TRA-1-60-positive. After sorting for TRA-1-60 or SSEA-4, >95% of the eluted cells were TRA-1-60-positive, illustrating the feasibility of using MACS to rescue a failing culture and to recover the remaining pluripotent cells. Grey histogram: unstained control; blue histogram: isotype control; orange histogram: TRA-1-60-PE stained sample.

These data taken together suggested that the initial process parameters, such as stirring rate and cell seeding density, were unable to maintain the pluripotency of the hiPSCs. While MACS was found to be suitable for the recovery of pluripotent cells in a differentiating culture, we aimed to find culture conditions that would support the maintenance of pluripotency and thus eliminate the need for further sorting by MACS. Therefore, optimisation of the process parameters was required. We hypothesised that the stirring rate was too low, and/or the cell seeding density was too high, resulting in coalescence of aggregates resulting in irregularly-sized aggregates. Furthermore, we reasoned that due to the large size of the aggregates, the cells in the core of the aggregates had decreased access to medium components responsible for the maintenance of pluripotency, thus resulting in spontaneous differentiation and the loss of pluripotency. Hence, we targeted the stirring rate, cell seeding density, and the medium processing procedures for further optimisation. These are highlighted in red dashed boxes in Figure 3.4.

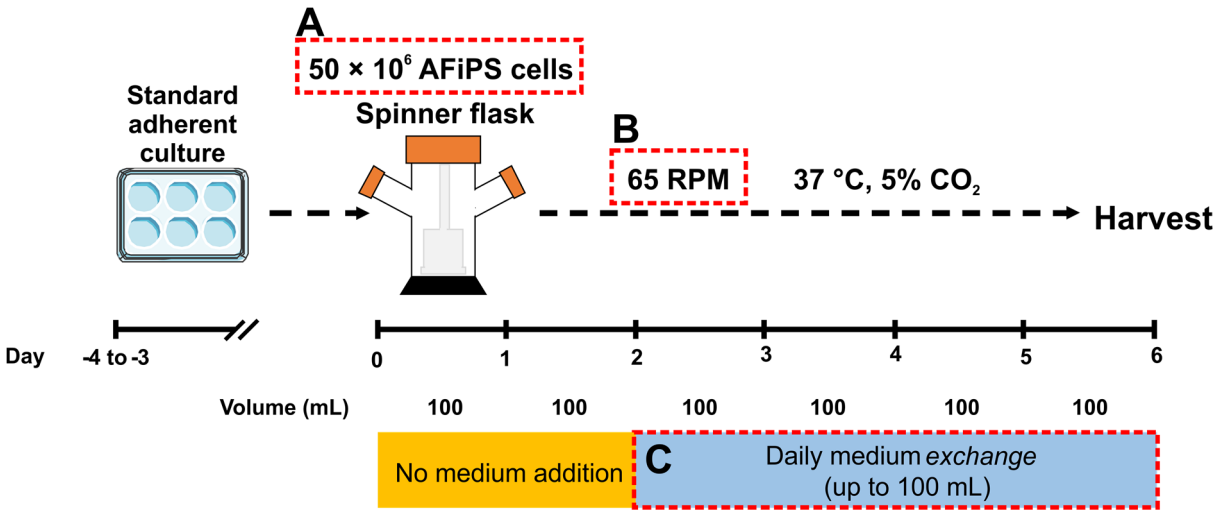

Figure 3.4 Identification of process parameters useful for optimisation of stirred suspension culture in spinner flasks. Since the pilot experiment only generated irregularly-sized aggregates with a decrease in pluripotency-associated markers, process parameters were identified that would have an impact on aggregate size. These parameters were (A) cell seeding density, (B) stirring rate, and (C) medium processing protocol.

Optimisation of stirring rate and cell seeding density

We tested two cell seeding densities: 2×10^5 cells/mL and 5×10^5 cells/mL, and a range of stirring rates from 65–85 RPM. Irregularly shaped aggregates of differing sizes were obtained at 65, 75, and 85 RPM at 5×10^5 cells/mL cell seeding density (Figure 3.5, bottom row), and a similar case was observed at 65 and 75 RPM at 2×10^5 cells/mL cell seeding density (Figure 3.5, top row). Strikingly, spherical aggregates of a more homogeneous size were generated at 85 RPM with 2×10^5 cells/mL cell seeding density.

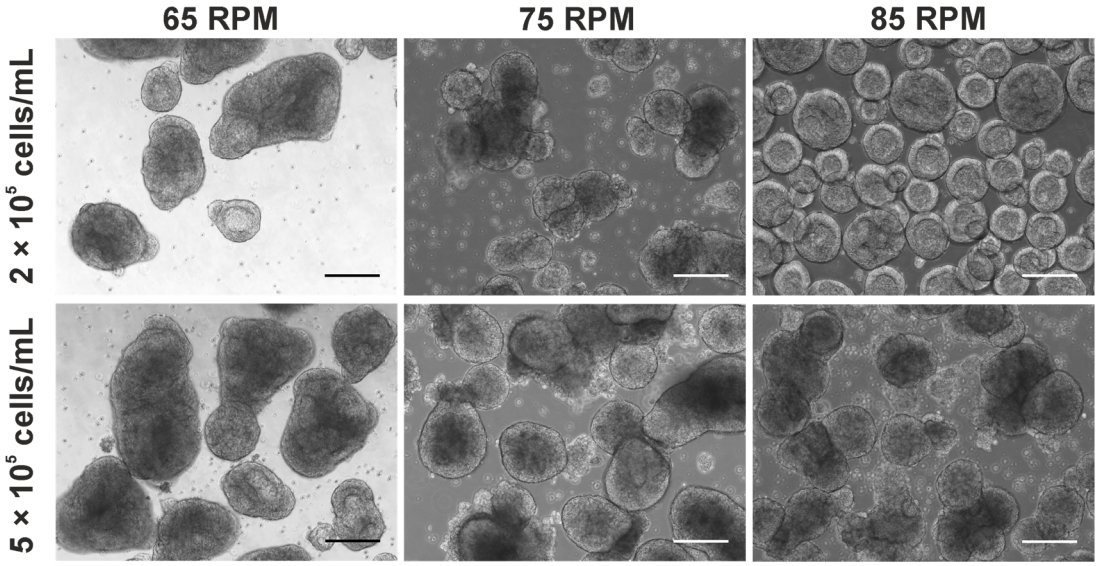

Figure 3.5 Titration of the stirring rate and cell seeding density reveals an optimal combination of parameters. Initial optimisation of stirring rate and cell seeding density was performed using the AFiPS cell line. We tested a range of different stirring rates and two cell seeding densities. We found that a cell seeding density of 2×10^5 cells/mL in a spinner flask stirred at 85 RPM proved to be ideal, generating spherical aggregates of more homogeneous diameter. Other combinations of stirring rate and cell seeding density produced irregularly shaped aggregates. Representative images of aggregates at day 3 are shown. Scale bar = 100 µm.

Optimisation of medium processing protocol

After establishing a "regular protocol" with the optimal cell seeding density (2×10^5 cells/ml) and stirring rate (85 RPM), we ran several spinner flask experiments to determine the process efficiency of the spinner flask method compared to standard adherent conditions. Process efficiency refers to the cell quantities harvested per unit of input medium. We found that stirred suspension culture with the regular protocol resulted in lower process efficiency than standard adherent culture (Figure 3.6B), with $636 \pm 24 \times 10^3$ hiPSCs/mL of medium under standard adherent conditions, in contrast to only $516 \pm 46 \times 10^3$ hiPSCs/mL of medium under stirred suspension culture with the "regular protocol" ($n=5$ per condition). To improve the process efficiency of stirred suspension culture in the spinner flasks, we aimed at reducing the medium consumption and minimising the loss of cell aggregates during medium exchange.

These two aims could be achieved by changing the medium processing protocol. The regular protocol starts with daily medium *exchange* from day 2 onwards, which involves the loss of small aggregates when removing the spent medium. In contrast, the optimised protocol uses medium *addition* on days 2 and 3, with daily medium *exchange* from day 4 onwards. This significantly reduces the total medium

consumption and reduces the loss of small aggregates. These protocols are summarised in a schematic in Figure 3.6A. By employing the "optimised protocol", we harvested 894 ± 180 × 10^3 hiPSCs/mL of medium (n=4), representing an improvement in process efficiency over both standard adherent conditions and stirred suspension with the regular protocol (Figure 3.6B).

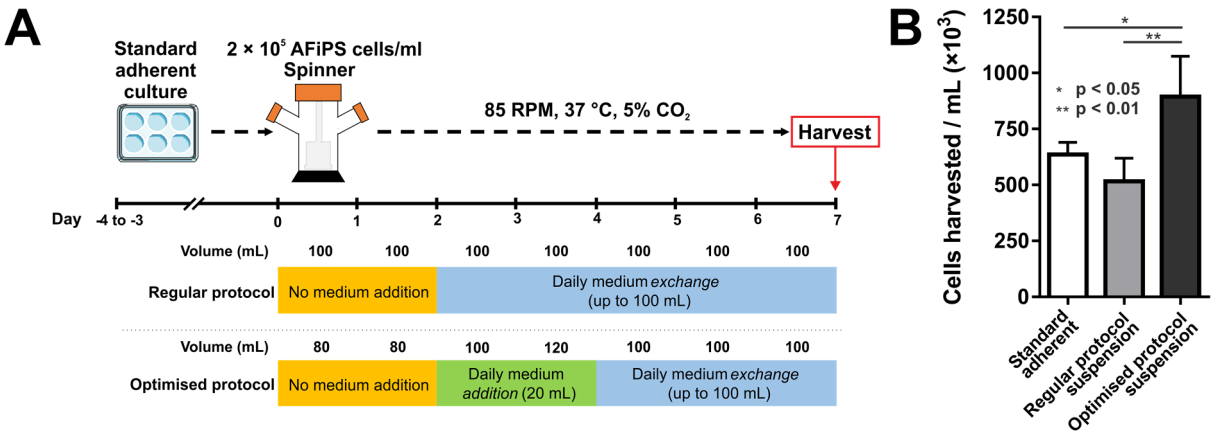

Figure 3.6 Optimisation of medium processing for stirred suspension culture results in better process efficiency over regular processing. (A) Schematic outlining differences between regular and optimised medium processing protocols. The key difference of the optimised protocol is the medium *addition* on days 2 and 3 (highlighted in green), whereas the regular protocol starts medium *exchange* on day 2. (B) Under standard adherent conditions, we harvested 636 ± 24 × 10^3 hiPSCs/ml of medium (n=5), representing a higher process efficiency than stirred suspension culture using the regular protocol for medium processing where we could only harvest 516 ± 46 × 10^3 hiPSCs/ml of medium (n=5). By changing the medium processing to the optimised protocol, the process efficiency was dramatically increased, as evidenced by the 894 ± 180 × 10^3 hiPSCs/ml of medium (n=4) that was harvested.

In spinners, FSiPS aggregates of 95 ± 17 µm diameter on day 2 grew into aggregates measuring 343 ± 76 µm on day 7, representing an increase in cell number from 21 ± 3 × 10^6 cells on day 2 and 204 ± 17 × 10^6 cells on day 7. Similarly, AFiPS aggregates measuring 112 ± 22 µm diameter on day 2 grew to 305 ± 61 µm on day 7, corresponding to a total cell number of 21 ± 0.3 × 10^6 cells on day 2 and 252 ± 8 × 10^6 cells on day 7. The growth curves and diameter development over time are presented in Figure 3.7. These data represent three biological replicates per cell line per day, with a minimum of 100 aggregates measured per cell line per day.

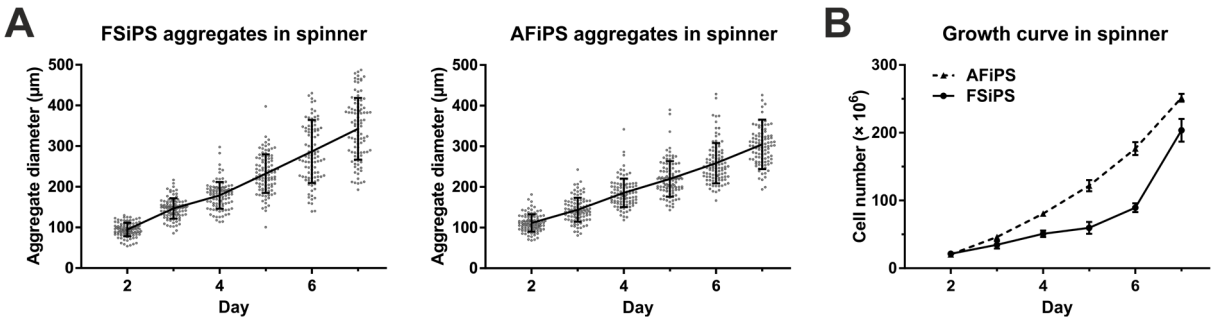

Figure 3.7 FSiPS and AFiPS cells proliferate as aggregates when cultured in spinners. (A) Both FSiPS and AFiPS aggregates grow over the course of one passage of 7 days. FSiPS aggregates grew from 95 ± 17 µm diameter on day 2 to 343 ± 76 µm on day 7, while AFiPS aggregates grew from 112 ± 22 µm diameter on day 2 to 305 ± 61 µm on day 7. (B) Cell quantities were counted over the course of one passage of 7 days. FSiPS grew from 21 ± 3 × 10^6 cells on day 2 to 204 ± 17 × 10^6 cells on day 7, whereas AFiPS grew from 21 ± 0.3 × 10^6 cells on day 2 and 252 ± 8 × 10^6 cells on day 7. Data from three biological replicates per cell line are shown, with a minimum of 100 aggregates measured per cell line per day.

3.1.1.2 Impact of cell culture additives on hiPSC growth

After optimising stirred suspension cultures in spinner flasks, to demonstrate scalability of the technique, we used 3 L bioreactors coupled to an ezControl controller. However, stirred suspension culture in bioreactors can differ significantly from standard adherent culture and spinner culture in terms of degree of environment sterility, shear stress on cells, and method of aeration of the culture medium. For example, in standard adherent culture the medium is sufficiently aerated through the overlaying, ambient air within the incubator due to a relatively high ratio of liquid-air interface area to volume. However, in a bioreactor this ratio is lower by more than an order of magnitude since the volume in a bioreactor is much higher. Therefore, the culture medium could require aeration by gas sparging to maintain cell viability. In a trial medium-only run with gas sparging through a bottom air inlet, foam was generated after overnight sparging (Figure 3.8), highlighting the possibility that antifoaming reagents could be required. As the bioreactor and controller were placed in the open in a laboratory, the risk of contamination was increased compared to a more controlled environment such as that within a cell culture incubator. These differences warranted an investigation into cell culture additives that could be required in sparged bioreactors.

Figure 3.8 Bioreactor with medium aerated by controlled gas sparging overnight results in significant foaming. A trial run using the bioreactor with only medium and no cells inoculated was carried out overnight with gas sparging as the aeration method to maintain dissolved oxygen (DO) levels. Gas sparging resulted in excessive formation of foam, indicating that measures to reduce or eliminate foam formation could be necessary. The bioreactor in this setup was maintained at 37 °C, with a stirring rate of 75 RPM.

Here we tested penicillin-streptomycin to prevent contamination, Poloxamer 188 to reduce shear stress, and antifoam C to prevent excessive formation of foam. To assess the impact of these cell culture additives on hiPSC growth, we cultured AFiPS cells under standard adherent conditions in mTeSR-1 medium only or mTeSR-1 supplemented with penicillin-streptomycin (50 or 100 U/mL), Antifoam C (37.5 ppm; Kehoe *et al.*, 2010), or Poloxamer 188 (0.02% w/v; Murhammer and Goochee, 1990) and monitored their growth over 6 days. At these additive concentrations, we did not observe any major change in growth kinetics compared to AFiPS cells cultured in mTeSR-1 only (Figure 3.9A). Additionally, no obvious morphological changes could be discerned between the AFiPS cells growing under all tested conditions (Figure 3.9B), suggesting that the additives did not significantly stimulate differentiation or stress the cells under adherent conditions.

While these additives were tested for potential toxic or other negative effects on hiPSCs, these additives were ultimately not required for the scaled-up bioreactor cultures. Sterility of the setup was maintained through gas line filters and tube welding systems, and gas sparging of the culture medium was not required as a gas overlay was adequate to permit cell growth, thus resulting in minimal formation of foam.

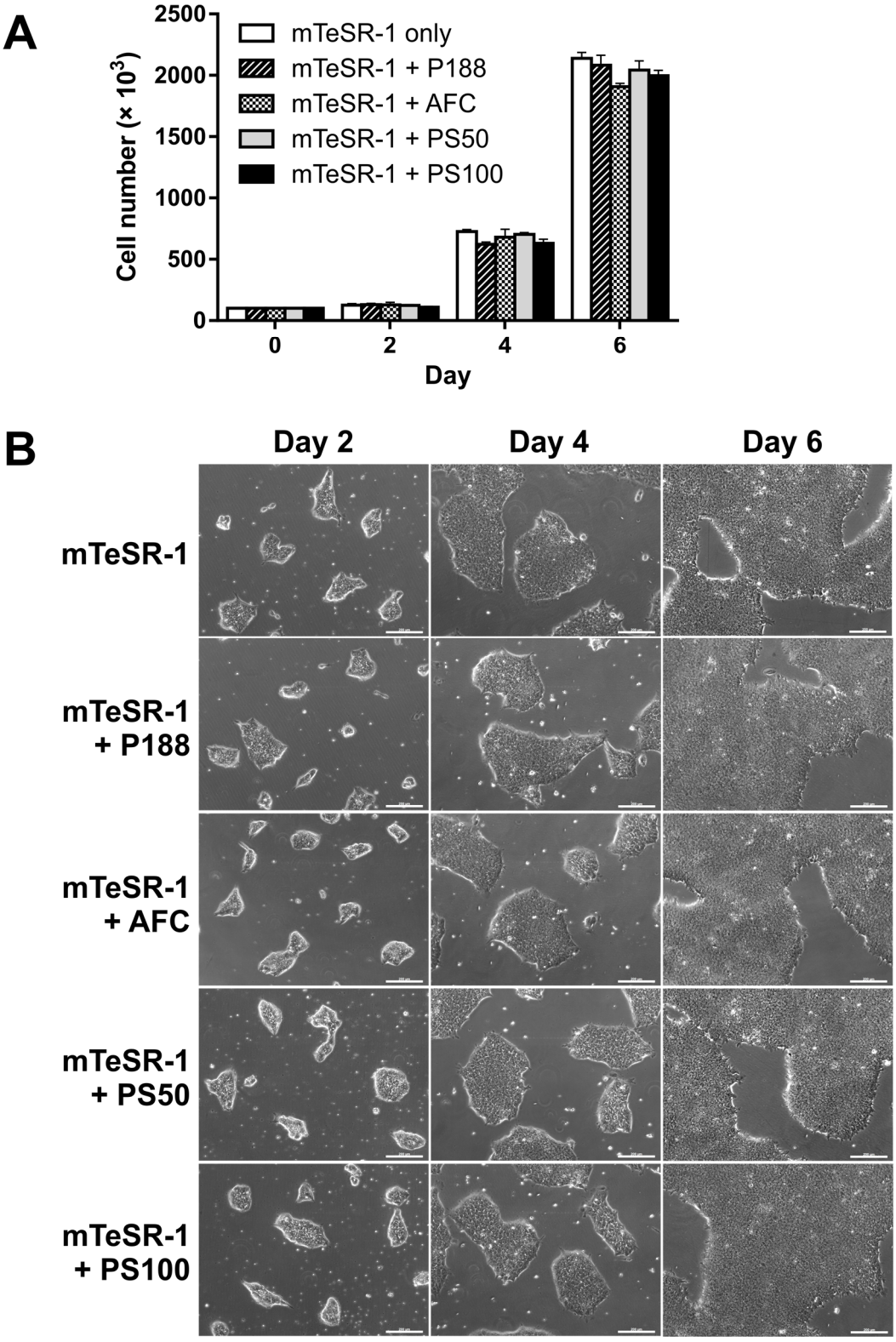

Figure 3.9 Additives potentially required for stirred suspension culture do not have a major impact on hiPSCs. hiPSCs were cultured over 6 days under standard adherent conditions with mTeSR-1 medium supplemented with or without cell culture additives. (A) No large differences between the growth kinetics of the cells with or without additives could be observed. Data represent mean ± S.D. of 3 replicates per condition per day. Results using AFiPS cells are presented. (B) hiPSCs cultured with or without additives exhibited typical hiPSC morphology, with high nuclear to cytoplasm ratios and sharp, well-defined colony edges. Scale bar = 200 µm. P188: 0.02% w/v Poloxamer 188; AFC: 37.5 ppm Antifoam C; PS50: 50 U/mL penicillin-streptomycin; PS100: 100 U/mL penicillin-streptomycin.

3.1.1.3 Scaling up the production of hiPSCs in bioreactors

After optimising the stirring parameters in spinner flasks, we were able to successfully culture hiPSCs as aggregates. With the cell quantities generated per spinner, reaching the target of >10^9 cells would require 4–5 spinners for each cell line. However, to demonstrate the scalability of the stirred suspension culture technique, the culture volume was scaled up while remaining at the same cell seeding density of 200,000 cells/mL. After treating the aggregates generated in spinners with Accutase, the resulting cell suspension was used as inoculum for culture in bioreactors (Figure 3.10).

However, the pilot experiment to generate aggregates in a bioreactor resulted in aggregates of heterogeneous diameter, with many small aggregates (~40 µm) and a few unusually large aggregates (>100 µm diameter). As illustrated in the top panels of Figure 3.11, when the cell suspension generated through Accutase treatment was directly seeded into medium without straining the cell suspension through a 40 µm cell strainer, small cell clumps could be found in the cell suspension (white arrowhead), which then grew into much larger aggregates by day 2. On day 2, a few large aggregates (~100 µm diameter) could be observed while most aggregates were 40–50 µm in diameter. To reduce the large variability in aggregate size, the cell suspension generated through Accutase treatment was first strained through a cell strainer to remove small cell clumps, which resulted in a more homogeneous single cell suspension. This resulted in a more homogeneously sized aggregate population after 2 days of bioreactor culture (bottom panels, Figure 3.11).

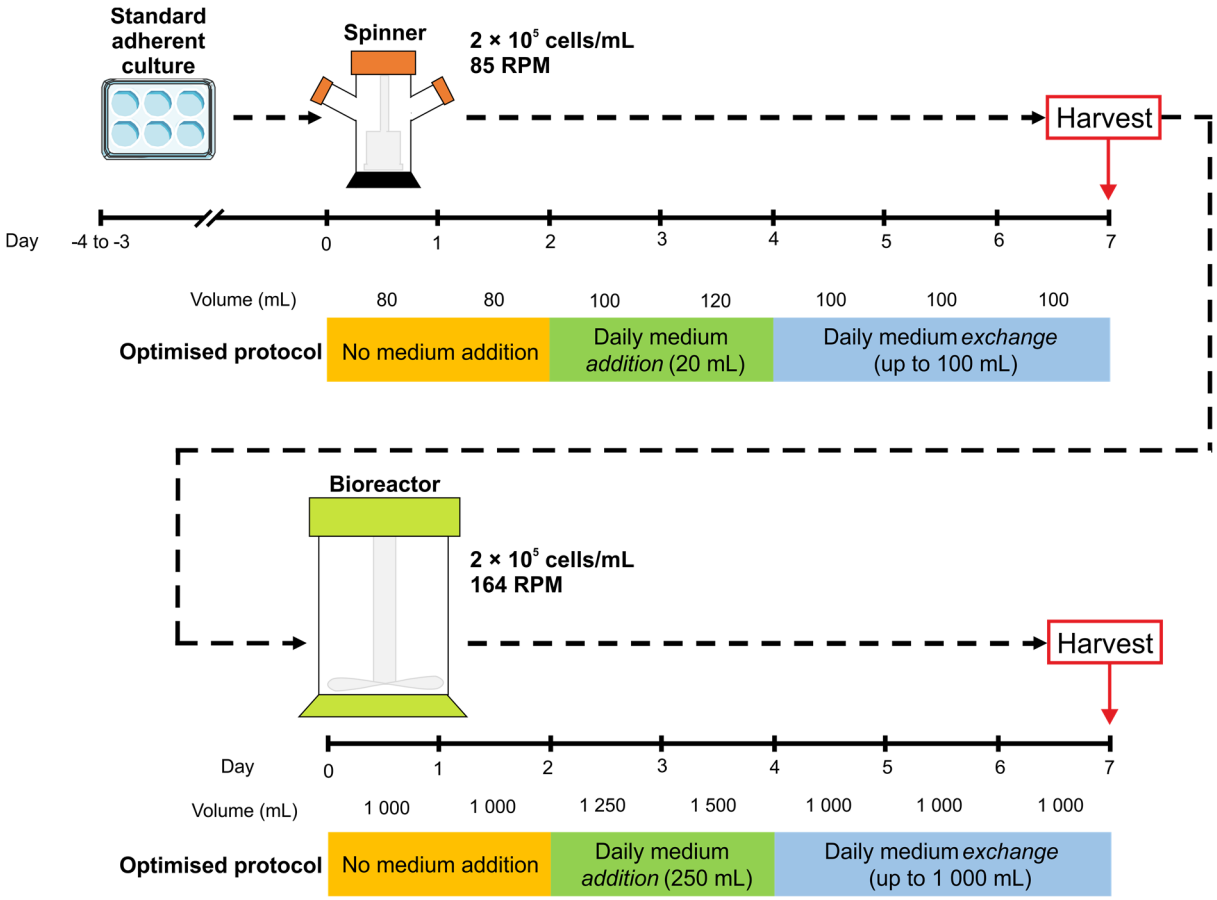

Figure 3.10 Schematic overview of stirred suspension culture and medium processing strategy for sequential expansion of hiPSCs in spinners then bioreactors. Starting from one confluent 6-well plate of hiPSCs grown in standard adherent culture, 16 × 10^6 cells were seeded into a spinner in 80 mL of mTeSR-1 medium (i.e. 200,000 cells/mL) supplemented with 10 µM Y27632, and stirred at 85 RPM in a 37 °C incubator. After 2 days of culture, 20 mL of fresh pre-warmed culture medium was *added* to bring the volume up to 100 mL. After another day, another 20 mL of culture medium was *added*. Thereafter, medium was *exchanged* daily and maintained at 100 mL culture volume for the following 3 days. After a total of 7 days of spinner culture, hiPSC aggregates were harvested and treated with Accutase to generate a cell suspension. This cell suspension was then brought into a bioreactor at the same cell seeding density of 200,000 cells/mL. The cells were cultured using the same medium processing approach of 2 days without medium addition, then 2 days of daily 250 mL medium *addition*, followed by 3 days of daily medium *exchange* up to 1,000 mL culture volume.

As shown in Figure 3.12, in bioreactors, FSiPS aggregates of 44 ± 8 µm diameter on day 2 grew to 197 ± 55 µm diameter on day 7, corresponding to a total cell number of 243 ± 31 × 10^6 cells on day 2 and 1,587 ± 99 × 10^6 cells on day 7. AFiPS aggregates measuring 54 ± 9 µm diameter on day 2 grew to 198 ± 62 µm diameter on day 7, representing a total cell number of 267 ± 7 × 10^6 cells on day 2 and 1,987 ± 86 × 10^6 cells on day 7. Four technical replicates per cell line per day were counted, with a minimum of 100 aggregates measured per cell line per day. In both hiPSC lines, the final harvest on day 7 of bioreactor culture yielded >1 × 10^9 cells per bioreactor, which was the targeted cell quantity.

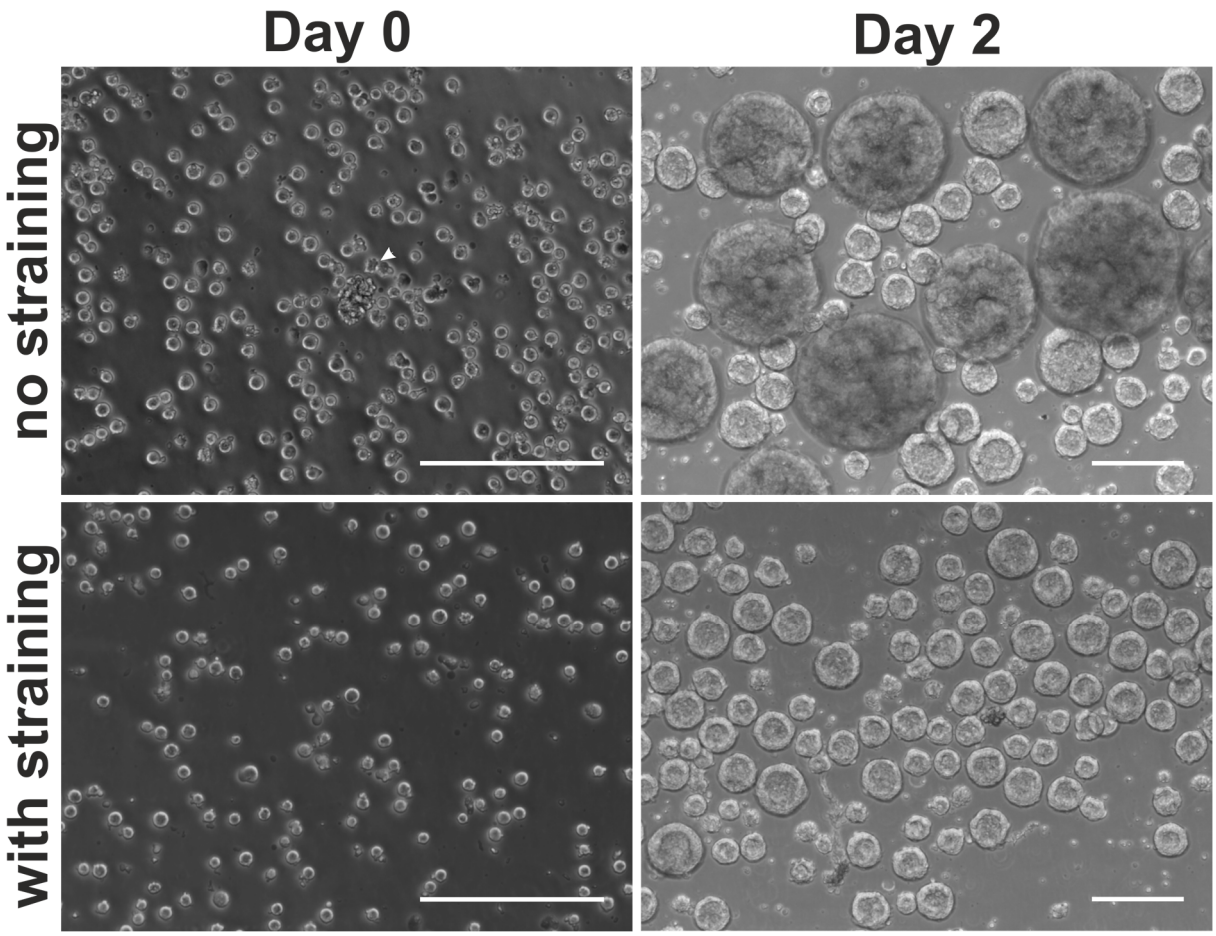

Figure 3.11 Straining cell suspensions to remove cell clumps before seeding into stirred suspension vessels improves size homogeneity of resultant aggregates. When cell suspensions generated by Accutase treatment of aggregates were directly seeded into culture medium in suspension culture vessels, some small cell clusters remained (white arrowhead). This gave rise to unusually large aggregates detectable on day 2. By straining the cell suspension through a cell strainer, cell clumps could be removed from the cell suspension, which resulted in a more homogeneous population of hiPSC aggregates. Scale bars = 100 µm.

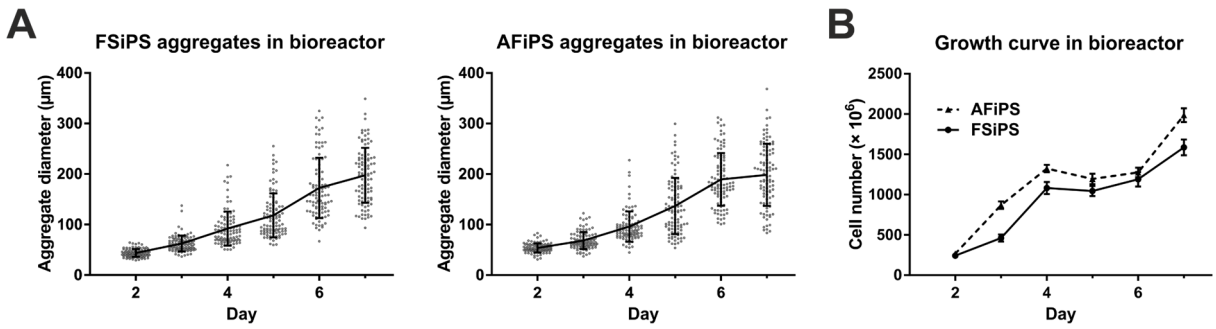

Figure 3.12 FSiPS and AFiPS cells proliferate as aggregates when cultured in bioreactors. (A) Both FSiPS and AFiPS aggregates grow over the course of one passage of 7 days. FSiPS aggregates grew from 44 ± 8 µm diameter on day 2 to 197 ± 55 µm on day 7, while AFiPS aggregates grew from 54 ± 9 µm diameter on day 2 to 198 ± 62 µm on day 7. (B) Cell quantities were counted over the course of one passage of 7 days. FSiPS grew from 243 ± 31 × 10^6 cells on day 2 to 1,587 ± 99 × 10^6 cells on day 7, whereas AFiPS grew from 267 ± 7 × 10^6 cells on day 2 to 1,987 ± 86 × 10^6 cells on day 7. Data from four technical replicates per cell line are shown, with a minimum of 100 aggregates measured per cell line per day.

To show that hiPSCs can be cultured as aggregates for extended periods of time, hiPSCs were serially passaged and expanded in spinners for 7 passages, with 7 days of culture between each passage. At the end of each passage, cells were counted and analysed by flow cytometry for viability and expression of pluripotency-associated markers. Both FSiPS and AFiPS cells could be serially expanded over 7 passages and showed stable and consistent proliferation. At the end of each passage, flow cytometric analysis showed that viability of the resulting cells was consistently >90%, and >90% of the cells co-expressed pluripotency markers TRA-1-60 and SSEA-4, suggesting that pluripotency and viability of the cells was maintained after 7 consecutive passages in stirred suspension culture in spinners (Figure 3.13).

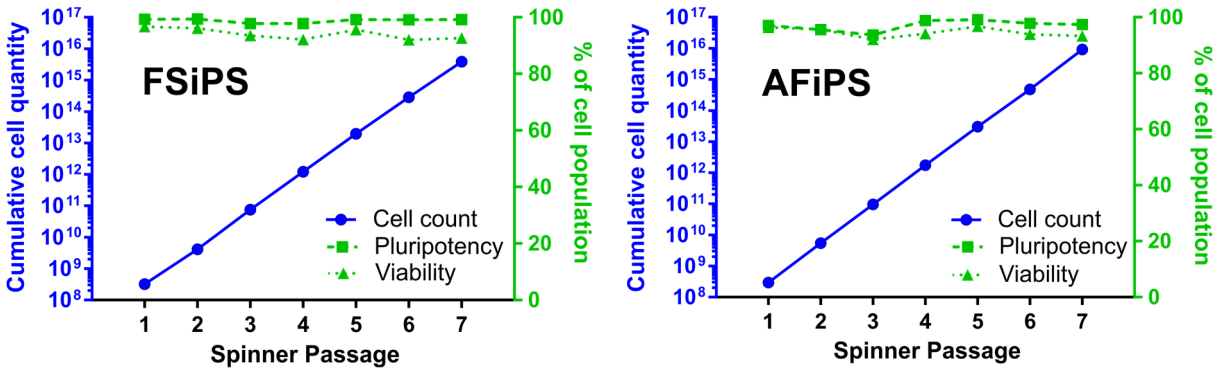

Figure 3.13 hiPSCs can be serially cultured as aggregates in stirred suspension culture for at least 7 weeks/passages. Both FSiPS and AFiPS showed stable proliferation over 7 passages in stirred suspension culture in spinners. At the end of each passage, cells were analysed by flow cytometry to quantify the fraction of viable and pluripotent cells remaining in the culture. Viability was consistently above 90%, and of the viable cells, >90% of them were double-positive for the pluripotency-associated markers TRA-1-60 and SSEA-4.

3.1.2 Characterisation and quality control of hiPSCs

To characterise a newly generated PSC line and to perform quality control on an existing PSC line, a battery of assays can be applied (Martí *et al.*, 2013). For example, the presence of pluripotency-associated markers can be examined by immunocytochemistry and flow cytometry, and the differentiation capacity of the PSC line to all three germ layers can be verified using undirected differentiation followed by analysis using immunocytochemistry. In the following, characterisation of a newly-generated hiPSC line (BJiPS) grown under standard adherent conditions is described. Similarly, the suite of tests was also applied to bioreactor-expanded FSiPS and AFiPS lines to demonstrate the maintenance of PSC quality after expansion in spinner flasks and bioreactors.

3.1.2.1 Characterisation of a hiPSC line in adherent culture

Immunocytochemical analysis revealed that BJiPS cells exhibit a range of pluripotency-associated markers NANOG, OCT4, SOX2, SSEA-4, and TRA-1-81 (Figure 3.14). The fraction of pluripotent cells in the BJiPS cultures was quantified using flow cytometry by labelling two pluripotency-associated surface markers SSEA-4 and TRA-1-60, which showed that >98% of the cells in the BJiPS cultures are double-positive for these two markers (Figure 3.15).

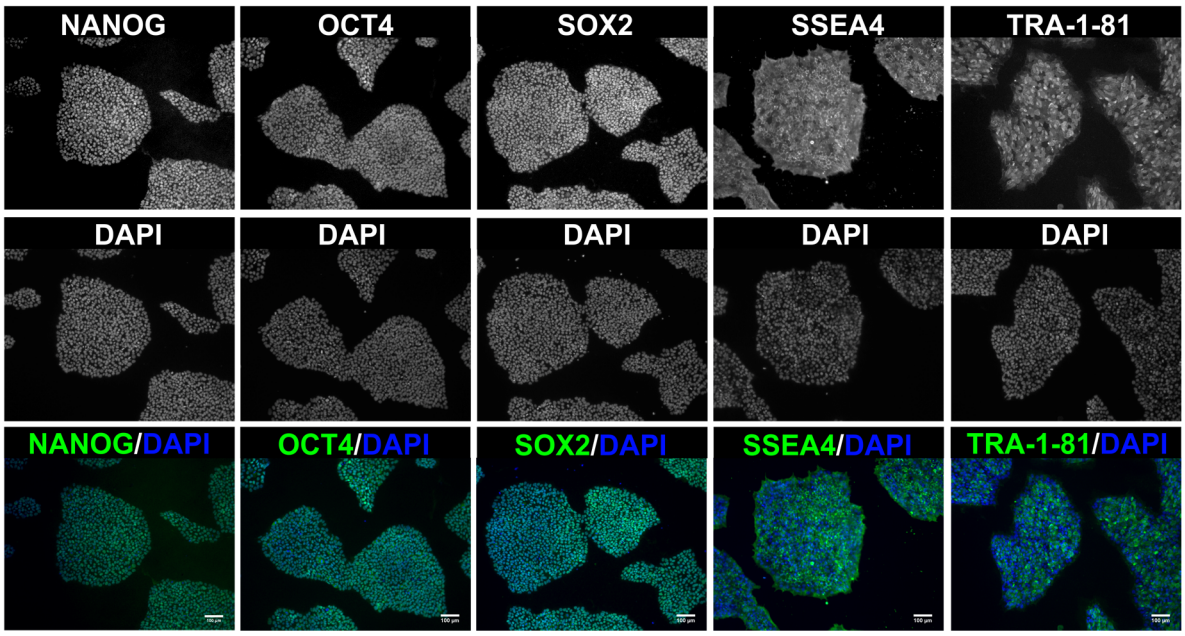

Figure 3.14 hiPSCs are positive for typical pluripotency-associated markers in standard adherent culture on hES MG-coated plates. hiPSCs express nuclear pluripotency-associated markers NANOG, OCT4, and SOX2, and exhibit cell surface pluripotency-associated markers SSEA-4 and TRA-1-81. Cell nuclei were counter-stained with DAPI. Scale bars = 100 µm.

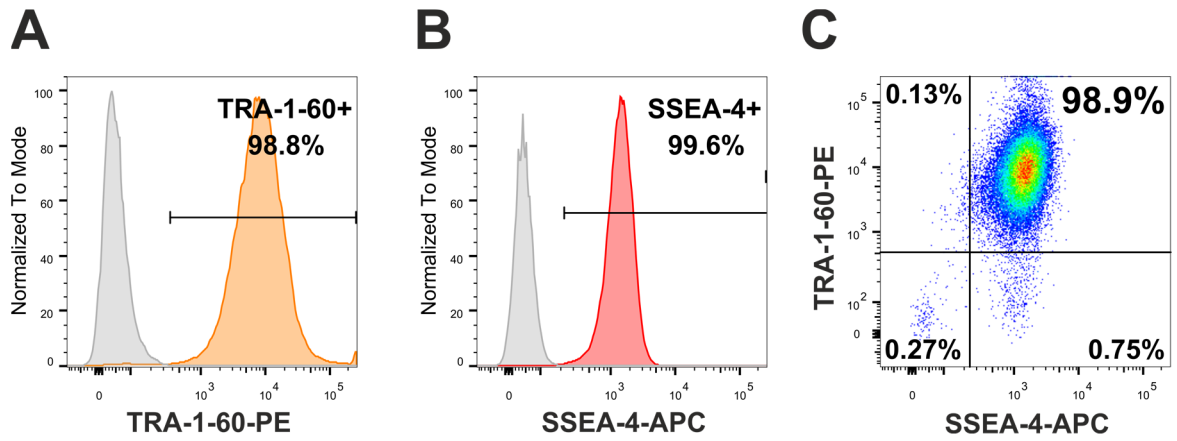

Figure 3.15 Flow cytometric analysis of hiPSCs cultured under standard adherent conditions reveal high homogeneity in presence of surface pluripotency-associated markers. BJiPS cells were co-stained for the cell surface pluripotency-associated markers TRA-1-60 and SSEA-4. (A) >98% of the cells are TRA-1-60-positive, and (B) >99% of the cells are SSEA-4 positive; grey peaks represent fluorophore-matched isotype controls. (C) >98% of the cells are double-positive for SSEA-4 and TRA-1-60.

To verify trilineage potential, BJiPS cells were cultured in undirected differentiation medium for a total of 28 days. The heterogeneous mix of cells was then analysed by immunocytochemistry to identify representative cells from each of the three germ layers. As shown in Figure 3.16, BJiPS cells can differentiate into cells positive for AFP, which was used as a marker of endodermal differentiation. Similarly, cells positive for SMA, a marker of mesodermal differentiation, or TUBB3, a marker of ectodermal differentiation, could be found in this mix of cells. This suggested that BJiPS cells possess trilineage potential as expected of PSCs.

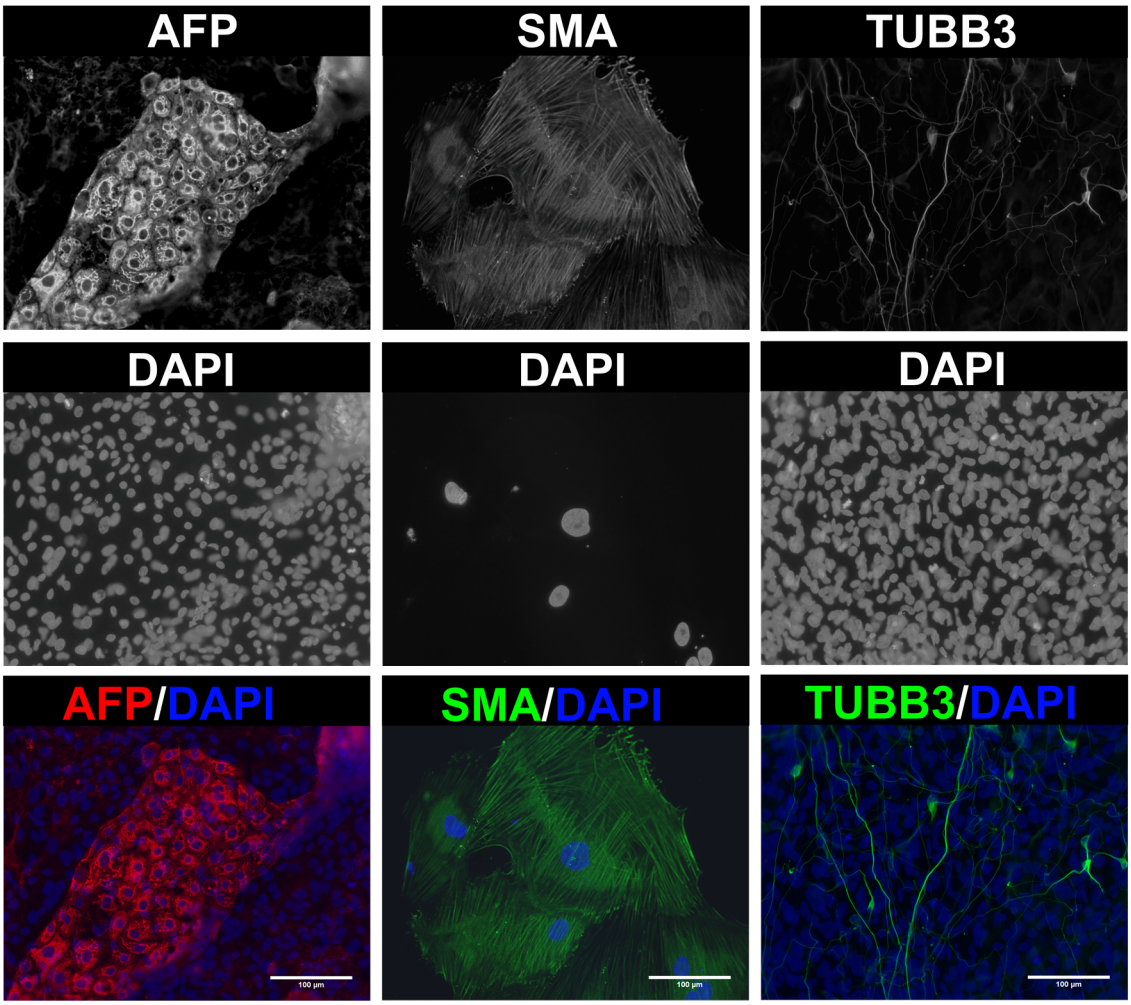

Figure 3.16 hiPSCs cultured under standard adherent conditions can be differentiated into all three germ layers. Cells were cultured in undirected differentiation medium for 28 days to allow differentiation into different germ layers. After differentiation, cells were stained for representative markers of the three germ layers. In this highly heterogeneous mixture of cells, AFP-positive (endodermal), SMA-positive (mesodermal), or TUBB3-positive (ectodermal) cells can be detected. Cells shown were differentiated from BJiPS cells. Scale bars = 100 µm.

3.1.2.2 Characterisation of bioreactor-expanded hiPSCs

Pluripotency-associated marker analyses of bioreactor-expanded hiPSCs

To verify the maintenance of pluripotency after sequential expansion in spinner flasks and then bioreactors, aggregates from the bioreactor were harvested and dissociated into a single cell suspension with Accutase. The single cell suspension was used for various downstream analyses as described below.

Firstly, the cells were analysed by flow cytometry using fluorescently-labelled antibodies against the pluripotency-associated surface markers TRA-1-60 and SSEA-4 (Figure 3.17). We included unstained and isotype controls to ensure the specificity of the immunolabelling. For both AFiPS and FSiPS lines, typically >95% of cells were double positive for both TRA-1-60 and SSEA-4, suggesting the maintenance of pluripotency of bioreactor-expanded hiPSCs.

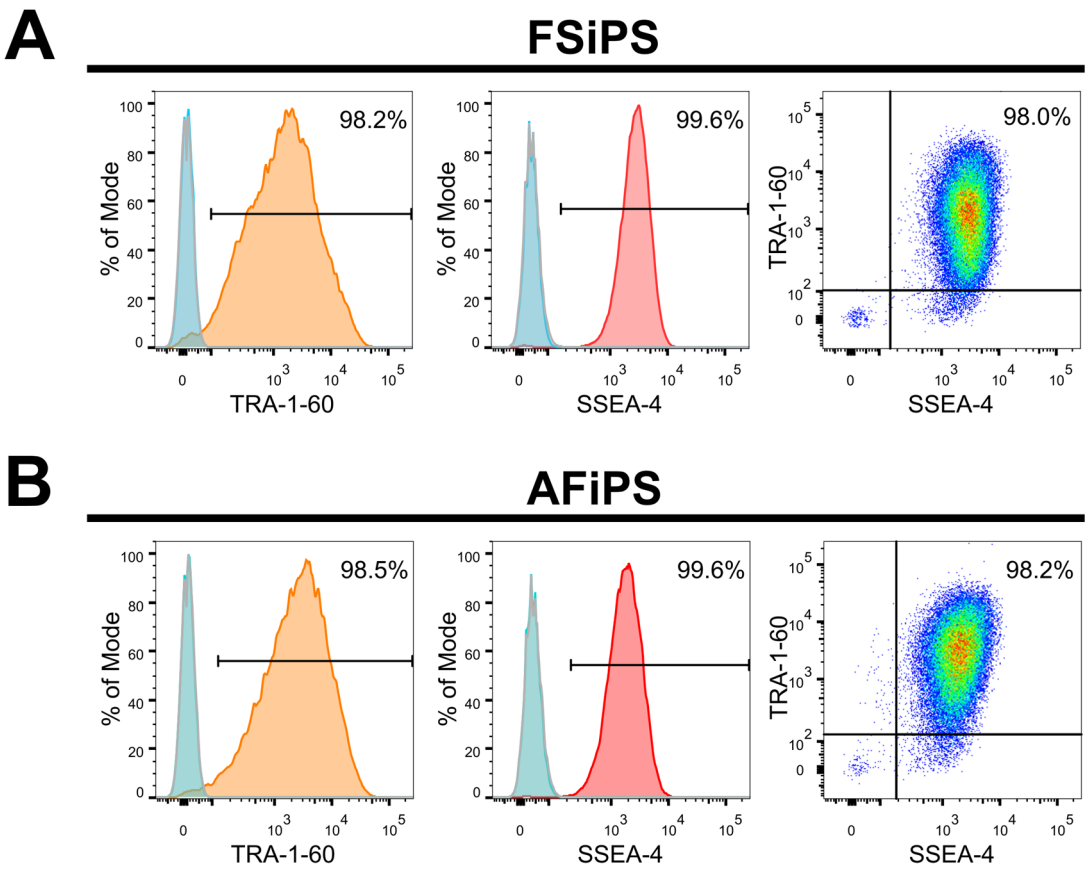

Figure 3.17 Bioreactor-expanded hiPSCs exhibit pluripotency-associated cell surface markers as assessed by flow cytometry. Aggregates grown in bioreactors were dissociated into a single cell suspension before staining for analysis by flow cytometry. Cells were stained for the pluripotency-associated surface markers TRA-1-60 (orange histograms) and SSEA-4 (red histograms). Unstained controls (grey histograms) and isotype controls (light blue histograms) were included to ensure a specific signal. Typically, for both the FSiPS (A) and AFiPS (B) cell lines, >95% of cells are positive for TRA-1-60, >99% of cells are positive for SSEA-4, and >95% are double positive for both markers. Representative histograms and density plots are shown.

Next, the cells were plated onto glass coverslips coated with hES MG for further immunocytochemical analysis (Figure 3.18). Cells were stained with an expanded panel of pluripotency-associated markers: for the surface markers, SSEA-4 or TRA-1-81 were stained; for the nuclear transcription factor markers, we stained for OCT4 or SOX2. In close agreement with the flow cytometry data, almost all the plated cells were positive for the expanded panel of pluripotency markers, suggesting the maintenance of a pluripotent state.

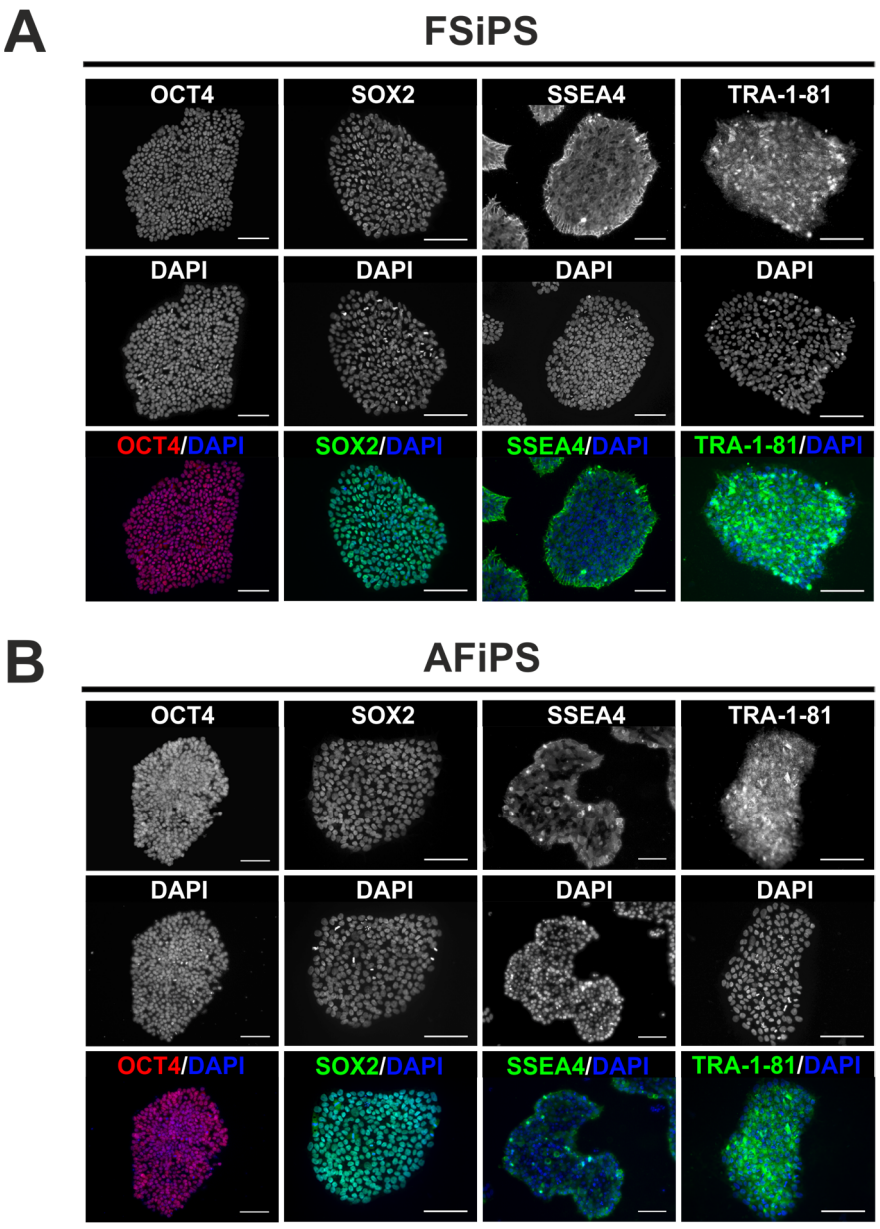

Figure 3.18 Bioreactor-expanded hiPSCs express various pluripotency-associated markers as assessed by immunocytochemical analyses. Aggregates grown in bioreactors were dissociated into a single cell suspension before plating onto hES-qualified Matrigel-coated glass coverslips and cultured for up to 3 days. FSiPS colonies (A) and AFiPS colonies (B) are both homogeneously positive for the nuclear pluripotency-associated markers OCT4 and SOX2, as well as the surface pluripotency-associated markers SSEA-4 and TRA-1-81. Cells were counterstained with DAPI to label nuclei. Scale bars = 100 µm.

Furthermore, we performed qRT-PCR to compare, at the transcript level, both pluripotency- and differentiation-associated markers in the FSiPS line grown in bioreactors to those grown under standard adherent conditions (Figure 3.19). We found high expression levels of the pluripotency markers *OCT4* (endogenous) and *NANOG* in both bioreactor-grown and standard adherent-grown FSiPS cells with no significant difference between them. Similarly, we found very low to no expression of the differentiation-associated markers *AFP* (endoderm), *T* (mesoderm), and *SOX1* (ectoderm), in both bioreactor-grown and standard adherent-grown FSiPS cells with no significant difference between them.

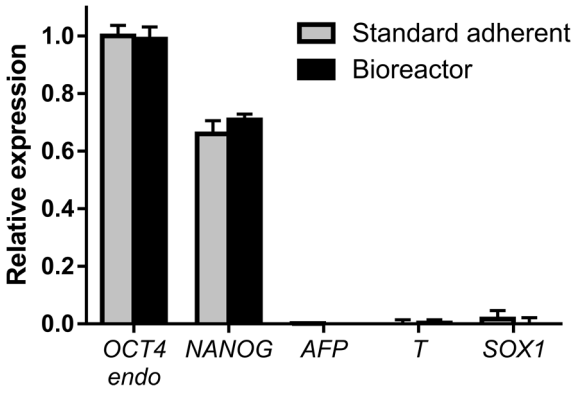

Figure 3.19 Similar levels of pluripotency- and differentiation-related marker transcripts are detected between bioreactor- and standard adherent-grown FSiPS cells. Expression of pluripotency markers *OCT4* (endogenous) and *NANOG* was high in both standard adherent FSiPS and bioreactor FSiPS, with no significant difference between the two. Expression of differentiation-associated markers *AFP* (endoderm), *T* (mesoderm), and *SOX1* (ectoderm) was very low or undetectable in both standard adherent FSiPS and bioreactor FSiPS, with no significant difference between the two. Gene expression was normalised to standard adherent FSiPS *OCT4* (set to 1), with *GAPDH* used as an internal reference. Data presented represents 3 technical replicates.

Differentiation-based analyses of bioreactor-expanded hiPSCs

A defining feature of pluripotency is the ability to further differentiate into cell types of all the three germ layers, namely the endoderm, mesoderm, and ectoderm. To assess this *in vitro*, we collected bioreactor-expanded aggregates and applied undirected differentiation on them for a total of 3–4 weeks. Both FSiPS and AFiPS cell lines expanded in bioreactors can differentiate into cells from all three germ layers, using AFP (endoderm), SMA (mesoderm), and TUBB3 (ectoderm) as markers for the indicated lineages (Figure 3.20).

Additionally, to examine whether bioreactor-expanded hiPSCs continued to be able to respond to specific differentiation cues, we applied a directed cardiomyocyte differentiation protocol on bioreactor-expanded FSiPS cells to generate cardiomyocyte-like cells. After cardiomyocyte differentiation for 8 days, FSiPS cells developed into spontaneously beating sheets of cells (Figure 3.21A,

Movie 1). Cardiac enrichment using glucose-depleted, lactate-based medium was then applied, and the resulting cells were re-plated. The remaining cells after enrichment continue to exhibit spontaneous contraction (Figure 3.21B, Movie 2), and express the cardiomyocyte-related markers cardiac troponin T2 (TNNT2) and alpha sarcomeric actinin (ACTN2) (Figure 3.21C). Analysis with flow cytometry showed that after cardiac enrichment, about 90% of the cells are positive for TNNT2 or the surface marker signal regulatory protein alpha (SIRPA; Figure 3.21D).

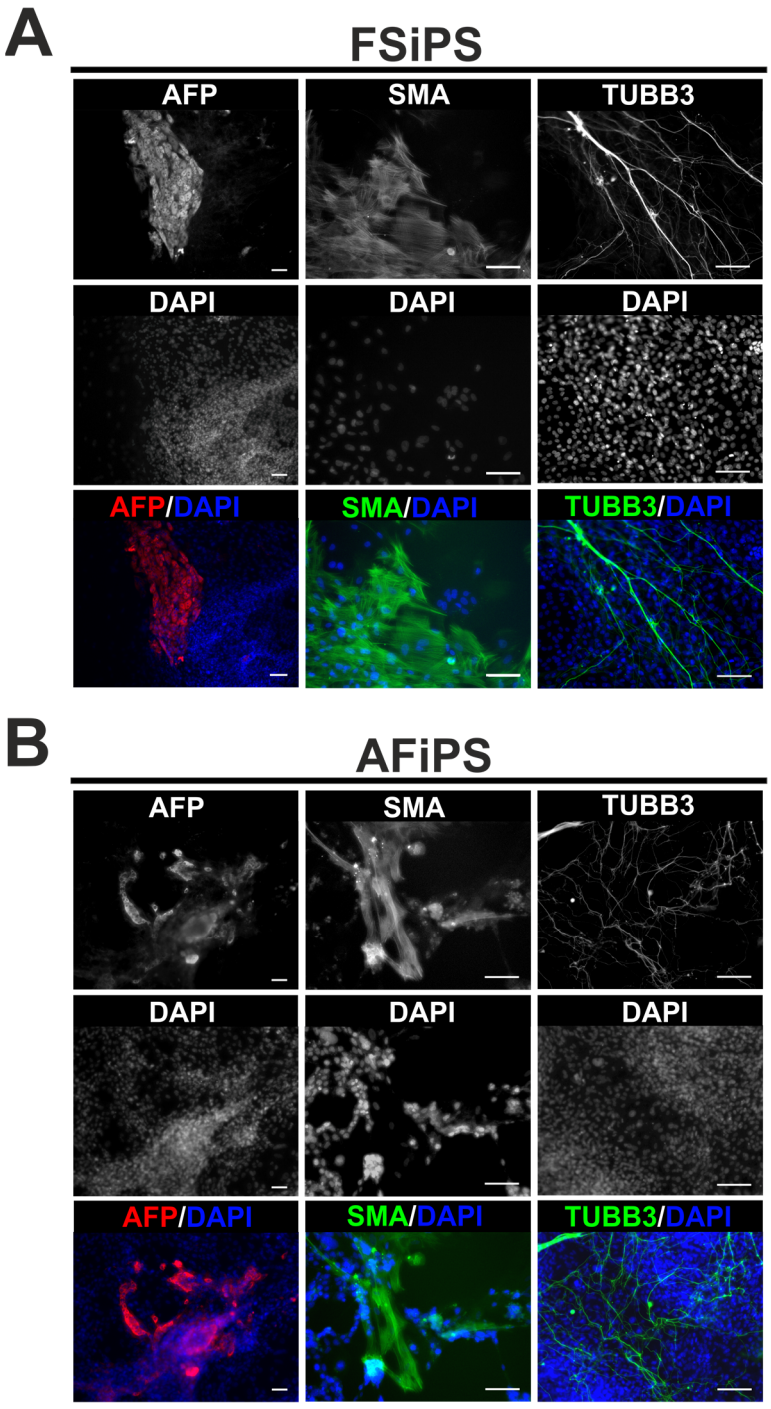

Figure 3.20 Bioreactor-expanded hiPSCs can differentiate into cells from all three germ layers. Aggregates of FSiPS or AFiPS were cultured as embryoid bodies in undirected differentiation medium for 7 days, then plated onto gelatin-coated glass coverslips for further differentiation. After up to 4 weeks of differentiation, differentiated cells derived from FSiPS cells (A) or AFiPS cells (B) could be detected that were positive for markers of the three different germ layers, using alpha-fetoprotein (AFP; endoderm), smooth muscle actin (SMA; mesoderm), and βIII-tubulin (TUBB3; ectoderm) as representative markers for these lineages. Scale bars = 100 µm.

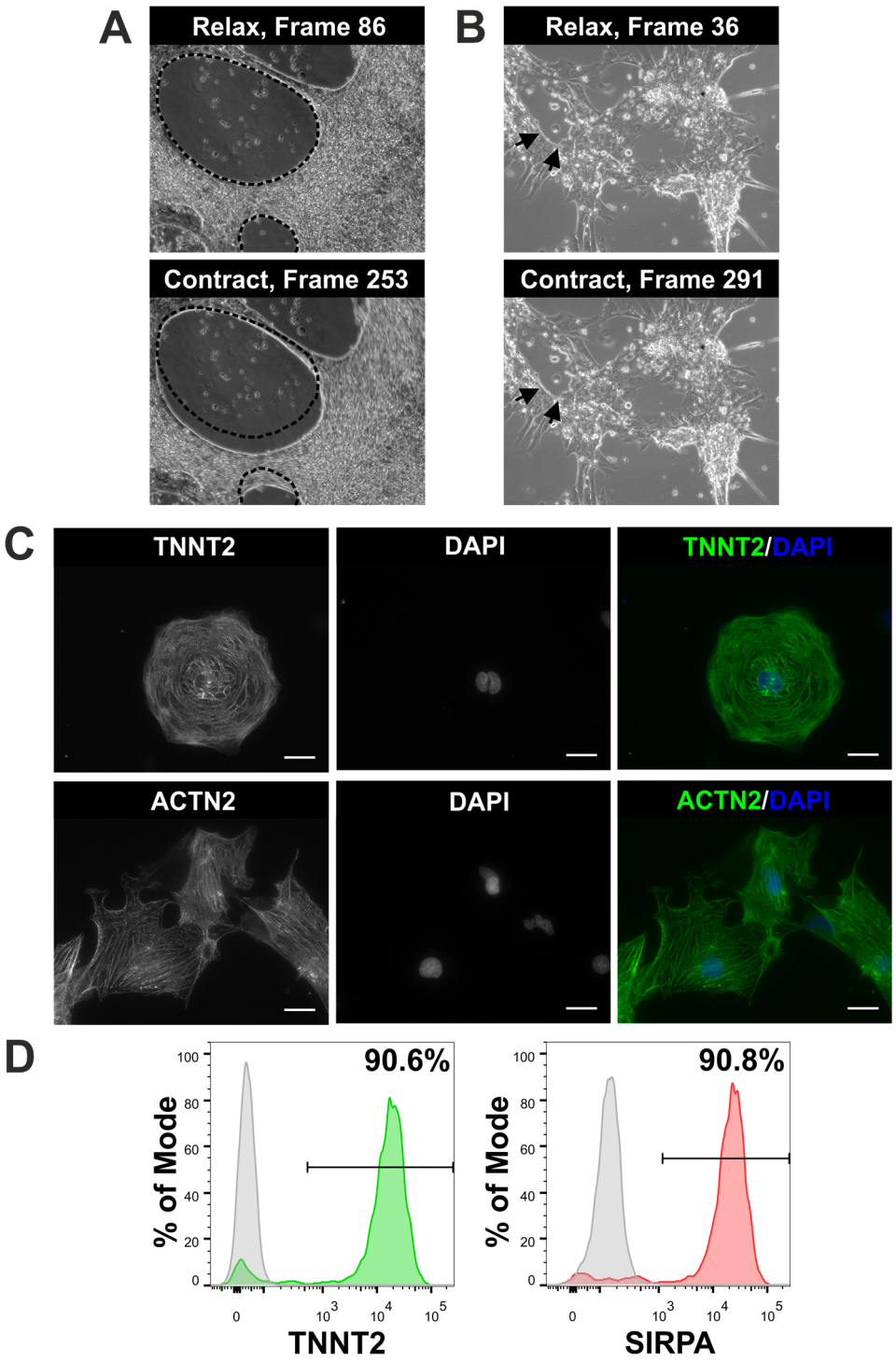

Figure 3.21 Bioreactor-expanded FSiPS cells respond to directed cardiac differentiation cues to generate cardiomyocyte-like cells. (A) After applying a cardiac differentiation protocol, sheets of beating cardiomyocyte-like cells were generated. Illustrative frames from movies of beating sheets are shown. Dashed outlines demarcate cell sheet borders in the relaxed frame. (B) After enriching the differentiated cells for cardiomyocytes by using glucose-depleted, lactate-based enrichment medium and replating on bMG-coated glass coverslips and cultureware, individual beating cells could be observed. Illustrative frames from movies of beating cells are shown. Arrows indicate a representative contracting area. (C) The enriched cells were positive for typical cardiomyocyte markers such as cardiac troponin T (TNNT2) and alpha sarcomeric actinin (ACTN2) using immunocytochemical analysis. Scale bars = 25 µm. (D) Further flow cytometric analysis revealed that ~90% of the enriched cells were positive for signal regulatory protein A (SIRPA), another cardiac marker. Grey peaks indicate fluorophore-matched isotype controls.

Karyotype analysis

To check for any gross chromosomal aberrations or translocations, bioreactor-expanded FSiPS cells were subjected to G-banding staining for karyotype analysis. In the 10 metaphases examined, no chromosome loss or gain could be detected, and no chromosomal translocations were observed. This is consistent with a normal human male karyotype, with 22 chromosome pairs, an X, and a Y chromosome. This suggests that bioreactor culture is compatible with the maintenance of genome integrity in proliferating hiPSCs. A representative karyogram is presented in Figure 3.22.

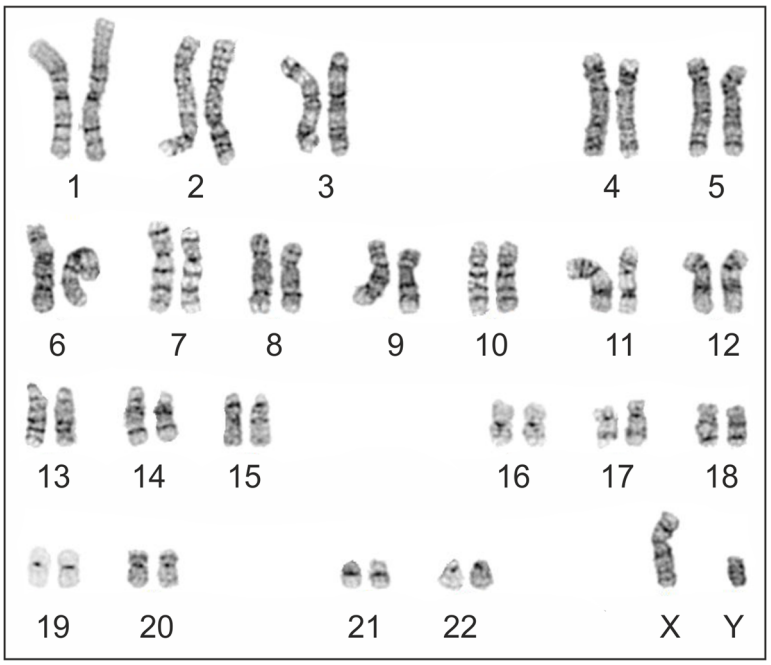

Figure 3.22 Bioreactor-expanded FSiPS cells maintain a normal karyotype. G-banding staining was performed on bioreactor-expanded FSiPS to visualise the chromosomes on a karyogram. In all 10 metaphases examined, 22 chromosome pairs, and X, and a Y chromosome could be seen, with no gain or loss of chromosome number. No chromosomal translocations or other aberrations could be detected, suggesting that bioreactor culture is compatible with the stable maintenance of the genome in hiPSCs.

Metabolite analysis

Monitoring of glucose and lactate in culture medium was performed when culturing FSiPS cells in bioreactors, with sampling carried out shortly before medium addition or exchange. Using the optimised suspension protocol, glucose concentration of the culture medium decreased day-on-day, even with medium addition and/or exchange until day 7, where concentrations remained above 167 ± 31 mg/dL (Figure 3.23). Correspondingly, lactate concentrations also increased day-on-day despite medium addition and/or exchange, reaching 15 ± 2 mM on day 7. Taken together, these data suggest that not only were cells respirating and viable, they were also proliferating, leading to increased per-day consumption of glucose, and increased

per-day production of lactate. Importantly, these curves suggest that glucose is not depleted on day 2 with the optimised medium processing protocol, and lactate concentrations on day 2–4 do not appear limiting despite the lack of waste medium removal.

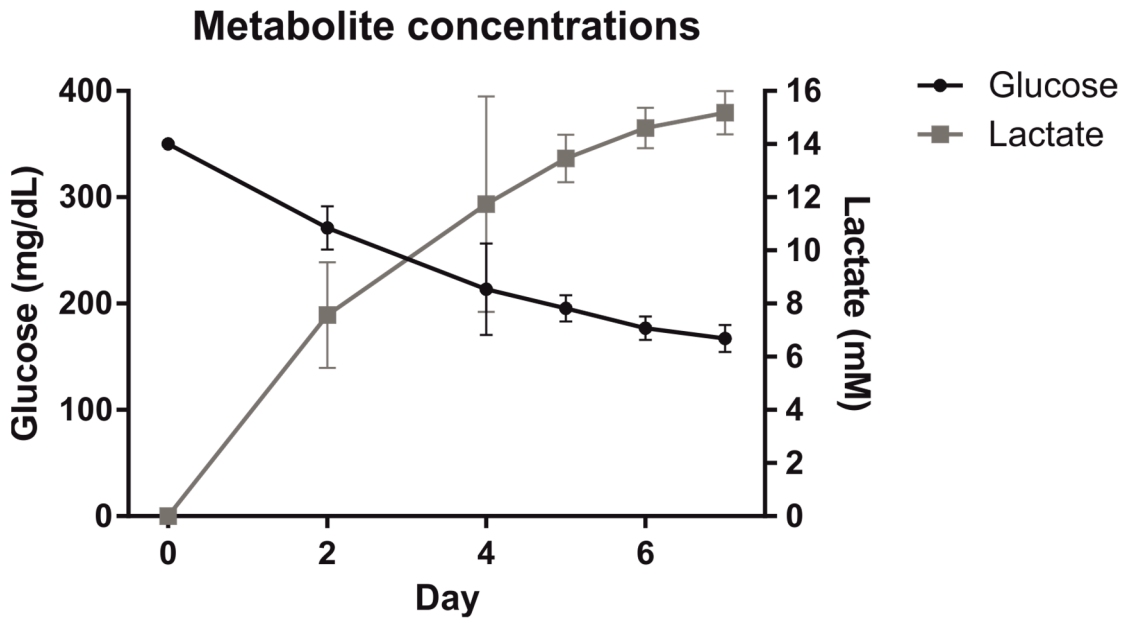

Figure 3.23 Glucose and lactate concentrations in culture medium change over time in a manner consistent with cell proliferation in bioreactors. If the FSiPS cells were respirating but not proliferating, glucose and lactate concentrations would be expected to be stable over time given medium addition and/or exchange. FSiPS cells cultured in bioreactors increase in quantity, leading to higher glucose consumption over time and consequently higher lactate production into the cell culture medium.

3.2 Alternative cell types towards cell therapy

Other than the use of hiPSCs in cell therapy applications, another paradigm is to use multipotent, lineage committed, but proliferative stem cells which are thought to possess lower teratoma or tumorigenic risk (Gao *et al.*, 2016; Goldring *et al.*, 2011). To this end, two types of stem/progenitor cell populations were studied in this thesis, namely cardiovascular progenitor cells (CVPCs) and induced neural stem cells (iNSCs).

3.2.1 Cardiovascular progenitor cells (CVPCs)

Induction of hiPSCs to CVPCs

The culture and *in vitro* expansion of undifferentiated CVPCs is challenging (Birket and Mummery, 2015; Chen and Wu, 2016), as conditions for their maintenance are not well-understood. While expandable CVPCs derived from hPSCs have been described (Birket *et al.*, 2015), it involved overexpression of *cMYC* mediated by lentivirus transduction. We attempted to replicate a previous study by Cao and co-workers by plating FSiPS and AFiPS in CVPC Induction Medium (CIM), supplemented with 5 μM Y27632 for the first 24 h, and cultured for 3 days with daily medium exchange (Cao *et al.*, 2013). With both hiPSC lines, the culture was proliferative under CIM conditions and grew to near confluence by day 3 of CVPC induction (Figure 3.24). On day 3, flow cytometry analysis for the differentiation marker stage-specific embryonic antigen-1 (SSEA-1) revealed that >90% of cells in both hiPSC lines were SSEA-1-positive after CVPC induction (Figure 3.24).

The cells were then passaged onto hES MG-coated plates at a 1:3–1:10 ratio in CVPC Propagation Medium (CPM), supplemented with 5 μM Y27632 for the first 24 h, and defined as Passage 1 CVPCs. At Passage 1, CVPCs from both hiPSC lines expressed the markers ISL LIM homeobox 1 (ISL1) and mesoderm posterior BHLH transcription factor 1 (MESP1) (Figure 3.25). These cells were then grown to ~80% confluence before passaging as described.

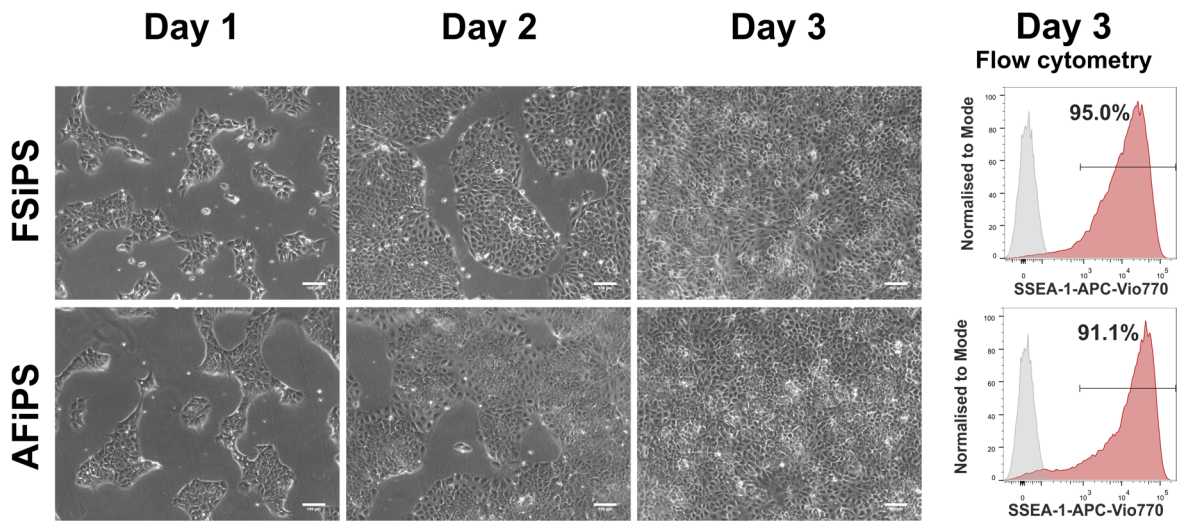

Figure 3.24 hiPSCs could be induced into CVPCs using CVPC induction medium (CIM) for 3 days. Over 3 days of induction, plated hiPSCs changed in morphology and proliferated to near confluence. The differentiation marker SSEA-1 could be detected in >90% of induced cells by day 3. Grey peaks indicate fluorophore-matched isotype controls. Scale bars = 100 µm.

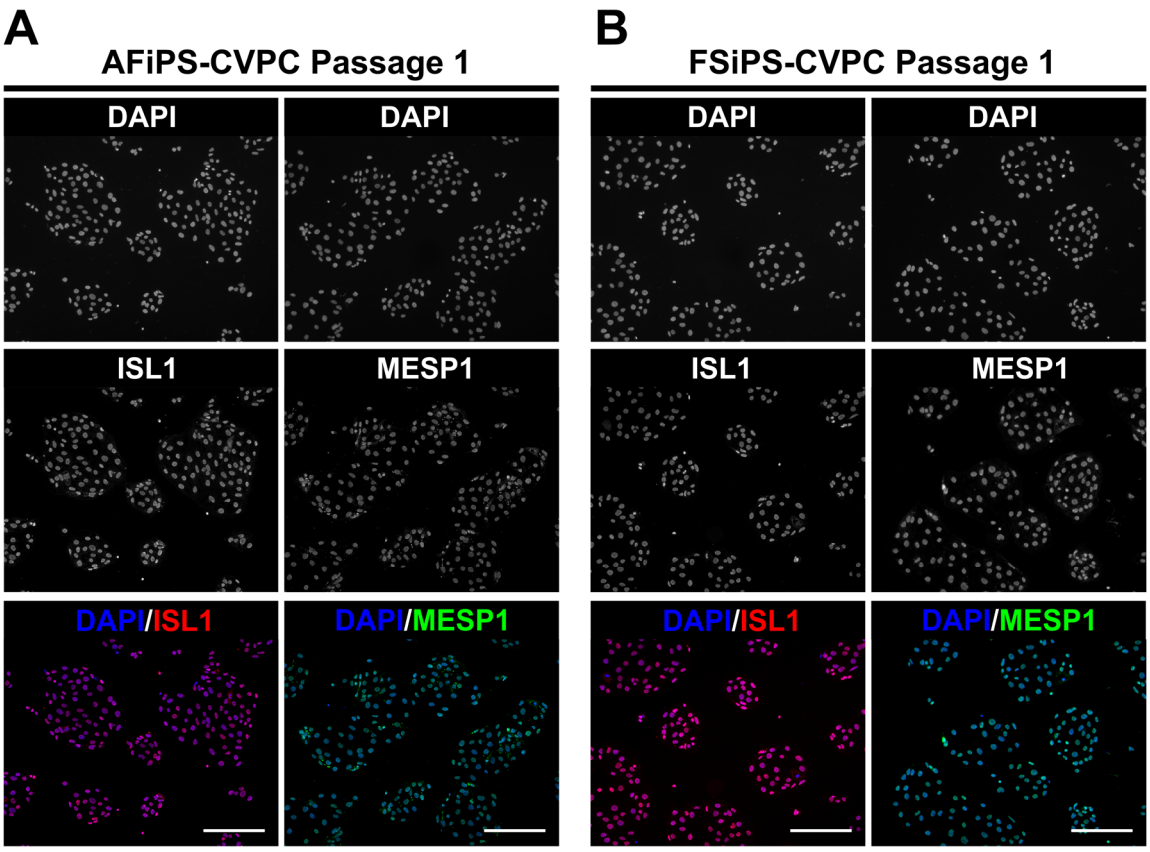

Figure 3.25 CVPCs derived from both AFiPS and FSiPS cell lines express cardiac progenitor markers after derivation. (A) AFiPS-derived CVPCs and (B) FSiPS-derived CVPCs were passaged onto hES MG-coated plates at a 1:3 ratio and stained for cardiac progenitor markers ISL1 and MESP1 at 5 days of culture. These markers could be detected in CVPCs derived from both cell lines. Scale bars = 200 µm.

However, these CVPCs exhibited a limited capacity for long-term expansion in CPM. With FSiPS-CVPCs, even at Passage 1, the cells were slow to proliferate compared to AFiPS-CVPCs, and cells were heterogeneous in morphology at Passage 2 after 7 days of culture (Figure 3.26A). With the AFiPS-CVPCs, they could typically be passaged until Passage 3–4, where cells exhibited low to no proliferation. At Passage 4 after 7 days of culture, heterogeneous morphology could be observed in the cells (Figure 3.26B). These suggest that CPM could not support the stable expansion of CIM-induced CVPCs.

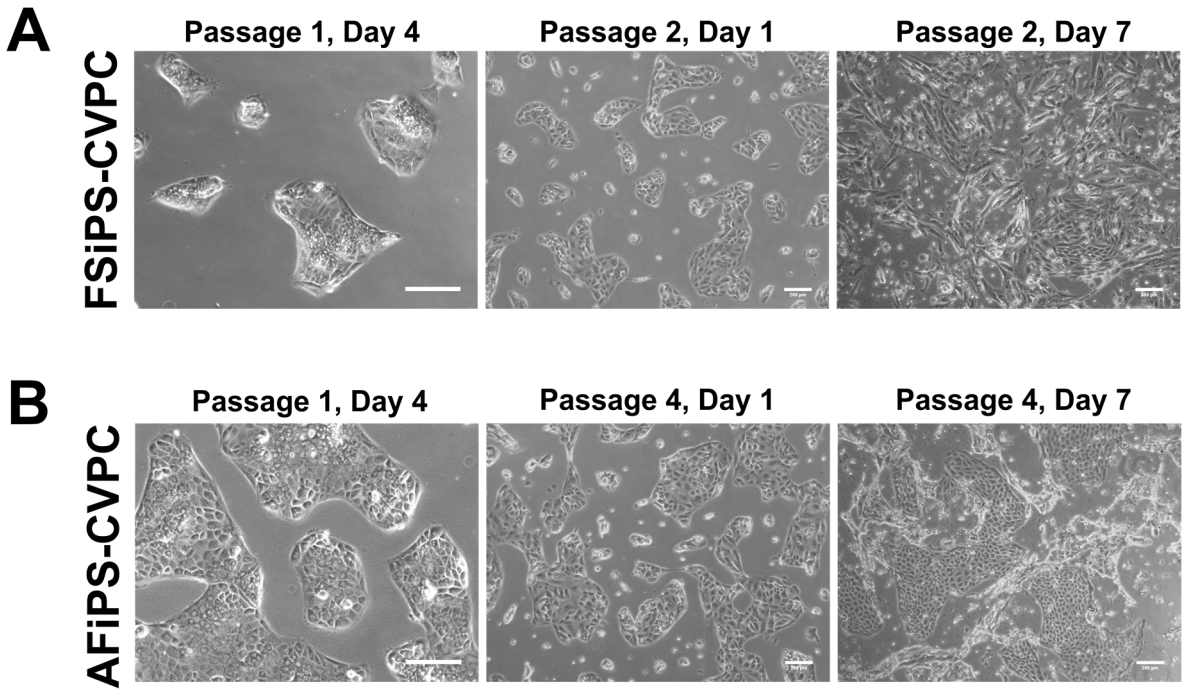

Figure 3.26 CVPCs derived from both FSiPS and AFiPS could not be stably expanded over more than a few passages in CVPC Propagation Medium (CPM). (A) FSiPS-derived CVPCs showed heterogeneous, potentially differentiated, morphology by 7 days of culture at Passage 2. (B) While AFiPS-derived CVPCs could be maintained in CPM for more passages, they showed heterogeneous morphology at 7 days of culture at Passage 4. Scale bars = 200 µm.

Assessment of an alternative approach to propagate CVPCs

Since CPM was unable to support the long-term expansion of the hiPSC-derived CVPCs, an alternative CVPC Expansion Medium (BACS) was tested (adapted from Zhang *et al.*, 2016). After induction with CIM, CVPCs were re-plated 1:3 on hES MG-coated plasticware in BACS, supplemented with 5 µM Y27632 for the first 24 h. BACS was then exchanged every other day for up to 18 days. After plating in BACS, FSiPS- and AFiPS-CVPCs proliferated (Figure 3.27).

Flow cytometric analysis of the CIM-induced cells after 3 days of induction but before BACS treatment is shown in Figure 3.28A, showing cells which were >90% SSEA-1-positive, 13–26% platelet-derived growth factor receptor alpha (PDGFRa)-positive, and <5% vascular endothelial growth factor receptor 2/kinase insert domain receptor (KDR)-positive. After treatment with BACS medium for another 18 days, of the resulting cells, >90% were still SSEA-1-positive, whereas >90% were now PDGFRa-positive, and 50–80% were positive for KDR (Figure 3.28B).

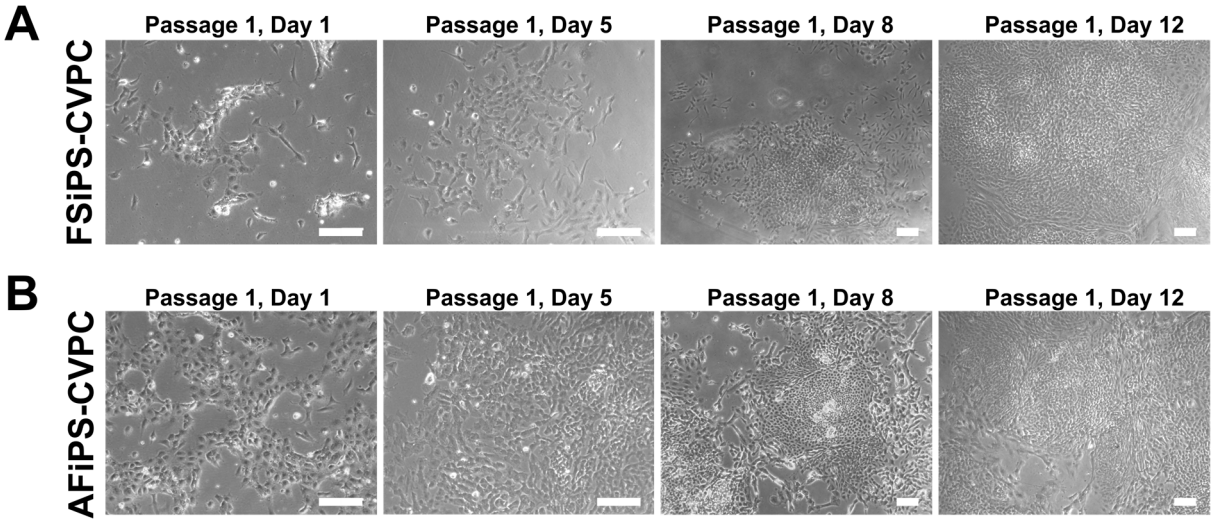

Figure 3.27 CVPCs re-plated in BACS medium proliferate during the first passage. (A) FSiPS-derived CVPCs and (B) AFiPS-derived CVPCs were re-plated after induction in BACS medium and could proliferate over 12 days. Scale bars = 200 µm.

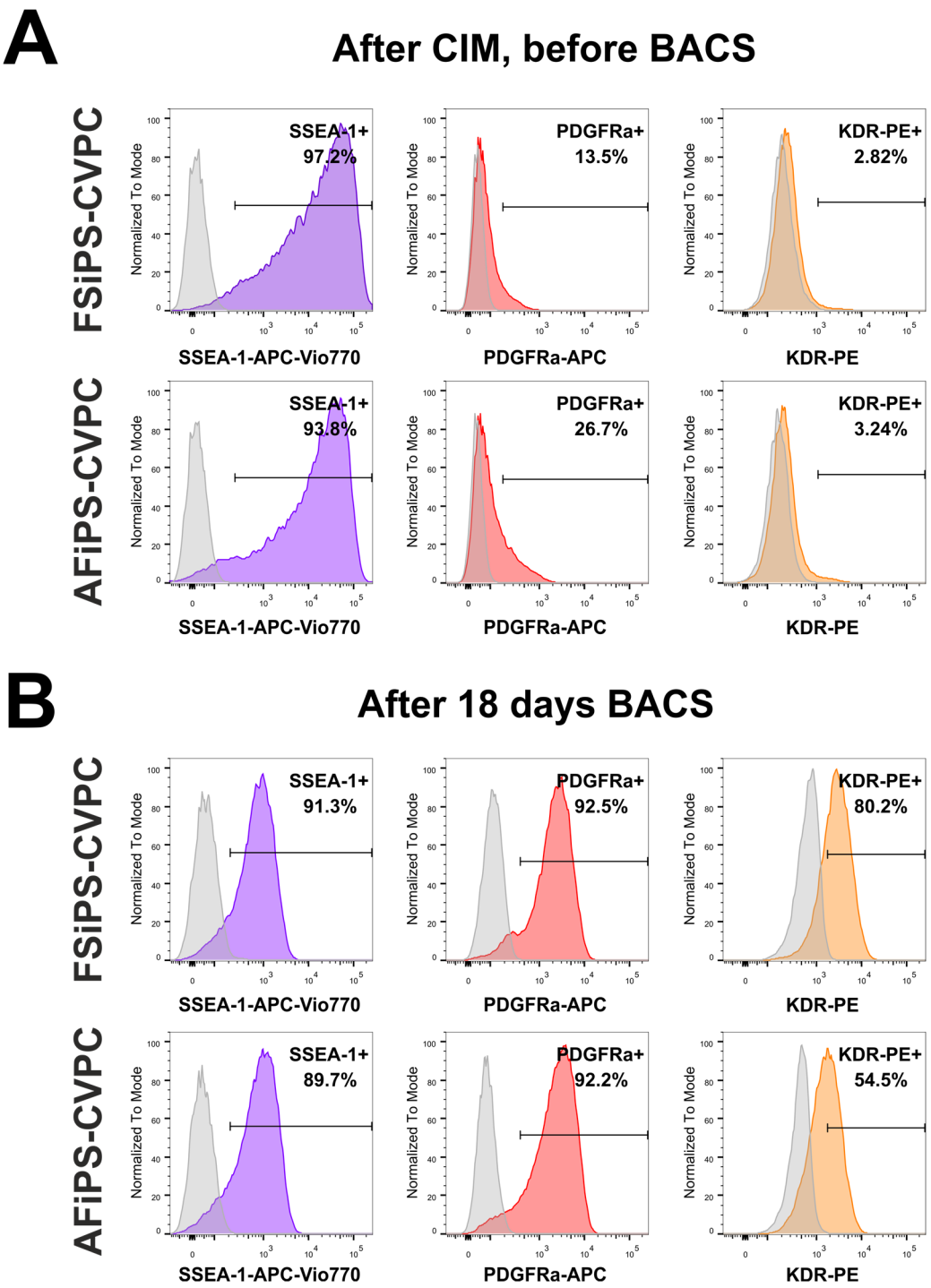

Figure 3.28 Flow cytometric analysis of CIM-induced CVPCs treated with the BACS cocktail reveals expression of key CVPC surface markers. (A) After CIM induction but before BACS treatment, both AFiPS- and FSiPS-CVPCs were >90% positive for SSEA-1, faintly positive (13–26%) for PDGFRa, and nearly negative (<5%) positive for KDR. (B) After 18 days of BACS treatment, cells exhibited a different surface marker profile. While they were still >90% SSEA-1-positive, >90% of the total cells were PDGFRa-positive, and 50–80% of them were KDR-positive. Grey peaks represent fluorophore-matched isotype controls.

3.2.2 Induced neural stem cells (iNSCs)

In contrast to cardiovascular progenitor cells, the conditions to maintain neural stem cells in culture are well-defined. Our group developed a protocol to directly convert human fibroblasts into iNSCs (Meyer *et al.*, 2015). Accordingly, BJ-iNSCs generated from BJ fibroblasts needed to be analysed first.

Marker expression profile of iNSCs

To ensure the integrity of the cryopreserved BJ-iNSCs, they were thawed between passage 9–12, cultured and expanded in the original medium (NIM) for at least 1 passage, and then analysed by immunocytochemistry. Immunocytochemical analysis revealed the expression of the neural stem cell markers Nestin (NES), paired box 6 (PAX6), SRY-box 1 (SOX1), and SRY-box 2 (SOX2). The proliferation marker Ki67 was also detected in the BJ-iNSCs, while the presence of the pluripotency marker OCT4 could not be detected (Figure 3.29). This expression profile was consistent with the BJ-iNSCs originally generated in this laboratory.

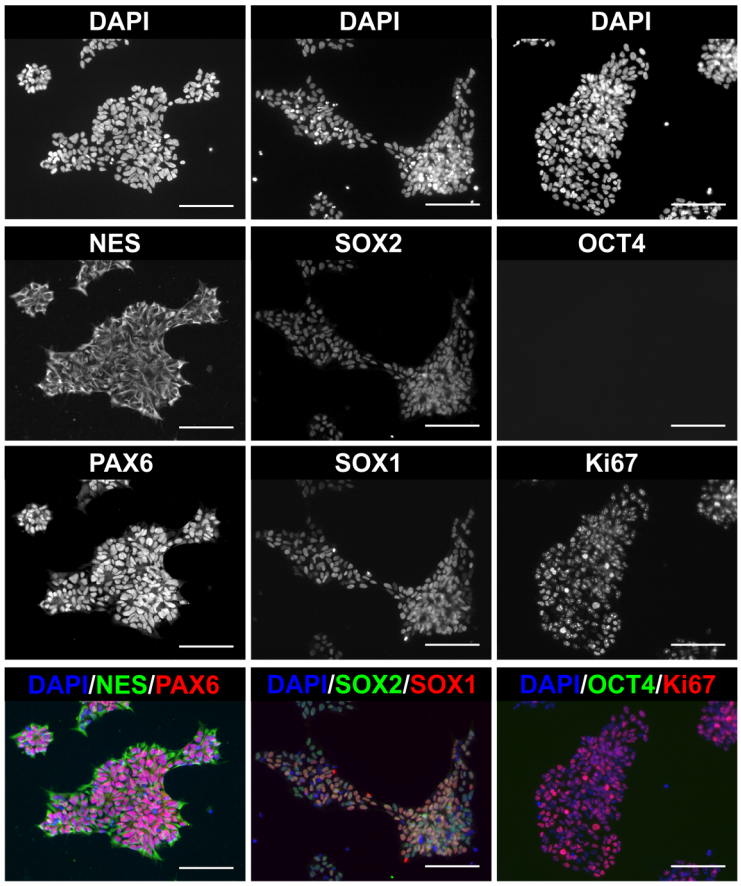

Figure 3.29 BJ-iNSCs express typical neural stem cell markers. Routine expansion of BJ-iNSCs in NIM yields a population of cells that express the neural stem cell markers NES, PAX6, SOX1, and SOX2. They also express the proliferation marker Ki67, but not the pluripotency marker OCT4. Scale bars = 100 µm.

Small molecule withdrawal to prepare iNSCs for transplantation

To mitigate the risk of excessive proliferation after transplantation, a protocol was developed to pre-differentiate the BJ-iNSCs by the withdrawal of small molecules from the culture medium. After 3 days of culture in medium without small molecules (denoted as NIM–), the confluency of BJ-iNSCs was reduced compared to control BJ-iNSCs that were cultured in complete NIM, and also exhibited a modest change in morphology, becoming more elongated with short neurite-like outgrowths (Figure 3.30).

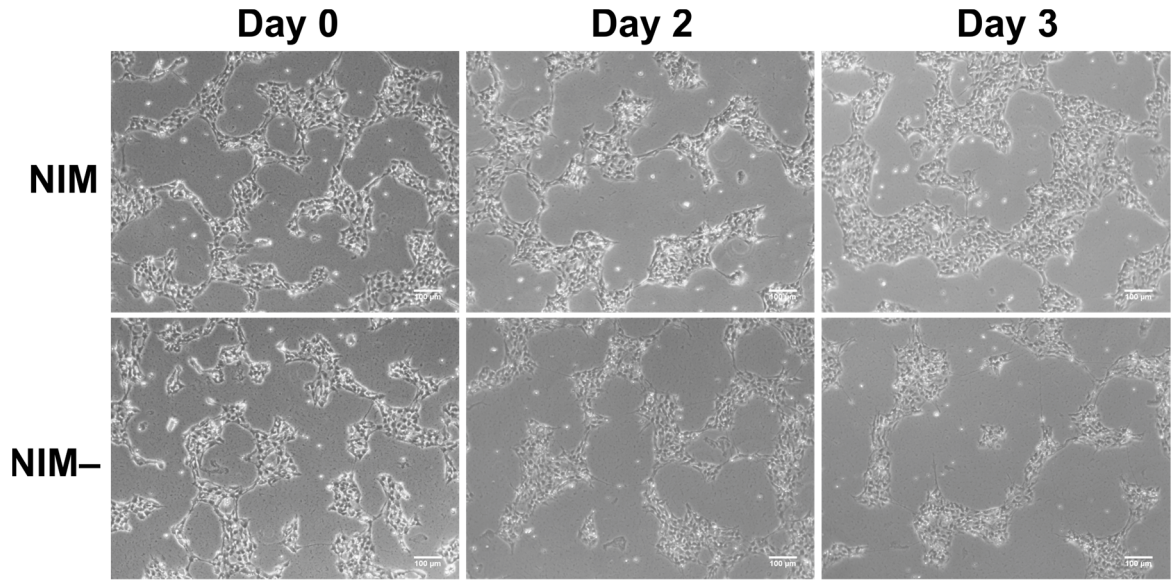

Figure 3.30 BJ-iNSCs treated with small molecule withdrawal exhibit lower confluency compared to BJ-iNSCs cultured in complete medium. This suggests that the removal of the small molecules lowers proliferation rate and may indicate pre-differentiation. NIM: neural induction medium; NIM–: neural induction medium without small molecules. Scale bars = 100 μm.

While a lower proliferation rate was evident, the stemness of the resulting BJ-iNSCs required examination. Immunocytochemical analysis of the BJ-iNSCs treated with NIM– revealed the continued presence of PAX6, but also a higher expression of βIII-tubulin (Tujl1). At this time-point of 3 days of small molecule withdrawal, BJ-iNSCs express both markers of stemness and differentiation, and could represent cells in a pre-differentiated transitory state between stem cells and differentiated cells. These pre-differentiated cells could be useful for further transplantation studies.

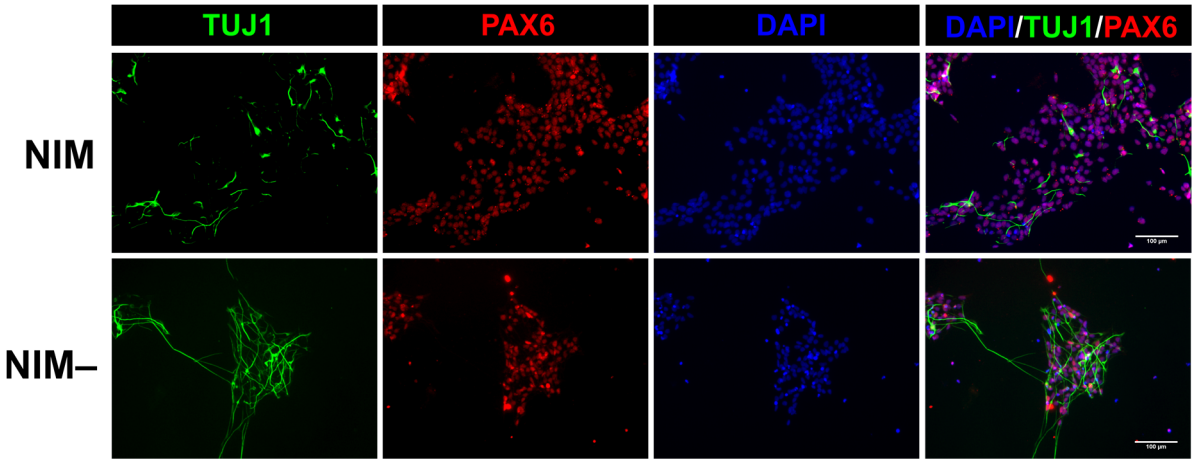

Figure 3.31 BJ-iNSCs treated with small molecule withdrawal express markers of both differentiation and stemness. Compared to BJ-iNSCs cultured in complete NIM, BJ-iNSCs that underwent small molecule withdrawal continue to contain similar levels of PAX6, a neural stem cell marker, while exhibiting a higher expression of βIII-tubulin (TUJ1), a differentiation marker. This suggested a pre-differentiated state which could be useful for transplantation studies. Nuclei were stained with DAPI. Scale bars = 100 µm.

Stirred suspension culture of iNSCs

The generation of large quantities of iNSCs for cell therapy applications may be required. To address this, the stirred suspension culture approach that was established with hiPSCs in Section 3.1.1 was assessed for its applicability to also generate large quantities of iNSCs. When seeded at 200,000 cells/mL in NIM, a few large aggregates were generated (black arrows, Figure 3.32A), with each aggregate measuring ~1 mm in diameter. In this initial experiment, 10×10^6 cells were expanded to 11.5×10^6 cells over 7 days.

These spinner-selected BJ-iNSCs were then used as a founder population and expanded in standard adherent bMG-coated plates. After expansion on bMG-coated plates, these were re-seeded in a second round of stirred suspension. After a second round of stirred suspension, only one large aggregate was generated (white arrow, Figure 3.32B). In this experiment, 10×10^6 cells were seeded, but only 5.7×10^6 cells were recovered after 7 days of culture.

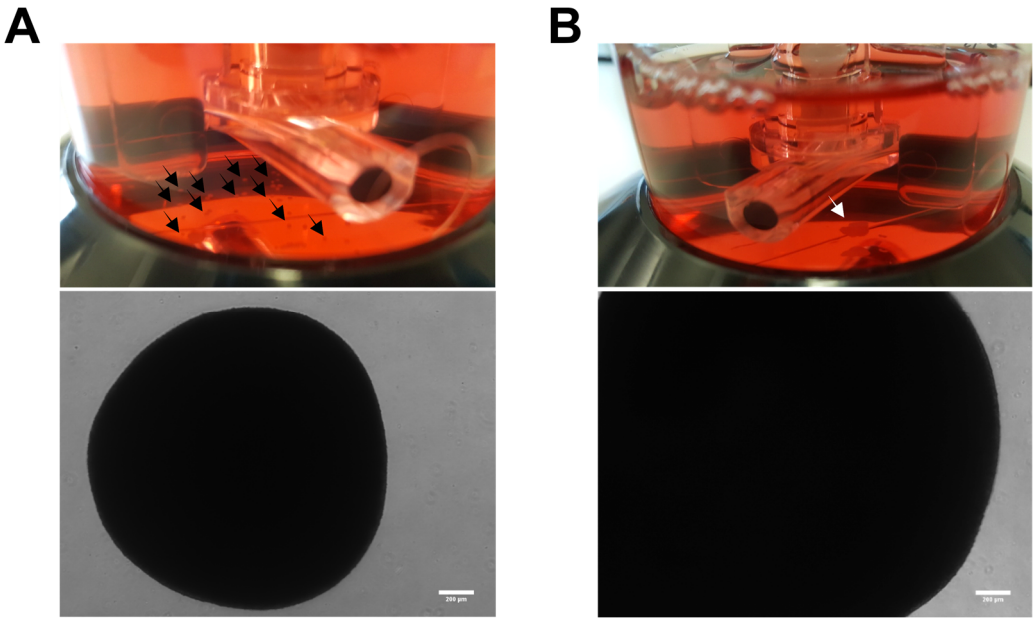

Figure 3.32 Initial stirred suspension cultures of BJ-iNSCs generated a few excessively large aggregates (A) After 7 days of suspension culture, the initial 10 × 10^6 cells grew to 11.5 × 10^6 cells as several large aggregates (black arrows) measuring approximately 1 mm in diameter. These cells were used as a founder population and expanded on bMG-coated plastic before further suspension culture. (B) Using the expanded founder population, 10 × 10^6 cells were brought into a new spinner. After 7 days of culture, only one large aggregate remained (white arrow) which contained 5.7 × 10^6 cells, representing a reduction in cell number compared to the seeded number of cells. Scale bars = 200 µm.

We then explored the possibility of culturing BJ-iNSCs in an alternative neural expansion medium (NEM) that was more recently described (Jovanovic *et al.*, 2018). To do this, BJ-iNSCs were brought into suspension culture in Petri dishes in NEM to test for aggregate formation. After seeding BJ-iNSCs as a single cell suspension in NEM supplemented with 10 µM Y27632 in Petri dishes, aggregates were generated (Day 4A, Figure 3.33) and could be maintained in NEM. However, some cells were observed to attach to the non-tissue culture treated Petri dishes (Day 4B), and aggregates also did not increase in diameter by day 6.

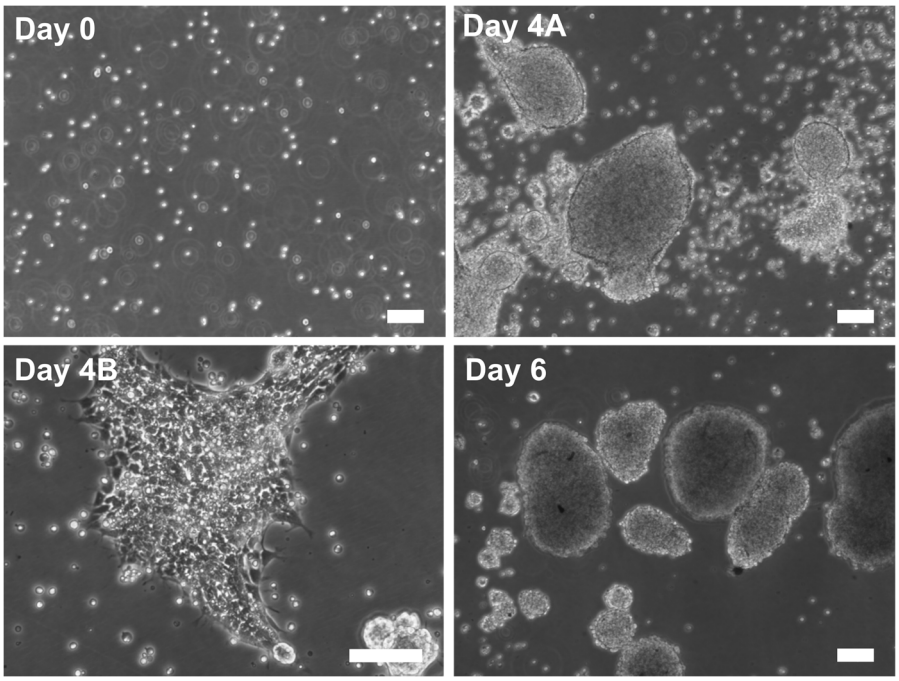

Figure 3.33 Adaptation of BJ-iNSCs to neural expansion medium (NEM) conditions shows feasibility of generating aggregates in suspension. The suitability of NEM as an expansion medium for suspension culture of BJ-iNSCs was tested by seeding BJ-iNSCs in Petri dishes in NEM as a single cell suspension. By Day 4, aggregates of cells could form, but some cells were also observed to attach to the non-tissue culture treated Petri dishes (Day 4B). After culture for another 2 days, aggregates did not increase in size. Scale bars = 100 µm.

BJ-iNSCs were also cultured using standard adherent culture conditions on bMG-coated plates to test whether an adaptation to NEM would induce any changes in the BJ-iNSC population. Compared to the control BJ-iNSCs expanded on bMG-coated plates in NIM, NEM-cultured BJ-iNSCs continued to homogeneously express SOX2 (>95%) but the fraction of PAX6-positive cells was decreased to ~75% (Figure 3.34A). Intriguingly, this decrease in PAX6 positive cells was not observed in immunocytochemical analysis, where PAX6 appeared to be homogeneously expressed in NEM-cultured BJ-iNSCs (Figure 3.34B).

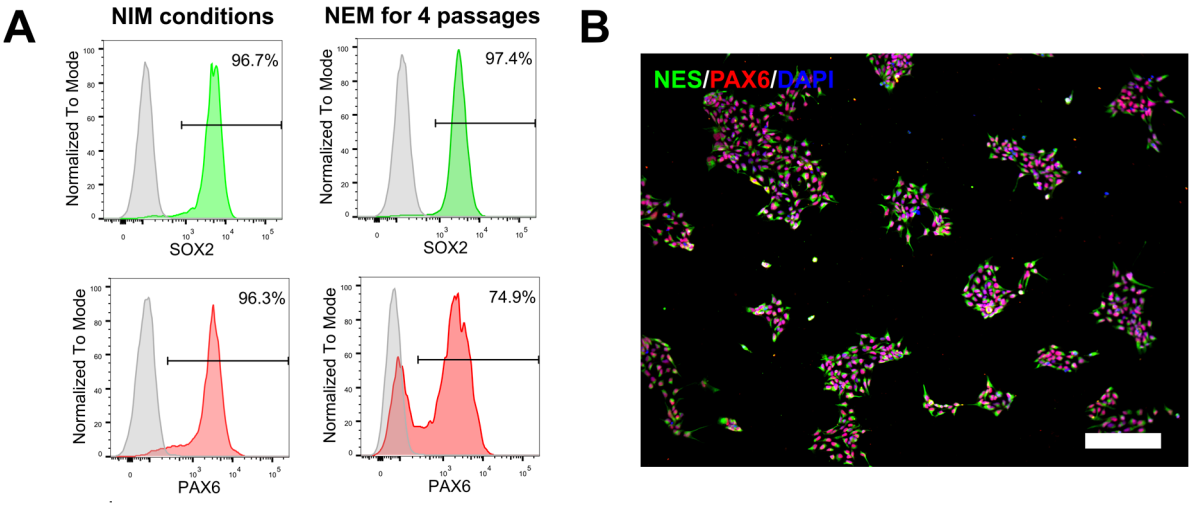

Figure 3.34 Adaptation of BJ-iNSCs to neural expansion medium (NEM) may be correlated with a loss of PAX6 expression. (A) After culturing the BJ-iNSCs in NEM for 4 passages, the fraction of cells expressing SOX2 was maintained at >95%. While control BJ-iNSCs cultured in NIM were 96% positive for PAX6, BJ-iNSCs cultured in NEM showed a decrease to ~75% PAX6-positive. Grey peaks represent isotype controls. (B) Immunocytochemical analysis for PAX6 in NEM-expanded BJ-iNSCs showed a homogeneously PAX6-positive population. Scale bar = 200 µm.

3.3 Biofabrication using hiPSCs

3.3.1 Assessment of materials for biofabrication

The aim of this section of the thesis was to identify materials that were not only cytocompatible with hiPSCs, but also printable when laden with hiPSCs. To this aim, we chose two materials that were previously shown to have good printability when laden with cells. These materials were recombinant spider silk proteins which were shown to be compatible with printing mouse and human fibroblasts (Schacht *et al.*, 2015), and gelatin-alginate hydrogel which has been printed laden with human MSCs (Paxton *et al.*, 2017). We cultured hiPSCs on these materials as an initial screen to test their suitability with hiPSCs.

3.3.1.1 Recombinant spider silk protein

In cooperation with the Chair of Biomaterials of the Faculty of Engineering Sciences of the University of Bayreuth headed by Prof. Dr. Thomas Scheibel, three variants of recombinant spider silk proteins, namely C16, C16-RGD, or K16 were prepared in two formats at the Scheibel laboratory by Dr. Kiran Pawar and Tamara Aigner, either cast as a film coating on plasticware, or as a sheet of non-woven fibres (Aigner, DeSimone, and Scheibel, 2018).

hiPSC attachment on recombinant spider silk protein films

AFiPS cells were plated onto C16, C16-RGD, or K16 recombinant spider silk films as a single-cell suspension at a density of 50,000 cells/cm^2 in mTeSR supplemented with 10 µM Y27632. AFiPS cells were plated on hES MG-coated plates under the same conditions as a control. Medium was exchanged daily, and hiPSC attachment and growth on these films was monitored over 7 days.

After one day of culture, a few clusters of cells appeared to have attached to C16-RGD and K16 films, but these were fewer compared to the hiPSCs plated on the control hES MG plate. Calcein AM staining revealed that at least some of the adherent clusters on C16-RGD and K16 were viable (Figure 3.35). In contrast, almost no viable cell attachment could be observed on C16 films.

Over a total of 7 days of culture, no cell attachment or cell growth could be observed on C16 films. While some cells could be seen remaining on K16 films, these cells were not viable based on calcein AM staining. Interestingly, C16-RGD films appeared to be able to partially support the attachment and growth of hiPSCs, and

some viable hiPSC colonies could be observed growing on this film (Figure 3.35). However, growth on C16-RGD was markedly lower than those grown on hES MG-coated plates.

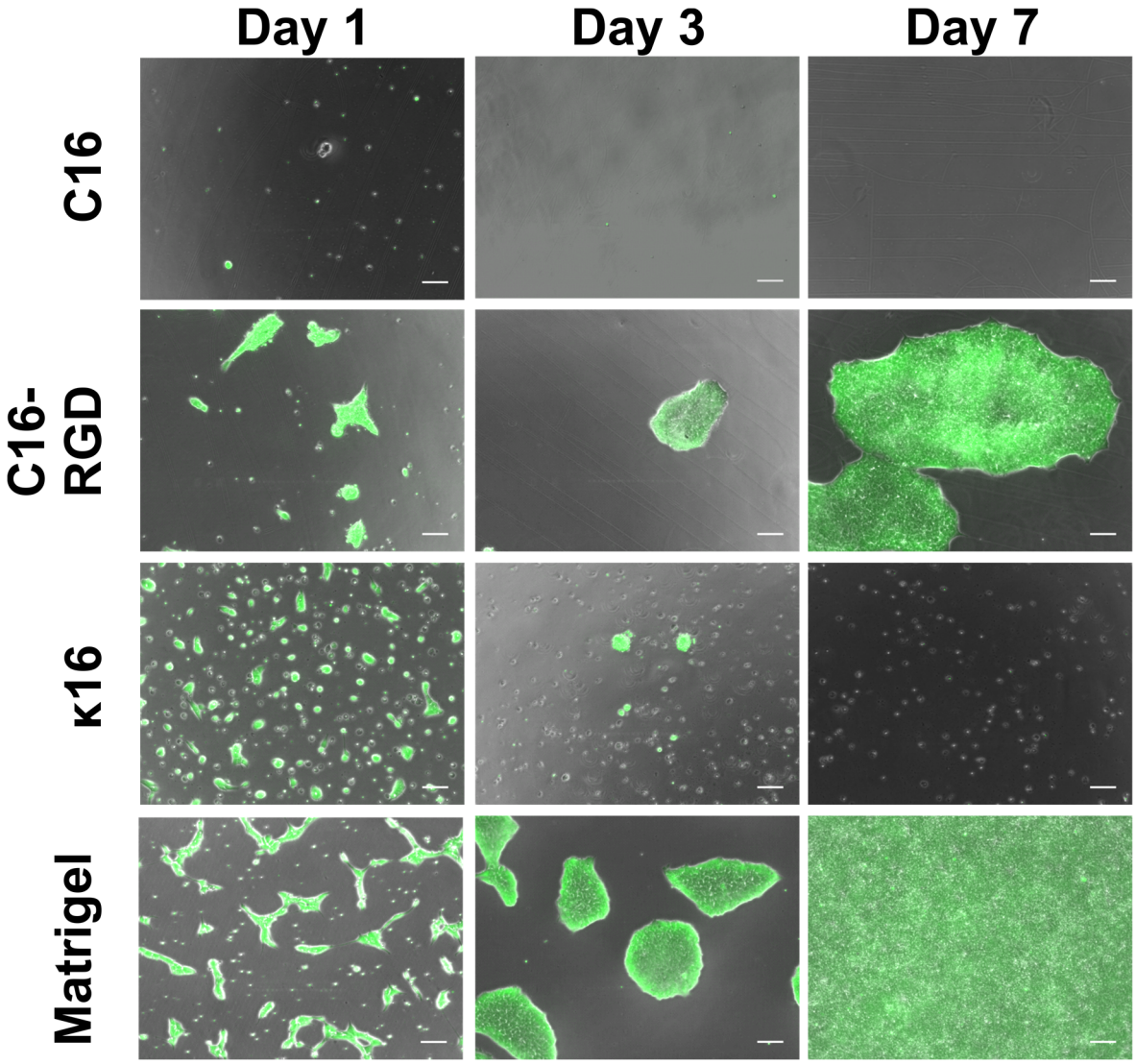

Figure 3.35 hiPSCs exhibit poor attachment to spider silk protein film coatings. hiPSCs were plated on C16, C16-RGD, and K16 films, as well as hES MG as a control. On days 1, 3, and 7, cells were labelled for viability with calcein AM (green). C16 films appear to be unable to support hiPSC attachment and growth, as no viable cells could be found after 7 days of culture. On C16-RGD films, modest hiPSC attachment and proliferation could be found, with some viable colonies remaining after 7 days. On K16 films, some viable cells initially appeared to attach on day 1, but through the culture process most of the cells that appear to attach to the film were no longer viable by day 7 and did not stain green with calcein AM. hiPSCs on hES MG grew to confluence by 7 days on hES MG and remained viable throughout the culture process. Scale bars = 100 µm.

hiPSC attachment on recombinant spider silk protein non-woven sheets

AFiPS cells were plated onto C16, C16-RGD, or κ16 recombinant spider silk fibres prepared as non-woven sheets as a single-cell suspension, at a density of 50,000 cells/cm^2 in mTeSR supplemented with 10 µM Y27632. As a control, AFiPS cells were plated on hES MG-coated plates under the same culture conditions. Medium was exchanged daily, and hiPSC attachment and growth on these non-woven fibre sheets was monitored over 4 days.

The opacity of the non-woven fibre sheets resulted in low visibility of cells using light microscopy. Therefore, cells were labelled with calcein AM to visualise live cells, and only fluorescence images of the calcein AM-stained cells are presented (Figure 3.36). On day 2 of culture on C16, C16-RGD, and κ16 sheets, viable AFiPS cells had formed large aggregates in the central portion of the sheet, with smaller cell clusters spread across the sheet. However, these cell clusters and aggregates were easily aspirated away during medium exchange, suggesting poor attachment of the cells to the spider silk sheets. On day 4 of culture, some aggregates remained on the C16 and κ16 sheets but did not form monolayer colonies. Intriguingly, some of the cells remaining on C16-RGD sheets were observed to attach to the sheets and form monolayer colonies, like the observation with C16-RGD films. As before, the growth of AFiPS cells on C16-RGD sheets was slower compared to growth on hES MG, as AFiPS cells grew to confluence by day 4 on hES MG, but on C16-RGD they were growing as separate colonies.

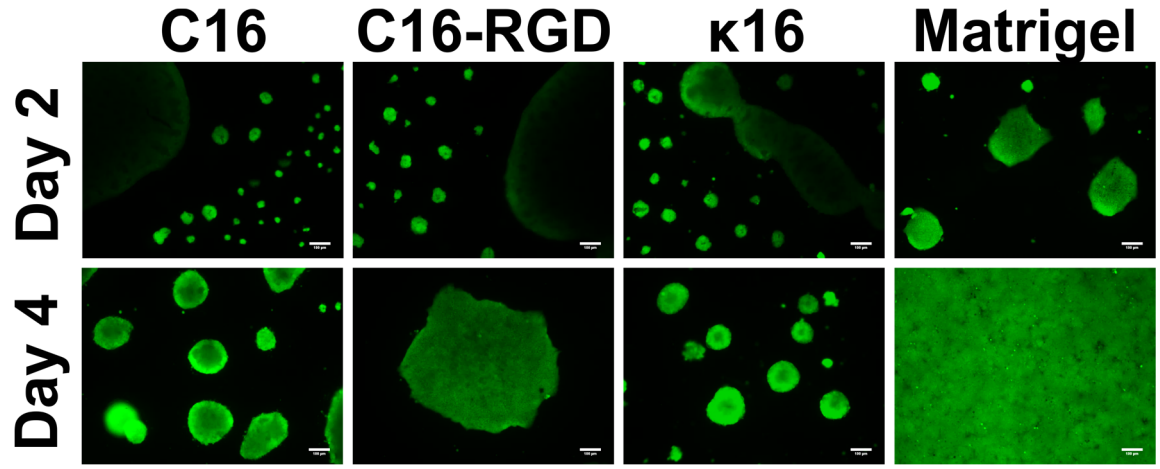

Figure 3.36 hiPSCs exhibit weak attachment to spider silk non-woven fibres. AFiPS cells were plated onto sheets of various spider silk protein non-woven fibres. AFiPS cells initially weakly attach to C16, C16-RGD, and κ16 non-woven fibres on day 2, but did not attach homogeneously across the non-woven fibres. At day 4, cells were contained in aggregate morphology on C16 and κ16 non-woven fibres but had a single large colony on C16-RGD. hiPSCs grown on hES Matrigel were used as a positive control. Scale bars = 100 µm.

3.3.1.2 Gelatin-alginate hydrogel

Gelatin-alginate hydrogels represent another widely-used material for loading cells for the purposes of bioprinting, owing to its thermoresponsivity, biocompatibility, and thinning properties. Gelatin-alginate hydrogels were prepared as described in Section 2.2.14.1 and extruded into 6-well plates to cover the surface. These were then incubated at 37 °C for 30 min to allow re-liquifying of the hydrogel, rotated to evenly coat the surface of the well, then cross-linked with Ca^{2+} for 10 min. Thereafter, the cross-linked hydrogels were rinsed with DPBS with 0.9 mM Ca^{2+} to remove precipitates. Then, hiPSCs were plated at 50,000 cells/cm² in StemMACS iPS-Brew XF, with 10 µM Y27632 for the first 24 h. Medium change was performed daily, and cells were stained with calcein AM/ethidium homodimer-1 to label live/dead cells on days 2 and 4 for analysis.

On day 2, live (green) hiPSC aggregates were maintained on the gelatin-hydrogel surface with a few dead (red) cells (Figure 3.37). On day 4, the aggregates had grown in size and most of the cells were still viable. This suggested compatibility of the gelatin-alginate hydrogel for culturing hiPSCs. Based on these findings, we continued with gelatin-alginate hydrogels as the material of choice for creating a printable bioink loaded with hiPSCs.

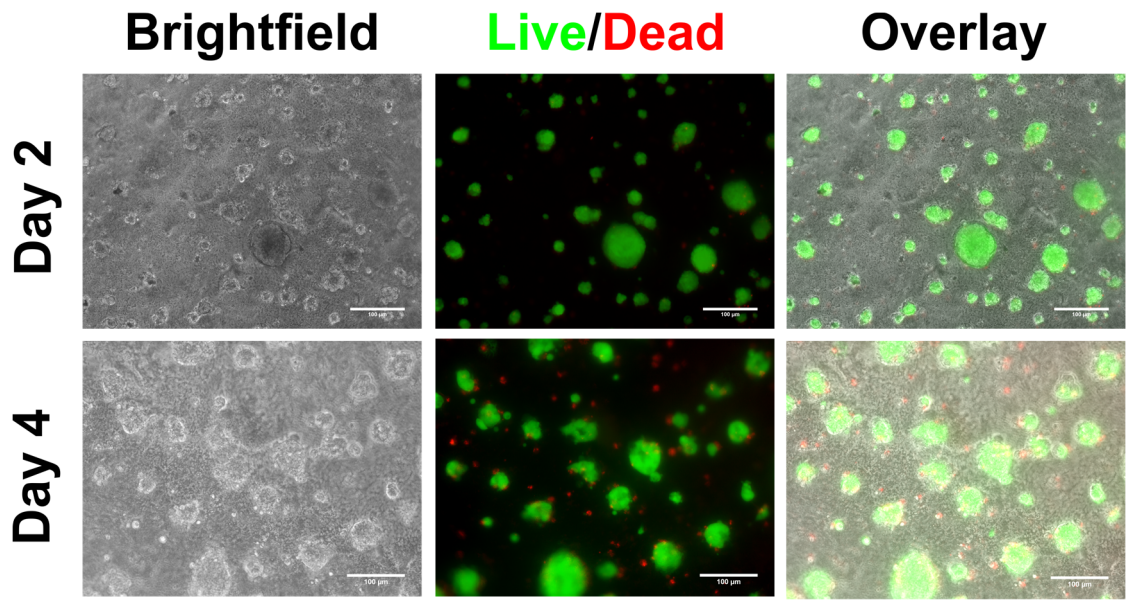

Figure 3.37 hiPSCs grow on gelatin-alginate hydrogel. AFiPS cells were plated onto cross-linked gelatin-alginate hydrogels. On days 2 and 4, cells were labelled with calcein AM (green, live) and ethidium homodimer-1 (red, dead), and analysed by microscopy. On day 2, some AFiPS cells had formed aggregates on the hydrogels with minimal cell death. These aggregates continued to grow over the next two days on the gelatin-alginate hydrogels, where most cells remained viable, with minimal dead cells. Scale bars = 100 µm.

3.3.2 Bioinks of gelatin-alginate loaded with hiPSCs as a single cell suspension

In cooperation with the Department for Functional Materials in Medicine and Dentistry of the University of Würzburg headed by Prof. Dr. Jürgen Groll, we set out to develop a printable bioink consisting of a gelatin-alginate hydrogel laden with hiPSCs. Initially, bioink loaded with hiPSCs was prepared by mixing hiPSCs as a single cell suspension into gelatin-alginate hydrogels. The hiPSC-loaded bioink was then either dispensed into disc-shaped silicone moulds to create non-printed discs or printed through a printing nozzle at varying pressures into the same silicone moulds to create printed discs. These discs were cross-linked with Ca^{2+} and cultured for the following 4 days in StemMACS iPS-Brew XF, with 10 µM Y27632 for the first 24 h.

At 2 days and 4 days post-printing, the cells were incubated with 2 µM calcein AM and 2 µM ethidium homodimer 1 to label live and dead cells respectively. As illustrated in Figure 3.38A, the non-printed and 1 bar-printed samples continued to contain live cells (labelled in green) on day 2, whereas the 3 bar-printed sample contained mostly dead cells (labelled in red). On day 4, the non-printed samples contained a few live cell clusters, but the vast majority of the printed hiPSCs in 1 bar and 3 bar samples were no longer viable (Figure 3.38B). Based on these results, 3 bar printed conditions were excluded from further experiments as hiPSC-loaded bioink could already be extruded from the nozzle at 1 bar pressure, and 3 bar pressure had a large and clear detrimental impact on cell viability.

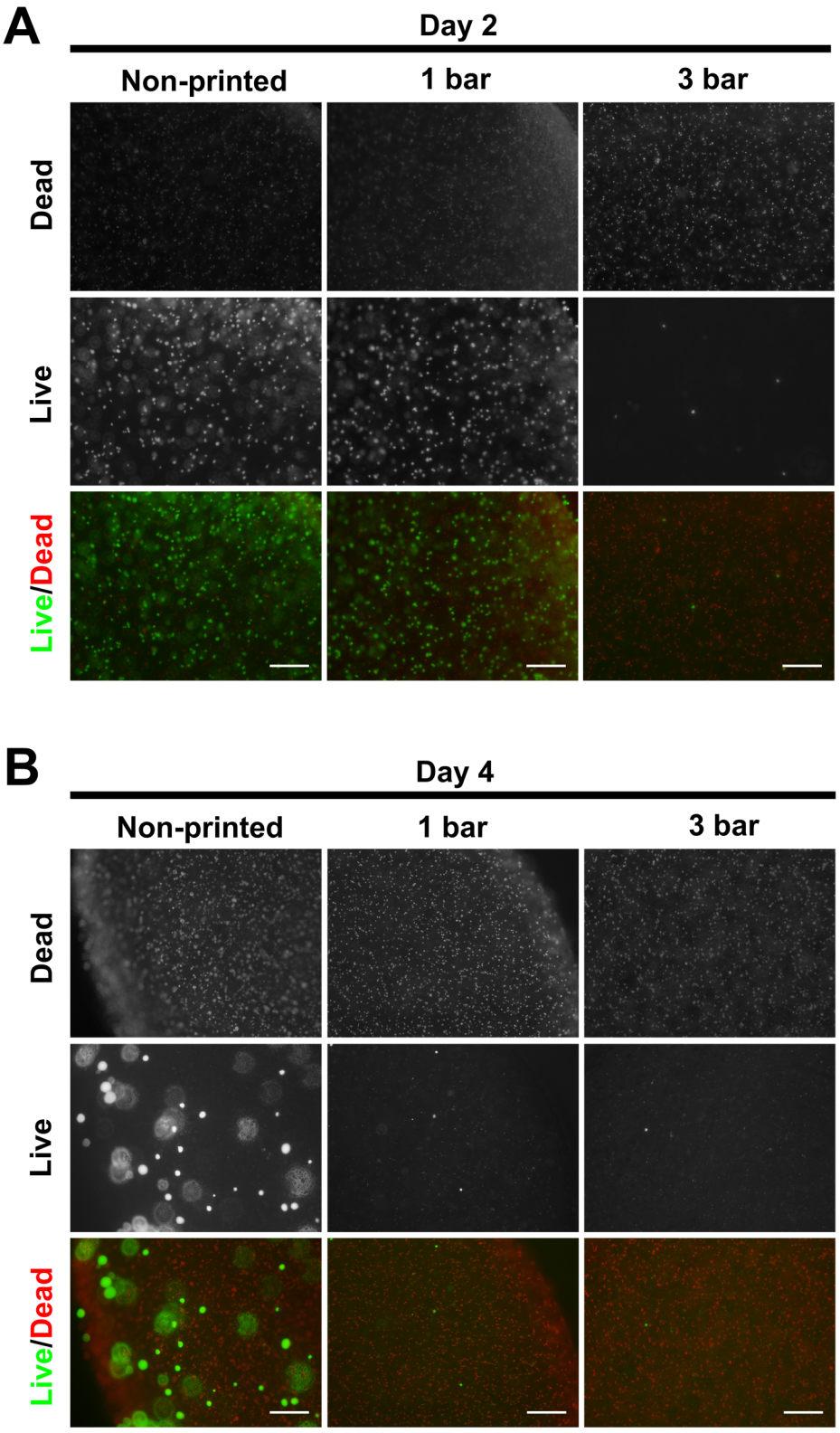

Figure 3.38 hiPSCs mixed into gelatin-alginate hydrogel as a single cell suspension exhibit low viability after 4 days of culture. Gelatin-alginate bioinks loaded with hiPSCs as a single cell suspension were either dispensed (non-printed) or printed (at 1 bar or 3 bar) into disc-shaped silicone moulds, cross-linked with Ca^{2+}, and cultured in StemMACS iPS-Brew XF with 10 µM Y27632 for the first 24 h. (A) At 2 days post-printing, live cells could still be detected in the non-printed and 1 bar printed samples (labelled with calcein AM, green); in contrast, almost all of the cells in the 3 bar printed sample were dead (labelled with ethidium homodimer 1, red). (B) By day 4, while a few live cell clusters could be detected in the non-printed sample, almost all cells in the 1 bar and 3 bar printed samples were dead. Scale bars = 200 µm.

Matrigel (MG) is used as a coating for plasticware to allow hiPSC attachment and survival. Therefore, it was hypothesised that incorporation of MG into the hydrogel could provide a more permissive environment for hiPSCs to grow and survive within the hydrogel. To test whether the addition of MG could improve the viability of printed hiPSCs in single cell suspension, gelatin-alginate hydrogel was prepared using MG dissolved in DPBS instead of DPBS alone. Thereafter, hiPSCs in single cell suspension were mixed into the gelatin-alginate-MG hydrogel to form the bioink, and the bioink was either dispensed or printed at 1 bar into disc-shaped silicone moulds. These discs were cross-linked and then cultured over the following 4 days in StemMACS iPS-Brew XF, with 10 µM Y27632 for the first 24 h. After 1 day or 4 days of culture, the viability of the cells in these gelatin-alginate-Matrigel discs was assessed. As shown in Figure 3.39, some viable cells were detected at 1 day after printing in both the non-printed and 1 bar printed samples. However, despite the addition of MG, cell viability was not improved at 4 days post-print as most of the cells in both non-printed and 1 bar-printed samples were dead. Other approaches to maintain viability of hiPSCs had to be investigated.

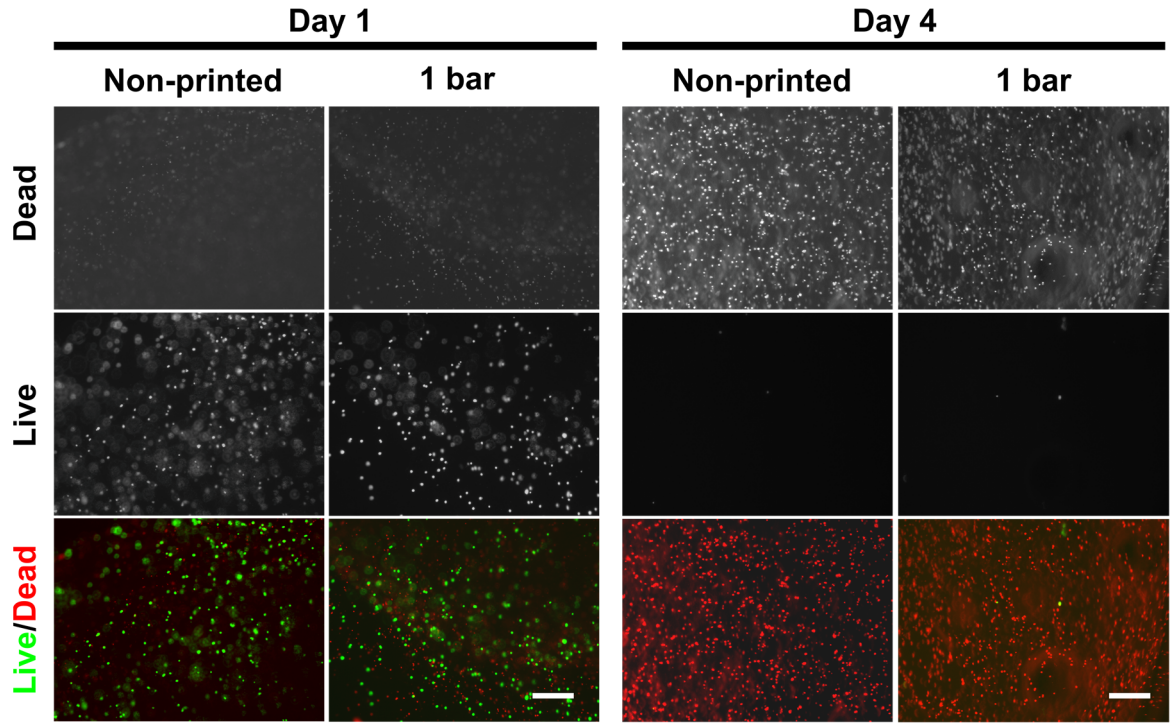

Figure 3.39 Inclusion of Matrigel in gelatin-alginate hydrogels does not improve hiPSC viability when the hiPSCs are loaded as a single cell suspension. Gelatin-alginate-Matrigel bioinks loaded with hiPSCs as a single cell suspension were either dispensed (non-printed) or printed into disc-shaped silicone moulds, cross-linked with Ca^{2+}, and cultured in StemMACS iPS-Brew XF with 10 µM Y27632 for the first 24 h. After 1 day, live cells were detected in the non-printed and 1 bar printed samples (labelled with calcein AM, green). However, after 4 days, almost all the cells in both the non-printed and printed samples were dead (labelled with ethidium homodimer 1, red). Scale bars = 200 µm.

3.3.3 Bioinks of gelatin-alginate loaded with hiPSCs as aggregates

Cell-cell contact has an impact on hiPSC survival (Li, Bennett, and Wang, 2012), and we hypothesised that mixing hiPSCs into the hydrogel as cell clusters or cell aggregates could be an approach to increase hiPSCs' viability for longer periods of time in hydrogels after printing. To assess this approach, hiPSCs were first cultured in suspension to generate hiPSC aggregates. These aggregates were then mixed into gelatin-alginate hydrogel to generate an aggregate-loaded bioink. This aggregate-loaded bioink was then dispensed or printed at 1 bar into disc-shaped silicone moulds, cross-linked, and cultured as before but without Y27632 supplementation.

After 1 day of culture, cells were assayed for viability, and cells comprising aggregates were found to remain viable as they were labelled green with calcein AM, with a few dead cells labelled red with ethidium homodimer 1 (Figure 3.40). In stark contrast to hiPSCs mixed in as single cells (Figure 3.38, Figure 3.39), the hiPSCs that were mixed in as aggregates continued to be viable even after 4 days of culture (Figure 3.40) and increased in size, suggesting proliferation. While some aggregates stained red and were inferred to be comprised of dead cells, this represented a significant improvement in the maintenance of viability of hiPSCs after printing.

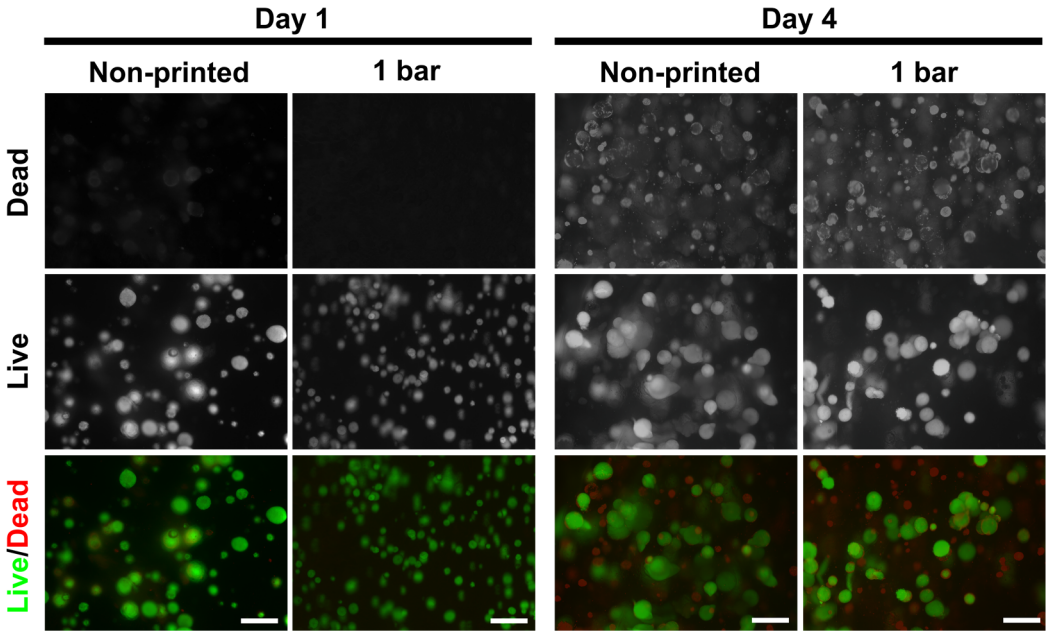

Figure 3.40 hiPSC viability is greatly improved when mixed into gelatin-alginate hydrogels as aggregates instead of single cells. Gelatin-alginate hydrogel was loaded with hiPSC aggregates to form aggregate-loaded bioink, and this was either dispensed (non-printed) or printed into disc-shaped silicone moulds, cross-linked with Ca^{2+}, and cultured in StemMACS iPS-Brew XF without Y27632 supplementation. After 1 day post-printing, live cells were present in both non-printed and 1 bar-printed discs (labelled with calcein AM, green), with a few dead cells (labelled with ethidium homodimer-1, red). After 4 days of culture, many live cell aggregates could still be found, in contrast to hiPSCs loaded as single cells. Scale bars = 200 µm.

To further quantify the fraction of viable cells remaining in the printed bioinks after 4 days of culture, the hydrogel was dissolved by EDTA and the recovered aggregates were processed with Accutase into a single cell suspension (see Section 2.2.14.4) for flow cytometric analysis. The single cell suspension containing cells recovered from the printed bioink was labelled with the fixable viability stain Viobility 405/452 to assess viability and labelled with antibodies against pluripotency-associated markers TRA-1-60 and SSEA-4 to assess the maintenance of pluripotency. A portion of the single cell suspension was re-plated onto hES MG-coated plasticware to verify whether cells were qualitatively viable and able to attach to hES MG and continue to proliferate. Flow cytometric analysis of the recovered cells revealed that ~70% of the cells were viable (Figure 3.41A), and of these viable cells, >95% of them continued to express both the pluripotency-associated markers (Figure 3.41B). The re-plated cells were also able to attach to hES MG-coated plasticware and continued to proliferate with typical hiPSC colony morphology (Figure 3.41C)

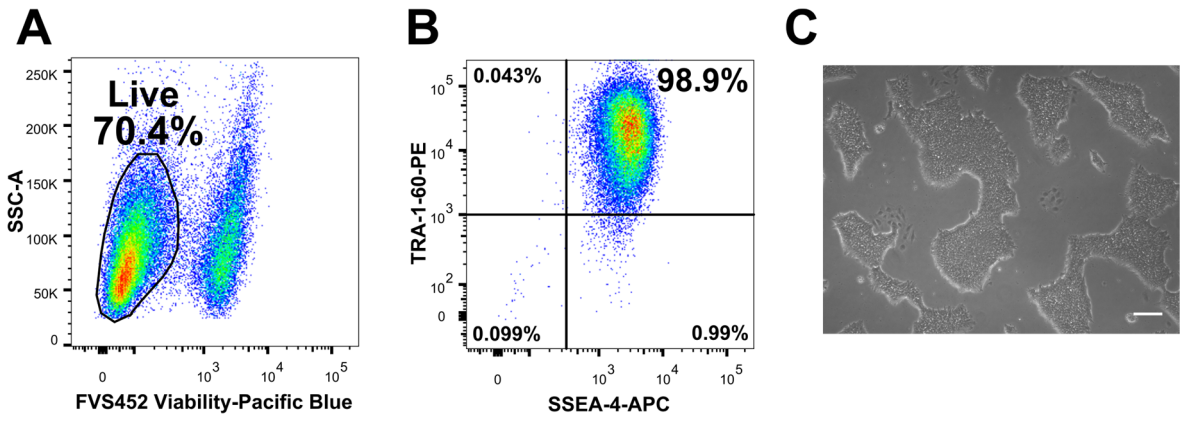

Figure 3.41 hiPSCs recovered from printed bioink discs after 4 days of culture remain viable and pluripotent. (A) 70% of the recovered printed hiPSCs from bioink discs remained viable. FVS452: fixable viability stain, Viobility 405/452. (B) Of the viable cells, >95% of these cells were double-positive for pluripotency-associated markers TRA-1-60 and SSEA-4. (C) Recovered printed hiPSCs were replated on hES MG-coated plates and cultured for another 4 days. Cells attached and continued to proliferate, exhibiting typical hiPSC morphology. Scale bar = 100 µm.

3.3.4 Biofabrication of constructs using hiPSC aggregate bioinks

After establishing the feasibility of printing hiPSC as aggregates mixed into gelatin-alginate hydrogel with sustained viability and maintenance of pluripotency in culture, the next aim was to use this aggregate-loaded bioink for the biofabrication of defined constructs of a specific shape. To illustrate this, square grid constructs with a crosshatch infill were printed onto chilled glass microscope coverslips using the aggregate-loaded bioink (Figure 3.42). These constructs measured 12 × 12 mm, with fibres of ~4.3 mm thickness, and 1.5 mm between fibres. After printing, the constructs were cross-linked with Ca^{2+}, and cultured for 4 days and analysed for viability and pluripotency.

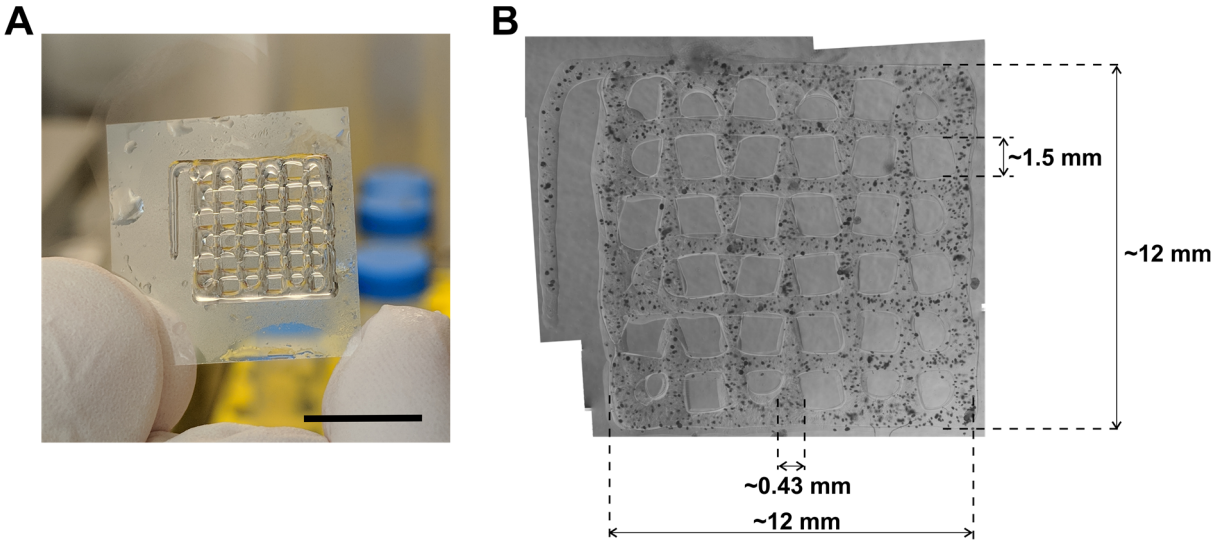

Figure 3.42 Biofabricated square grid constructs with crosshatch infill using hiPSC-loaded bioink. (A) Biofabricated construct shortly after printing, before cross-linking with Ca^{2+}. Scale bar = 10 mm. (B) Microscope images of the biofabricated construct were taken and stitched together in software. Fibres of ~0.43 mm were extruded from the bioprinter set at 1 bar pressure, with ~1.5 mm between fibres. Aggregates of hiPSCs can be observed encapsulated in the gelatin-alginate hydrogel.

Like the results from printed discs, after 1 day of culture, hiPSC aggregates in biofabricated square grids remained alive with some dead cells (Figure 3.43, left). After 4 days of culture, hiPSC aggregates grew in size indicating proliferation, while some dead cells could also be observed, notably around the periphery of live aggregates, or in small aggregates (Figure 3.43, right).

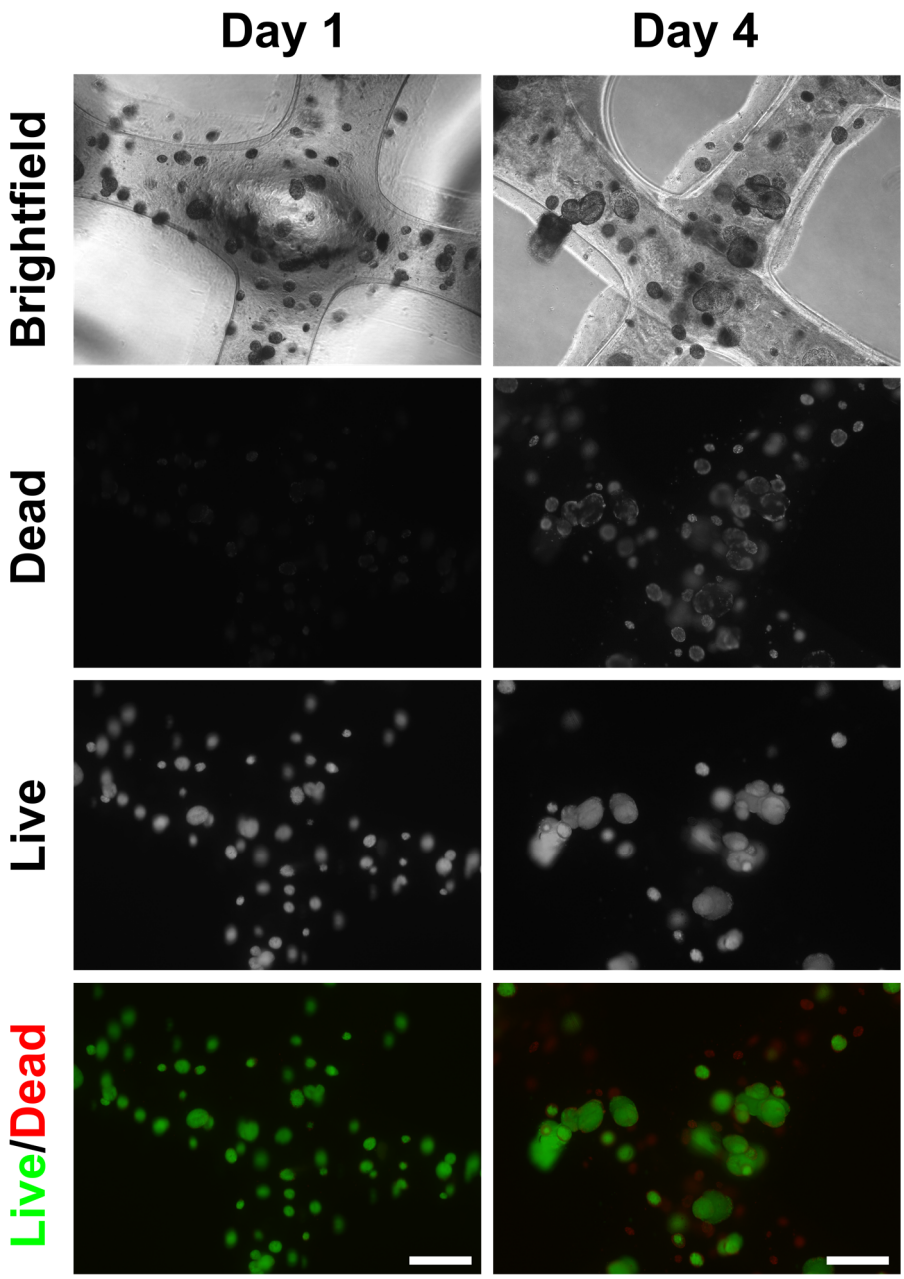

Figure 3.43 hiPSCs as aggregates loaded into gelatin-alginate hydrogels can be printed into a defined pattern and survive after 4 days of culture. Biofabricated square grids were cultured in StemMACS iPS-Brew XF without Y27632 supplementation. After 1 day of culture post-printing, live cells in aggregates could be detected (labelled with calcein AM, green), with a few dead cells (labelled with ethidium homodimer-1, red). With the same analysis done after 4 days of culture, some dead cells could be detected, but many aggregates had grown and contained live cells. Scale bars = 200 µm.

Quantification of the percentage of viable cells in this biofabricated construct was performed by first dissolving the hydrogel with EDTA, then recovering the aggregates, and then processing the aggregates into a single cell suspension for analysis. Through flow cytometric analysis, ~68% of the cells were found to be viable (Figure 3.44A), and >95% of these viable cells were double-positive for pluripotency-

associated markers TRA-1-60 and SSEA-4 (Figure 3.44B). By re-plating these cells onto hES MG-coated plasticware, viability could be verified by the observation that the cells could attach to the plates and proliferated to form small colonies after 2 days of culture, with typical colony morphology expected of hiPSCs (Figure 3.44C).

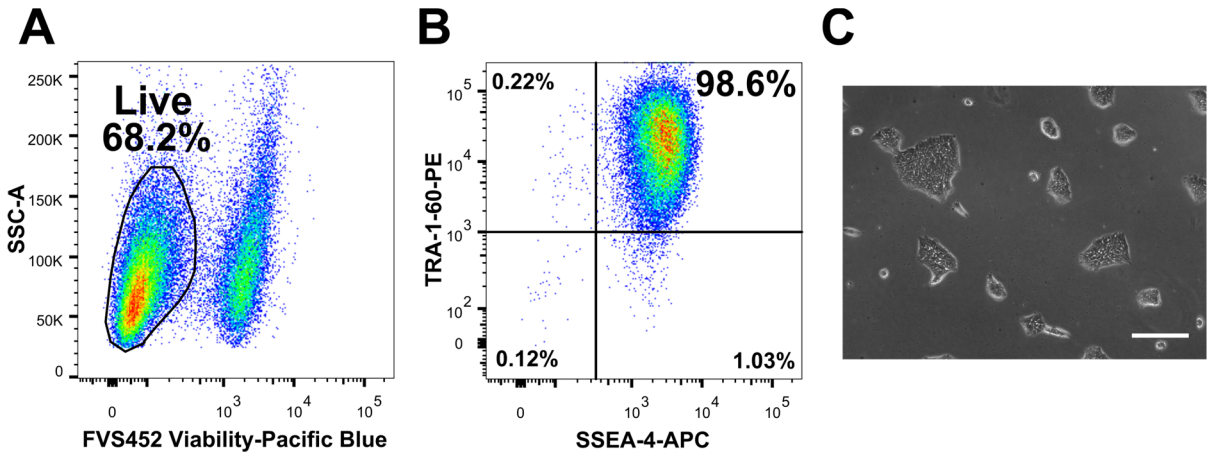

Figure 3.44 hiPSCs recovered from printed square grids after 4 days of culture remain viable and pluripotent. (A) ~68% of the recovered printed hiPSCs from biofabricated square grids remained viable after 4 days. FVS452: fixable viability stain, Viobility 405/452. (B) Of the viable cells, >95% of these cells were double-positive for pluripotency-associated markers TRA-1-60 and SSEA-4. (C) Similar to printed bioink discs, the hiPSCs recovered were re-plated on hES MG-coated plates and cultured for 2 days. Resultant colonies had typical hiPSC morphology. Scale bar = 200 µm.

3.3.5 Neuronal differentiation of biofabricated constructs

While the results shown above demonstrate that hiPSCs can survive as aggregates when printed and encapsulated in gelatin-alginate hydrogel, the possibility to differentiate the printed hiPSCs into a more committed lineage should be assessed. To address this, the hiPSCs in biofabricated square grids were directed to differentiate into neurons as a proof-of-principle.

The printed constructs containing hiPSC aggregates were switched from maintenance medium (StemMACS iPS-Brew XF) to the various differentiation media as outlined in Section 2.2.14.3. After applying the neuronal differentiation protocol, the differentiated constructs were imaged, focus-Z-stacked, and stitched as described to generate an overview image (Figure 3.45A). Neurite-like projections could be observed growing out of aggregates at higher magnifications (Figure 3.45B, C).

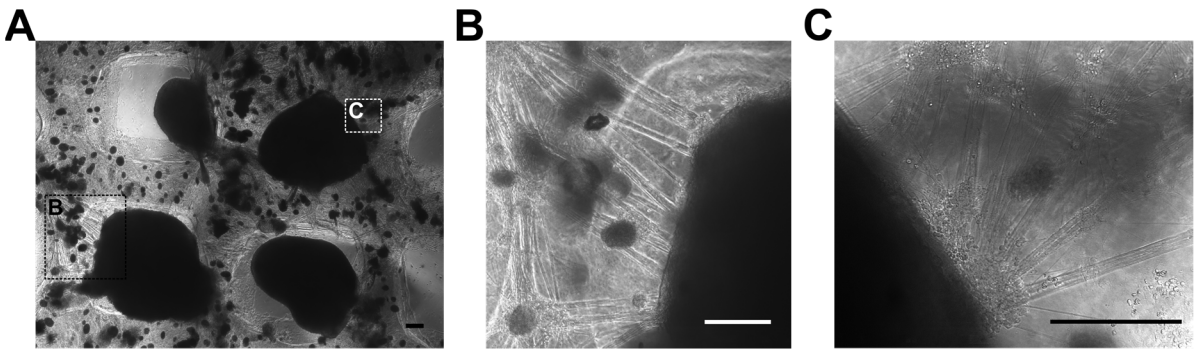

Figure 3.45 hiPSCs printed as aggregates respond to differentiation cues and differentiate into cells resembling neurons with neurite-like outgrowth.(A) Focus-Z-stacked and stitched image of printed aggregates after more than 3 weeks of neuronal differentiation. Fields B and C are shown at higher magnifications (B) and (C) respectively. Neurite-like projections from aggregates can be observed, suggesting a putative neuronal identity. Scale bars = 200 µm.

To further characterise the resulting cells, these putative neuronal constructs were then fixed and analysed by immunocytochemistry, staining for the pan-neuronal marker βIII-tubulin (TUBB3). As shown in Figure 3.46, these cells stain positive for TUBB3, and have neuronal bundle-like morphology projecting out from the differentiating aggregates. These data suggest that the earlier printed hiPSC aggregates could survive over several days and differentiate into neurons when provided with the appropriate signals by the medium.

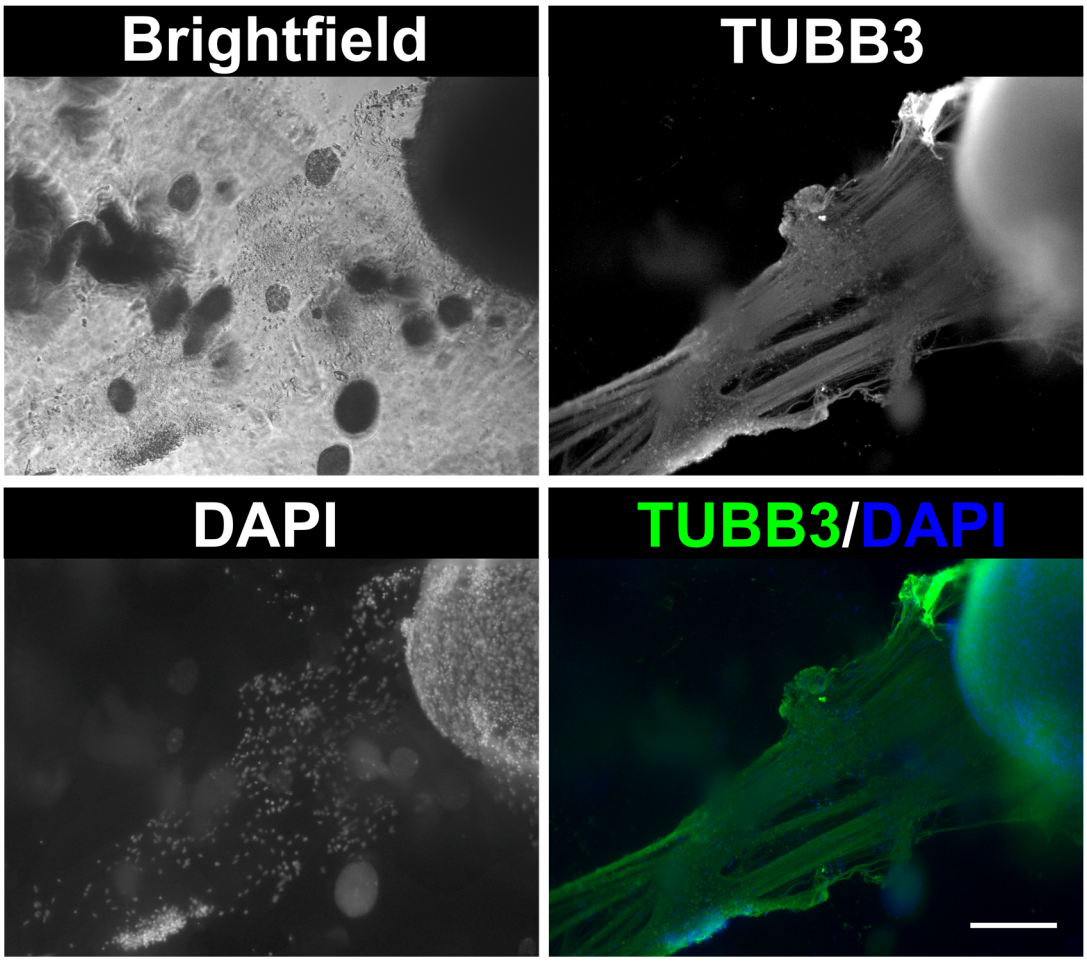

Figure 3.46 Printed hiPSCs differentiate into neurons upon neuronal differentiation as evidenced by TUBB3. After neuronal differentiation, the printed construct was fixed and stained for the neuronal marker TUBB3. Neuronal bundles projecting out of earlier hiPSC aggregates are positive for TUBB3, suggesting a neuronal identity. Scale bar = 200 µm.

4. Discussion

4.1 Stirred suspension culture for hiPSC expansion is feasible and scalable

4.1.1 hiPSCs can be cultured as cell-only aggregates in stirred spinner flasks

The scale-up procedure described in this thesis enables the medium scale generation of hiPSCs as cell-only aggregates in stirred spinner flasks. Starting with a seeding population of 16×10^6 hiPSCs that were cultured under adherent culture conditions, we successfully expanded them into $>250 \times 10^6$ hiPSCs over 7 days in spinner flasks, representing a ~16-fold increase. The hiPSCs cultured in spinner flasks exhibit pluripotency-associated markers such as TRA-1-60 and SSEA-4 and remain viable for further expansion and downstream processing, and can be serially passaged in these spinner flasks for at least 7 weeks.

Our pilot experiment was based on previously published work (Amit *et al.*, 2011; Zweigerdt *et al.*, 2011), and while we could generate hiPSC aggregates using culture parameters from those studies, our pilot aggregates had unexpectedly non-uniform morphology with large variation in their dimensions. Moreover, they had started to lose pluripotency-associated factors such as OCT4 and TRA-1-60 (Figure 3.2). It was evident that while the previous reports were useful as a blueprint for starting suspension cultures, troubleshooting steps to establish suspension culture in our laboratory were necessary. Potential explanations for the different processing parameters could be i) different spinner flask/bioreactor designs and ii) cell line-to-cell line variability cannot be ruled out. Previous reports had suggested that aggregate sizes had to be controlled during suspension culture to minimise differentiation of cells in larger aggregates (Abbasalizadeh *et al.*, 2012; Krawetz *et al.*, 2009). We reasoned that the non-uniform morphology of our initial aggregates was resulting in unwanted differentiation, and such non-uniform morphology could be due to agglomeration of aggregates in our spinner flasks. Therefore, we performed a titration experiment with different cell seeding densities and agitation speeds to identify a combination suitable for our specific spinner flask design and for the hiPSC lines developed in our laboratory. Through the titration experiment (Figure 3.5), we could identify a combination of parameters suited to our spinner flasks and cell lines (85 RPM, 2×10^5 hiPSC/mL seeding density). Once these parameters were determined, we could reliably and reproducibly culture hiPSCs as aggregates in

spinner flasks, further confirming that the general approach of culturing hiPSCs in cell-only aggregates in stirred suspension is feasible.

After establishing optimal stirring speeds and cell inoculation density, we sought to improve upon the medium exchanging protocol and could demonstrate that we could improve the process efficiency by i) reducing medium consumption and ii) increasing aggregate retention within the spinner flasks. Most previous publications rely on medium *exchange* on day 2 and daily medium exchange thereafter, which we termed the "regular protocol". However, we noticed that day 2 aggregates were around 80–100 µm in diameter and a significant portion of these aggregates would be aspirated away during medium exchange, even if we allowed the aggregates to sediment before medium removal. Additionally, excessive durations of sedimentation would also lead to the fusing of individual aggregates to form large, irregular chains and networks of cells, leading to loss of control over aggregate sizes (data not shown). To overcome both of these difficulties, we optimised the medium exchange protocol by changing the time point of the first medium exchange. Elanzew and colleagues found that medium *addition* instead of medium *exchange* on days 2 and 3 was still able to maintain hiPSC viability and pluripotency (Elanzew *et al.*, 2015). While they opted to passage cells after 4 days of culture with completely no medium exchange, we instead extended the culture process for another 3 days with medium exchange on those additional days and we termed this the "optimised protocol" (Figure 3.6). This resulted in improved cell yields over a 7-day passage, with the maintenance of pluripotency and viability. At day 7, aggregates were about 300–350 µm in diameter on average depending on cell line, and given that necrosis and other effects of nutrient and gas diffusion limits occur around 300 µm and above (Kinney, Sargent, and Mcdevitt, 2011; Wu *et al.*, 2014), this was defined as the end-point of one "passage" in suspension culture.

Another aspect of suspension cultures that is not frequently addressed in the literature is whether hPSCs can be maintained long-term in suspension culture with minimal loss in viability or pluripotency. We demonstrated sequential expansion of hiPSCs over 7 passages of 7 days per passage (up to 49 days), while maintaining high viability of cells (>90%) and >90% of cells remained positive for pluripotency-associated markers SSEA-4 and TRA-1-60 (Figure 3.13). This illustrated the feasibility of maintaining hiPSCs in suspension culture for extended periods of time.

With the above, we have shown that stirred spinner flasks offer the possibility to scale up the culture of hiPSCs. However, there are still some open questions regarding the applicability of spinner flasks to all hiPSC lines. As outlined previously in Section 1.1.1.2, there are now a plethora of cell sources and reprogramming methods that can be used to derive hiPSCs. These may all result in cells that have the hallmarks of PSCs and pass all characterisation checks, but these might also result in variances between cell lines not only in their differentiation potential, but also their amenability to be cultured in suspension culture. Indeed, there has been at least one report of a clinically compliant hESC cell line that has been well-characterised for its pluripotency, but fails to stably expand as undifferentiated aggregates in suspension culture in mTeSR-1 medium (Singh *et al.*, 2010). Even some commonly used hPSC lines, such as the hESC line HES-3 and the hiPSC line IMR90 (Yu *et al.*, 2007), have been shown to be sensitive to shear forces that are present in stirred suspension cultures that trigger differentiation (Leung *et al.*, 2011). To further complicate the matter, there is now a wide variety of culture media for feeder-free culture of hPSCs (Dakhore, Nayer, and Hasegawa, 2018), and each formulation would require careful validation for its compatibility with specific cell lines and suitability for stirred suspension culture. Therefore, we concur and join others in recommending that small scale aggregation experiments are performed to screen hPSC lines before undertaking larger scale up studies (Zweigerdt *et al.*, 2011), and to establish and standardise optimal cell inoculation and passaging for suspension cultures (Chen *et al.*, 2014b). It also remains to be seen if these spinner flasks can be used to expand other hPSC lines, or whether any adaptation is required.

4.1.2 hiPSCs can be cultured as cell-only aggregates in stirred bioreactors

We processed the hiPSCs generated in spinner flasks into a single cell suspension and used it as the inoculum (2×10^5 hiPSCs/mL seeding density) for further scaling up the culture process in bioreactors. To ensure a homogeneously sized aggregate population, we also found it crucial to remove small cell clumps arising from incomplete aggregate digestion (Figure 3.11). Our strategy was to strain the cell suspension through a 40 µm strainer before inoculation into the bioreactor. By setting the bioreactor agitation rate to 164 RPM and aerating through a gas overlay, we used the same "optimised protocol" for medium exchange and could successfully expand 200×10^6 hiPSCs into nearly 2×10^9 hiPSCs over 7 days, representing a ~10-fold increase. The hiPSCs cultured in bioreactors continue to exhibit pluripotency-associated markers, maintain the ability to differentiate into cells of all three germ

layers, can respond to specific directed differentiation cues, and maintain a stable karyotype. We therefore achieved the aim of generating 1–2 × 10^9 hiPSCs in the bioreactor which was a fair approximation of the cells required for most cell replacement therapies (Section 1.1.3, Laflamme and Murry, 2011; Mummery, 2005; Zweigerdt, 2009).

While there are several research groups working towards scaling up the culture of cells as described in Section 1.2, many of these studies showed the feasibility of suspension culture in volumes <300 mL, while the question of *scalability* to volumes higher than that were not adequately addressed. In contrast, this thesis presents further data to show the *scalability* of the stirred suspension culture approach. Not only is the volume different between spinner flasks (~125 mL) and bioreactors (~2.4 L), the spinner fin design is different as well. Therefore, the agitation rate of 85 RPM in spinners had to be converted for the bioreactor. Based on earlier studies on the 3 L Mobius Single-use bioreactor (Kehoe *et al.*, 2010; Mollet *et al.*, 2007), we determined that the corresponding agitation rate for the bioreactor would be 164 RPM.

To our knowledge, the spinner flask-to-bioreactor two-phase approach developed in this thesis is the first demonstration of expanding cells in a smaller spinner flask before using the generated cells as inoculum for a larger bioreactor. We initially encountered problems with generating a single cell suspension from digestion of aggregates from spinner flasks. This problem was solved by our strategy of running the cell suspension through a 40 µm cell strainer before usage as inoculum. Therefore, cell straining may be used as a method to obtain a more homogeneous single cell suspension from difficult-to-dissociate populations such as hPSC aggregates.

Metabolite analysis of the culture medium during suspension culture in bioreactor also revealed that lactate concentrations were consistently below 16 mM. Interestingly, even on day 7 of bioreactor culture, aggregates of both hiPSC lines were only ~200 µm in diameter, and lactate concentrations within the culture medium were only at about 15 mM. Since lactate is suggested to be limiting around 22 mM (Chen *et al.*, 2010b) and ~300 µm is suggested to be the limit for aggregate sizes beyond which necrosis and other nutrient-diffusion effects start to occur (Kinney, Sargent, and Mcdevitt, 2011; Wu *et al.*, 2014), the aggregate size of ~200 µm and lactate concentration of 15 mM may indicate that it could have been possible to further

extend the culture duration of the hiPSC aggregates in bioreactors to more than 7 days in order to harvest more cells. It would certainly be an interesting follow-up investigation to further increase yield and process efficiency.

To ensure the quality of hiPSCs expanded from bioreactors, not only did we perform a battery of tests to characterise PSCs (Martí *et al.*, 2013), we additionally showed that they could respond to specific differentiation cues to differentiate into beating cardiomyocyte-like cells (see Section 3.1.2.2, Figure 3.21, Movies 1 and 2). While other suspension culture scale-up studies regularly perform standard hPSC characterisation on resulting hPSCs, the further step of showing responsivity to specific differentiation cues is rarely shown. Taken together, we showed that we could produce high quality hiPSCs in bioreactors while maintaining their pluripotency and in high quantities suitable for further differentiation for cell therapy and other biomedical applications.

4.1.3 Sequential spinner-to-bioreactor scale up is efficient

With the workflow developed in this thesis, with spinner flasks, we observe a 16-fold increase in cell quantity over 7 days of culture. In bioreactors, we achieve nearly 10-fold increase in cell quantity over 7 days of culture.

Currently, there is no commonly accepted approach to evaluate the efficiency of the various methods used to culture hPSCs either in adherent or suspension conditions, and no gold standard exists for hPSC culture. A recent review proposed the use of a metric, fold increase per day (FIPD; Chen *et al.*, 2014b), to quickly estimate the growth rate of hPSCs cultured in various formats and perform comparisons between these methods. This FIPD value can be derived by taking the fold increase in cell number and dividing it by the number of days of culture required to produce the final number of cells. When our spinner flask or bioreactor cultures are considered independently, our FIPD values of 2.28 (spinner flasks) and 1.42 (bioreactors) fall within the ranges reported thus far (Table 4.1).

However, if we consider the expansion protocol as an integrated sequential two-phase (spinner phase and bioreactor phase) process, we can then perform the following calculation. Starting with 16×10^6 cells harvested from standard adherent culture as inoculum for spinner flasks, we then expand this starter population into nearly 2×10^9 cells, representing a 125-fold increase over 14 days for an FIPD of 8.92. This surpasses the currently reported FIPD values of other expansion systems and suggests an appreciably higher efficiency of the 14-day workflow that we developed.

Table 4.1 Comparison of representative suspension culture studies (Modified from Chen *et al.*, 2014b)

Cell type	Inoculation method	Vessel type	Max. FIPD	Reference
hiPSCs	Single cells	Spinner flask + bioreactor	8.92	Kwok *et al.*, 2018 (this thesis)
hiPSCs	Single cells	Spinner flask only	2.28	Kwok *et al.*, 2018 (this thesis)
hiPSCs	Single cells	Bioreactor only	1.42	Kwok *et al.*, 2018 (this thesis)
hiPSCs	Single cells	Bioreactor	5.0	Elanzew *et al.*, 2015
hiPSCs	Single cells	Bioreactor	2.0	Abecasis *et al.*, 2017
hiPSCs	Single cells	Spinner flask	1.5	Zweigerdt *et al.*, 2011
hiPSCs	Single cells	Bioreactor	0.96	Kropp *et al.*, 2016
hESCs	Clumps	Erlenmeyer	2.5	Amit *et al.*, 2010
hESCs	Clumps with microcarriers	Spinner flask	5.6	Lock and Tzanakakis, 2009
hESCs	Single cells	Bioreactor	4.2	Krawetz *et al.*, 2009
hESCs (WA09)	Single cells	Spinner flask	4.2	Chen *et al.*, 2012
hESCs (HES-3)	Clumps with microcarriers	Spinner flask	4.0	Oh *et al.*, 2009
hESCs	Single cells	Spinner flask	0.7	Steiner *et al.*, 2010

While the FIPD of our developed protocol is higher than those reported by others, there is still room for further improvement. Our medium exchange protocol relies on batch feeding, which involves exchange of ~70-80% of spent culture medium with fresh medium. The reliance on batch feeding is a limitation of the current bioreactor and controller design. The batch feeding approach has been reported to result in large fluctuations in culture environment in terms of glucose availability, waste metabolite concentrations, and dissolved oxygen (Kropp *et al.*, 2016). In contrast, a perfusion approach using slow and continuous waste medium removal and fresh medium replacement eliminates such large fluctuations, which correlates with significant increases in growth rates and therefore higher quantities of cells harvested. In terms of FIPD, a calculation based on Kropp and colleagues' (2016) data suggest an FIPD of 0.66 using batch feeding, compared to an FIPD of 0.96 using

perfusion feeding methods. Thus, a bioreactor re-design or addition of modules to the controller to enable controlled perfusion feeding may offer another approach to further increase the process efficiency of our protocol.

The unique needs of suspension culture can also be taken into consideration for further optimisation of stirred suspension culture. For example, a drawback of suspension culture systems is the loss of suspended aggregates during medium exchange. Even though time is allowed for aggregates to sediment, the aspiration forces to remove spent medium frequently also inadvertently remove a portion of cell aggregates. Longer sedimentation time could partially alleviate this problem but results in another issue of agglomeration of aggregates after excessive sedimentation times, thereby greatly reducing the ability to control homogeneous aggregate sizes. Therefore, a reduction in the number of medium exchanges can contribute to higher retention of aggregates in the culture vessel. While our protocol already includes optimisation to reduce the number of medium exchanges (see Section 3.1.1.1 and Figure 3.6), an additional solution is to develop medium formulations that support this particular demand of suspension culture. As the field is increasingly recognising the importance of 3D culture formats, whether for cell expansion or for organoid culture, more medium formulations are being made available to suit the needs of 3D culture systems. An example of a hPSC culture medium formulation that is now commercially available is mTeSR 3D. It is based on mTeSR-1, the medium used in our study. To minimise medium exchange, culturing cells in mTeSR 3D does not require medium exchange but relies only on adding a mixture of supplements containing growth factors and nutrients to the “spent” medium, hence eliminating the loss of aggregates.

It is also worthy to note that across the various groups investigating bioreactor culture of hPSCs, there is no consensus on initial cell seeding densities, medium formulation, and duration of culture, as these rely in part on bioreactor designs and may also be affected by cell line-to-line variability (Serra *et al.*, 2010; Zweigerdt *et al.*, 2011). This highlights a weakness of using FIPD alone to evaluate the efficiency and should be used in combination with other parameters such as growth curves to compare between differing protocols and instrumentation.

4.2 Spinner flask culture does not support the expansion of iNSCs

We attempted to culture iNSCs using the same stirred spinner flasks, but such an approach proved unfeasible as we were unable to efficiently culture proliferating iNSCs in the reported culture medium NIM (Meyer *et al.*, 2015). An alternative expansion medium NEM (Jovanovic *et al.*, 2018) was assessed for its suitability to culture iNSCs in suspension as well as in adherent conditions, but this was associated with signs of a reduced fraction of PAX6-positive cells as analysed by flow cytometry. Intriguingly, these NEM cultured iNSCs continued to stain positive for PAX6 in immunofluorescence analysis (Section 3.2.2).

Current publications have described the suspension culture of NSCs as neurospheres (Jensen and Parmar, 2006; Pacey *et al.*, 2006), or cultured on microcarriers in a rotating wall vessel-type bioreactor (Srinivasan *et al.*, 2018). Crucially, neurosphere cultures are either static suspension cultures or suspension cultures on rotators, both of which involve relatively low shear stress. Rotating wall vessel-type bioreactors are also associated with lower shear stress, thus suggesting that shear stress may be an important factor in suspension cultures of NSCs. This may help to explain why iNSCs appear to be incompatible with the stirred spinner flasks used in this thesis, which are associated with relatively high amounts of shear stress due to the fin design. Additionally, given the discrepancies between flow cytometry and immunofluorescence data, the difference in clonality of the antibodies used in these analyses may impact on the interpretation of PAX6-positivity. Further study into this phenomenon is required to elucidate the true impact of NEM on the expansion of iNSCs.

While scaled up production of iNSCs has not been demonstrated thus far, alternative methods have been considered. Since iNSCs grow and proliferate under standard adherent conditions on MG in NIM, higher quantity production of these sensitive cells can be achieved through a scale out strategy. This could, for example, include methods such as using multi-layer flasks (Section 1.2.1) coated with MG to expand these iNSCs. In the meantime, these iNSCs are attractive potential candidates for cell therapy applications for diseases such as multiple sclerosis (Martino *et al.*, 2010; Pluchino *et al.*, 2009). Currently, there is an ongoing clinical trial in phase 1 assessing the safety of human foetal-derived NSCs for the treatment of multiple sclerosis (ClinicalTrials.gov ID: NCT03269071). Similar studies may also benefit from autologously-derived iNSCs which can be generated and directly converted from

fibroblasts of patients (Meyer *et al.*, 2015). These iNSCs are currently being tested in collaboration with the Pluchino group in various contexts (Peruzzotti-Jametti *et al.*, 2018), including investigating their effects and differentiation upon transplantation into *Olig*-deficient mice as part of *in vivo* testing in mouse models that is required before human trials.

4.3 hiPSC aggregate-loaded gelatin-alginate hydrogel is a printable bioink

In this thesis, the utility of hiPSC aggregates is further demonstrated by their incorporation into gelatin-alginate hydrogels to form a hiPSC-loaded bioink. hiPSCs loaded as aggregates showed ~70% viability 4 days after printing, continued to exhibit pluripotency-associated markers SSEA-4 and TRA-1-60, and could be recovered from the bioprint and further propagated. Bioprinted hiPSC aggregates could also respond to differentiation cues provided by the culture media, and we demonstrate the neuronal differentiation of a bioprint over the course of 4 weeks, giving rise to TUBB3-positive neurons.

Paxton and colleagues proposed a workflow to determine the printability of bioinks – as an initial, rapid screening process, the bioink could be manually extruded to identify useful concentrations and combinations that were compatible with cell survival (Paxton *et al.*, 2017). To that end, we initially assessed hiPSCs loaded as single cells in gelatin-alginate hydrogel or gelatin-alginate-MG hydrogel. However, hiPSCs printed in this way do not survive past 2 days (Figure 3.38). While a previous report of hPSCs printed as a single cell suspension in an alginate hydrogel using a valve-based cell printer system showed viability of ~60–86%, these viability stains were performed after just 30 min post-print (Faulkner-Jones *et al.*, 2015). We reasoned that since cell-cell contact has been shown to be important for hiPSC survival mediated through E-cadherin (Li, Bennett, and Wang, 2012; Rodin *et al.*, 2014), the loading of hiPSCs as cell aggregates instead of single cells should aid in cell viability post-printing. Therefore, we generated hiPSC aggregates using suspension culture for 1 day before mixing these hiPSC aggregates into the gelatin-alginate mixtures. After printing this hiPSC aggregate-laden gelatin-alginate hydrogel into disc-shaped silicone moulds, we noted that while some small aggregates were dead after 4 days of culture, the remaining aggregates remained viable in the printed hydrogel discs, labelled with calcein (Figure 3.40). After recovering these printed aggregates by EDTA treatment, they were dissociated into a single cell suspension and quantitatively analysed for viability and pluripotency-associated markers by

flow cytometry. We showed that after 4 days of culture encapsulated in the gelatin-alginate hydrogel, ~70% of the cells remained viable, and of these viable cells, >90% of them were double-positive for the surface pluripotency-associated markers SSEA-4 and TRA-1-60 (Figure 3.41), indicating that pluripotency was preserved in the live cells. Furthermore, viability was functionally shown by plating the cells from the recovered aggregates onto hES MG-coated plates and typical hiPSC morphology and growth was observed.

The results of this thesis further demonstrate that not only can these hiPSC aggregate-laden hydrogels be printed into moulds, they can also be printed as fibres into a 4-layer crosshatch infill pattern. The aggregates recovered from printed patterns also showed similar viability and pluripotency markers compared to the printed discs. Moreover, as a proof-of-principle, over a time period of 4 weeks we differentiated the printed hiPSC constructs towards a neural stem cell lineage using a previously published protocol for hiPSC aggregates (Reinhardt *et al.*, 2013), and further differentiated them into TUBB3-positive neurons (modified from Borghese *et al.*, 2010; Yan *et al.*, 2013), suggesting that the hiPSCs in these printed constructs have access to the differentiation cues supplied by the different culture media. This contrasts with existing publications regarding hPSC printing and differentiation. Faulkner-Jones and colleagues pre-differentiated hPSCs to hepatocyte-like cells for 6 days in adherent cultures before printing the differentiating cells with alginate hydrogel and continuing differentiation for another 17 days (Faulkner-Jones *et al.*, 2015), whereas Koch, Deiwick and colleagues used laser bioprinting to print hiPSC aggregates in hyaluronic acid/fibrinogen or hyaluronic acid/E8 medium onto MG-coated plates or coverslips before starting cardiac differentiation for ~20 days (Koch *et al.*, 2018). Other cell types have also been printed while loaded in other materials. For example, mouse and human fibroblasts have been loaded into highly concentrated spider silk protein solutions for extrusion. In these studies, survival of BALB/3T3 mouse fibroblasts for at least 18 days of culture (DeSimone *et al.*, 2017) and survival of human fibroblasts for at least 2 days of culture (Schacht *et al.*, 2015) were reported. Considering the relative robustness of fibroblasts in comparison to relatively sensitive hiPSCs, the survival of printed hiPSC constructs and subsequent differentiation over 4 weeks compares favourably and is in line with other reports of printing and differentiating cells.

Since alginate molecules can also be functionalised by coupling to peptides such as RGD motifs, one could utilise differentially functionalised alginate-based

bioinks to print specific shapes to guide growth. For example, GRGGL has been reported to be a peptide sequence suitable for neuronal attachment and network formation (An *et al.*, 2015). By coupling this peptide to alginate, one could imagine printing lines of GRGGL-functionalised alginate hydrogel to guide neuronal outgrowth and network formation, and use calcium imaging to visualise functional coupling of neuron networks (Grienberger and Konnerth, 2012).

4.4 Future perspectives

The contribution of the work presented in this thesis to biomedical applications of stem cells is graphically represented in Figure 4.1, and described in more detail in the following.

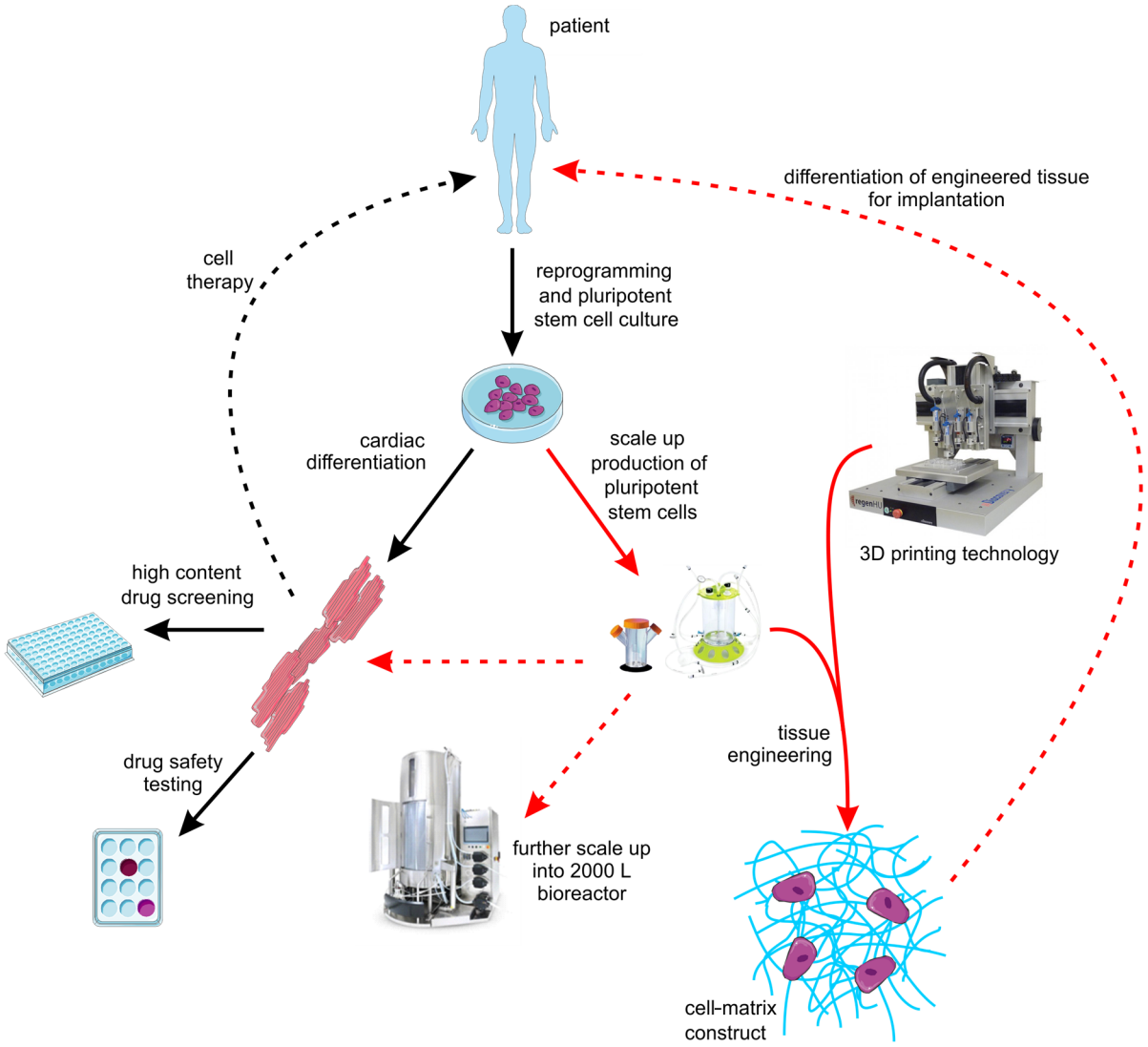

Figure 4.1 Future perspectives and applications of the current work. Represented by the red solid arrows, we have shown that we can use a combination of spinners and bioreactors to scale up the production of hiPSCs and combine these hiPSC aggregates with gelatin-alginate hydrogels to form a printable bioink. Using this bioink, we have printed a 4-layer construct of hiPSCs, and further differentiated this construct into neuronal cells. Potential future developments stemming from this work are represented by the red dashed arrows: Based on our data from 3 L scale Mobius bioreactors, further scale up into Mobius 1000 or 2000 L bioreactors could be performed to support hiPSC banking efforts. Bioreactor-generated hiPSC aggregates could continue to be differentiated into other cells such as cardiomyocytes to produce billions of cardiomyocytes for further downstream applications and potentially cell therapy. Further differentiation and maturation of bioprinted hiPSC constructs into tissue-specific constructs containing other cell types may one day be used for tissue implantation as a form of cell replacement therapy. (Modified from Braam, Passier, and Mummery, 2009 using elements contributed by Servier Medical Art, RegenHU's website, and the websites of Merck KGaA/MilliporeSigma)

4.4.1 Further scale-up and culture intensification

While a lot of excitement and interest has been generated around the possibility of autologous, highly personalised hiPSCs for deriving patient-specific cells for cell therapy, the costs associated with generating and validating hiPSC lines compliant with current Good Manufacturing Practices (cGMP) renders such an approach commercially unfeasible, as it has been estimated to cost US$800,000 for one line (Bravery, 2014). Therefore, the establishment of standardised, cGMP-qualified, and genetically-defined allogeneic iPSC banks may contribute to lowering the cost of iPSC-based therapies (Shi *et al.*, 2016).

Taking Japan as an example, it has been estimated that 50 hiPSC lines with well-defined human leukocyte antigen (HLA) haplotypes could already be matched to 90.7% of the Japanese population (Nakatsuji, Nakajima, and Tokunaga, 2008). For the UK, it has been estimated that 150 lines could match 93% of the UK population (Taylor *et al.*, 2012). The establishment of such banks would require very high quantities of hiPSCs per line, as each line would be matched to not just one patient but a significant proportion of the population. In this regard, further culture intensification and development of scale-up processes must be developed with cGMP-compliance in mind. The work in this thesis contributes to the groundwork for using the Mobius family of bioreactors for culturing hiPSCs. While we have demonstrated stirred suspension culture of hiPSCs in 3 L Mobius Single-use bioreactors, this family of bioreactors scales up to 2000 L, which may be more relevant to producing the large batches of hiPSCs required by these banks.

Currently, different banks of hiPSCs are being built up for various countries and applications (Kim *et al.*, 2017). Some of these hiPSCs are cGMP-compliant allogeneic hiPSCs (Turner *et al.*, 2013), while others are banks of hiPSCs derived from patient with specific diseases such as Parkinson's disease (Holmqvist *et al.*, 2016). For applications that do not require cGMP-grade hiPSCs, such as disease modelling, autologous hiPSC lines can be generated for comparatively less. For these applications which may benefit from high-throughput analyses, high cell quantities may also be beneficial, but not to the extent of the haplotype banks described earlier. For these lower scale requirements, the workflow described in this thesis could be used to generate the cell quantities required, either through a scale-up (e.g. bioreactor) or scale-out (e.g. several spinner flasks) approach.

4.4.2 Scale up production of hiPSC derivatives

The utility of hiPSCs is realised when the hiPSCs are differentiated into other cell types. Various groups have endeavoured to use stirred suspension culture to produce large quantities of hiPSCs, and further use the bioreactors to aid in differentiating these hiPSCs into other cells such as cardiomyocytes (Kempf *et al.*, 2015) and pancreatic cells (Pagliuca *et al.*, 2014). It is expected that greater quantities of such cells can be manufactured at greater scale in larger bioreactors.

4.4.3 Differentiation of printed construct for implantation

The hiPSC aggregate printing described by this thesis opens further possibilities of printing cells and differentiating these cells into different lineages. While we have demonstrated that printing hiPSCs in a gelatin-alginate hydrogel is feasible, other directions that future work could explore include the combination of hiPSC aggregates with other novel hydrogels such as hydrogels of spider silk proteins. For example, eADF4(K16) films have recently been shown to be a substratum suitable for the attachment of cardiomyocytes (Petzold *et al.*, 2017). One could imagine printing hiPSC aggregates in eADF4(K16) hydrogel into a patch-like construct and differentiating the hiPSCs into cardiac cells such as cardiomyocytes to create a cardiac patch for cell replacement therapy following myocardial infarction.

5. References

Aasen, T., Raya, A., Barrero, M.J., Garreta, E., Consiglio, A., Gonzalez, F., Vassena, R., Bilić, J., Pekarik, V., Tiscornia, G., Edel, M., Boué, S., and Belmonte, J.C.I. (2008). Efficient and rapid generation of induced pluripotent stem cells from human keratinocytes. *Nat. Biotechnol.* **26** (11): 1276–1284.

Abbasalizadeh, S., Larijani, M.R., Samadian, A., and Baharvand, H. (2012). Bioprocess Development for Mass Production of Size-Controlled Human Pluripotent Stem Cell Aggregates in Stirred Suspension Bioreactor. *Tissue Eng. Part C Methods* **18** (11): 831–851.

Abecasis, B., Aguiar, T., Arnault, É., Costa, R., Gomes-Alves, P., Aspegren, A., Serra, M., and Alves, P.M. (2017). Expansion of 3D human induced pluripotent stem cell aggregates in bioreactors: Bioprocess intensification and scaling-up approaches. *J. Biotechnol.* **246**: 81–93.

Abraham, E.J., Slater, K.A., Sanyal, S., Linehan, K., Flaherty, P.M., and Qian, S. (2011). Scale-Up of Mammalian Cell Culture using a New Multilayered Flask. *J. Vis. Exp.* (58): e3418.

Aigner, T.B., DeSimone, E., and Scheibel, T. (2018). Biomedical Applications of Recombinant Silk-Based Materials. *Adv. Mater.* **30** (19): 1–28.

Amit, M., Chebath, J., Margulets, V., Laevsky, I., Miropolsky, Y., Shariki, K., Peri, M., Blais, I., Slutsky, G., Revel, M., and Itskovitz-Eldor, J. (2010). Suspension Culture of Undifferentiated Human Embryonic and Induced Pluripotent Stem Cells. *Stem Cell Rev. Reports* **6** (2): 248–259.

Amit, M., Laevsky, I., Miropolsky, Y., Shariki, K., Peri, M., and Itskovitz-Eldor, J. (2011). Dynamic suspension culture for scalable expansion of undifferentiated human pluripotent stem cells. *Nat. Protoc.* **6** (5): 572–579.

An, B., Tang-Schomer, M.D., Huang, W., He, J., Jones, J.A., Lewis, R. V, and Kaplan, D.L. (2015). Physical and biological regulation of neuron regenerative growth and network formation on recombinant dragline silks. *Biomaterials* **48**: 137–146.

Ashok, P., Fan, Y., Rostami, M.R., and Tzanakakis, E.S. (2016). Aggregate and Microcarrier Cultures of Human Pluripotent Stem Cells in Stirred-Suspension Systems. In Bioreactors in Stem Cell Biology. Methods in Molecular Biology, K. Turksen, ed. (New York, NY: Springer New York), pp. 35–52.

Atchison, L., Zhang, H., Cao, K., and Truskey, G.A. (2017). A Tissue Engineered Blood Vessel Model of Hutchinson-Gilford Progeria Syndrome Using Human iPSC-derived Smooth Muscle Cells. *Sci. Rep.* **7**: 8168.

Ban, H., Nishishita, N., Fusaki, N., Tabata, T., Saeki, K., Shikamura, M., Takada, N., Inoue, M., Hasegawa, M., Kawamata, S., and Nishikawa, S.-I. (2011). Efficient generation of transgene-free human induced pluripotent stem cells (iPSCs) by temperature-sensitive Sendai virus vectors. *Proc. Natl. Acad. Sci.* **108** (34): 14234–14239.

Becker, A.J., McCulloch, E.A., and Till, J.E. (1963). Cytological Demonstration of the Clonal Nature of Spleen Colonies Derived from Transplanted Mouse Marrow Cells. *Nature* **197** (4866): 452–454.

Bellin, M., Marchetto, M.C., Gage, F.H., and Mummery, C.L. (2012). Induced pluripotent stem cells: The new patient? *Nat. Rev. Mol. Cell Biol.* **13** (11): 713–726.

Berman, B. (2012). 3-D printing: The new industrial revolution. *Bus. Horiz.* **55** (2): 155–162.

Biehl, J.K., and Russell, B. (2009). Introduction to stem cell therapy. *J. Cardiovasc. Nurs.* **24** (2): 98–105.

Birket, M.J., and Mummery, C.L. (2015). Pluripotent stem cell derived cardiovascular progenitors – A developmental perspective. *Dev. Biol.* **400** (2): 169–179.

Birket, M.J., Ribeiro, M.C., Verkerk, A.O., Ward, D., Leitoguinho, A.R., den Hartogh, S.C., Orlova, V. V, Devalla, H.D., Schwach, V., Bellin, M., Passier, R., and Mummery, C.L. (2015). Expansion and patterning of cardiovascular progenitors derived from human pluripotent stem cells. *Nat. Biotechnol.* **33** (9): 970–979.

Boland, T., Mironov, V., Gutowska, A., Roth, E.A., and Markwald, R.R. (2003). Cell and organ printing 2: Fusion of cell aggregates in three-dimensional gels. *Anat. Rec. - Part A Discov. Mol. Cell. Evol. Biol.* **272** (2): 497–502.

Borghese, L., Dolezalova, D., Opitz, T., Haupt, S., Leinhaas, A., Steinfarz, B., Koch, P., Edenhofer, F., Hampl, A., and Brüstle, O. (2010). Inhibition of notch signaling in human embryonic stem cell-derived neural stem cells delays G1/S phase transition and accelerates neuronal differentiation in vitro and in vivo. *Stem Cells* **28** (5): 955–964.

Bose, B., and Sudheer, P.S. (2016). In Vitro Differentiation of Pluripotent Stem Cells into Functional β Islets Under 2D and 3D Culture Conditions and In Vivo Preclinical Validation of 3D Islets. In Embryonic Stem Cell Protocols, K. Turksen, ed. (New York, NY: Springer New York), pp. 257–284.

Bosnali, M., and Edenhofer, F. (2008). Generation of transducible versions of transcription factors Oct4 and Sox2. *Biol. Chem.* **389**: 851–861.

Braam, S.R., Passier, R., and Mummery, C.L. (2009). Cardiomyocytes from human pluripotent stem cells in regenerative medicine and drug discovery. *Trends Pharmacol. Sci.* **30** (10): 536–545.

Bravery, C.A. (2014). Do Human Leukocyte Antigen-Typed Cellular Therapeutics Based on Induced Pluripotent Stem Cells Make Commercial Sense? *Stem Cells Dev.* **24** (1): 1–10.

Briggs, R., and King, T.J. (1952). Transplantation of Living Nuclei From Blastula Cells into Enucleated Frogs' Eggs. *Proc. Natl. Acad. Sci. U. S. A.* **38** (5): 455–463.

Briggs, J.A., Mason, E.A., Ovchinnikov, D.A., Wells, C.A., and Wolvetang, E.J. (2013). Concise Review: New Paradigms for Down Syndrome Research Using Induced Pluripotent Stem Cells: Tackling Complex Human Genetic Disease. *Stem Cells Transl. Med.* **2** (3): 175–184.

Bruyneel, A.A., McKeithan, W.L., Feyen, D.A., and Mercola, M. (2018). Will iPSC-cardiomyocytes revolutionize the discovery of drugs for heart disease? *Curr. Opin. Pharmacol.* **42**: 55–61.

Buganim, Y., Faddah, D.A., Cheng, A.W., Itskovich, E., Markoulaki, S., Ganz, K., Klemm, S.L., van Oudenaarden, A., and Jaenisch, R. (2012). Single-cell expression analyses during cellular reprogramming reveal an early stochastic and a late hierarchic phase. *Cell* **150** (6): 1209–1222.

Burridge, P.W., Matsa, E., Shukla, P., Lin, Z.C., Churko, J.M., Ebert, A.D., Lan, F., Diecke, S., Huber, B., Mordwinkin, N.M., Plews, J.R., Abilez, O.J., Cui, B., Gold, J.D., and Wu, J.C. (2014). Chemically defned generation of human cardiomyocytes. *Nat. Methods* **11** (8): 855–860.

Calne, R.Y., Gan, S.U., and Lee, K.O. (2010). Stem cell and gene therapies for diabetes mellitus. *Nat. Rev. Endocrinol.* **6** (3): 173–177.

Campbell, P.G., Miller, E.D., Fisher, G.W., Walker, L.M., and Weiss, L.E. (2005). Engineered spatial patterns of FGF-2 immobilized on fibrin direct cell organization. *Biomaterials* **26** (33): 6762–6770.

Cao, N., Liang, H., Huang, J., Wang, J., Chen, Y., Chen, Z., and Yang, H.-T. (2013). Highly efficient induction and long-term maintenance of multipotent cardiovascular progenitors from human pluripotent stem cells under defined conditions. *Cell Res.* **23** (9): 1119–1132.

Cayo, M.A., Mallanna, S.K., Di Furio, F., Jing, R., Tolliver, L.B., Bures, M., Urick, A., Noto, F.K., Pashos, E.E., Greseth, M.D., Czarnecki, M., Traktman, P., Yang, W., Morrisey, E.E., Grompe, M., Rader, D.J., and Duncan, S.A. (2017). A Drug Screen using Human iPSC-Derived Hepatocyte-like Cells Reveals Cardiac Glycosides as a Potential Treatment for Hypercholesterolemia. *Cell Stem Cell* **20** (4): 478–489.e5.

Chambers, S.M., Fasano, C.A., Papapetrou, E.P., Tomishima, M., Sadelain, M., and Studer, L. (2009). Highly efficient neural conversion of human ES and iPS cells by dual inhibition of SMAD signaling. *Nat. Biotechnol.* **27** (3): 275–280.

Chen, I.Y., and Wu, J.C. (2016). Finding expandable induced cardiovascular progenitor cells. *Circ. Res.* **119** (1): 16–20.

Chen, A.K.-L., Reuveny, S., and Oh, S.K.W. (2013). Application of human mesenchymal and pluripotent stem cell microcarrier cultures in cellular therapy. *Biotechnol. Adv.* **31** (7): 1032–1046.

Chen, A.K.-L., Chen, X., Lim, Y.M., Reuveny, S., and Oh, S.K.W. (2013). Inhibition of ROCK–Myosin II Signaling Pathway Enables Culturing of Human Pluripotent Stem Cells on Microcarriers Without Extracellular Matrix Coating. *Tissue Eng. Part C Methods* **20** (3): 227–238.

Chen, A.K., Chen, X., Choo, A.B.H., Reuveny, S., and Oh, S.K.W. (2010a). Expansion of Human Embryonic Stem Cells on Cellulose Microcarriers. In Current Protocols in Stem Cell Biology, (John Wiley & Sons, Ltd), p. 1C.11.1-1C.11.14.

Chen, C.-H., Lee, M.-Y., Shyu, V.B.-H., Chen, Y.-C., Chen, C.-T., and Chen, J.-P. (2014a). Surface modification of polycaprolactone scaffolds fabricated via selective laser sintering for cartilage tissue engineering. *Mater. Sci. Eng. C* **40**: 389–397.

Chen, K.G., Mallon, B.S., McKay, R.D.G., and Robey, P.G. (2014b). Human pluripotent stem cell culture: considerations for maintenance, expansion, and therapeutics. *Cell Stem Cell* **14** (1): 13–26.

Chen, V.C., Couture, S.M., Ye, J., Lin, Z., Hua, G., Huang, H.-I.P., Wu, J., Hsu, D., Carpenter, M.K., and Couture, L.A. (2012). Scalable GMP compliant suspension culture system for human ES cells. *Stem Cell Res.* **8** (3): 388–402.

Chen, X., Chen, A., Woo, T.L., Choo, A.B.H., Reuveny, S., and Oh, S.K.W. (2010b). Investigations into the Metabolism of Two-Dimensional Colony and Suspended Microcarrier Cultures of Human Embryonic Stem Cells in Serum-Free Media. *Stem Cells Dev.* **19** (11): 1781–1792.

Chestkov, I. V, Vasilieva, E.A., Illarioshkin, S.N., Lagarkova, M.A., and Kiselev, S.L. (2014). Patient-Specific Induced Pluripotent Stem Cells for SOD1-Associated Amyotrophic Lateral Sclerosis Pathogenesis Studies. *Acta Naturae* **6** (1): 54–60.

Clevers, H. (2016). Modeling Development and Disease with Organoids. *Cell* **165** (7): 1586–1597.

Côme, J., Nissan, X., Aubry, L., Tournois, J., Girard, M., Perrier, A.L., Peschanski, M., and Cailleret, M. (2008). Improvement of Culture Conditions of Human Embryoid Bodies Using a Controlled Perfused and Dialyzed Bioreactor System. *Tissue Eng. Part C Methods* **14** (4): 289–298.

Conti, L., and Cattaneo, E. (2010). Neural stem cell systems: Physiological players or in vitro entities? *Nat. Rev. Neurosci.* **11** (3): 176–187.

Cowan, C.A., Atienza, J., Melton, D.A., and Eggan, K. (2005). Nuclear Reprogramming of Somatic Cells After Fusion with Human Embryonic Stem Cells. *Science* **309** (5739): 1369–1373.

Dakhore, S., Nayer, B., and Hasegawa, K. (2018). Human Pluripotent Stem Cell Culture: Current Status, Challenges, and Advancement. *Stem Cells Int.* : 7396905.

Das, A.K., and Pal, R. (2010). Induced pluripotent stem cells (iPSCs): the emergence of a new champion in stem cell technology-driven biomedical applications. *J. Tissue Eng. Regen. Med.* **4** (6): 413–421.

DeSimone, E., Schacht, K., Pellert, A., and Scheibel, T. (2017). Recombinant spider silk-based bioinks. *Biofabrication* **9** (4).

DiBernardo, A.B., and Cudkowicz, M.E. (2006). Translating preclinical insights into effective human trials in ALS. *Biochim. Biophys. Acta - Mol. Basis Dis.* **1762** (11–12): 1139–1149.

Doblhofer, E., and Scheibel, T. (2015). Engineering of Recombinant Spider Silk Proteins Allows Defined Uptake and Release of Substances. *J. Pharm. Sci.* **104** (3): 988–994.

Docherty, K., Bernardo, A.S., and Vallier, L. (2007). Embryonic stem cell therapy for diabetes mellitus. *Semin. Cell Dev. Biol.* **18** (6): 827–838.

Doke, S.K., and Dhawale, S.C. (2015). Alternatives to animal testing: A review. *Saudi Pharm. J.* **23** (3): 223–229.

Duan, B., Hockaday, L.A., Kang, K.H., and Butcher, J.T. (2013). 3D Bioprinting of heterogeneous aortic valve conduits with alginate/gelatin hydrogels. *J. Biomed. Mater. Res. A* **101** (5): 1255–1264.

Ebert, A.D., Yu, J., Rose Jr, F.F., Mattis, V.B., Lorson, C.L., Thomson, J.A., and Svendsen, C.N. (2009). Induced pluripotent stem cells from a spinal muscular atrophy patient. *Nature* **457** (7227): 277–280.

Ebert, A.D., Liang, P., and Wu, J.C. (2012). Induced pluripotent stem cells as a disease modeling and drug screening platform. *J. Cardiovasc. Pharmacol.* **60** (4): 408–416.

Egli, D., Chen, A.E., Saphier, G., Ichida, J., Fitzgerald, C., Go, K.J., Acevedo, N., Patel, J., Baetscher, M., Kearns, W.G., Goland, R., Leibel, R.L., Melton, D.A., and Eggan, K. (2011). Reprogramming within hours following nuclear transfer into mouse but not human zygotes. *Nat. Commun.* **2**: 488.

Eibl, R., Werner, S., and Eibl, D. (2010). Bag Bioreactor Based on Wave-Induced Motion: Characteristics and Applications. In Disposable Bioreactors. Advances in Biochemical Engineering / Biotechnology, R. Eibl, and D. Eibl, eds. (Berlin, Heidelberg: Springer Berlin Heidelberg), pp. 55–87.

Elanzew, A., Sommer, A., Pusch-Klein, A., Brüstle, O., and Haupt, S. (2015). A reproducible and versatile system for the dynamic expansion of human pluripotent stem cells in suspension. *Biotechnol. J.* **10** (10): 1589–1599.

Evans, M.J., and Kaufman, M.H. (1981). Establishment in culture of pluripotential cells from mouse embryos. *Nature* **292** (5819): 154–156.

Fatima, A., Kaifeng, S., Dittmann, S., Xu, G., Gupta, M.K., Linke, M., Zechner, U., Nguemo, F., Milting, H., Farr, M., Hescheler, J., and Šarić, T. (2013). The Disease-Specific Phenotype in Cardiomyocytes Derived from Induced Pluripotent Stem Cells of Two Long QT Syndrome Type 3 Patients. *PLoS One* **8** (12): e83005.

Faulkner-Jones, A., Fyfe, C., Cornelissen, D.-J., Gardner, J., King, J., Courtney, A., and Shu, W. (2015). Bioprinting of human pluripotent stem cells and their directed differentiation into hepatocyte-like cells for the generation of mini-livers in 3D. *Biofabrication* **7** (4): 44102.

Firth, A.L., Menon, T., Parker, G.S., Qualls, S.J., Lewis, B.M., Ke, E., Dargitz, C.T., Wright, R., Khanna, A., Gage, F.H., and Verma, I.M. (2015). Functional Gene Correction for Cystic Fibrosis in Lung Epithelial Cells Generated from Patient iPSCs. *Cell Rep.* **12** (9): 1385–1390.

Fonoudi, H., Ansari, H., Abbasalizadeh, S., Blue, G.M., Aghdami, N., Winlaw, D.S., Harvey, R.P., Bosman, A., and Baharvand, H. (2016). Large-Scale Production of Cardiomyocytes from Human Pluripotent Stem Cells Using a Highly Reproducible Small Molecule-Based Differentiation Protocol. *J. Vis. Exp.* (113): e54276.

Forbester, J.L., Goulding, D., Vallier, L., Hannan, N., Hale, C., Pickard, D., Mukhopadhyay, S., and Dougan, G. (2015). Interaction of Salmonella enterica Serovar Typhimurium with Intestinal Organoids Derived from Human Induced Pluripotent Stem Cells. *Infect. Immun.* **83** (7): 2926 LP-2934.

Ford, K.A. (2016). Refinement, reduction, and replacement of animal toxicity tests by computational methods. *ILAR J.* **57** (2): 226–233.

Ford, C.E., Hamerton, J.L., Barnes, D.W.H., and Loutit, J.F. (1956). Cytological Identification of Radiation-Chimæras. *Nature* **177** (4506): 452–454.

Frank, S., Zhang, M., Schöler, H.R., and Greber, B. (2012). Small molecule-assisted, line-independent maintenance of human pluripotent stem cells in defined conditions. *PLoS One* **7** (7): e41958.

Fridley, K.M., Fernandez, I., Li, M.-T.A., Kettlewell, R.B., and Roy, K. (2010). Unique Differentiation Profile of Mouse Embryonic Stem Cells in Rotary and Stirred Tank Bioreactors. *Tissue Eng. Part A* **16** (11): 3285–3298.

Friedenstein, A.J., Chailakhyan, R.K., Latsinik, N. V, Panasyuk, A.F., and Keiliss-Borok, I. V (1974). Stromal Cells Responsible for Transferring the Microenvironment of the Hemopoietic Tissues: Cloning In Vitro and Retransplantation In Vivo. *Transplantation* **17** (4): 331–340.

Fusaki, N., Ban, H., Nishiyama, A., Saeki, K., and Hasegawa, M. (2009). Efficient induction of transgene-free human pluripotent stem cells using a vector based on Sendai virus, an RNA virus that does not integrate into the host genome. *Proc. Japan Acad. Ser. B* **85** (8): 348–362.

Gage, F.H., and Temple, S. (2013). Neural stem cells: Generating and regenerating the brain. *Neuron* **80** (3): 588–601.

Gao, M., Yao, H., Dong, Q., Zhang, H., Yang, Z., Yang, Y., Zhu, J., Xu, M., and Xu, R. (2016). Tumourigenicity and Immunogenicity of Induced Neural Stem Cell Grafts Versus Induced Pluripotent Stem Cell Grafts in Syngeneic Mouse Brain. *Sci. Rep.* **6**: 29955.

Garattini, S., and Grignaschi, G. (2017). Animal testing is still the best way to find new treatments for patients. *Eur. J. Intern. Med.* **39**: 32–35.

Gerecht-Nir, S., Cohen, S., and Itskovitz-Eldor, J. (2004). Bioreactor cultivation enhances the efficiency of human embryoid body (hEB) formation and differentiation. *Biotechnol. Bioeng.* **86** (5): 493–502.

Goldring, C.E.P., Duffy, P.A., Benvenisty, N., Andrews, P.W., Ben-David, U., Eakins, R., French, N., Hanley, N.A., Kelly, L., Kitteringham, N.R., Kurth, J., Ladenheim, D., Laverty, H., McBlane, J., Narayanan, G., Patel, S., Reinhardt, J., Rossi, A., Sharpe, M., *et al.* (2011). Assessing the safety of stem cell therapeutics. *Cell Stem Cell* **8** (6): 618–628.

Grienberger, C., and Konnerth, A. (2012). Imaging Calcium in Neurons. *Neuron* **73** (5): 862–885.

Groll, J., Boland, T., Blunk, T., Burdick, J.A., Cho, D.-W., Dalton, P.D., Derby, B., Forgacs, G., Li, Q., Mironov, V.A., Moroni, L., Nakamura, M., Shu, W., Takeuchi, S., Vozzi, G., Woodfield, T.B.F., Xu, T., Yoo, J.J., and Malda, J. (2016). Biofabrication: reappraising the definition of an evolving field. *Biofabrication* **8** (1): 013001.

Günther, K., Appelt-Menzel, A., Kwok, C.K., Walles, H., Metzger, M., and Edenhofer, F. (2016). Rapid Monolayer Neural Induction of induced Pluripotent Stem Cells Yields Stably Proliferating Neural Stem Cells. *J. Stem Cell Res. Ther.* **6** (5): 1–6.

Guo, S., Zi, X., Schulz, V.P., Cheng, J., Zhong, M., Koochaki, S.H.J., Megyola, C.M., Pan, X., Heydari, K., Weissman, S.M., Gallagher, P.G., Krause, D.S., Fan, R., and Lu, J. (2014). Nonstochastic reprogramming from a privileged somatic cell state. *Cell* **156** (4): 649–662.

Gurdon, J.B. (1962). The Developmental Capacity of Nuclei taken from Intestinal Epithelium Cells of Feeding Tadpoles. *J. Embryol. Exp. Morphol.* **10** (4): 622–640.

Gurdon, J.B., and Melton, D.A. (2008). Nuclear Reprogramming in Cells. *Science* **322** (5909): 1811 LP-1815.

Häcker, V. (1892). Die Kernteilungsvorgänge bei der Mesoderm- und Entodermbildung bei Cyclops. *Arch. f. Mikr. Anat.* (39): 556–581.

Haeckel, E. (1868). Natürliche Schöpfungsgeschichte (Berlin).

Hagbard, L., Cameron, K., August, P., Penton, C., Parmar, M., Hay, D.C., and Kallur, T. (2018). Developing defined substrates for stem cell culture and differentiation. *Philos. Trans. R. Soc. Lond., B. Biol. Sci.* **373** (1750).

Han, C., Chaineau, M., Chen, C.X.Q., Beitel, L.K., and Durcan, T.M. (2018). Open science meets stem cells: A new drug discovery approach for neurodegenerative disorders. *Front. Neurosci.* **12**: 47.

Hanna, J., Saha, K., Pando, B., van Zon, J., Lengner, C.J., Creyghton, M.P., van Oudenaarden, A., and Jaenisch, R. (2009). Direct cell reprogramming is a stochastic process amenable to acceleration. *Nature* **462** (7273): 595–601.

Hartman, M.E., Dai, D.-F., and Laflamme, M.A. (2016). Human pluripotent stem cells: Prospects and challenges as a source of cardiomyocytes for in vitro modeling and cell-based cardiac repair. *Adv. Drug Deliv. Rev.* **96**: 3–17.

He, Y., Yang, F., Zhao, H., Gao, Q., Xia, B., and Fu, J. (2016). Research on the printability of hydrogels in 3D bioprinting. *Sci. Rep.* **6**: 29977.

Heng, B.C., Li, J., Chen, A.K.-L., Reuveny, S., Cool, S.M., Birch, W.R., and Oh, S.K.-W. (2011). Translating Human Embryonic Stem Cells from 2-Dimensional to 3-Dimensional Cultures in a Defined Medium on Laminin- and Vitronectin-Coated Surfaces. *Stem Cells Dev.* **21** (10): 1701–1715.

Holmqvist, S., Lehtonen, Š., Chumarina, M., Puttonen, K.A., Azevedo, C., Lebedeva, O., Ruponen, M., Oksanen, M., Djelloul, M., Collin, A., Goldwurm, S., Meyer, M., Lagarkova, M., Kiselev, S., Koistinaho, J., and Roybon, L. (2016). Creation of a library of induced pluripotent stem cells from Parkinsonian patients. *NPJ Park. Dis* **2**: 16009.

Holzapfel, B.M., Hutmacher, D.W., Nowlan, B., Barbier, V., Thibaudeau, L., Theodoropoulos, C., Hooper, J.D., Loessner, D., Clements, J.A., Russell, P.J., Pettit, A.R., Winkler, I.G., and Levesque, J.P. (2015). Tissue engineered humanized bone supports human hematopoiesis in vivo. *Biomaterials* **61**: 103–114.

Huemmerich, D., Helsen, C.W., Quedzuweit, S., Oschmann, J., Rudolph, R., and Scheibel, T. (2004). Primary Structure Elements of Spider Dragline Silks and Their Contribution to Protein Solubility. *Biochemistry* **43** (42): 13604–13612.

Hung, S.S.C., Khan, S., Lo, C.Y., Hewitt, A.W., and Wong, R.C.B. (2017). Drug discovery using induced pluripotent stem cell models of neurodegenerative and ocular diseases. *Pharmacol. Ther.* **177**: 32–43.

Hunt, N.C., Hallam, D., Karimi, A., Mellough, C.B., Chen, J., Steel, D.H.W., and Lako, M. (2017). 3D culture of human pluripotent stem cells in RGD-alginate hydrogel improves retinal tissue development. *Acta Biomater.* **49**: 329–343.

Inoue, H., and Yamanaka, S. (2011). The Use of Induced Pluripotent Stem Cells in Drug Development. *Clin. Pharmacol. Ther.* **89** (5): 655–661.

Jaenisch, R., and Young, R. (2008). Stem cells, the molecular circuitry of pluripotency and nuclear reprogramming. *Cell* **132** (4): 567–582.

Jansch, C., Günther, K., Waider, J., Ziegler, G.C., Forero, A., Kollert, S., Svirin, E., Pühringer, D., Kwok, C.K., Ullmann, R., Maierhofer, A., Flunkert, J., Haaf, T., Edenhofer, F., and Lesch, K.-P. (2018). Generation of a human induced pluripotent stem cell (iPSC) line from a 51-year-old female with attention-deficit/hyperactivity disorder (ADHD) carrying a duplication of SLC2A3. *Stem Cell Res.* **28**: 136–140.

Jenkins, M.J., and Farid, S.S. (2015). Human pluripotent stem cell-derived products: Advances towards robust, scalable and cost-effective manufacturing strategies. *Biotechnol. J.* **10** (1): 83–95.

Jensen, J.B., and Parmar, M. (2006). Strengths and limitations of the neurosphere culture system. *Mol. Neurobiol.* **34** (3): 153–161.

Jovanovic, V.M., Salti, A., Tilleman, H., Zega, K., Jukic, M.M., Zou, H., Friedel, R.H., Prakash, N., Blaess, S., Edenhofer, F., and Brodski, C. (2018). BMP/SMAD Pathway Promotes Neurogenesis of Midbrain Dopaminergic Neurons *In Vivo* and in Human Induced Pluripotent and Neural Stem Cells. *J. Neurosci.* **38** (7): 1662–1676.

Jung, P., Sato, T., Merlos-Suárez, A., Barriga, F.M., Iglesias, M., Rossell, D., Auer, H., Gallardo, M., Blasco, M.A., Sancho, E., Clevers, H., and Batlle, E. (2011). Isolation and in vitro expansion of human colonic stem cells. *Nat. Med.* **17** (10): 1225–1227.

Jüngst, T., Smolan, W., Schacht, K., Scheibel, T., and Groll, J. (2016). Strategies and Molecular Design Criteria for 3D Printable Hydrogels. *Chem. Rev.* **116** (3): 1496–1539.

Kadari, A., Lu, M., Li, M., Sekaran, T., Thummer, R.P., Guyette, N., Chu, V., and Edenhofer, F. (2014). Excision of viral reprogramming cassettes by Cre protein transduction enables rapid, robust and efficient derivation of transgene-free human induced pluripotent stem cells. *Stem Cell Res. Ther.* **5** (2): 47.

Kaji, K., Norrby, K., Paca, A., Mileikovsky, M., Mohseni, P., and Woltjen, K. (2009). Virus-free induction of pluripotency and subsequent excision of reprogramming factors. *Nature* **458**: 771.

Kami, D., Watakabe, K., Yamazaki-Inoue, M., Minami, K., Kitani, T., Itakura, Y., Toyoda, M., Sakurai, T., Umezawa, A., and Gojo, S. (2013). Large-scale cell production of stem cells for clinical application using the automated cell processing machine. *BMC Biotechnol.* **13**.

Kattman, S.J., Huber, T.L., and Keller, G.M. (2006). Multipotent Flk-1+ cardiovascular progenitor cells give rise to the cardiomyocyte, endothelial, and vascular smooth muscle lineages. *Dev. Cell* **11** (5): 723–732.

Kehoe, D.E., Jing, D., Lock, L.T., and Tzanakakis, E.S. (2010). Scalable Stirred-Suspension Bioreactor Culture of Human Pluripotent Stem Cells. *Tissue Eng. Part A* **16** (2): 405–421.

Kempf, H., Kropp, C., Olmer, R., Martin, U., and Zweigerdt, R. (2015). Cardiac differentiation of human pluripotent stem cells in scalable suspension culture. *Nat. Protoc.* **10** (9): 1345–1361.

Khudiakov, A., Kostina, D., Zlotina, A., Yany, N., Sergushichev, A., Pervunina, T., Tomilin, A., Kostareva, A., and Malashicheva, A. (2017). Generation of iPSC line from patient with arrhythmogenic right ventricular cardiomyopathy carrying mutations in PKP2 gene. *Stem Cell Res.* **24**: 85–88.

Kim, J.-H., Kurtz, A., Yuan, B.-Z., Zeng, F., Lomax, G., Loring, J.F., Crook, J., Ju, J.H., Clarke, L., Inamdar, M.S., Pera, M., Firpo, M.T., Sheldon, M., Rahman, N., O'Shea, O., Pranke, P., Zhou, Q., Isasi, R., Rungsiwiwut, R., *et al.* (2017). Report of the International Stem Cell Banking Initiative Workshop Activity: Current Hurdles and Progress in Seed-Stock Banking of Human Pluripotent Stem Cells. *Stem Cells Transl. Med.* **6** (11): 1956–1962.

Kim, M.H., Takeuchi, K., and Kino-oka, M. (2018). Role of cell-secreted extracellular matrix formation in aggregate formation and stability of human induced pluripotent stem cells in suspension culture. *J. Biosci. Bioeng.* **127** (3): 372–380.

Kinney, M.A., Sargent, C.Y., and Mcdevitt, T.C. (2011). The Multiparametric Effects of Hydrodynamic Environments on Stem Cell Culture. *Tissue Eng. Part B* **17** (4): 249–262.

Kishino, Y., Seki, T., Fujita, J., Yuasa, S., Tohyama, S., Kunitomi, A., Tabei, R., Nakajima, K., Okada, M., Hirano, A., Kanazawa, H., and Fukuda, K. (2014). Derivation of transgene-free human induced pluripotent stem cells from human peripheral T cells in defined culture conditions. *PLoS One* **9** (5): e97397.

Klein, T., Günther, K., Kwok, C.K., Edenhofer, F., and Üçeyler, N. (2018). Generation of the human induced pluripotent stem cell line (UKWNLi001-A) from skin fibroblasts of a woman with Fabry disease carrying the X-chromosomal heterozygous c.708 G > C (W236C) missense mutation in exon 5 of the alpha-galactosidase–A gene. *Stem Cell Res.* **31**: 222–226.

Kleinman, H.K., McGarvey, M.L., Liotta, L.A., Robey, P.G., Tryggvason, K., and Martin, G.R. (1982). Isolation and Characterization of Type IV Procollagen, Laminin, and Heparan Sulfate Proteoglycan from the EHS Sarcoma. *Biochemistry* **21** (24): 6188–6193.

Klimanskaya, I., Chung, Y., Becker, S., Lu, S.-J., and Lanza, R. (2006). Human embryonic stem cell lines derived from single blastomeres. *Nature* **444** (7118): 481–485.

Ko, H.C., and Gelb, B.D. (2014). Concise Review: Drug Discovery in the Age of the Induced Pluripotent Stem Cell. *Stem Cells Transl. Med.* **3** (4): 500–509.

Koch, L., Deiwick, A., Franke, A., Schwanke, K., Haverich, A., Zweigerdt, R., and Chichkov, B. (2018). Laser bioprinting of human induced pluripotent stem cells—the effect of printing and biomaterials on cell survival, pluripotency, and differentiation. *Biofabrication* **10**: 035005.

Koch, P., Breuer, P., Peitz, M., Jungverdorben, J., Kesavan, J., Poppe, D., Doerr, J., Ladewig, J., Mertens, J., Tüting, T., Hoffmann, P., Klockgether, T., Evert, B.O., Wüllner, U., and Brüstle, O. (2011). Excitation-induced ataxin-3 aggregation in neurons from patients with Machado-Joseph disease. *Nature* **480** (7378): 543–546.

Konagaya, S., Ando, T., Yamauchi, T., Suemori, H., and Iwata, H. (2015). Long-term maintenance of human induced pluripotent stem cells by automated cell culture system. *Sci. Rep.* **5**: 1–9.

Krawetz, R., Taiani, J.T., Liu, S., Meng, G., Li, X., Kallos, M.S., and Rancourt, D.E. (2009). Large-Scale Expansion of Pluripotent Human Embryonic Stem Cells in Stirred-Suspension Bioreactors. *Tissue Eng. Part C Methods* **16** (4): 573–582.

Kropp, C., Kempf, H., Halloin, C., Robles-Diaz, D., Franke, A., Scheper, T., Kinast, K., Knorpp, T., Joos, T.O., Haverich, A., Martin, U., Zweigerdt, R., and Olmer, R. (2016). Impact of Feeding Strategies on the Scalable Expansion of Human Pluripotent Stem Cells in Single-Use Stirred Tank Bioreactors. *Stem Cells Transl. Med.* **5** (10): 1289–1301.

Kropp, C., Massai, D., and Zweigerdt, R. (2017). Progress and challenges in large-scale expansion of human pluripotent stem cells. *Process Biochem.* **59** (B): 244–254.

Kumar, A., and Starly, B. (2015). Large scale industrialized cell expansion: Producing the critical raw material for biofabrication processes. *Biofabrication* **7** (4): 044103.

Kwok, C.K., Ueda, Y., Kadari, A., Günther, K., Ergün, S., Heron, A., Schnitzler, A.C., Rook, M., and Edenhofer, F. (2018). Scalable stirred suspension culture for the generation of billions of human induced pluripotent stem cells using single-use bioreactors. *J. Tissue Eng. Regen. Med.* **12** (2): e1076–e1087.

Laflamme, M.A., and Murry, C.E. (2011). Heart regeneration. *Nature* **473** (7347): 326–335.

Lancaster, M.A., Renner, M., Martin, C.A., Wenzel, D., Bicknell, L.S., Hurles, M.E., Homfray, T., Penninger, J.M., Jackson, A.P., and Knoblich, J.A. (2013). Cerebral organoids model human brain development and microcephaly. *Nature* **501** (7467): 373–379.

Leal-Egaña, A., and Scheibel, T. (2010). Silk-based materials for biomedical applications. *Biotechnol. Appl. Biochem.* **55** (3): 155–167.

Lee, A.S., Tang, C., Rao, M.S., Weissman, I.L., and Wu, J.C. (2013). Tumorigenicity as a clinical hurdle for pluripotent stem cell therapies. *Nat. Med.* **19** (8): 998–1004.

Leung, H.W., Cand, P.D., Chen, A., Ph, D., Choo, A.B.H., Ph, D., Reuveny, S., Ph, D., Oh, S.K.W., and Ph, D. (2011). Agitation can Induce Differentiation of Human Pluripotent Stem Cells in Microcarrier Cultures. *Tissue Eng. Part C Methods* **17** (2): 165–172.

Li, L., Bennett, S.A.L., and Wang, L. (2012). Role of E-cadherin and other cell adhesion molecules in survival and differentiation of human pluripotent stem cells. *Cell Adhes. Migr.* **6** (1): 59–70.

Lian, Q., Zhang, Y., Zhang, J., Zhang, H.K., Wu, X., Zhang, Y., Lam, F.F.-Y., Kang, S., Xia, J.C., Lai, W.-H., Au, K.-W., Chow, Y.Y., Siu, C.-W., Lee, C.-N., and Tse, H.-F. (2010). Functional Mesenchymal Stem Cells Derived From Human Induced Pluripotent Stem Cells Attenuate Limb Ischemia in Mice. *Circulation* **121** (9): 1113–1123.

Lian, X., Zhang, J., Azarin, S.M., Zhu, K., Hazeltine, L.B., Bao, X., Hsiao, C., Kamp, T.J., and Palecek, S.P. (2012). Directed cardiomyocyte differentiation from human pluripotent stem cells by modulating Wnt/β-catenin signaling under fully defined conditions. *Nat. Protoc.* **8** (1): 162–175.

Lipson, H., and Kurman, M. (2013). Fabricated: The New World of 3D Printing (John Wiley & Sons, Ltd).

Liu, C., Oikonomopoulos, A., Sayed, N., and Wu, J.C. (2018). Modeling human diseases with induced pluripotent stem cells: from 2D to 3D and beyond. *Development* **145** (5): dev156166.

Liu, G.-H., Barkho, B.Z., Ruiz, S., Diep, D., Qu, J., Yang, S.-L., Panopoulos, A.D., Suzuki, K., Kurian, L., Walsh, C., Thompson, J., Boue, S., Fung, H.L., Sancho-Martinez, I., Zhang, K., III, J.Y., and Belmonte, J.C.I. (2011). Recapitulation of premature ageing with iPSCs from Hutchinson–Gilford progeria syndrome. *Nature* **472**: 221.

Lock, L.T., and Tzanakakis, E.S. (2009). Expansion and Differentiation of Human Embryonic Stem Cells to Endoderm Progeny in a Microcarrier Stirred-Suspension Culture. *Tissue Eng. Part A* **15** (8): 2051–2063.

Loh, Y.-H.H., Hartung, O., Li, H., Guo, C., Sahalie, J.M., Manos, P.D., Urbach, A., Heffner, G.C., Grskovic, M., Vigneault, F., Lensch, M.W., Park, I.-H., Agarwal, S., Church, G.M., Collins, J.J., Irion, S., and Daley, G.Q. (2010). Reprogramming of T Cells from Human Peripheral Blood. *Cell Stem Cell* **7** (1): 15–19.

Lu, X., and Zhao, T. (2013). Clinical Therapy Using iPSCs: Hopes and Challenges. *Genomics Proteomics Bioinformatics* **11** (5): 294–298.

MacIntosh, A.C., Kearns, V.R., Crawford, A., and Hatton, P. V (2008). Skeletal tissue engineering using silk biomaterials. *J. Tissue Eng. Regen. Med.* **2** (2-3): 71–80.

Maherali, N., Ahfeldt, T., Rigamonti, A., Utikal, J., Cowan, C., and Hochedlinger, K. (2008). A High-Efficiency System for the Generation and Study of Human Induced Pluripotent Stem Cells. *Cell Stem Cell* **3** (3): 340–345.

Malda, J., Visser, J., Melchels, F.P., Jüngst, T., Hennink, W.E., Dhert, W.J.A., Groll, J., and Hutmacher, D.W. (2013). 25th Anniversary Article: Engineering Hydrogels for Biofabrication. *Adv. Mater.* **25** (36): 5011–5028.

Mallon, B.S., Park, K.-Y., Chen, K.G., Hamilton, R.S., and McKay, R.D.G. (2006). Toward xeno-free culture of human embryonic stem cells. *Int. J. Biochem. Cell Biol.* **38** (7): 1063–1075.

Mandai, M., Watanabe, A., Kurimoto, Y., Hirami, Y., Morinaga, C., Daimon, T., Fujihara, M., Akimaru, H., Sakai, N., Shibata, Y., Terada, M., Nomiya, Y., Tanishima, S., Nakamura, M., Kamao, H., Sugita, S., Onishi, A., Ito, T., Fujita, K., *et al.* (2017). Autologous Induced Stem-Cell–Derived Retinal Cells for Macular Degeneration. *N. Engl. J. Med.* **376** (11): 1038–1046.

Martí, M., Mulero, L., Pardo, C., Morera, C., Carrió, M., Laricchia-Robbio, L., Esteban, C.R., and Belmonte, J.C.I. (2013). Characterization of pluripotent stem cells. *Nat. Protoc.* **8** (2): 223–253.

Martin, G.R. (1981). Isolation of a pluripotent cell line from early mouse embryos cultured in medium conditioned by teratocarcinoma stem cells. *Proc. Natl. Acad. Sci. U. S. A.* **78** (12): 7634–7638.

Martin, U. (2017). Therapeutic Application of Pluripotent Stem Cells: Challenges and Risks. *Front. Med. (Lausanne)* **4**: 229.

Martino, G., Franklin, R.J.M., Van Evercooren, A.B., Kerr, D.A., and the Stem Cells in Multiple Sclerosis (STEMS) Consensus Group (2010). Stem cell transplantation in multiple sclerosis: current status and future prospects. *Nat. Rev. Neurol.* **6** (5): 247–255.

McMurtrey, R.J. (2016). Multi-compartmental biomaterial scaffolds for patterning neural tissue organoids in models of neurodevelopment and tissue regeneration. *J Tissue Eng* **7**: 2041731416671926.

Mei, Y., Saha, K., Bogatyrev, S.R., Yang, J., Hook, A.L., Kalcioglu, Z.I., Cho, S.-W., Mitalipova, M., Pyzocha, N., Rojas, F., Van Vliet, K.J., Davies, M.C., Alexander, M.R., Langer, R., Jaenisch, R., and Anderson, D.G. (2010). Combinatorial development of biomaterials for clonal growth of human pluripotent stem cells. *Nat. Mater.* **9** (9): 768–778.

Merkert, S., Bednarski, C., Göhring, G., Cathomen, T., and Martin, U. (2017). Generation of a gene-corrected isogenic control iPSC line from cystic fibrosis patient-specific iPSCs homozygous for p.Phe508del mutation mediated by TALENs and ssODN. *Stem Cell Res.* **23**: 95–97.

Merkle, F.T., and Eggan, K. (2017). Culturing human pluripotent stem cells from diverse culture histories. *Protoc. Exch.*

Meyer, S., Wörsdörfer, P., Günther, K., Thier, M., and Edenhofer, F. (2015). Derivation of Adult Human Fibroblasts and their Direct Conversion into Expandable Neural Progenitor Cells. *J. Vis. Exp.* **101** (101): e52831.

Mironov, V., Boland, T., Trusk, T., Forgacs, G., and Markwald, R.R. (2003). Organ printing: Computer-aided jet-based 3D tissue engineering. *Trends Biotechnol.* **21** (4): 157–161.

Mollet, M., Godoy-Silva, R., Berdugo, C., and Chalmers, J.J. (2007). Acute Hydrodynamic Forces and Apoptosis: A Complex Question. *Biotechnol. Bioeng.* **98** (4): 772–788.

Morrison, S.J., Shah, N.M., and Anderson, D.J. (1997). Regulatory Mechanisms in Stem Cell Biology. *Cell* **88** (3): 287–298.

Mota, C., Puppi, D., Chiellini, F., and Chiellini, E. (2015). Additive manufacturing techniques for the production of tissue engineering constructs. *J. Tissue Eng. Regen. Med.* **9** (3): 174–190.

Mummery, C.L. (2005). Solace for the broken-hearted? *Nature* **433** (7026): 585–587.

Murhammer, D.W., and Goochee, C.F. (1990). Structural features of nonionic polyglycol polymer molecules responsible for the protective effect in sparged animal cell bioreactors. *Biotechnol. Prog.* **6** (2): 142–148.

Murphy, S. V., and Atala, A. (2014). 3D bioprinting of tissues and organs. *Nat. Biotechnol.* **32** (8): 773–785.

Nakatsuji, N., Nakajima, F., and Tokunaga, K. (2008). HLA-haplotype banking and iPS cells. *Nat. Biotechnol.* **26**: 739.

Nobel Media, A.B. (2012). The Nobel Prize in Physiology or Medicine 2012.

Norotte, C., Marga, F.S., Niklason, L.E., and Forgacs, G. (2009). Scaffold-free vascular tissue engineering using bioprinting. *Biomaterials* **30** (30): 5910–5917.

Oh, S.K.W., Chen, A.K., Mok, Y., Chen, X., Lim, U.M., Chin, A., Choo, A.B.H., and Reuveny, S. (2009). Long-term microcarrier suspension cultures of human embryonic stem cells. *Stem Cell Res.* **2** (3): 219–230.

Okita, K., Ichisaka, T., and Yamanaka, S. (2007). Generation of germline-competent induced pluripotent stem cells. *Nature* **448** (7151): 313–317.

Olmer, R., Haase, A., Merkert, S., Cui, W., Paleček, J., Ran, C., Kirschning, A., Scheper, T., Glage, S., Miller, K., Curnow, E.C., Hayes, E.S., and Martin, U. (2010). Long term expansion of undifferentiated human iPS and ES cells in suspension culture using a defined medium. *Stem Cell Res.* **5** (1): 51–64.

Olmer, R., Lange, A., Selzer, S., Kasper, C., Haverich, A., Martin, U., and Zweigerdt, R. (2012). Suspension Culture of Human Pluripotent Stem Cells in Controlled, Stirred Bioreactors. *Tissue Eng. Part C Methods* **18** (10): 772–784.

Pacey, L., Stead, S., Gleave, J., Tomczyk, K., and Doering, L. (2006). Neural Stem Cell Culture: Neurosphere generation, microscopical analysis and cryopreservation .

Pagliuca, F.W., Millman, J.R., Gürtler, M., Segel, M., Van Dervort, A., Ryu, J.H., Peterson, Q.P., Greiner, D., and Melton, D.A. (2014). Generation of functional human pancreatic β cells in vitro. *Cell* **159** (2): 428–439.

Park, C.-Y., Kim, D.H.D.-W., Son, J.S., Sung, J.J., Lee, J., Bae, S., Kim, J.-S.J.-H., Kim, D.H.D.-W., and Kim, J.-S.J.-H. (2015). Functional Correction of Large Factor VIII Gene Chromosomal Inversions in Hemophilia A Patient-Derived iPSCs Using CRISPR-Cas9. *Cell Stem Cell* **17** (2): 213–220.

Park, I.-H., Arora, N., Huo, H., Maherali, N., Ahfeldt, T., Shimamura, A., Lensch, M.W., Cowan, C., Hochedlinger, K., and Daley, G.Q. (2008). Disease-Specific Induced Pluripotent Stem Cells. *Cell* **134** (5): 877–886.

Paxton, N., Smolan, W., Böck, T., Melchels, F., Groll, J., and Jungst, T. (2017). Proposal to assess printability of bioinks for extrusion-based bioprinting and evaluation of rheological properties governing bioprintability. *Biofabrication* **9** (4): 044107.

Peitz, M., Bechler, T., Thiele, C.C., Veltel, M., Bloschies, M., Fliessbach, K., Ramirez, A., and Brüstle, O. (2018). Blood-derived integration-free iPS cell line UKBi011-A from a diagnosed male Alzheimer's disease patient with APOE ε4/ε4 genotype. *Stem Cell Res.* **29**: 250–253.

Perlman, R.L. (2016). Mouse models of human disease: An evolutionary perspective. *Evol. Med. Public Heal.* **2016** (1): 170–176.

Peruzzotti-Jametti, L., Bernstock, J.D., Vicario, N., Costa, A.S.H., Kwok, C.K., Leonardi, T., Booty, L.M., Bicci, I., Balzarotti, B., Volpe, G., Mallucci, G., Manferrari, G., Donegà, M., Iraci, N., Braga, A., Hallenbeck, J.M., Murphy, M.P., Edenhofer, F., Frezza, C., *et al.* (2018). Macrophage-Derived Extracellular Succinate Licenses Neural Stem Cells to Suppress Chronic Neuroinflammation. *Cell Stem Cell* **22** (3): 355–368.e13.

Petzold, J., Aigner, T.B., Touska, F., Zimmermann, K., Scheibel, T., and Engel, F.B. (2017). Surface Features of Recombinant Spider Silk Protein eADF4(κ16)-Made Materials are Well-Suited for Cardiac Tissue Engineering. *Adv. Funct. Mater.* **27** (36): 1701427.

Phillips, B.W., Horne, R., Lay, T.S., Rust, W.L., Teck, T.T., and Crook, J.M. (2008). Attachment and growth of human embryonic stem cells on microcarriers. *J. Biotechnol.* **138** (1–2): 24–32.

Pluchino, S., Gritti, A., Blezer, E., Amadio, S., Brambilla, E., Borsellino, G., Cossetti, C., Del Carro, U., Comi, G., Hart, B., Vescovi, A., and Martino, G. (2009). Human Neural Stem Cells Ameliorate Autoimmune Encephalomyelitis in Non-human Primates. *Ann. Neurol.* **66** (3): 343–354.

Polo, J.M., Anderssen, E., Walsh, R.M., Schwarz, B.A., Nefzger, C.M., Lim, S.M., Borkent, M., Apostolou, E., Alaei, S., Cloutier, J., Bar-Nur, O., Cheloufi, S., Stadtfeld, M., Figueroa, M.E., Robinton, D., Natesan, S., Melnick, A., Zhu, J., Ramaswamy, S., *et al.* (2012). A molecular roadmap of reprogramming somatic cells into iPS cells. *Cell* **151** (7): 1617–1632.

Qian, X., Nguyen, H.N., Song, M.M., Hadiono, C., Ogden, S.C., Hammack, C., Yao, B., Hamersky, G.R., Jacob, F., Zhong, C., Yoon, K., Jeang, W., Lin, L., Li, Y., Thakor, J., Berg, D.A., Zhang, C., Kang, E., Chickering, M., *et al.* (2016). Brain-Region-Specific Organoids Using Mini-bioreactors for Modeling ZIKV Exposure. *Cell* **165** (5): 1238–1254.

Ramalho-Santos, M., and Willenbring, H. (2007). On the Origin of the Term "Stem Cell." *Cell Stem Cell* **1** (1): 35–38.

Reinhardt, P., Glatza, M., Hemmer, K., Tsytsyura, Y., Thiel, C.S., Höing, S., Moritz, S., Parga, J.A., Wagner, L., Bruder, J.M., Wu, G., Schmid, B., Röpke, A., Klingauf, J., Schwamborn, J.C., Gasser, T., Schöler, H.R., and Sterneckert, J. (2013). Derivation and Expansion Using Only Small Molecules of Human Neural Progenitors for Neurodegenerative Disease Modeling. *PLoS One* **8** (3): e59252.

Rodin, S., Antonsson, L., Niaudet, C., Simonson, O.E., Salmela, E., Hansson, E.M., Domogatskaya, A., Xiao, Z., Damdimopoulou, P., Sheikhi, M., Inzunza, J., Nilsson, A.S., Baker, D., Kuiper, R., Sun, Y., Blennow, E., Nordenskjöld, M., Grinnemo, K.H., Kere, J., *et al.* (2014). Clonal culturing of human embryonic stem cells on laminin-521/E-cadherin matrix in defined and xeno-free environment. *Nat. Commun.* **5**: 3195.

Rodrigues, A.L., Rodrigues, C.A.V., Gomes, A.R., Vieira, S.F., Badenes, S.M., Diogo, M.M., and Cabral, J.M.S. (2018). Dissolvable Microcarriers Allow Scalable Expansion And Harvesting Of Human Induced Pluripotent Stem Cells Under Xeno-Free Conditions. *Biotechnol. J.* : 1800461.

Rodrigues, C.A.V., Fernandes, T.G., Diogo, M.M., da Silva, C.L., and Cabral, J.M.S. (2011). Stem cell cultivation in bioreactors. *Biotechnol. Adv.* **29** (6): 815–829.

Rowley, J., Abraham, E., Campbell, A., Brandwein, H., and Oh, S. (2012). Meeting Lot-Size Challenges of Manufacturing Adherent Cells for Therapy. *Bioprocess Int.* **10** (3): 16–22.

Ruoslahti, E. (1988). Fibronectin and its receptors. *Annu. Rev. Biochem.* **57**: 375–413.

Sampaziotis, F., Cardoso de Brito, M., Madrigal, P., Bertero, A., Saeb-Parsy, K., Soares, F.A.C., Schrumpf, E., Melum, E., Karlsen, T.H., Bradley, J.A., Gelson, W.T.H., Davies, S., Baker, A., Kaser, A., Alexander, G.J., Hannan, N.R.F., and Vallier, L. (2015). Cholangiocytes derived from human induced pluripotent stem cells for disease modeling and drug validation. *Nat. Biotechnol.* **33** (8): 845–852.

Sart, S., Schneider, Y.J., Li, Y., and Agathos, S.N. (2014). Stem cell bioprocess engineering towards cGMP production and clinical applications. *Cytotechnology* **66** (5): 709–722.

Schacht, K., Jüngst, T., Schweinlin, M., Ewald, A., Groll, J., and Scheibel, T. (2015). Biofabrication of Cell-Loaded 3D Spider Silk Constructs. *Angew. Chemie Int. Ed.* **54** (9): 2816–2820.

Schindelin, J., Arganda-Carreras, I., Frise, E., Kaynig, V., Longair, M., Pietzsch, T., Preibisch, S., Rueden, C., Saalfeld, S., Schmid, B., Tinevez, J.-Y., White, D.J., Hartenstein, V., Eliceiri, K., Tomancak, P., and Cardona, A. (2012). Fiji: an open-source platform for biological-image analysis. *Nat. Methods* **9** (7): 676–682.

Scott, S., Kranz, J.E., Cole, J., Lincecum, J.M., Thompson, K., Kelly, N., Bostrom, A., Theodoss, J., Al-Nakhala, B.M., Vieira, F.G., Ramasubbu, J., and Heywood, J.A. (2008). Design, power, and interpretation of studies in the standard murine model of ALS. *Amyotroph. Lateral Scler.* **9** (1): 4–15.

Seki, T., Yuasa, S., Oda, M., Egashira, T., Yae, K., Kusumoto, D., Nakata, H., Tohyama, S., Hashimoto, H., Kodaira, M., Okada, Y., Seimiya, H., Fusaki, N., Hasegawa, M., and Fukuda, K. (2010). Generation of Induced Pluripotent Stem Cells from Human Terminally Differentiated Circulating T Cells. *Cell Stem Cell* **7** (1): 11–14.

Seok, J., Warren, H.S., Cuenca, A.G., Mindrinos, M.N., Baker, H. V, Xu, W., Richards, D.R., McDonald-Smith, G.P., Gao, H., Hennessy, L., Finnerty, C.C., López, C.M., Honari, S., Moore, E.E., Minei, J.P., Cuschieri, J., Bankey, P.E., Johnson, J.L., Sperry, J., *et al.* (2013). Genomic responses in mouse models poorly mimic human inflammatory diseases. *Proc. Natl. Acad. Sci. U. S. A.* **110** (9): 3507–3512.

Serra, M., Brito, C., Sousa, M.F.Q., Jensen, J., Tostões, R., Clemente, J., Strehl, R., Hyllner, J., Carrondo, M.J.T., and Alves, P.M. (2010). Improving expansion of pluripotent human embryonic stem cells in perfused bioreactors through oxygen control. *J. Biotechnol.* **148** (4): 208–215.

Serra, M., Brito, C., Correia, C., and Alves, P.M. (2012). Process engineering of human pluripotent stem cells for clinical application. *Trends Biotechnol.* **30** (6): 350–359.

Shapiro, A.M.J., Lakey, J.R.T., Ryan, E.A., Korbutt, G.S., Toth, E., Warnock, G.L., Kneteman, N.M., and Rajotte, R. V (2000). Islet Transplantation in Seven Patients with Type 1 Diabetes Mellitus Using a Glucocorticoid-Free Immunosuppressive Regimen. *N. Engl. J. Med.* **343** (4): 230–238.

Shi, Y., Inoue, H., Wu, J.C., and Yamanaka, S. (2016). Induced pluripotent stem cell technology: a decade of progress. *Nat. Rev. Drug Discov.* **16**: 115.

Siminovitch, L., McCulloch, E.A., and Till, J.E. (1963). The distribution of colony-forming cells among spleen colonies. *J. Cell. Comp. Physiol.* **62** (3): 327–336.

Singh, H., Mok, P., Balakrishnan, T., Rahmat, S.N.B., and Zweigerdt, R. (2010). Up-scaling single cell-inoculated suspension culture of human embryonic stem cells. *Stem Cell Res.* **4** (3): 165–179.

Singh, V.K., Kalsan, M., Kumar, N., Saini, A., and Chandra, R. (2015). Induced pluripotent stem cells: applications in regenerative medicine, disease modeling, and drug discovery. *Front. Cell Dev. Biol.* **3**: 2.

Smith, A.G., Heath, J.K., Donaldson, D.D., Wong, G.G., Moreau, J., Stahl, M., and Rogers, D. (1988). Inhibition of pluripotential embryonic stem cell differentiation by purified polypeptides. *Nature* **336** (6200): 688–690.

Smithies, O., Gregg, R.G., Boggs, S.S., Koralewski, M.A., and Kucherlapati, R.S. (1985). Insertion of DNA sequences into the human chromosomal β-globin locus by homologous recombination. *Nature* **317** (6034): 230–234.

Soares, F.A.C., Chandra, A., Thomas, R.J., Pedersen, R.A., Vallier, L., and Williams, D.J. (2014). Investigating the feasibility of scale up and automation of human induced pluripotent stem cells cultured in aggregates in feeder free conditions. *J. Biotechnol.* **173** (1): 53–58.

Soejitno, A., and Prayudi, P.K.A. (2011). The prospect of induced pluripotent stem cells for diabetes mellitus treatment. *Ther. Adv. Endocrinol. Metab.* **2** (5): 197–210.

Soldner, F., and Jaenisch, R. (2012). iPSC Disease Modeling. *Science* **338** (6111): 1155–1156.

Soldner, F., Hockemeyer, D., Beard, C., Gao, Q., Bell, G.W., Cook, E.G., Hargus, G., Blak, A., Cooper, O., Mitalipova, M., Isacson, O., and Jaenisch, R. (2009). Parkinson's Disease Patient-Derived Induced Pluripotent Stem Cells Free of Viral Reprogramming Factors. *Cell* **136** (5): 964–977.

Somers, A., Jean, J.-C., Sommer, C.A., Omari, A., Ford, C.C., Mills, J.A., Ying, L., Sommer, A.G., Jean, J.M., Smith, B.W., Lafyatis, R., Demierre, M.-F., Weiss, D.J., French, D.L., Gadue, P., Murphy, G.J., Mostoslavsky, G., and Kotton, D.N. (2010). Generation of transgene-free lung disease-specific human induced pluripotent stem cells using a single excisable lentiviral stem cell cassette. *Stem Cells* **28** (10): 1728–1740.

Sommer, C.A., Stadtfeld, M., Murphy, G.J., Hochedlinger, K., Kotton, D.N., and Mostoslavsky, G. (2008). Induced Pluripotent Stem Cell Generation Using a Single Lentiviral Stem Cell Cassette. *Stem Cells* **27** (3): 543–549.

Song, S.J., Choi, J., Park, Y.D., Hong, S., Lee, J.J., Ahn, C.B., Choi, H., and Sun, K. (2011). Sodium Alginate Hydrogel-Based Bioprinting Using a Novel Multinozzle Bioprinting System. *Artif. Organs* **35** (11): 1132–1136.

Srinivasan, G., Morgan, D., Varun, D., Brookhouser, N., and Brafman, D.A. (2018). An integrated biomanufacturing platform for the large-scale expansion and neuronal differentiation of human pluripotent stem cell-derived neural progenitor cells. *Acta Biomater.* **74**: 168–179.

Stadtfeld, M., Nagaya, M., Utikal, J., Weir, G., and Hochedlinger, K. (2008a). Induced Pluripotent Stem Cells Generated Without Viral Integration. *Science* **322** (5903): 945–949.

Stadtfeld, M., Maherali, N., Breault, D.T., and Hochedlinger, K. (2008b). Defining molecular cornerstones during fibroblast to iPS cell reprogramming in mouse. *Cell Stem Cell* **2** (3): 230–240.

Staerk, J., Dawlaty, M.M., Gao, Q., Maetzel, D., Hanna, J., Sommer, C.A., Mostoslavsky, G., and Jaenisch, R. (2010). Reprogramming of Human Peripheral Blood Cells to Induced Pluripotent Stem Cells. *Cell Stem Cell* **7** (1): 20–24.

Steiner, D., Khaner, H., Cohen, M., Even-Ram, S., Gil, Y., Itsykson, P., Turetsky, T., Idelson, M., Aizenman, E., Ram, R., Berman-Zaken, Y., and Reubinoff, B. (2010). Derivation, propagation and controlled differentiation of human embryonic stem cells in suspension. *Nat. Biotechnol.* **28**: 361.

Sugawara, T., Nishino, K., Umezawa, A., and Akutsu, H. (2012). Investigating cellular identity and manipulating cell fate using induced pluripotent stem cells. *Stem Cell Res. Ther.* **3** (2): 8.

Suntharalingam, G., Perry, M.R., Ward, S., Brett, S.J., Castello-Cortes, A., Brunner, M.D., and Panoskaltsis, N. (2006). Cytokine Storm in a Phase 1 Trial of the Anti-CD28 Monoclonal Antibody TGN1412. *N. Engl. J. Med.* **355** (10): 1018–1028.

Szabo, E., Rampalli, S., Risueño, R.M., Schnerch, A., Mitchell, R., Fiebig-Comyn, A., Levadoux-Martin, M., and Bhatia, M. (2010). Direct conversion of human fibroblasts to multilineage blood progenitors. *Nature* **468** (7323): 521–526.

Tachibana, M., Amato, P., Sparman, M., Gutierrez, N.M., Tippner-Hedges, R., Ma, H., Kang, E., Fulati, A., Lee, H.-S., Sritanaudomchai, H., Masterson, K., Larson, J., Eaton, D., Sadler-Fredd, K., Battaglia, D., Lee, D., Wu, D., Jensen, J., Patton, P., *et al.* (2013). Human Embryonic Stem Cells Derived by Somatic Cell Nuclear Transfer. *Cell* **153** (6): 1228–1238.

Takahashi, K., and Yamanaka, S. (2006). Induction of pluripotent stem cells from mouse embryonic and adult fibroblast cultures by defined factors. *Cell* **126** (4): 663–676.

Takahashi, K., Tanabe, K., Ohnuki, M., Narita, M., Ichisaka, T., Tomoda, K., and Yamanaka, S. (2007). Induction of Pluripotent Stem Cells from Adult Human Fibroblasts by Defined Factors. *Cell* **131** (5): 861–872.

Takao, K., and Miyakawa, T. (2015). Genomic responses in mouse models greatly mimic human inflammatory diseases. *Proc. Natl. Acad. Sci. U. S. A.* **112** (4): 1167–1172.

Takebe, T., Sekine, K., Enomura, M., Koike, H., Kimura, M., Ogaeri, T., Zhang, R.-R., Ueno, Y., Zheng, Y.-W., Koike, N., Aoyama, S., Adachi, Y., and Taniguchi, H. (2013). Vascularized and functional human liver from an iPSC-derived organ bud transplant. *Nature* **499** (7459): 481–484.

Tang, X., Wang, S., Bai, Y., Wu, J., Fu, L., Li, M., Xu, Q., Xu, Z.Q.D., Alex Zhang, Y., and Chen, Z. (2016). Conversion of adult human peripheral blood mononuclear cells into induced neural stem cell by using episomal vectors. *Stem Cell Res.* **16** (2): 236–242.

Taylor, C.J., Peacock, S., Chaudhry, A.N., Bradley, J.A., and Bolton, E.M. (2012). Generating an iPSC Bank for HLA-Matched Tissue Transplantation Based on Known Donor and Recipient HLA Types. *Cell Stem Cell* **11** (2): 147–152.

Theunissen, T.W., and Jaenisch, R. (2014). Molecular control of induced pluripotency. *Cell Stem Cell* **14** (6): 720–734.

Thier, M., Münst, B., and Edenhofer, F. (2011). Exploring refined conditions for reprogramming cells by recombinant Oct4 protein. *Int. J. Dev. Biol.* **54** (11–12): 1713–1721.

Thier, M., Wörsdörfer, P., Lakes, Y.B., Gorris, R., Herms, S., Opitz, T., Seiferling, D., Quandel, T., Hoffmann, P., Nöthen, M.M., Brüstle, O., and Edenhofer, F. (2012). Direct conversion of fibroblasts into stably expandable neural stem cells. *Cell Stem Cell* **10** (4): 473–479.

Thier, M.C., Hommerding, O., Panten, J., Pinna, R., García-González, D., Berger, T., Wörsdörfer, P., Assenov, Y., Scognamiglio, R., Przybylla, A., Kaschutnig, P., Becker, L., Milsom, M.D., Jauch, A., Utikal, J., Herrmann, C., Monyer, H., Edenhofer, F., and Trumpp, A. (2019). Identification of Embryonic Neural Plate Border Stem Cells and Their Generation by Direct Reprogramming from Adult Human Blood Cells. *Cell Stem Cell* **24** (1): 166–182.e13.

Thomas, K.R., Folger, K.R., and Capecchi, M.R. (1986). High frequency targeting of genes to specific sites in the mammalian genome. *Cell* **44** (3): 419–428.

Thomas, R.J., Anderson, D., Chandra, A., Smith, N.M., Young, L.E., Williams, D., and Denning, C. (2008). Automated, scalable culture of human embryonic stem cells in feeder-free conditions. *Biotechnol. Bioeng.* **102** (6): 1636–1644.

Thomson, J.A., Itskovitz-Eldor, J., Shapiro, S.S., Waknitz, M.A., Swiergiel, J.J., Marshall, V.S., and Jones, J.M. (1998). Embryonic Stem Cell Lines Derived from Human Blastocysts. *Science* **282** (5391): 1145–1147.

Tohyama, S., Hattori, F., Sano, M., Hishiki, T., Nagahata, Y., Matsuura, T., Hashimoto, H., Suzuki, T., Yamashita, H., Satoh, Y., Egashira, T., Seki, T., Muraoka, N., Yamakawa, H., Ohgino, Y., Tanaka, T., Yoichi, M., Yuasa, S., Murata, M., *et al.* (2013). Distinct metabolic flow enables large-scale purification of mouse and human pluripotent stem cell-derived cardiomyocytes. *Cell Stem Cell* **12** (1): 127–137.

Turner, M., Leslie, S., Martin, N.G., Peschanski, M., Rao, M., Taylor, C.J., Trounson, A., Turner, D., Yamanaka, S., and Wilmut, I. (2013). Toward the Development of a Global Induced Pluripotent Stem Cell Library. *Cell Stem Cell* **13** (4): 382–384.

Villa-Diaz, L.G., Nandivada, H., Ding, J., Nogueira-de-Souza, N.C., Krebsbach, P.H., O'Shea, K.S., Lahann, J., and Smith, G.D. (2010). Synthetic polymer coatings for long-term growth of human embryonic stem cells. *Nat. Biotechnol.* **28** (6): 581–583.

Villa-Diaz, L.G., Brown, S.E., Liu, Y., Ross, A.M., Lahann, J., Parent, J.M., and Krebsbach, P.H. (2012). Derivation of Mesenchymal Stem Cells from Human Induced Pluripotent Stem Cells Cultured on Synthetic Substrates. *Stem Cells* **30** (6): 1174–1181.

Villa-Diaz, L.G., Ross, A.M., Lahann, J., and Krebsbach, P.H. (2013). Concise review: The evolution of human pluripotent stem cell culture: From feeder cells to synthetic coatings. *Stem Cells* **31** (1): 1–7.

Völkner, M., Zschätzsch, M., Rostovskaya, M., Overall, R.W., Busskamp, V., Anastassiadis, K., and Karl, M.O. (2016). Retinal Organoids from Pluripotent Stem Cells Efficiently Recapitulate Retinogenesis. *Stem Cell Reports* **6** (4): 525–538.

Vosough, M., Omidinia, E., Kadivar, M., Shokrgozar, M.-A., Pournasr, B., Aghdami, N., and Baharvand, H. (2013). Generation of Functional Hepatocyte-Like Cells from Human Pluripotent Stem Cells in a Scalable Suspension Culture. *Stem Cells Dev.* **22** (20): 2693–2705.

Wang, H., Luo, X., Yao, L., Lehman, D.M., and Wang, P. (2015). Improvement of Cell Survival During Human Pluripotent Stem Cell Definitive Endoderm Differentiation. *Stem Cells Dev.* **24** (21): 2536–2546.

Wang, Z.S., Feng, Z.H., Wu, G.F., Bai, S.Z., Dong, Y., Chen, F.M., and Zhao, Y.M. (2016). The use of platelet-rich fibrin combined with periodontal ligament and jaw bone mesenchymal stem cell sheets for periodontal tissue engineering. *Sci. Rep.* **6**: 28126.

Warren, L., Manos, P.D., Ahfeldt, T., Loh, Y.-H., Li, H., Lau, F., Ebina, W., Mandal, P.K., Smith, Z.D., Meissner, A., Daley, G.Q., Brack, A.S., Collins, J.J., Cowan, C., Schlaeger, T.M., and Rossi, D.J. (2010). Highly Efficient Reprogramming to Pluripotency and Directed Differentiation of Human Cells with Synthetic Modified mRNA. *Cell Stem Cell* **7** (5): 618–630.

Watanabe, K., Ueno, M., Kamiya, D., Nishiyama, A., Matsumura, M., Wataya, T., Takahashi, J.B., Nishikawa, S., Nishikawa, S., Muguruma, K., and Sasai, Y. (2007). A ROCK inhibitor permits survival of dissociated human embryonic stem cells. *Nat. Biotechnol.* **25** (6): 681–686.

Wiedemann, P.M., Simon, J., Schicktanz, S., and Tannert, C. (2004). The future of stem-cell research in Germany. *EMBO Rep.* **5** (10): 927–931.

Wilkinson, D.C., Alva-Ornelas, J.A., Sucre, J.M.S., Vijayaraj, P., Durra, A., Richardson, W., Jonas, S.J., Paul, M.K., Karumbayaram, S., Dunn, B., and Gomperts, B.N. (2017). Development of a Three-Dimensional Bioengineering Technology to Generate Lung Tissue for Personalized Disease Modeling. *Stem Cells Transl. Med.* **6** (2): 622–633.

Williams, R.L., Hilton, D.J., Pease, S., Willson, T.A., Stewart, C.L., Gearing, D.P., Wagner, E.F., Metcalf, D., Nicola, N.A., and Gough, N.M. (1988). Myeloid leukaemia inhibitory factor maintains the developmental potential of embryonic stem cells. *Nature* **336** (6200): 684–687.

Wilmut, I., Schnieke, A.E., McWhir, J., Kind, A.J., and Campbell, K.H.S. (1997). Viable offspring derived from fetal and adult mammalian cells. *Nature* **385** (6619): 810–813.

Wohlrab, S., Müller, S., Schmidt, A., Neubauer, S., Kessler, H., Leal-Egaña, A., and Scheibel, T. (2012). Cell adhesion and proliferation on RGD-modified recombinant spider silk proteins. *Biomaterials* **33** (28): 6650–6659.

Woltjen, K., Michael, I.P., Mohseni, P., Desai, R., Mileikovsky, M., Hämäläinen, R., Cowling, R., Wang, W., Liu, P., Gertsenstein, M., Kaji, K., Sung, H.-K., and Nagy, A. (2009). piggyBac transposition reprograms fibroblasts to induced pluripotent stem cells. *Nature* **458** (7239): 766–770.

Wörsdörfer, P., Thier, M., Kadari, A., and Edenhofer, F. (2013). Roadmap to Cellular Reprogramming - Manipulating Transcriptional Networks with DNA, RNA, Proteins and Small Molecules. *Curr. Mol. Med.* **13** (5): 868–878.

Wu, J., Rostami, M.R., Cadavid Olaya, D.P., Tzanakakis, E.S., and Pappalardo, F. (2014). Oxygen Transport and Stem Cell Aggregation in Stirred-Suspension Bioreactor Cultures. *PLoS One* **9** (7): e102486.

Wüst, S., Müller, R., and Hofmann, S. (2015). 3D Bioprinting of complex channels—Effects of material, orientation, geometry, and cell embedding. *J. Biomed. Mater. Res. A* **103** (8): 2558–2570.

Xu, C., Inokuma, M.S., Denham, J., Golds, K., Kundu, P., Gold, J.D., and Carpenter, M.K. (2001). Feeder-free growth of undifferentiated human embryonic stem cells. *Nat. Biotechnol.* **19** (10): 971–974.

Yamanaka, S. (2009). Elite and stochastic models for induced pluripotent stem cell generation. *Nature* **460** (7251): 49–52.

Yan, Y., Shin, S., Jha, B.S., Liu, Q., Sheng, J., Li, F., Zhan, M., Davis, J., Bharti, K., Zeng, X., Rao, M., Malik, N., and Vemuri, M.C. (2013). Efficient and Rapid Derivation of Primitive Neural Stem Cells and Generation of Brain Subtype Neurons From Human Pluripotent Stem Cells. *Stem Cells Transl. Med.* **2** (11): 862–870.

Ying, Q., Nichols, J., Chambers, I., and Smith, A. (2003). BMP Induction of Id Proteins Suppresses Differentiation and Sustains Embryonic Stem Cell Self-Renewal in Collaboration with STAT3. *Cell* **115** (3): 281–292.

Youssef, A., Hollister, S.J., and Dalton, P.D. (2017). Additive manufacturing of polymer melts for implantable medical devices and scaffolds. *Biofabrication* **9** (1): 012002.

Yu, J., Vodyanik, M.A., Smuga-Otto, K., Antosiewicz-Bourget, J., Frane, J.L., Tian, S., Nie, J., Jonsdottir, G.A., Ruotti, V., Stewart, R., Slukvin, I.I., and Thomson, J.A. (2007). Induced Pluripotent Stem Cell Lines Derived from Human Somatic Cells. *Science* **318** (5858): 1917–1920.

Yu, J., Hu, K., Smuga-Otto, K., Tian, S., Stewart, R., Slukvin, I.I., and Thomson, J.A. (2009). Human Induced Pluripotent Stem Cells Free of Vector and Transgene Sequences. *Science* **324** (5928): 797–801.

Yu, J., Du, K.T., Fang, Q., Gu, Y., Mihardja, S.S., Sievers, R.E., Wu, J.C., and Lee, R.J. (2010). The use of human mesenchymal stem cells encapsulated in RGD modified alginate microspheres in the repair of myocardial infarction in the rat. *Biomaterials* **31** (27): 7012–7020.

Zhang, Y., Cao, N., Huang, Y., Spencer, C.I., Fu, J.D., Yu, C., Liu, K., Nie, B., Xu, T., Li, K., Xu, S., Bruneau, B.G., Srivastava, D., and Ding, S. (2016). Expandable Cardiovascular Progenitor Cells Reprogrammed from Fibroblasts. *Cell Stem Cell* **18** (3): 368–381.

Zhou, H., Wu, S., Joo, J.Y., Zhu, S., Han, D.W., Lin, T., Trauger, S., Bien, G., Yao, S., Zhu, Y., Siuzdak, G., Schöler, H.R., Duan, L., and Ding, S. (2009). Generation of Induced Pluripotent Stem Cells Using Recombinant Proteins. *Cell Stem Cell* **4** (5): 381–384.

Zhou, T., Benda, C., Dunzinger, S., Huang, Y., Ho, J.C., Yang, J., Wang, Y., Zhang, Y., Zhuang, Q., Li, Y., Bao, X., Tse, H.F., Grillari, J., Grillari-Voglauer, R., Pei, D., and Esteban, M.A. (2012). Generation of human induced pluripotent stem cells from urine samples. *Nat. Protoc.* **7** (12): 2080–2089.

Zweigerdt, R. (2009). Large Scale Production of Stem Cells and Their Derivatives. In Engineering of Stem Cells, U. Martin, ed. (Berlin, Heidelberg, Germany: Springer), pp. 201–235.

Zweigerdt, R., Olmer, R., Singh, H., Haverich, A., and Martin, U. (2011). Scalable expansion of human pluripotent stem cells in suspension culture. *Nat. Protoc.* **6** (5): 689–700.

List of Figures

List of Tables

Publication list

Peer-reviewed articles

1. **Kwok, C.K.***, Ueda, Y.*, Kadari, A., Günther, K., Ergün, S., Heron, A., Schnitzler, A.C., Rook, M., and Edenhofer, F. (2018). Scalable stirred suspension culture for the generation of billions of human induced pluripotent stem cells using single-use bioreactors. *J. Tissue Eng. Regen. Med.* **12** (2): e1076–e1087.

2. Günther, K.*, Appelt-Menzel, A.*, **Kwok, C.K.**, Walles, H., Metzger, M., and Edenhofer, F. (2016). Rapid Monolayer Neural Induction of induced Pluripotent Stem Cells Yields Stably Proliferating Neural Stem Cells. *J. Stem Cell Res. Ther.* **06**: 1–6.

3. Peruzzotti-Jametti, L., Bernstock, J.D.*, Vicario, N.*, Costa, A.S.H., **Kwok, C.K.**, Leonardi, T., Booty, L.M., Bicci, I., Balzarotti, B., Volpe, G., Mallucci, G., Manferrari, G., Donegà, M., Iraci, N., Braga, A., Hallenbeck, J.M., Murphy, M.P., Edenhofer, F., Frezza, C., and Pluchino, S. (2018). Macrophage-Derived Extracellular Succinate Licenses Neural Stem Cells to Suppress Chronic Neuroinflammation. *Cell Stem Cell* **22** (3): 355–368.e13.

4. Jansch, C., Günther, K., Waider, J., Ziegler, G.C., Forero, A., Kollert, S., Svirin, E., Pühringer, D., **Kwok, C.K.**, Ullmann, R., Maierhofer, A., Flunkert, J., Haaf, T., Edenhofer, F., and Lesch, K.-P. (2018). Generation of a human induced pluripotent stem cell (iPSC) line from a 51-year-old female with attention-deficit/hyperactivity disorder (ADHD) carrying a duplication of SLC2A3. *Stem Cell Res.* **28**: 136–140.

5. Mekala, S.R.*, Wörsdörfer, P.*, Bauer, J., Stoll, O., Wagner, N., Reeh, L., Loew, K., Eckner, G., **Kwok, C.K.**, Wischmeyer, E., Dickinson, M.E., Stegner, D., Benndorf, R.A., Edenhofer, F., Pfeiffer, V., Kuerten, S., Frantz, S., and Ergün, S. (2018). Generation of Cardiomyocytes from Vascular Adventitia-Resident Stem Cells. *Circ. Res.* **123** (6): 686–699.

6. Klein, T., Henkel, L., Klug, K., **Kwok, C.K.**, Klopocki, E., and Üçeyler, N. (2018). Generation of the human induced pluripotent stem cell line UKWNLi002-A from dermal fibroblasts of a woman with a heterozygous c.608C > T (p.Thr203Met) mutation in exon 3 of the nerve growth factor gene potentially associated with hereditary sensory and autonomic neuropathy type. *Stem Cell Res.* **33**: 171–174.

7. Klein, T.*, Günther, K.*, **Kwok, C.K.**, Edenhofer, F., and Üçeyler, N. (2018). Generation of the human induced pluripotent stem cell line (UKWNLi001-A) from skin fibroblasts of a woman with Fabry disease carrying the X-chromosomal heterozygous c.708 G > C (W236C) missense mutation in exon 5 of the alpha-galactosidase−A gene. *Stem Cell Res.* **31**: 222−226.
8. Klein, T., Klug, K., Henkel, L., **Kwok, C.K.**, Edenhofer, F., Klopocki, E., Kurth, I., and Üçeyler, N. (2019). Generation of two induced pluripotent stem cell lines from skin fibroblasts of sisters carrying a c.1094C > A variation in the SCN10A gene potentially associated with small fiber neuropathy. *Stem Cell Res.* **35**: 101396.

*These authors contributed equally.

Abstracts for oral presentation

1. Stirred suspension culture for the scalable generation of billions of human induced pluripotent stem cells. **4th International Annual Conference of the German Stem Cell Network, September 2016, Hannover, Germany**.
2. Single-use stirred suspension culture vessels for the generation of billions of human induced pluripotent stem cells in cell-only aggregates. **9th Austrian Society for Molecular Biotechnology and 8th Life Science Meeting Innsbruck, September 2017, Innsbruck, Austria.**
3. Scalable Suspension Culture for the Generation of Billions of Human Induced Pluripotent Stem Cells using Single-Use Bioreactors. **Merck Millipore/ MilliporeSigma Webinar Series, April 2017**. https://www.merckmillipore.com/DE/en/20141201_203345?Pname=131

Abstracts for poster presentation

1. **Kwok, C.K.**†, Ueda, Y., Kadari, A., Günther, K., Heron, A., Schnitzler, A., Rook, M., Edenhofer, F. (2016). Stirred suspension culture for scalable generation of billions of human induced pluripotent stem cells. **11th GSLS Symposium, October, Würzburg, Germany.**

2. **Kwok, C.K.**†, Ueda, Y., Kadari, A., Günther, K., Heron, A., Schnitzler, A., Rook, M., Edenhofer, F. (2017). Production of billions of human induced pluripotent stem cells as cell-only aggregates in single-use stirred suspension bioreactors. **15th Annual Meeting of the International Society of Stem Cell Research (ISSCR), June, Boston, MA, USA.**

3. **Kwok C.K.**†, Ueda, Y., Jüngst, T., Di Lascio, A., Groll, J., Edenhofer, F. (2018). Bioreactor-expanded human induced pluripotent stem cells and printable hydrogels for biofabrication. **16th Annual Meeting of the International Society of Stem Cell Research (ISSCR), June, Melbourne, Australia.**

4. **Kwok, C.K.**, Ueda, Y., Lawson, T.†, Verma, A., Pease, M., Kadari, A., Günther, K., Schnitzler, A., Heron, A., Rook, M., Edenhofer, F., Murrell, J. (2016). Expansion of human induced pluripotent stem cells in scalable stirred suspension culture. **World Stem Cell Summit 2016, December, West Palm Beach, FL, USA**

5. Ueda, Y.†, **Kwok, C.K.**, Kadari, A., Hertlein, S., Edenhofer, F. (2016). Efficient human pluripotent stem cell bioprocess development — Upscaling of expansion and differentiation potential. **Stem Cell Models of Neural Regeneration and Disease International Symposium (ISSCR-CRTD), February, Dresden, Germany.**

6. Ueda, Y.†, **Kwok, C.K.**, Nose, N., Kadari, A., Edenhofer, F. (2016). Cardiac differentiation of human induced pluripotent stem cells in scalable stirred suspension culture. **Stem Cell Society of Singapore Symposium 2016, November, Singapore.**

7. Peruzzotti-Jametti, L.†, Bernstock, J., Vicario, N., **Kwok, C.K.**, Leonardi, T., Booty, L., Bicci, I., Balzarotti, B., Volpe, G., Mallucci, G., Manferrari, G., Donegà, M., Iraci, N., Braga, A., Hallenbeck, J., Murphy, M., Edenhofer, F., Frezza, C., Pluchino, S. (2018). Macrophage-derived extracellular succinate licenses neural stem cells to suppress chronic neuroinflammation. **16th Annual Meeting of the International Society of Stem Cell Research (ISSCR), June, Melbourne, Australia.**

8. Peruzzotti-Jametti, L.†, Vicario, N., Braga, A., Rizzi, S., **Kwok, C.K.**, Volpe, G., Balzarotti, B., D'Amico, G., Bernstock, J., Parenti, R., Zhao, C., Franklin, R., Edenhofer, F., Pluchino, S. (2018). Remyelination of chronic demyelinated lesions of the spinal cord with directly induced neural stem cells. **16th Annual Meeting of the International Society of Stem Cell Research (ISSCR), June, Melbourne, Australia.**

† Presenting author

Affidavit/Eidesstattliche Erklärung

I hereby confirm that my thesis entitled “Scaling up production of reprogrammed cells for biomedical applications” is the result of my own work. I did not receive any help or support from commercial consultants. All sources and/or materials applied are listed and specified in the thesis.

Furthermore, I confirm that this thesis has not yet been submitted as part of another examination process neither in identical nor in similar form.

Würzburg,

Place, Date	**Signature**

Hiermit erkläre ich an Eides statt, die Dissertation „Skalierung der Produktion von reprogrammierten Zellen für biomedizinische Anwendungen“ eigenständig, das heißt insbesondere selbständig und ohne Hilfe eines kommerziellen Promotionsberaters, angefertigt und keine anderen als die von mir angegebenen Quellen und Hilfsmittel verwendet zu haben.

Ich erkläre außerdem, dass die Dissertation weder in gleicher noch in ähnlicher Form bereits in einem anderen Prüfungsverfahren vorgelegen hat.

Würzburg,

Ort, Datum	**Unterschrift**

Acknowledgments

First and foremost, my heartfelt gratitude goes to my supervisor **Prof. Dr. Frank Edenhofer** who provided me with the opportunity to perform my doctoral work on this great project. Thank you for your patience, your always encouraging and enthusiastic attitude, your invaluable guidance and fruitful suggestions during our discussions and meetings, and your support to let me explore different directions during my doctoral work.

Next, I thank **Prof. Dr. Jürgen Groll**, **Prof. Dr. Thomas Scheibel**, and **Prof. Dr. Heike Walles** for their support as my thesis committee. Thank you for your active participation in our annual meetings, for contributing your feedback on the progress of my doctoral work, and for providing insights from different perspectives. I would also like to thank **Prof. Dr. Süleyman Ergün** for his hospitality at the Institute of Anatomy and Cell Biology, and for his comments and discussions during our regular lab meetings. To all of you, thank you — my work has doubtlessly been enriched through our consultation sessions.

I count my lucky stars every day, for I have had the immense pleasure of working with some of the most helpful and wonderful colleagues and friends. To **Dr. Yuichiro Ueda**, thank you for your guidance and infectious enthusiasm, and I admire your resilience and tenacity and it will always be a source of inspiration for me. Thanks also for all your efforts to create a friendly atmosphere in the working group. Your countless onigiri and okonomiyaki parties will be sorely missed, and I hope they were not inspired by “Have you had lunch yet?”. Thanks also for helping to proof-read and comment on this thesis despite your other commitments.

On my first day in the Edenhofer lab as an intern, **Dr. Katharina Günther** was responsible for introducing me to the world of stem cells and cell culture techniques. I remember with fond memories the first time we made dTomato lentiviral particles and made cells light up in red, or when you showed me stained neurons in the dish. I do not believe in magic, but this experience came very close to that. Outside of the lab, I will always remember our many explorations at different restaurants in Würzburg, fuelled by our passion for food (and coffee!).

To **Dr. Philipp Wörsdörfer**, thank you for sharing all your scientific knowledge and being so welcoming throughout my stay in the laboratory. You were always willing to help and answer questions, and all students should be so lucky to have a mentor like you! Thanks also for helping with the translation of my summary into German. To **Dr. Dirk Pühringer**, thanks for all the thought-provoking

discussions during lab meetings, and for being the Chilli Meister and my office coffee buddy. Thanks also go to **Dr. Asifiqbal Kadari** for teaching your cardiomyocyte differentiation protocol and for starting the collaboration work regarding stirred suspension culture of hiPSCs. Seeing those cardiomyocytes beating in the dish was one of the most unforgettable things I have seen in my scientific career. Thanks also to **Dr. Sandra Meyer** for teaching me about your induced neural stem cells, and **Dr. Damiano Rovituso** for sharing your expertise in flow cytometry, teaching and guiding me to becoming an independent user of the machine. Thanks also to **Tobias Königer**, for being a great fellow doctoral student and reliable sounding board, and I will always smile when I look back at our times shared during the organisation of the Eureka GSLS Symposium. To **Dr. Takashi I**, **Dr. Manju Nandigama**, and **Dr. Leyla Doğan,** although our time in the lab together was short, you were always friendly and open to discussion, not to mention your generosity with treats and goodies! Thanks also go to the Innsbruck Stem Cell group for discussions during our "Würzbruck" retreat and meetings, especially **Dr. Sandra Rizzi** and **Marta Suarez-Cubero** for discussions about iNSCs and the examination of their profiles by flow cytometry.

One also cannot forget the monumental contribution to the lab from our outstanding technicians **Martina Gebhardt**, **Heike Arthen**, and **Ursula Roth.** Thank you for your work in maintaining the lab in tip-top condition so that we can always carry out our experiments, and for your great help in performing some of the routine but important assays.

My time in the institute was also made enjoyable by the many students and co-workers coming through our lab; a special shout-out to **Nahide Dalda**, **Berin Upcin**, **Naoko Nose, Simon Hertlein**, **Anna Kern**, **Anna Janz**, **Helena Dambacher**, **Sven Schmidt**, **Sarah Krüger**, and **Endi Kashari**. Thank you for contributing to the nice working atmosphere!

I would also like to thank our external collaborators. To **Dr. Tomasz Jüngst** from the Groll lab, thank you for sharing your expertise with 3D printing and for our joint work in printing hiPSCs. Thanks also go to **Dr. Kiran Pawar** and **Tamara Aigner** from the Scheibel lab for their efforts in generating the recombinant spider silk protein non-woven fibres and cast films, and for general discussions regarding cell culture on these novel substrata. Thanks also to fellow doctoral researchers **Thomas Klein** and **Charline Jansch** for our collaborative work together and for joining us in our neuro journal club, and to **Julia Flunkert** and **Anna Maierhofer** from **Prof. Dr. Thomas Haaf**'s group for the G-banding analysis. To **Dr. Stefano Pluchino's team**,

especially **Dr. Luca Peruzzotti-Jametti** and **Beatrice Balzarotti**, I am so happy that our collaboration has been fruitful so far, and thanks for the fond memories of Cambridge and Thorpe Park. Thanks also go to our collaborators at **Merck KGaA/MilliporeSigma Cell Therapy Bioprocessing**. To **Dr. Antoine Heron**, thanks for your input and efforts surrounding the hiPSC scale-up project and for visiting the GSLS Symposium as a career session panellist. **Dr. Aletta Schnitzler**, thank you for your helpful suggestions during our monthly Skype calls about the project, and being such a wizard at coordinating my visit at your facilities in Bedford. Special thanks also to **Tristan Lawson** for being a wonderful guide at Bedford, and for introducing me to Handkäs mit Musik.

The **Graduate School of Life Sciences team**, including **Dr. Stephan Schröder-Köhne**, **Dr. Gabriele Blum-Oehler**, **Dr. Franz-Xaver Kober, Jennifer Heilig**, **Katrin Lichosik**, **Felizitas Berninger** and **Sebastian Michel,** has also been instrumental in running and coordinating many of the aspects of the doctoral programme. Thank you to each of you for all your efforts in helping to make my doctoral phase a smooth, fulfilling, and enriching one. Thank you also for the financial support provided by the GSLS through my doctoral fellowship which afforded me the opportunity to attend several overseas conferences and pursue side projects.

To my expanded FOKUS family, **Prathi**, **Alok**, **Rohini**, **Andrea**, **Diyaa**, **Moataz**, **Gayathri**, **Manju**, **Ana Maria**, **Manli**, and **Ashley**, we embarked on this journey together some 5–6 years ago, and I have to say thank you to you for being my support system away from home. To my closest friends from home, **Gopal**, **Andee**, **Yong Ping**, **Zarina**, **Rachel**, **Sue Ann**, and **Mingjie**, thank you for believing in me and for your friendship. Special mention goes to **Johannes**, the one who planted the seed of pursuing my doctorate in Germany, thank you for all your support, your fierce friendship, and for telling me things the way they are, even if they are things I do not particularly want to hear. Thanks also to your family who have been nothing but warm and welcoming all throughout my time here in Germany.

Last, but certainly not least, none of this could have been possible without the unconditional love and endless support from my parents **Kwok Seh In** and **Fong Yin Chee**. Thank you for giving up so much so that I could succeed. To my siblings **Kwok Chee May** and **Kwok Chee How**, thanks for your support and keeping the homesickness at bay with your stream of pictures and updates from home. I love you all.